Environmental
Studies
Research
Funds

094 Dynamics of Iceberg Grounding and Scouring

Volume 1 — The Field Experiment

Canada

June 1988

The Environmental Studies Research Funds are financed from special levies on the oil and gas industry and administered by the Canada Oil and Gas Lands Administration for the Minister of Energy, Mines and Resources, and by the Northern Affairs Program for the Minister of Indian Affairs and Northern Development.

The Environmental Studies Research Funds and any person acting on their behalf assume no liability arising from the use of the information contained in this document. The opinions expressed are those of the authors and do not necessarily reflect those of the Environmental Studies Research Funds agencies. The use of trade names or identification of specific products does not constitute an endorsement or recommendation for use.

Dynamics of Iceberg Grounding and Scouring

This report is published in two volumes.

Volume I contains the results of the field experiment.

Volume II contains the maps and charts that are discussed in the text of Volume I.

Ten Appendices containing data on observations made during the field experiment are archived at the Atlantic Geoscience Centre, Bedford Institute of Oceanography, Dartmouth, Nova Scotia.

ENVIRONMENTAL STUDIES RESEARCH FUNDS
REPORT NO. 094, VOLUME I
JUNE, 1988

THE DYNAMICS OF ICEBERG GROUNDING AND SCOURING (DIGS) EXPERIMENT AND REPETITIVE MAPPING OF THE EASTERN CANADIAN CONTINENTAL SHELF

Editors:
G.J. Hodgson[1]
J.H. Lever[2]
C.M.T. Woodworth-Lynas[2]
and
C.F.M. Lewis[3]

[1] GEONAUTICS LIMITED
St. John's, Newfoundland

and

[2] CENTRE FOR COLD OCEAN RESOURCES ENGINEERING (C-CORE)
Memorial University of Newfoundland
St. John's, Newfoundland

and

[3] ATLANTIC GEOSCIENCE CENTRE (AGC)
Geologic Survey of Canada
Bedford Institute of Oceanography
Dartmouth, Nova Scotia

Scientific Advisers: C.F.M. Lewis and D.R. Parrott

89-06081/

The correct citation for this report is:

Hodgson, G.J., J.H. Lever, C.M.T. Woodworth-Lynas, and C.F.M. Lewis, (editors). 1988. The dynamics of iceberg grounding and scouring (DIGS) experiment and repetitive mapping of the eastern Canadian continental shelf. Environmental Studies Research Funds Report No. 094. Two vols. Ottawa. 315 p.

Published under the auspices of the Environmental Studies Research Funds.
ISBN 0-920783-83-7
c 1988 - Geonautics Ltd.

PREFACE

The Dynamics of Iceberg Grounding and Scouring experiment (DIGS) was conceived in 1984 and formulated by an ad hoc committee comprising J.V. Barrie (C-CORE), S. Hotzel (Petro-Canada), H.W. Josenhans (AGC), J.H. Lever (C-CORE), C.F.M. Lewis (AGC, Chairman), D.R. Parrott (AGC), S.D. Smith (DFO), and C.M.T. Woodworth-Lynas (C-CORE). The recommendations of this group were accepted and developed by the ESRF Committee on Seabottom Scouring under the chairmanship of W.R. Livingstone (Gulf Resources Canada). Following a discussion of the proposal (Lewis et al., 1986; Lewis 1986; Lever 1986; Josenhans 1986; Moran 1986) at a workshop on ice scour research in early 1985, the experiment was authorized by the Environmental Studies Research Funds (ESRF) who selected Geonautics Limited, St. John's, Newfoundland, to implement the program. The DIGS results, as reported in this volume, are the culmination of a co-ordinated effort under scientific guidance of the ad hoc committee, comprising the ESRF work under the advisorship of C.F.M. Lewis and D.R. Parrott, a submersible research program (jointly sponsored by EMR and DFO) under the direction of H.W. Josenhans and J.V. Barrie, and a research study of wave-induced ice motion (WIIM study, funded by NSERC) under the direction of J.H. Lever.

The following materials are archived at the Atlantic Geoscience Centre as a Geological Survey of Canada Open File Report and may be accessed by writing to:

Atlantic Geoscience Centre
Geological Survey of Canada
Bedford Institute of Oceanography
P.O. Box 1006
Dartmouth, Nova Scotia
B2Y 4A2

Included are:

- All photographs
- BRUTIV film and logs
- OSPS iceberg profile tape including format and file structure
- Motion sensor tape including format and file structure
- Navigation tape of iceberg positions including format and file structure
- full-size charts
- all sounder, sidescan sonar and Huntec DTS data

TABLE OF CONTENTS

Page

Preface....................iii

List of Figures....................xi

List of Tables....................xvi

List of Charts....................xvii

Acknowledgements....................xviii

SUMMARY....................xxi

RESUME....................xxiv

INTRODUCTION

C.F.M. Lewis and J.H. Lever.................... 1

DYNAMICS OF ICEBERG GROUNDING AND SCOURING (DIGS) EXPERIMENT.................... 2

Objectives.................... 6

Strategy and methods used for the DIGS experiment.................... 7

REPETITIVE MAPPING OF THE EASTERN CANADIAN CONTINENTAL SHELF....................13

CHAPTER 1

METHODS AND OPERATIONS

OPERATIONS OVERVIEW

W. Carter and M. Dyke....................14

Operational setting....................14

Operational strategy....................17

Field systems and facilities....................19

DATA COLLECTION AND ANALYTICAL TECHNIQUES....................25

Navigation and position fixing

M. Dyke....................25

Iceberg tracking

W. Carter and M. Dyke....................27

Iceberg dimensioning
W. Carter....30
Iceberg motions
J.H. Lever and K. Klein....35
Atmospheric and oceanographic measurements
D. Finlayson....43
Seabed mapping and profiling
W. Carter....48
Observations from submersible
W. Carter....51
Sediment tracer techniques
J.V. Barrie....51

CHAPTER 2

PHYSICAL AND ENVIRONMENTAL SETTING

PHYSIOGRAPHIC AND GEOLOGIC SETTING
W. Carter and H.W. Josenhans....55
METEOROLOGIC AND OCEANOGRAPHIC SETTING
D. Finlayson....62

CHAPTER 3

ICEBERG OBSERVATIONS AND RELATED DATA

METEOROLOGIC AND OCEANOGRAPHIC DATA
D. Finlayson....66
Winds and weather....66
Waves....68
Currents and tides....70
Water properties....72
Sea ice and icebergs
D. Finlayson and W. Carter....72

SUMMARY OF DATA ON ALL ICEBERGS INVESTIGATED
D. Diemand and J.H. Lever..........................73
Iceberg "Anastasia"................................75
Iceberg "Bertha"...................................78
Iceberg "Cordelia".................................80
Iceberg "Deborah"..................................81
Iceberg "Erica/Hermione"...........................82
Iceberg "Frieda"...................................83
Iceberg "Gladys"...................................87
Iceberg "Isadora"..................................93
Iceberg "Julianna".................................94
Iceberg "Kit Kat"..................................96
Iceberg "Lucretia".................................97

DETAILED ICEBERG OBSERVATIONS.......................99
Iceberg shape and volume
J.H. Lever...99
Iceberg motions
J.H. Lever and K. Klein...........................129

CHAPTER 4

ICEBERG SCOUR AND SEDIMENT TRANSPORT OBSERVATIONS

OBSERVATIONS FROM SUBMERSIBLE
C.M.T. Woodworth-Lynas, H.W. Josenhans,
J.V. Barrie and D.R. Parrott......................152
Makkovik Bank, "Bertha" grounding site
J.V. Barrie and H.W. Josenhans....................154
Makkovik Bank, "Anastasia" grounding site
J.V. Barrie and C.M.T. Woodworth-Lynas............157
Makkovik Bank, "Big Makk," Repetitive Mapping mosaic
H.W. Josenhans, J.V. Barrie,
C.M.T. Woodworth-Lynas and D.R. Parrott...........158

Western Makkovik Bank, shallow tracer sand site
J.V. Barrie and H. Mairs..........................163
Western Edge of Makkovik Bank (Dive 1658-9)
H.W. Josenhans and C.M.T. Woodworth-Lynas........163
Southeastern Makkovik Bank, "Gladys" grounding site
J.V. Barrie and D. Locke..........................168
Saglek Bank
J.V. Barrie, H.W. Josenhans and
C.M.T. Woodworth-Lynas............................169
South Baffin Island Shelf
C.M.T. Woodworth-Lynas and J.V. Barrie...........174
DESCRIPTION OF SIDESCAN MOSAICS
W. Carter and R.T. Gillespie......................177
Repetitive mapping mosaic.........................177
"Bertha" mosaic...................................190
"Anastasia/Deborah" mosaic........................196
"Gladys" sidescan composite.......................202
SEDIMENT TRANSPORT
J.V. Barrie.......................................205
Sediment tracer results...........................205
Predicted sediment transport......................206

CHAPTER 5

ICEBERG DYNAMICS AND SEDIMENT RESPONSE

ANALYSIS OF OBSERVED ICEBERG/SEABED INTERACTIONS
J.H. Lever and D.W. Bass..........................209
"Bertha" roll and pitting event...................214
"Gladys" split/grounding event....................224
"Gladys" post-grounding behaviour
J.H. Lever..242

"Julianna" post-grounding behaviour
J.H. Lever..244
ICEBERG DETERIORATION AND ITS INFLUENCE ON SEABED INTERACTION
J.H. Lever and D. Diemand.........................245
ICEBERG SCOUR PROCESSES...........................250
Iceberg dynamics
J.H. Lever..250
Ice keel adjustments
C.M.T. Woodworth-Lynas............................253
Seabed modifications
C.M.T. Woodworth-Lynas............................258
Regional aspects of iceberg scouring
W. Carter and H.W. Josenhans.......................272
Iceberg scour degradation
J.V. Barrie, H.W. Josenhans and
C.M.T. Woodworth-Lynas............................281

CHAPTER 6

CONCLUSIONS AND RECOMMENDATIONS
G.J. Hodgson, J.H. Lever, C.M.T. Woodworth-Lynas
C.F.M. Lewis, W. Carter, D. Diemand
J.V. Barrie, H.W. Josenhans and D.R. Parrott.....288
Strategy and Methodology..........................288
Accomplishments and Recommendations of the Repetitive Mapping Program.......................296
Advances in Understanding of Scour Processes.........298

REFERENCES

APPENDICES

1 Operations Log

2 Current Meter Locations and Specifications

3 Meteorological Conditions, August 1985 (including time series plots and histograms)

4 Wave Rider Buoy Data Summary, August 1985

5 Tides and Bottom Currents on Makkovik Bank, August 1985

6 Temperature and Salinity Profiles and Corresponding Time Series Plots for August, 1985

7 Iceberg Deterioration Observations and Temperature Measurements

8 Iceberg Dimensioning Data; Methodology and 3-D Projections of Above- and Below-Water Iceberg Shapes

9 Submersible Dive Logs

10 Measured Iceberg Scour Data From Sidescan Mosaics

LIST OF FIGURES

Page

FIGURE

1 Forces acting on an iceberg during scouring.......... 8
2 Angular motions of a scouring iceberg................ 10
3 General DIGS study area.............................. 12
4 Summary of operations................................ 15
5 Operational strategy................................. 18
6 Vessel configuration and equipment layout............ 21
7 Communication systems................................ 24
8 Navigation systems................................... 26
9 Iceberg tracking and plotting........................ 28
10 Illustration of underwater iceberg dimensioning.. 32
11 C-CORE motion sensor package........................ 38
12 Helicopter lifts a C-CORE motion sensor package...... 40
13 C-CORE motion sensor package on "Gladys"............ 41
14 Current meter tripod configuration.................. 44
15 Barrel used for deployment of pollucite 53
16 Physiography of Labrador Shelf...................... 56
17 Surficial geology of Labrador Shelf 60
18 Percent exceedence of wind speed.................... 67
19 Percent exceedence of significant wave height........ 71
20 "Anastasia" roll sequence........................... 77
21 Icebergs "Frieda" and "Gladys"...................... 85
22 Sediment on iceberg "Frieda"........................ 86
23 Sidescan sonogram across the trajectory of iceberg "Gladys".. 89
24 Iceberg "Gladys" before and after split............. 91
25 Computer generated perspectives of iceberg "Bertha", above- and below-water......................102
26 "Bertha" waterline contour..........................103

27 Surface photographs of iceberg "Bertha"..............104
28 Surface photographs of iceberg "Bertha"..............105
29 Aerial photograph of iceberg "Bertha"................106
30 Surface photographs of iceberg "Gladys" (before split)...109
31 Surface photographs of iceberg "Gladys" (before split).....................................110
32 Aerial photograph of iceberg "Gladys" (before split).....................................111
33 Surface photographs of iceberg "Gladys" (after split)...112
34 Aerial photograph of the free-floating portion of iceberg "Gladys" after split.....................113
35 Surface photographs of grounded portion of iceberg "Gladys" after split..................................114
36 Surface photographs of grounded portion of iceberg "Gladys" after split..................................115
37 Aerial photograph of grounded portion of iceberg "Gladys" after split..................................116
38 Computer generated perspectives of grounded portion of iceberg "Gladys", above- and below-water..117
39 "Gladys" waterline contour, grounded portion.........118
40 Surface photographs of iceberg "Julianna"............121
41 Surface photographs of iceberg "Julianna"............122
42 Aerial photograph of iceberg "Julianna"..............123
43 Computer generated perspectives of iceberg "Julianna", above- and below-water...................124
44 "Julianna" waterline contour.........................125
45 Surface photographs of iceberg "Lucretia"............126
46 Surface photographs of iceberg "Lucretia"............127
47 Aerial photograph of iceberg "Lucretia"..............128
48 "Lucretia" waterline contour.........................130
49 Sensor package measurement convention................132

50 Compressed time series plot, iceberg "Bertha"........133
51 "Bertha" roll/pitting event AX, TX...................135
52 "Bertha" roll/pitting event AY, TY...................136
53 "Bertha" roll/pitting event AZ, Compass..............137
54 Compressed time series plot, iceberg "Gladys", deployment D-2.......................................139
55 Compressed time series plot, iceberg "Gladys" deployment D-3.......................................140
56 "Gladys" split/roll event AX, TX.....................142
57 "Gladys" split/roll event AY, TY.....................143
58 "Gladys" split/roll event AZ, Compass................144
59 "Gladys" event #2 AX, TX.............................146
60 "Gladys" event #2 AY, TY.............................147
61 "Gladys" event #2 AZ, Compass........................148
62 Compressed time series plot, iceberg "Lucretia"......149
63 Compressed time series plot, iceberg "Julianna"......151
64 _Pisces IV_ dive locations, Makkovik Bank..............153
65 A sidescan sonogram showing the "Bertha" pits........155
66 Iceberg "Bertha" grounding site (Dive number 5)......156
67 "Big Makk" site, Repetitive Mapping area (Dive numbers 7 and 12)..............................159
68 Sidescan sonogram of "Big Makk"......................160
69 Western edge, Makkovik Bank (Dive number 9)..........164
70 Western edge, Makkovik Bank (Dive number 13).........167
71 _Pisces IV_ dive locations, Saglek Bank and southeast Baffin Island Shelf...................................170
72 Sidescan mosaic, Saglek Bank.........................171
73 Mosaic area, Saglek Bank (Dive number 15)............173
74 Iceberg "Caroline" scour, Saglek Bank (Dive number 17)...................................175
75 DTS profile of moraine on Repetitive Mapping site....180
76 Sidescan sonogram from Repetitive Mapping site.......181
77 DTS profile of scours in Qeovik Silt, Repetitive Mapping site...182

78 Sidescan sonogram of degraded iceberg scour and symmetrical ripples, Repetitive Mapping site.........184
79 Iceberg scour orientations, >120 m water depth, Repetitive Mapping site..............................186
80 Iceberg scour orientations, <120 m water depth, Repetitive Mapping site..............................187
81 Histograms of iceberg scour dimensions, Repetitive Mapping site..188
82 DTS profile illustrating geological units, iceberg "Bertha" site...............................191
83 Sidescan sonogram of scours, iceberg "Bertha" site...193
84 Iceberg scour orientations, iceberg "Bertha" site....194
85 Iceberg scour dimensions, iceberg "Bertha" site......195
86 DTS profile illustrating geological units, and iceberg scours, "Anastasia"/"Deborah" site...........197
87 Sidescan sonogram of iceberg scours and pits, "Anastasia"/"Deborah" site..........................198
88 Sidescan sonogram illustrating a partially infilled iceberg scour, "Anastasia"/"Deborah" site...........200
89 Iceberg scour orientations, "Anastasia"/"Deborah" site...201
90 Sidescan sonogram illustrating iceberg scours, iceberg "Gladys" site..............................204
91 Potential energy plot for "Bertha"..................215
92 Simulated motions of "Bertha", X-axis translation and rotation.......................................219
93 Simulated motions of "Bertha", Y-axis translation and rotation.......................................220
94 Simulated motions of "Bertha", Z-axis translation and rotation.......................................221
95 Potential energy plot for the grounded portion of "Gladys"..226
96 Schematic representation of "Gladys" split/grounding event..229

97 Simulated motions of "Gladys", X-axis translation and rotation....238
98 Simulated motions of "Gladys", Y-axis translation and rotation....239
99 Simulated motions of "Gladys", Z-axis translation and rotation....240
100 Potential energy plot for "Julianna"....246
101 Iceberg deterioration processes and their possible consequences....248
102 Thin section of ice from grounded keel of iceberg "Gladys"....255
103 The former keel of a grounded iceberg....256
104a Massive blocks on the "Caroline" scour berm....260
104b Radial fracture on berm block, "Caroline" scour....261
105a Ridge-and-groove microtopography, "Caroline" scour..263
105b Ridge-and-groove microtopography, "Big Makk" scour..264
106 Flat-topped mound, "Big Makk" scour....267
107 Fractured blocks in situ on the berm of the "Caroline" scour....269
108 Inner berm - outer berm transition, "Caroline" site..271
109 Makkovik Bank bathymetry and location of mosaics....273
110 Schematic diagram of an iceberg scour....274
111 Scour depth vs. width for the mosaic areas on Makkovik Bank....278

LIST OF TABLES

TABLE Page

1 Vessel specifications, MV *Polar Circle*............... 20
2 C-CORE motion sensor package deployments............. 42
3 Meteorological conditions............................ 47
4 Grain size distribution of pollucite................. 52
5 Correlation of geologic units........................ 59
6 Frequency of visibility observations................. 69
7 Original iceberg shape data files....................100
8 Tracer sediment analysis.............................207
9 Simulation conditions for "Bertha"...................218
10 Simulation conditions for "Gladys" 237

LIST OF CHARTS

Chart

1 Bathymetry of Makkovik Bank
2 Surficial geology of Makkovik Bank
3 Survey locations, Makkovik Bank
4 Iceberg drift tracks from radar observations, August 1985
5 Iceberg trajectories
6 Survey track plot, Repetitive Mapping site
7 Survey track plot, "Bertha" site
8 Survey track plot, "Anastasia/Deborah" site
9 Survey track plot, "Gladys" site
10 Survey track plot, "Julianna" site
11 Bathymetry, Repetitive Mapping site
12 Sidescan mosaic and representative profile, Repetitive Mapping site
13 Bathymetry, "Bertha" site
14 Sidescan mosaic and representative profile, "Bertha" site
15 Bathymetry, "Anastasia/Deborah" site
16 Sidescan mosaic and representative profile, "Anastasia/Deborah" site
17 Bathymetry, "Gladys" site
18 Sidescan composite and representative profile, "Gladys" site

ACKNOWLEDGEMENTS

A project of this complexity could only succeed with support from many sources. In this respect the DIGS Experiment and Eastern Canadian Continental Shelf Repetitive Mapping project was a fortunate recipient, having received thoughtful consideration from the outset in early 1985 during discussion of its plan at the Calgary Workshop on Ice Scour, through to early 1988 when the reviews were received and the final report compiled.

It is a pleasure to acknowledge the interest of the Ice Scour Committee of ESRF which recognized the potential of the work despite it being an undertaking of high risk. W.R. Livingstone, Chairman, who provided support throughout, was particularly effective in guiding the project quickly through the approval and initiation phases, even though new procedures had to be developed. The interest, support and patience of the ESRF administration were exemplary, as represented by director Olav Løken and by program officers, Peter Wood who inaugurated the project and David Milburn who succeeded Peter in 1986.

We are grateful to many groups and individuals who aided the project in different ways: Stu Hotzel and John Miller of Petro-Canada generously shared their iceberg experience with us; and Ice Reconnaissance Division of the Atmospheric Environment Service, Canada Department of Environment provided a timely survey of iceberg distribution on Makkovik Bank. The Department of Fisheries and Oceans contributed its manned submersible Pisces IV and tender vessel M.V. Pandora II, a tool that facilitated extraordinarily effective observations for this project. These facilities were expertly outfitted for the DIGS experiment by the

Program Support Subdivision of the Atlantic Geoscience Centre. The scientists who participated in this project from the Canada Department of Energy, Mines and Resources received financial support from the Geological Survey of Canada and the Office of Energy Research and Development. Scientists and engineers from the Centre for Cold Ocean Resources Engineering of Memorial University were supported, in part, by grants from the offshore oil and gas industry and the Canada Natural Sciences and Engineering Research Council. We acknowledge that the opportunity to complete a project of this magnitude was possible because of the positive attitudes of industry, government and academic research organizations towards the development of cooperative multidisciplinary ventures.

The groups which participated in the field activities of the project are identified in the text of the report. Here, we wish to acknowledge and emphasize the contribution of individuals who were responsible for the safe and successful management of key logistic operations on which the outcome of the experiment depended: Monty Dyke, Geonautics Ltd., who co-ordinated the offshore activities: Captain R. Hesp, master of the M.V. Polar Circle; Captain R. Burt, helicopter pilot; Captain S. Gulati, Master of the M.V. Pandora II; Frank Chambers, chief pilot of the Pisces IV submersible; Denny Christian, C-CORE, who managed the onshore facilities at Makkovik, Labrador, and Charlie Randell, C-CORE, who was responsible for the construction and upkeep of the motion packages.

Finally, we are pleased to acknowledge the improvements to the report which have resulted from the critical and constructive comments by reviewers R. Frederking (National Research Council of Canada), W.R. Livingstone (Gulf

Resources Canada) and S.D. Smith (Physical and Chemical Sciences, Canada Department of Fisheries and Oceans, Bedford Institute of Oceanography). In addition, many improvements to the manuscript were made by J.T. Buckley (ESRF) who contributed to its technical edit and by Bill Carter Geonautics Limited who patiently implemented uncounted revisions and produced this final report. Jean-Paul Nadreau, C-CORE, provided the French translation.

SUMMARY

The Dynamics of Iceberg Grounding and Scouring (DIGS) experiment was carried out concurrently with the Repetitive Mapping of the Eastern Canadian Continental Shelf surveys and a submersible program on Makkovik Bank, Labrador, in August 1985. In addition, data were collected for the wave-induced iceberg motion (WIIM) study, the results of which have been compiled in a separate report (Lever and Diemand, 1988).

DIGS focused on the dynamics and effects of four iceberg groundings identified and subsequently selected from about 100 iceberg incursions onto Makkovik Bank during the study period.

A primary objective of DIGS was to determine the iceberg forces on the seabed during scouring events and to document the response of the seabed to these forces. The possible constraining effects of seabed contact on iceberg drift trajectories and how this contact may hydrodynamically induce sediment redistribution was to be investigated also. Finally, the DIGS program was to evaluate the dynamics of seafloor sediment and to infer the long-term degradation of iceberg scours due to sedimentary and biologic processes. To fulfil the aims of the repetitive mapping program, a series of sites were surveyed and mosaiced and the distribution and dimensions of iceberg scours accurately defined to serve as a basis for the establishment of a repetitive mapping network.

The combined DIGS-Repetitive Mapping field program resulted in the collection of a unique data set which has contributed greatly to understanding the processes acting upon free-floating and grounded icebergs and to the seabed features produced under different grounding scenarios.

Iceberg motion data acquired through the placement of motion sensor packages on five icebergs allowed for good quality computer modelling of iceberg dynamics. This capability has enhanced confidence in the understanding of the forces acting upon an iceberg during scouring.

Seabed impact from the rolling of an unstable iceberg had been suspected but was never documented prior to this field program. The DIGS experiment suggests that splitting and subsequent rolling of icebergs is likely a common occurrence and may be a primary cause of seabed pits. The data show clearly that during the scouring process not only is seabed sediment modified by iceberg keels but also that the keel ice is itself modified.

Iceberg scour analyses were carried out at four sidescan mosaic locations that were established to fulfil the requirements of the Repetitive Mapping program. In-depth geologic interpretations were prepared for these sites and the resultant data used as a basis to compare variations in scour dimensions under different geographic, bathymetric and geologic conditions.

Observations from submersible revealed the existence within scour troughs of "ridge and groove" microtopographic features which had previously been observed only once before (from a seabed photograph, pers. comm. H.J. Josenhans, 1988) on the eastern Canadian continental shelf. These features are believed to be directly related to the morphology of the trailing edge of the scouring keel and may indicate the direction of iceberg movement. A series of flat-topped mounds observed in the trough of one scour is believed to be the first observation of deposition of reworked sediment beneath a scouring keel. Also, the observation of apparently extruded material in a scour berm may indicate lateral movement of cohesive sediment from beneath the scouring keel.

An understanding of the processes affecting iceberg scour degradation is very important in the calculation of scour obliteration rates under different geologic and hydrodynamic conditions. Information acquired through the DIGS experiment suggests that degradation begins during the actual scouring process with localized redistribution of cohesive sediment followed by slumping and fracturing. Post-scouring degradation, attributed to the bioturbation effects of benthic organisms, current erosion, and the migration of sediment into the scour may erode microfeatures over a few years. However, large scale features, such as boulder-armoured berms, may endure for several hundreds of years.

The DIGS experiment was one of the most ambitious iceberg research experiments ever undertaken. Because of the nature of the project it was recognized during the planning stage that there existed a relatively high potential for failure. In fact some setbacks in data acquisition were realized, yet the program was extremely successful in advancing knowledge of iceberg dynamics and iceberg scour. The acquired data set not only met most of the requirements of the original DIGS and Repetitive Mapping experimental designs but will provide a solid base for future research work in several disciplines.

RÉSUMÉ

Le programme DIGS (Dynamics of Iceberg Grounding and Scouring) décrit dans le présent rapport a été réalisé parallèlement à d'autres activités, notamment des travaux de cartographie répétitive de la plate-forme continentale de l'est du Canada et une étude informatique sur les caractéristiques sous-marines du banc Makkovik, dans le Labrador, en août 1985. En outre, des données ont été recueillies sur le mouvement des icebergs causé par les vagues (l'étude WIIM, Wave-Induced Ice Motion Study). Les résultats de cette étude sont présentés dans un rapport distinct (Lever and Diemand, 1988).

Le programme DIGS portait principalement sur la dynamique et les effets de quatre icebergs échoués au banc Makkovik choisis parmi les quelque 100 icebergs observés dans cette région pendant l'étude.

L'un des objectifs principaux du programme DIGS consistait à déterminer la force exercée par l'iceberg sur le fond marin pendant l'affouillement et à décrire la réaction du fond marin. On a également étudié les effets de contrainte éventuels occasionnés par le contact du fond marin aux trajectoires de dérive des icebergs, et tenté de voir comment ce contact pouvait provoquer la redistribution des sédiments de façon hydrodynamique. Enfin, le programme DIGS visait à évaluer la dynamique des sédiments du fond marin et à tirer des conclusions quant à la dégradation à long terme des affouillements par les icebergs causée par la sédimentation et par certains facteurs biologiques.

Pour satisfaire aux objectifs du programme de cartographie répétitive, des levés ont été effectués à plusieurs emplacements et on servi à composer des mosaiques. En outre, des données sur la distribution et la dimension des affouillements par les icebergs ont été définies aussi exactement que possible et serviront à établir un réseau de cartographie répétitive.

Les travaux sur le chantier réalisés dans le cadre du programme DIGS et du programme de cartographie répétitive ont mené à l'acquisition de données uniques qui nous permettront de

mieux comprendre les processus qui interviennent lors de l'interaction entre les icebergs flottants ou échoués et le fond marin, selon les différents aspects des traces d'affouillement laissées par les icebergs.

Les données sur le mouvement des icebergs recueillies au moyen des dispositifs de détection des mouvements apposés sur cinq icebergs, ont permis de modéliser la dynamique des icebergs. Ces données amélioreront nos connaissances sur les forces qui agissent sur un iceberg pendant l'affouillement.

On se doutait depuis un certain temps déjà qu'un iceberg instable en mouvement influait considérablement sur le fond marin, un phénomène qui n'avait cependant jamais été étudié. Or, les résultats du programme DIGS montrent que la fission et le labourage subséquent des icebergs est un phénomène assez fréquent qui constitue l'une des causes principales des trous sur le fond marin. Les données indiquent clairement qu'au cours de l'affouillement, non seulement les sédiments du fond marin sont modifiés par la quille de glace, mais la glace est elle-même modifiée par l'abrasion.

Des analyses de l'affouillement par les icebergs ont été effectués à quatre emplacements où des balayages latéraux ont été effectués et composés en mosaiques, en réponse aux exigences du programme de cartographie répétitive. Des interprétations géologiques approfondies ont été préparées pour chacun de ces emplacements, et les données obtenues constituent la base d'une étude comparative de la dimension des traces d'affouillement selon les différentes conditions géographiques, bathymétriques et géologiques.

Les observations faites à partir du submersible ont mis au jour l'existence, à l'intérieur des dépressions causées par l'affouillement, de crêtes et de rainures microtopographiques qui avaient été observées une seule fois auparavant (sur une photographie du fond marin, remarques personnelles H.J. Josenhans, 1988), sur le talus continental de l'est du Canada. On estime que ces traits marquant sont directement liés à la morphologie du bord de la fuite de la quille de glace et constituent un indice quant à la direction du mouvement de l'iceberg. Par ailleurs, on croit avoir observé une série de monticules applatis à la surface à l'intérieur de la dépression d'une trace d'affouillement. Ce serait la première fois qu'on o observe des dépôts de sédiments remaniés par l'affouillement d'une quille de glace. En outre, on a observé, dans une berme de la trace d'affouillement, du matériel qui aurait été expulsé, ce qui indique que les sédiments en cohésion effectuent un mouvement latéral sous la quille de glace.

Il est très important de comprendre les processus qui interviennent dans la dégradation des traces d'affouillement des icebergs pour calculer la vitesse d'effacement des traces selon différentes conditions géologiques et hydrodynamiques. L'information acquise grâce au programme DIGS suggère que la dégradation commence dès l'affouillement, avec une certaine redistribution des sédiments en cohésion, puis la rupture et de l'affaissement des bermes. Ensuite, la dégradation s'explique par la bioturbation des organismes benthiques, l'érosion causée par les courants et la migration des sédiments à l'intérieur des traces d'affouillement, ce qui peut provoquer l'érosion des micro-éléments au fil du temps. Cependant, les traits importants, par exemple les bermes de roches, peuvent durer plusieurs centaines d'années.

Le programme DIGS constitue l'une des recherche sur les icebergs les plus ambitieuses jamais entreprise. Vu la nature du programme, on a reconnu, au stade de la planification, que les risques d'échec étaient assez considérables. En fait, malgré certains contretemps dans l'acquisition de données, il n'en reste pas moins que le programme a clairement été un succès. Les données acquises ont non seulement respectées la plupart des exigences du programme DIGS et du programme de cartographie répétitive, mais elles fourniront une base solide pour les recherches futures dans plusieurs domaines connexes.

INTRODUCTION

Interactions between icebergs and the seabed may place seabed structures, such as pipelines and wellheads, at risk. The potential need for, and design of, protective measures raise engineering questions concerning, for example, the level of risk, forces on the seabed, probable depth of ice scour, stresses on buried structures, or the chance of ice scouring in protective glory holes (seafloor excavations). To interpret and calculate the results of such interactions requires an understanding of ice scouring processes. However, observations of ice in contact with the seabed are difficult to obtain and are rare. The dynamic response of large ice features interacting with the seabed has never been measured. Consequently, existing models of ice scour have been based largely on intuition and supported by the results of physical modelling.

The question of protection from iceberg scour applies principally to the northeastern continental margin of Canada where hydrocarbons have been discovered beneath continental shelves which are subject to iceberg incursion and seabed scour. On average about 3000 icebergs drift annually into the Labrador Shelf area from Baffin Bay, of which perhaps 400 (Anderson 1971; Ebbesmeyer et al. 1980) penetrate waters of the northern Grand Banks of Newfoundland where oil production is being considered. On the banks of the Labrador Shelf, about 5 to 6% of these icebergs ground in water depths down to about 200 m (El-Tahan et al. 1985; Woodworth-Lynas et al. 1985), and on the northern margin of the Grand Banks, annual scouring rates in the order of 0.1 to 1 scour/100 km^2 have been estimated for a similar range of water depths (Lewis et al. 1987).

Two related projects were conducted to address the issues of 1) understanding the mechanics of iceberg scour, and 2) determining the risk of iceberg contact with the seabed. The Dynamics of Iceberg Grounding and Scouring (DIGS) experiment addressed the first issue through field studies which focused on iceberg dynamics and seabed observations of fresh (recently formed) iceberg scour marks. The Eastern Canadian Continental Shelf Repetitive Mapping project addresses the second issue and consists of sidescan sonar and seismic mapping of the seabed in preparation for comparison with future surveys to detect the incidence of new scours. Since the operations and data requirements of the two projects were complementary, both were implemented in a fully integrated field program. The data are also complementary to the objectives of both projects and, hence, are integrated into the structure of this combined report.

DYNAMICS OF ICEBERG GROUNDING AND SCOURING (DIGS) EXPERIMENT

Concepts for the mechanics of iceberg scouring were first considered by Chari and Allen (1972), Chari (1979) and Chari et al. (1980). Of the many dynamic scenarios which they recognized to be possible for iceberg-seabed interaction, they developed one for deformable sediments which should yield the "maximum likely scour depth", from which the safe burial depth for bottom structures could be designed. In this scenario soil (sediment) failure was the critical criterion; the seabed was thought to have a low shear strength while the iceberg was relatively strong. Iceberg motion was envisaged with one degree of freedom, with the iceberg moving horizontally, without tilt or uplift, into a seabed slope. The scouring process was modelled as a ploughing phenomenon in which the sediment in front of the iceberg keel was heaved up in a series of passive failure surfaces and displaced to the sides as the iceberg moved progressively forward. When the kinetic energy of the iceberg was dissipated and the current and wind drag forces acting upon it fully resisted, the iceberg became grounded. In general, the resulting scour resembled a long trench or furrow of gradually increasing depth with berms on both sides.

Similar work-energy balance models were constructed for bulldozing of sediments by keels of sea ice ridges in the Beaufort Sea by Kovacs and Mellor (1974) and by FENCO Consultants Ltd. (1975) and Kivisild (1981). The FENCO study also developed a dynamic model with three degrees of freedom by solving the basic equations of motion for a body being driven into a sloping seabed. Further refinements of the basic Chari model were added to account for hydrodynamic drag of currents (Chari et al. 1980; Lopez 1981), type of seabed sediments (Chari and Green 1981; Chari and Peters 1981), forces transmitted into the sediment beneath the passing ice keel (Green and Chari 1981; Green et al. 1983), and seabed scour following iceberg roll (Prasad and Chari 1985).

Since no uplift or rotation of the iceberg was considered, the seabed furrow of "maximum likely depth" predicted by the Chari model was of finite length and its depth increased progressively from beginning to end. For the conditions existing on the Labrador Shelf, the maximum predicted scour depths varied between 1.8 and 15 m and the maximum scour lengths ranged between 0.43 and 14.5 km, more or less in agreement with the available scour statistics (Chari 1979). At that time, only furrow-type iceberg scours of 30 m average width were recognized (Harris 1974; Harris and Jollymore 1974; van der Linden et al. 1976), and these ranged in depth up to 10 m in extreme cases with maximum lengths of 3 km where scour lengths could be discerned. Thus, the theoretical values were accepted in that they were in the range of reported field data.

Offshore research in the 1980s, using sidescan sonar, high resolution seismic profiling and direct observation with submersibles, began to reveal a wide variety of scour shapes and settings, which suggested that other modes of iceberg motion, as originally thought possible by Chari (1979) and Chari et al. (1980), were at work during the formation of iceberg scours. Early assessments of the character, setting and distribution of iceberg scours from seabed acoustic mapping and profiling data (Barrie 1980; Lewis et al. 1980; d'Apollonia and Lewis 1981; Fader and King 1981; and Lewis and Barrie 1981), coupled with the first seabed observations of iceberg scours from manned submersibles (Josenhans and Barrie 1982; Lewis et al. 1982; Maclean 1982; Syvitski et al. 1983; Collins and Diemand 1983; Lewis and Fader 1985) showed that very long scours exist, probably in excess of 14 km; some scours traverse up and down slope with elevation changes of several metres; many scours are much wider than they are deep and often are flat-bottomed, and that short circular to elliptical scours, termed pits or craters, are present. Some pits were found to be anomalously deeper than furrows on the Grand Banks of Newfoundland (Barrie et al. 1986).

Recently, more detailed analysis of sidescan sonar data (Woodworth-Lynas et al. 1986; Todd 1986) and inferences of grounding dynamics from drill-rig radar surveillance of iceberg trajectories (Woodworth-Lynas et al. 1985) demonstrated several examples of upslope and downslope scours traversing 15 m (vertical) with an extreme inference of 45 m. Scouring events over 200 km long were inferred. These observations clearly suggest that during many interactions with the seabed, icebergs must rotate and tilt, changing their draft to adjust to variations in bathymetry and to maintain contact with the seabed over long distances.

The offshore observations also revealed, as expected, that the scour morphology, particularly the side slopes of scour berms, varied with the sedimentary substrate; steeper slopes being developed in stiff clay or boulder-rich substrates and shallower slopes being more typical of sandy environments. Variations in degradation of scoured surfaces have been recognized in three major sedimentary environments - stiff clay, bouldery till and sand (Barrie 1983). For example, in bouldery clay till, bioturbation by benthic fauna (sediment mixing and disaggregation) and winnowing by bottom currents (erosion and transport of fine-grained sediment fractions) had given rise to deflated gravelly to bouldery surfaces on scour berms and patches of mobile sand in scour troughs and on the adjacent seafloor. Thus, it was inferred that scours degraded, changing their appearance and morphology (e.g., relief) with the passage of time. Moreover, sand resting in relict scours excavated in studies on shore, suggested that trenches may be rapidly backfilled by resedimentation immediately following the passage of currents flowing past a scouring iceberg keel (Woodworth-Lynas et al. 1986).

Clearly, the growing body of field evidence was suggesting that a number of factors, particularly variations in iceberg motion and sediment type, would be required to account for the variety of features developed on the seabed in response to iceberg contact. It was timely, therefore, to advance the understanding of ice scouring processes by observing the action of icebergs in the ocean, and, if suitable observations could be made, to develop case histories and dynamic models to explain the observed seabed features of iceberg scouring.

Objectives

The DIGS experiment examined the seabed effects of iceberg scouring at selected localities on the Labrador Shelf and focused on the dynamic behaviour and effects of four natural iceberg groundings identified from about 100 iceberg incursions onto Makkovik Bank during three weeks in August 1985. In addition to the work on Makkovik Bank, the submersible, Pisces IV, was used to investigate a fresh scour feature on Saglek Bank 400 km to the northwest of Makkovik Bank. Although this work was not done as part of the DIGS experiment, the results of it are presented in this report because of the relevance of the observations to DIGS. The specific objectives were:

- to determine iceberg forces on the seabed,
- to document the response of the seabed to iceberg forces during scouring events,
- to investigate the possible constraining effects of seabed contact on iceberg drift trajectories during long scouring (i.e., furrow making) events,
- to verify the possible occurrence of hydrodynamically-induced sediment redistribution during scouring events,
- to evaluate the dynamics (mobility as a result of current shear) of seafloor sediment and to infer the long term degradation of iceberg scours because of sedimentary and biologic processes.

Strategy and methods used for the DIGS experiment

One method to estimate the horizontal force exerted on the seabed by a scouring iceberg was proposed by Banke and Smith (1984). The winds and currents measured in the vicinity of a scouring iceberg were used to compute the drift trajectory. The difference between this computed open water trajectory and the observed trajectory was attributed to the seabed force. While straightforward, this method has several drawbacks. Firstly, it yields no information on the vertical seabed force. Secondly, because of the difficulties in the determination of the current and wind forces acting on the iceberg, large uncertainties could be transmitted to the estimation of the seabed force.

It was decided that the general case of iceberg-seabed interaction should be examined, where the iceberg is free to respond in all six rigid body degrees-of-freedom. The rotational behaviour of a scouring iceberg, in particular, should be governed primarily by the seabed force. Hence, the uncertainties arising from the other environmental loads would be less significant in the analysis (Lever 1986).

The forces acting on a scouring iceberg are summarized in Figure 1. These include wind drag, water drag, gravity, Coriolis force and the buoyancy force shown offset from the centre of gravity (CG). The seabed force can be resolved into vertical and horizontal components. The drag forces depend on the shape of the iceberg and increase as the square of the velocity of the iceberg relative to the wind or water. The Coriolis force is related to the mass multiplied by the Coriolis parameter, which is a function of the earth's rotation, latitude, and the relative velocity of the body in water. The buoyancy force will be approximately equal to the weight of the displaced water if the vertical

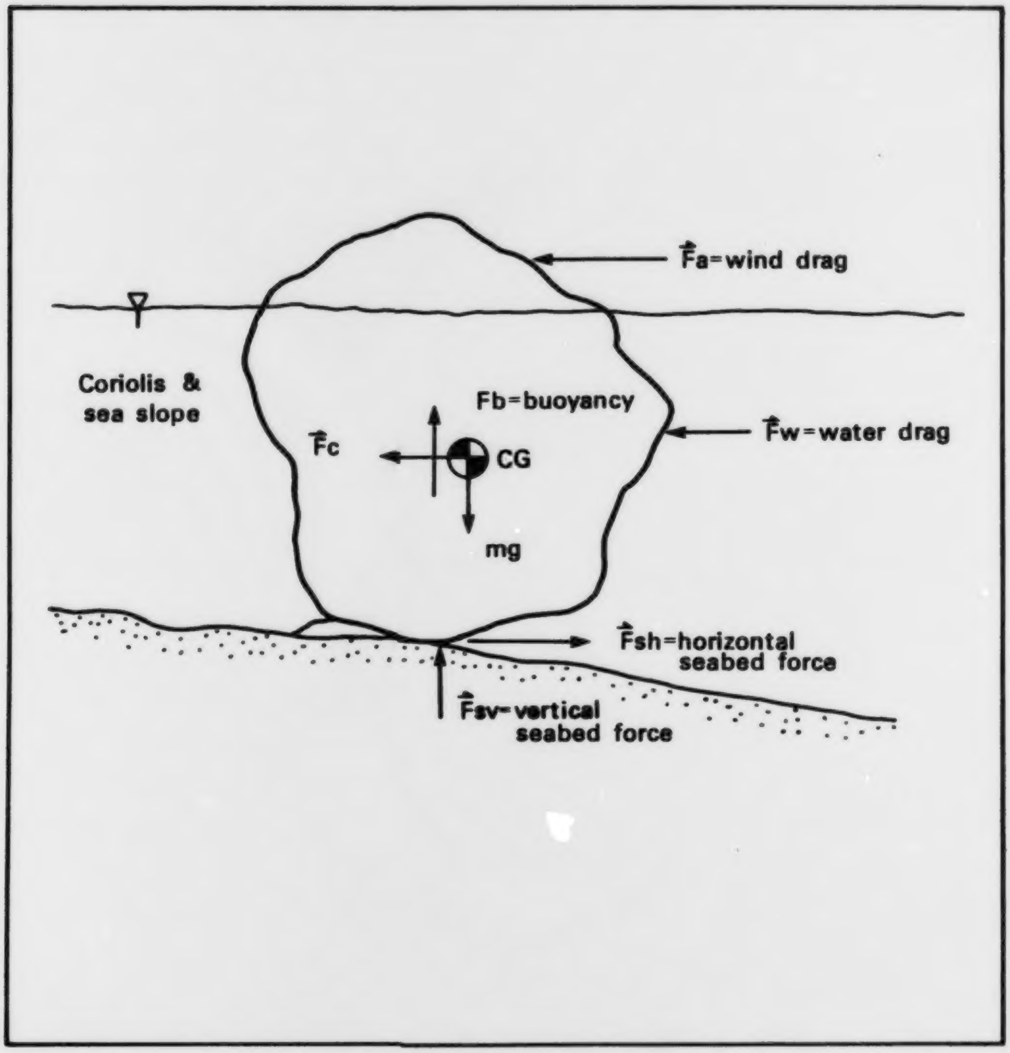

$\vec{F}a$=wind drag
Coriolis & sea slope
Fb=buoyancy
$\vec{F}w$=water drag
$\vec{F}c$
CG
mg
$\vec{F}sh$=horizontal seabed force
$\vec{F}sv$=vertical seabed force

Figure 1. Forces acting on an iceberg during scouring (from Lever 1986).

component of the seabed force is small compared with the total weight of the iceberg. The gravity and buoyancy forces can be easily estimated if good information about the shape of the iceberg is available. Shape information is also needed to estimate the wind and water drag forces (Lever 1986).

In the general scouring case, the contact of the seabed with the iceberg will not be directly below its CG. Also, the two environmental forces, wind drag and water drag, will not necessarily be coincident with the CG. While the rotations of the iceberg (pitch, roll, yaw) are thought to be small when it is driven by the environmental forces only (Lever 1986), the rotations induced by seabed contact may be significant.

As a free-floating iceberg contacts the seabed, a force imbalance occurs with the introduction of the seabed force. As a result, angular rotations are induced in the horizontal (yaw) and/or vertical (roll) planes (Figure 2). The environmental forces will not necessarily be negligible, but their effects will be reasonably constant until the pitch and yaw angles increase significantly. That is, the wind and current forces will not significantly affect the initial angular acceleration rates; here the seabed force predominates. Thus, the angular accelerations of an iceberg during its initial contact with the seabed provide good information regarding the interaction forces.

Once equilibrium is reached, the buoyancy force acting upward through the metacentre (M), counterbalances the seabed force. This shift in the buoyancy force is a function of the angle of rotation and the stability of the iceberg. If the iceberg is very stable, then the angle is small, and the seabed force is quickly counterbalanced by

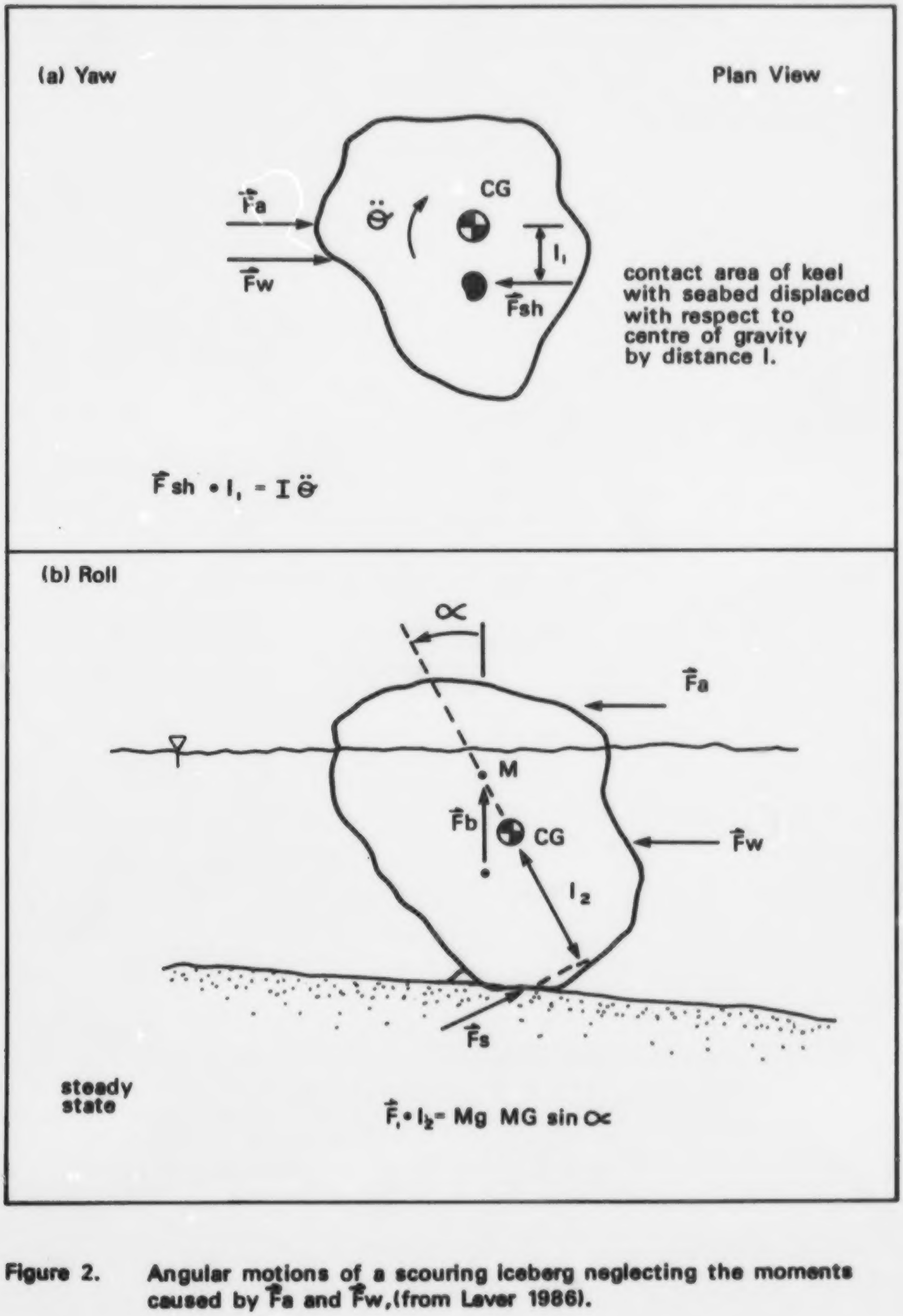
(a) Yaw
Plan View
$\vec{F}a$
$\vec{F}w$
$\ddot{\theta}$
CG
l_1
$\vec{F}sh$
contact area of keel with seabed displaced with respect to centre of gravity by distance l.
$\vec{F}sh \cdot l_1 = I\ddot{\theta}$
(b) Roll
$\propto$
$\vec{F}a$
M
$\vec{F}b$
CG
$\vec{F}w$
l_2
$\vec{F}s$
steady state
$\vec{F}_1 \cdot l_2 = Mg\ MG \sin\propto$

Figure 2. Angular motions of a scouring iceberg neglecting the moments caused by $\vec{F}a$ and $\vec{F}w$,(from Lever 1986).

the shift in buoyancy force. If the iceberg is not very stable, then a large rolling effect will be generated by the same seabed force. The seabed force can be calculated from the steady-state roll and the stability characteristics provided good shape information and the motion of the iceberg in six degrees of freedom are obtained. As is the case for rotational acceleration, the seabed force predominates over the other environmental forces in the determination of the steady-state roll angle. Only if the iceberg is very stable about all axes will roll not occur during scouring; then the seabed force is determined from the iceberg's linear deceleration. Thus it is possible to reconstruct the seabed forces acting on a scouring iceberg provided its shape is known and its motions are monitored in six degrees-of-freedom, and the environmental forces acting on it are estimated. By focusing attention on the iceberg's rotational behavior, the computed seabed forces should not be sensitive to uncertainties in the other environmental forces (Lever 1986).

The DIGS experiment was conducted from the observation vessel M.V. Polar Circle, in an area of the Labrador Shelf between latitudes 55° and 56° N (Figure 3). Iceberg drift trajectories were monitored by ship's radar and potential grounding candidates were identified on the basis of their size and trajectory with relation to the surrounding bathymetry. Once an iceberg was targeted for grounding, its shape was measured, its motions were recorded, and the wind and current around it were monitored. Where possible, the seabed was mapped with geophysical surveys before and after a grounding event and follow-up observations of the seabed were made with the manned submersible Pisces IV, operated from M.V. Pandora II. Additional submersible observations

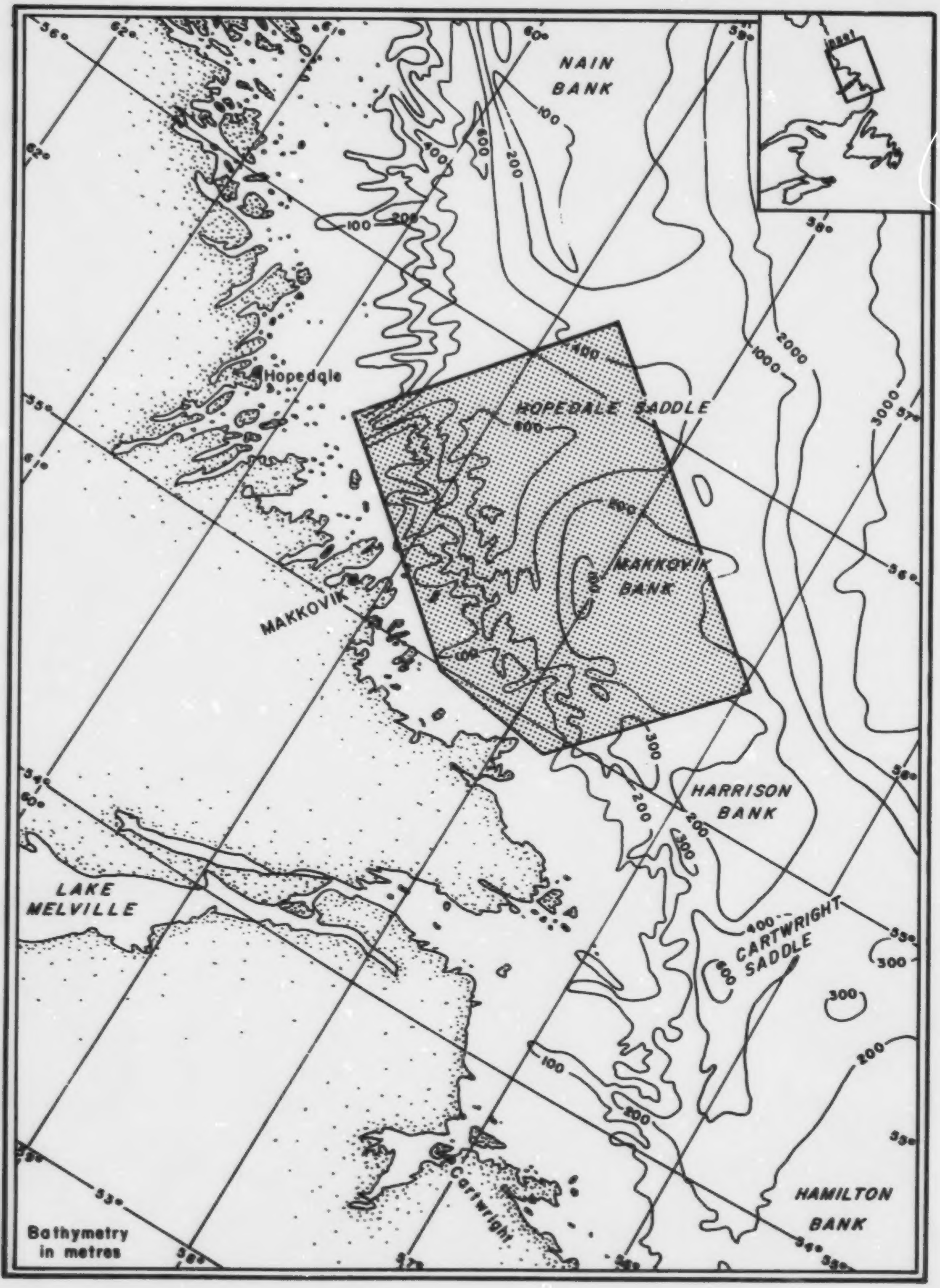
NAIN BANK
HOPEDALE SADDLE
MAKKOVIK BANK
Hopedale
MAKKOVIK
HARRISON BANK
LAKE MELVILLE
CARTWRIGHT SADDLE
HAMILTON BANK
Cartwright
inset
Bathymetry in metres
100
200
300
400
600
1000
2000
3000
56°
55°
54°
53°
62°
61°
60°
59°
58°
57°

Figure 3. Regional chart of Labrador Shelf indicating the area of activity during the DIGS experiment.

which led to critical inferences concerning the processes of ice scour formation were obtained from other recently formed ice scours, detected by the Repetitive Mapping operations. At the outset of the experiment, icebergs which were already aground were selected for instrumentation and measurement to ensure acquisition of data for icebergs in contact with the seabed. Two sites were also selected for monitoring of sediment transport by deployment of non-radioactive tracer material and moored oceanographic equipment. Geotechnical investigation of the ice-disturbed seabed was not attempted in this project, but remains a highly desirable follow-up study.

REPETITIVE MAPPING OF THE EASTERN CANADIAN CONTINENTAL SHELF

The methodology of repetitive mapping to determine the rate of incidence of ice scours is well known and widely applied in the Beaufort Sea for the detection of sea ice scours (Shearer et al. 1986). A mapping network has been designed for similar studies off the east coast of Canada by Geonautics Limited (1987). The Geonautics study proposes the establishment of control corridors for repetitive mapping on the Grand Banks of Newfoundland and on Hamilton and Makkovik Banks of the Labrador Shelf. The control corridors are to be mapped with a mosaic comprising at least four lines of high-resolution, short-range, sidescan sonar imagery to ensure recognition of large and small scour features and to circumvent all potential problems arising from navigational uncertainty. In the present project, the control mosaic for Makkovik Bank was completed. In addition, at least two other mosaics, completed for the DIGS experiment, will also serve as high-quality control areas for future repetitive mapping.

CHAPTER 1

METHODS AND OPERATIONS

OPERATIONS OVERVIEW

Operational setting

Field operations were conducted in an area of the Labrador Shelf between latitudes 55° to 56° N (Figure 3). The DIGS experiment included iceberg tracking and dimensioning in the area north of Makkovik Bank with the main data collection taking place on the Bank. Repetitive sea bed mapping networks were established in various areas of Makkovik Bank whereas the WIIM study (Lever and Diemand 1988) was concentrated in the nearshore area around Makkovik.

Operations in the Makkovik Bank area were conducted primarily from the observation vessel M.V. Polar Circle. These operations included meteorologic and oceanographic data collection, iceberg tracking and dimensioning, remotely operated vehicle (ROV) video and towed camera (BRUTIV) transects along with geophysical profiling. The M.V. Polar Circle was supported by a helicopter for aerial photography, iceberg reconnaissance, and transport, and by the longliner vessel M.V. Amanda J. A shore base was established in Makkovik to provide accommodation for the crew and support personnel of the helicopter and the longliner, and as well acting as a centralized communication base. The observation vessel was positioned using Sercel Syledis land-based stations with secondary position data contributed by satellite and Loran-C. The bar graph (Figure 4) illustrates

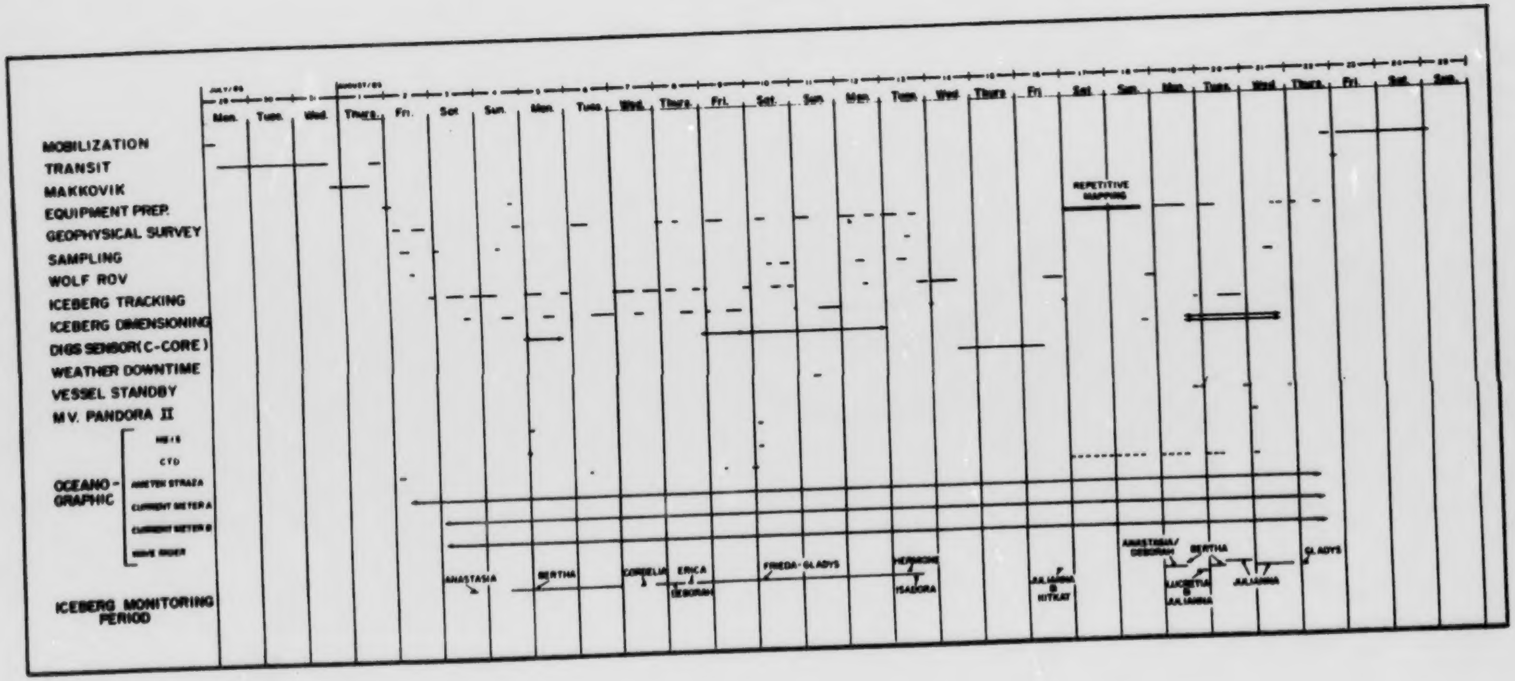

Figure 4. Summary of operations.

the sequence of events and use of equipment during the field program. Additional information on the major systems and facilities is presented later in the report.

Mobilization of the M.V. Polar Circle commenced on July 23, 1985, with the vessel departing St. John's early on July 29. Upon arrival in Makkovik on July 31, the shore-base personnel and equipment, including the navigation stations, were transferred ashore. The helicopter departed St. John's on July 31, following installation and calibration of the aerial photograpic equipment and arrived at the shore base that evening. The M.V. Amanda J arrived in Makkovik on August 1.

The experimental program on Makkovik Bank commenced on August 1 and continued until August 22 when the M.V. Polar Circle departed the survey area. Visual observations and video coverage of the sea bed were conducted from the Pisces IV submersible supplied by Atlantic Geoscience Centre. These operations were carried out between August 19 to August 22 from the M.V. Pandora II.

Following a brief port call in Makkovik to transfer the shore-based equipment, the M.V. Polar Circle returned to St. John's arriving on August 25. Demobilization of the vessel was completed on August 26 and all systems were returned to their points of origin.

A more detailed account of the operational sequence is provided in the next section and in Appendix 1. Summaries of the data collection are presented later in the text.

Operational Strategy

Owing to the complexity of the combined DIGS experiment and Repetitive Mapping of the eastern Canadian continental shelf, and the number of individual tasks required to satisfy the program objectives, an operational strategy was formulated as summarized in Figure 5.

Upon arrival on Makkovik Bank, sites were assessed and selected for deployment of tracer sediments and moored oceanographic equipment. Throughout this time iceberg drift patterns were being monitored using the methods described in the next chapter. Potential grounding candidates were selected on the basis of their size and trajectory with respect to local bathymetry. Draft measurements and water-line stereo photography were performed on icebergs of most interest and the candidates given a code name.

Initially, a grounded iceberg was chosen for documentation to observe its dynamic behaviour while aground and to assess and refine documentation techniques to establish a realistic time frame required to fully investigate a grounding event. Having established this, a free-drifting iceberg, selected as a potential grounding candidate, was observed and the documentation process repeated. When possible, attempts were made to run pre- and post-grounding geophysical surveys to acquire evidence of iceberg-seabed interaction. A remotely operated vehicle (ROV) was intended as a means of observing the actual iceberg-seabed interaction, and the Pisces IV submersible was available for follow-up visual observation of scour features.

A detailed account of all activities carried out during the study is included in Appendix 1.

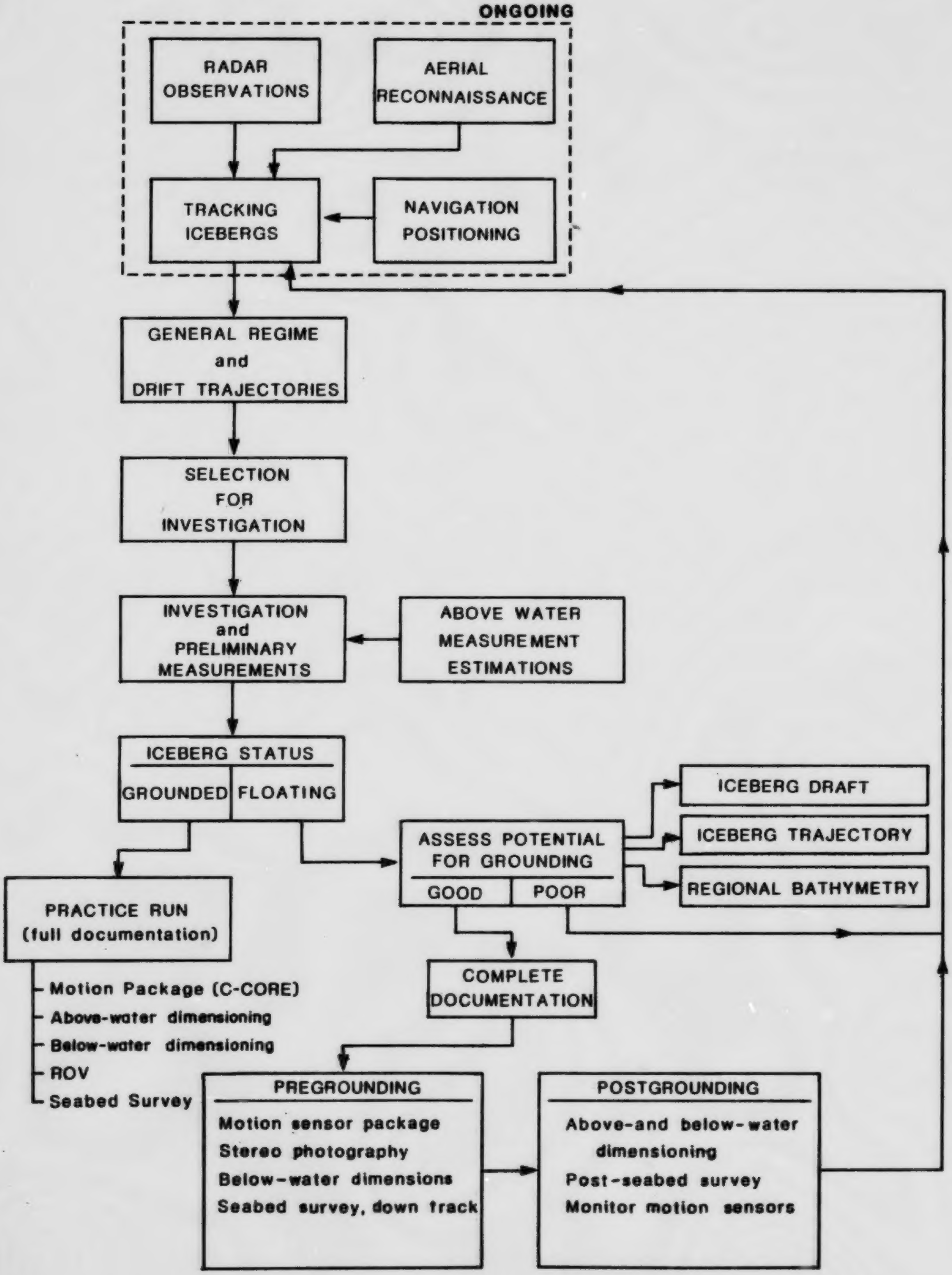
ONGOING
RADAR OBSERVATIONS
AERIAL RECONNAISSANCE
TRACKING ICEBERGS
NAVIGATION POSITIONING
GENERAL REGIME and DRIFT TRAJECTORIES
SELECTION FOR INVESTIGATION
INVESTIGATION and PRELIMINARY MEASUREMENTS
ABOVE WATER MEASUREMENT ESTIMATIONS
ICEBERG STATUS
GROUNDED
FLOATING
ASSESS POTENTIAL FOR GROUNDING
GOOD
POOR
ICEBERG DRAFT
ICEBERG TRAJECTORY
REGIONAL BATHYMETRY
PRACTICE RUN (full documentation)
Motion Package (C-CORE)
Above-water dimensioning
Below-water dimensioning
ROV
Seabed Survey
COMPLETE DOCUMENTATION
PREGROUNDING
Motion sensor package
Stereo photography
Below-water dimensions
Seabed survey, down track
POSTGROUNDING
Above-and below-water dimensioning
Post-seabed survey
Monitor motion sensors

Figure 5. **Operational strategy**

Field Systems and Facilities

The following is a description of the major survey and support equipment and facilities used during the DIGS experiment.

The main observation and survey vessel employed for the DIGS experiment was the M.V. Polar Circle. The Polar Circle is a DNV Class 1A1 icebreaker/sealer and was chartered from Carino Co., St. John's, Newfoundland. Vessel specifications are given in Table 1. Figure 6 shows the general layout of scientific equipment aboard the vessel during the study program.

For the DIGS experiment, a 12 m trailer was installed in the sheltered main deck cargo hold as an instrument laboratory. With the exception of the Wolf Sub-Ocean ROV control cabin, all of the major navigation and scientific recording equipment were placed in this facility.

Towed sensors such as the Huntec DeepTow Seismic (DTS) system, Klein sidescan sonar and BRUTIV camera sled were deployed from the after deck. The Ametek Straza Doppler Current Profiler was mounted on an outrigger off the port side. The Atlas-Deso 20 echo sounder and Hydrostar acoustic positioning transducers were mounted on a vertical boom on the starboard side (Figure 6).

Acoustic measurements of below-water iceberg dimensions, Neil Brown Direct Reading Current Meter (DRCM) measurements and Guildline Current-Temperature-Depth (CTD) profiles were all performed from a davit mounted on the port bow of the vessel.

TABLE 1

VESSEL SPECIFICATIONS

M.V. POLAR CIRCLE

GENERAL

Designed for scientific and/or transport expedition in arctic and antarctic areas. Class: DnV + IAI - icebreaker - sealer. Norwegian Shipcontrol for unrestricted trade. International load line. Built 1976.

MAIN DIMENSIONS

Length overall	49,615 m
Length between p.p.	42,350 m
Breadth moulded	11,500 m
Depth moulded main deck	4,830 m
Depth moulded shelterdeck	8,630 m
Draught summer mean	4,793 m

CAPACITIES

Fuel oil	370 m^3
Water ballast	17 m^3
Stabilizing tank	33 m^3
Fresh Water	114 m^3
Fresh water generating capacity	5 tons/24 h
Helicopter fuel	25 m^3
Lube Oil	7,73 m^3
Facilities for supply of fuel oil and water	
Lower hold bale	350 m^3
Upper hold bale	1,105 m^3
Deadweight	590 tons
Gross tonnage	495,71 tons
Net tonnage	148,14 tons

NORMAL SPEED

13 Knots

CONSUMPTION

Fuel Oil: 7,5 tons/24 hours
Lube oil: max 40 litres/24 hours

MANOEUVRING

Completecontrol stands in wheelhouse and crows nest

RIGGING

15 Meter 25 tons SWL derrick. Cargowinch, toppingwinch, slewingwinches and windlass of make Hydraulik, Brattvag. Helicopter deck and helicopter fuel tank with necessary pumps all approved by Norwegian authorities. One side door each side maindeck 2,5 X 1,7 m. Sterngate 4 X 3,8 m - axial load 8,5 tons. Part of helicopter deck can be moved forward on wheels to come within reach of derrick. De-icing system on necessary places.

ACCOMODATION

12 double cabins, 1 four berth cabin, 5 single cabins. 1 hospital (2 berths). Total 33 crew/officers/expedition members. Total crew from 11 - 12, rest of accomodation for charterers disposal. Accomodations fully airconditioned. Life-saving equipment for 40 persons.

MACHINERY

MaK main engine type 9M452AK 2.495 IHP directly coupled to Liaaen c.p. propeller with propeller nozzle. 2 of Deutz auxiliaries type BF 6 M 716each running a Stamford AC-generator 175 Kva, 440 v, 60 Hz transformed to 220 v for lighting etc.

ELECTRONIC AND NAVIGATION EQUIPMENT

Gyro compass with autopilot, make Anschutz. Direction finder. Taiyo type TDAI 30 - 8M. Echo sounder, Simrad type EN.
2 of Decca radars 3 cm type RM 1216 and RM 916.
Loran, Simrad Loran C.
Radio station, Skanti type TRP 5000.
VHF, SRA type ME 30.
El.magnetic log, Sagem LH.
Anemometer and Wind wane, Walker XMSI and XMDI.
Automatic telephone, Siemens (to all cabins and dayrooms).
Soundpowered telephone, Phonico type P - 2015 Hailer, Phonico type PFK - 5.
Helicopter homing beacon, Nera RS - 110.
Aero VHF, Becker type GS 2010.

SUNDRY

Incinerator for garbage and sludge. Separator for bilge water. Tunnel for bow-thruster 300 bhp installed. Arrangements made for installation of Decca Navigator.

Scientifical Echo Sounder, Simrad type EK with transducer 67 CA-12khz

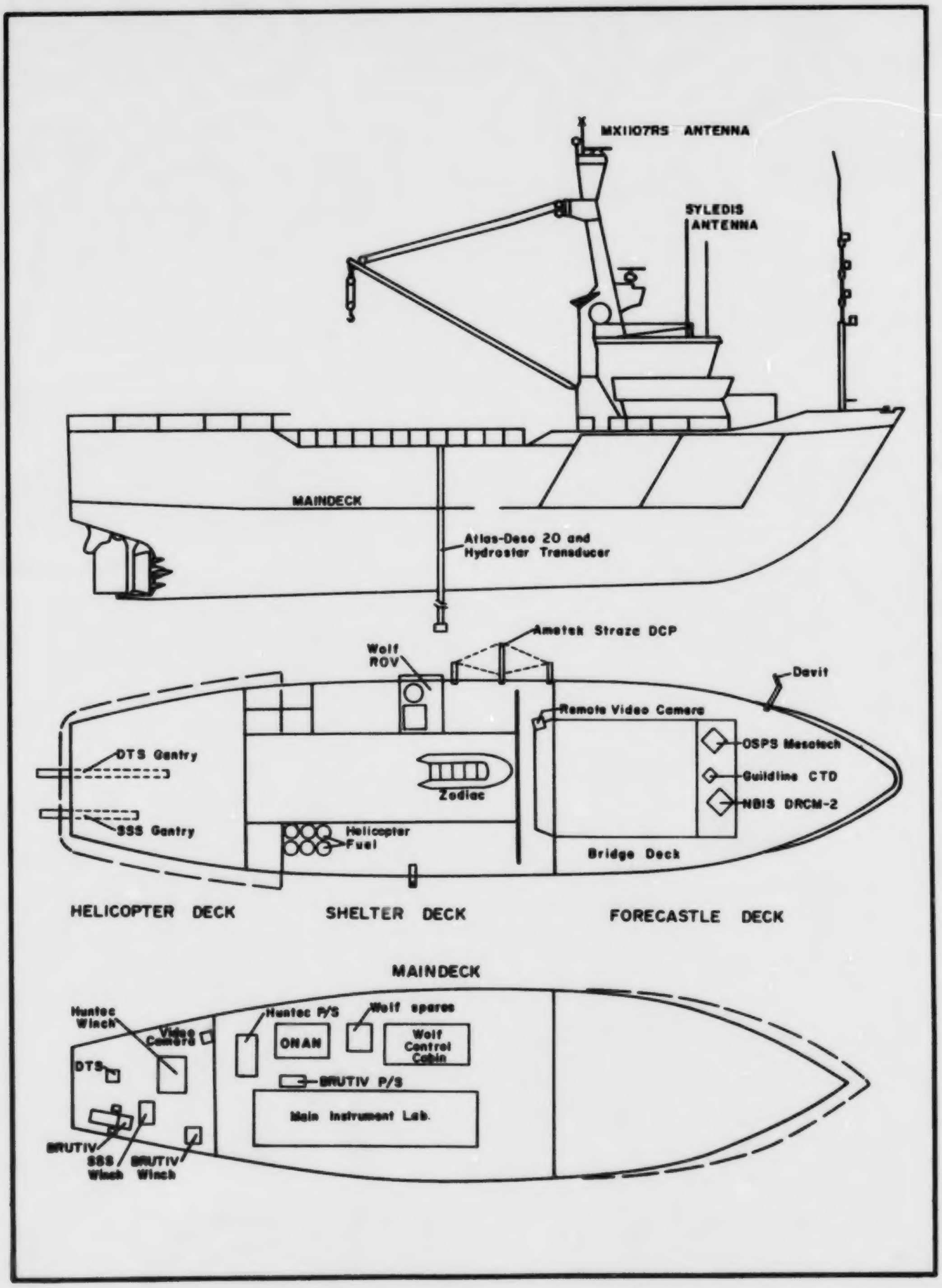
MX1107RS ANTENNA
SYLEDIS ANTENNA
MAINDECK
Atlas-Deso 20 and Hydrostar Transducer
Ametek Straza DCP
Wolf ROV
Davit
Remote Video Camera
DTS Gantry
OSPS Mesotech
Guildline CTD
Zodiac
NBIS DRCM-2
SSS Gantry
Helicopter Fuel
Bridge Deck
HELICOPTER DECK
SHELTER DECK
FORECASTLE DECK
MAINDECK
Huntec Winch
Video Camera
Huntec P/S
Wolf spares
ONAN
Wolf Control Cabin
DTS
BRUTIV P/S
Main Instrument Lab.
BRUTIV
SSS Winch
BRUTIV Winch

Figure 6. Vessel configuration and equipment layout of M.V. Polar Circle.

An Onan 50 kVa generator and power distribution system was provided to facilitate the hook-up of winches, the ROV, and other equipment to ship's power and to act as a back-up source if necessary.

The shore base established in Makkovik, supported the offshore and nearshore activities. The normal staff complement consisted of 2 WIIM study personnel, a navigation technician, a helicopter pilot and engineer and three crew members of the longliner, Amanda J, used for the WIIM study (Lever and Diemand 1988).

An Aerospatiale twin-engined "Twin Star" helicopter was chartered from Sealand Helicopters Limited of St. John's, Newfoundland for the DIGS experiment. This aircraft was capable of both nearshore and offshore work and was equipped with an Omega navigation system.

Major tasks undertaken by the helicopter included mobilization and demobilization of the coastal navigation stations, deployment and recovery of the DIGS and WIIM sensor packages, aerial reconnaissance and stereo photography of icebergs, and the movement of personnel and cargo between Makkovik and the Polar Circle.

A 13.7 m longliner, the Amanda J, was chartered for the duration of the field program. It carried a normal complement of three crew members and up to two scientific personnel. The vessel was used exclusively for the WIIM study (Lever and Diemand 1988), departing from and returning to Makkovik daily.

The M.V. Pandora II, carrying the Pisces IV submersible, overlapped its scientific program with that of the Polar Circle. Locations of interest, documented during the DIGS experiment, were passed on to the Pandora II as potential dive targets. Initially, Pandora II was put on location using the Polar Circle's Syledis navigation system. Eventually, however, this system was transferred to Pandora II for independent use.

In addition to visual documentation of grounding sites from Pisces IV, the Pandora II carried geoscientists for other related work including analysis of seabed samples.

For safety and efficiency an extensive communications network was established (Figure 7).

During all operations involving the helicopter, a non-directional beacon onboard the Polar Circle was in operation and the aircraft followed this until the pilot established visual contact with his destination. When in range, and during operations, the helicopter used aeronautical VHF to communicate with support vessels and the shore base. Generally, communications between all other parties were provided through single side band (SSB) radios.

Zodiac operations from the Polar Circle made use of portable marine VHF radios. These radios were also useful during onboard operations when activities, such as iceberg dimensioning, took place.

Onboard the Polar Circle, the ship's intercom was used to communicate between the bridge, laboratory, and decks. A separate dedicated intercom was run between the bridge, laboratory and ROV control van. Additionally, a remotely controlled colour video camera was mounted on the vessel's superstructure to monitor deck activities from the main laboratory, while a fixed black and white video camera was used to monitor after-deck operations.

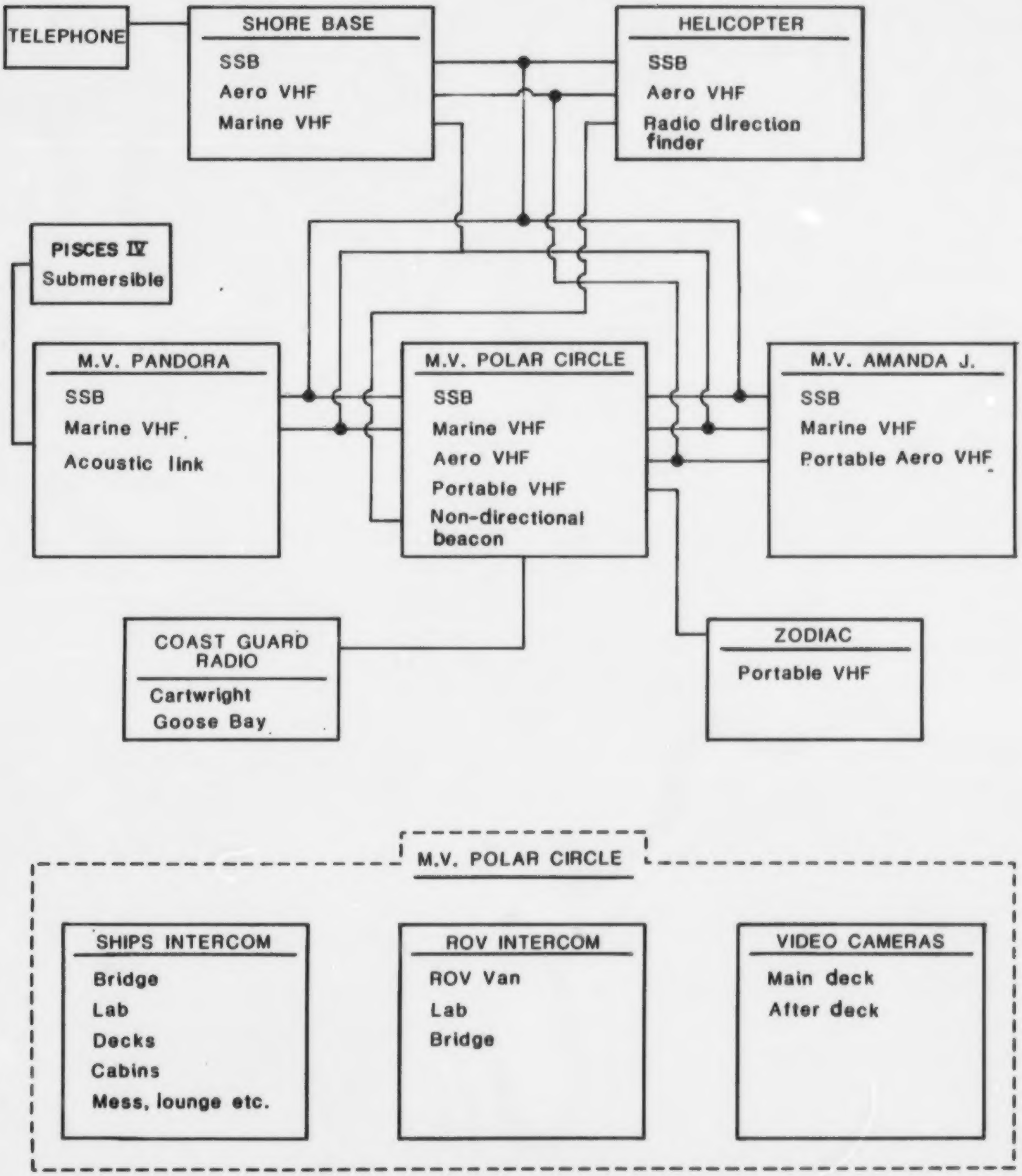
TELEPHONE
SHORE BASE
SSB
Aero VHF
Marine VHF
HELICOPTER
SSB
Aero VHF
Radio direction finder
PISCES IV
Submersible
M.V. PANDORA
SSB
Marine VHF
Acoustic link
M.V. POLAR CIRCLE
SSB
Marine VHF
Aero VHF
Portable VHF
Non-directional beacon
M.V. AMANDA J.
SSB
Marine VHF
Portable Aero VHF
COAST GUARD RADIO
Cartwright
Goose Bay
ZODIAC
Portable VHF
M.V. POLAR CIRCLE
SHIPS INTERCOM
Bridge
Lab
Decks
Cabins
Mess, lounge etc.
ROV INTERCOM
ROV Van
Lab
Bridge
VIDEO CAMERAS
Main deck
After deck

Figure 7. Communication systems.

DATA COLLECTION AND ANALYTICAL TECHNIQUES

Navigation and Position Fixing

Navigation services were provided by Cansite Surveys Limited of Calgary. The Cansite system consisted of an integrated navigation hardware/software package (Figure 8).

For seabed survey operations, fix marks were generated automatically at specific intervals and fed to individual recording systems.

During iceberg tracking operations, range and bearing information was passed from the ice observers to the navigators who, simultaneously, took a vessel position fix and entered range/bearing/gyro information into the computer manually. These data were processed onboard to produce a plot of geographic positions of iceberg targets.

The following shore-based stations provided LORAN-C navigation:

- Fox Harbour
- Cape Race
- Angissoc

The following shore-based stations provided Sercel Syledis navigation:

- Holt
- Strawberry
- Gust
- Cape Harrigan

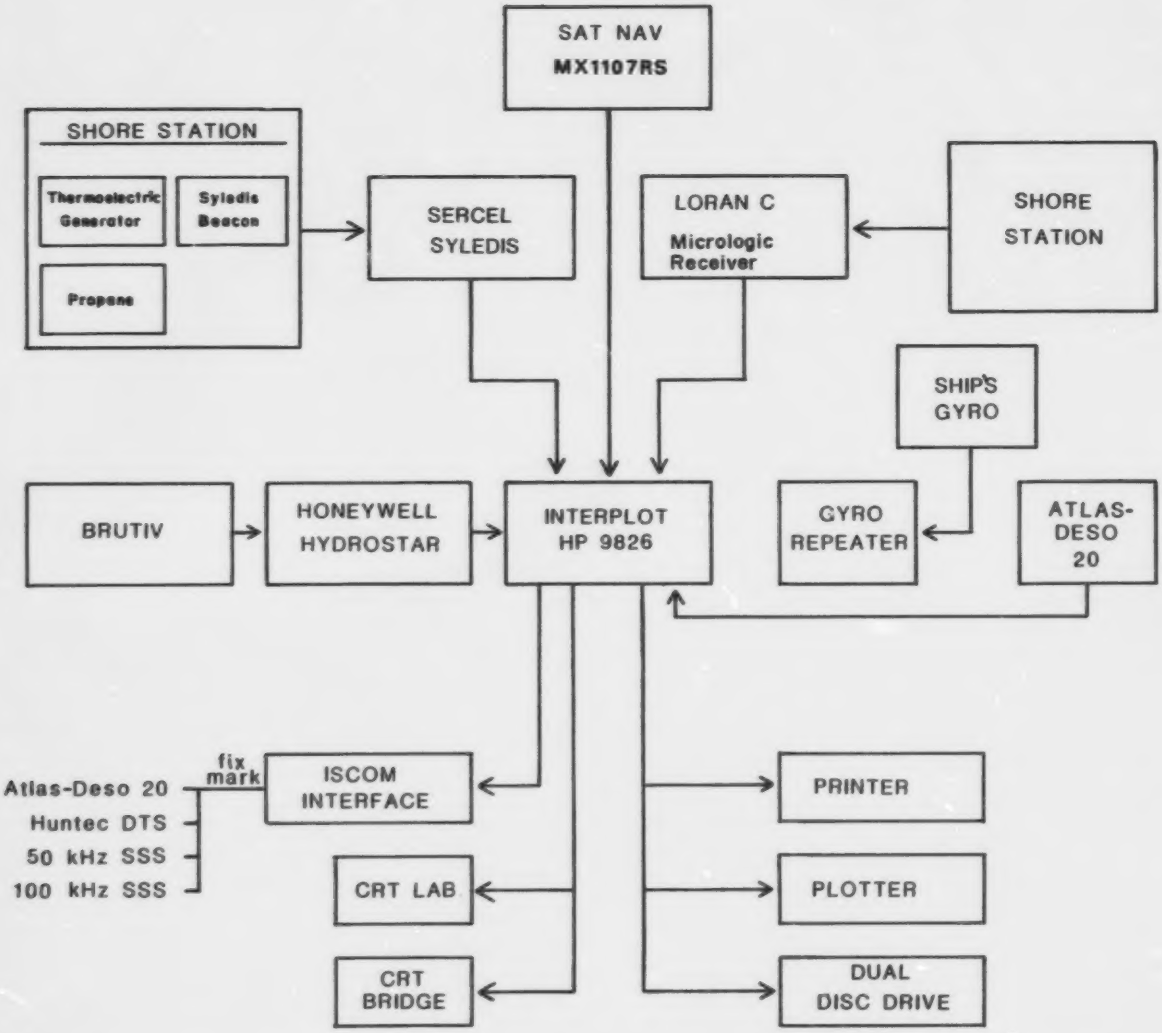
SAT NAV
MX1107RS
SHORE STATION
Thermoelectric Generator
Syledis Beacon
Propane
SERCEL SYLEDIS
LORAN C
Micrologic Receiver
SHORE STATION
SHIP'S GYRO
BRUTIV
HONEYWELL HYDROSTAR
INTERPLOT HP 9826
GYRO REPEATER
ATLAS-DESO 20
Atlas-Deso 20
Huntec DTS
50 kHz SSS
100 kHz SSS
fix mark
ISCOM INTERFACE
CRT LAB
CRT BRIDGE
PRINTER
PLOTTER
DUAL DISC DRIVE

Figure 8. Navigation systems.

Iceberg Tracking

Iceberg tracking and plotting were performed by the onboard ice and meteorological observers and navigators using equipment and procedures outlined in Figure 9.

Iceberg tracking and plotting were performed nominally at hourly intervals. Because the survey vessel was engaged in other tasks and was constantly manoeuvering, and because of the large number of icebergs present, it was not practical to identify individual icebergs with a unique code. Therefore, each target was treated individually and given a sequential number. Individual icebergs were identified and tracked when radar targets were plotted and compared with the positions of previous targets.

The tracking and plotting procedure may be summarized as follows:

- the ice observer and navigator co-ordinated data collection via the vessel's internal telephone system.

- beginning at the top of the radar screen (zero degrees relative to ship's heading) and continuing in a clockwise direction, the range and bearing to each target was recorded.

- coincident with the reading of range/bearing information, the navigator logged the vessel's heading from a gyro-repeater in the main instrument laboratory and took a position fix.

This procedure was repeated for all targets visible on the radar screen and subsequently the information was keyed

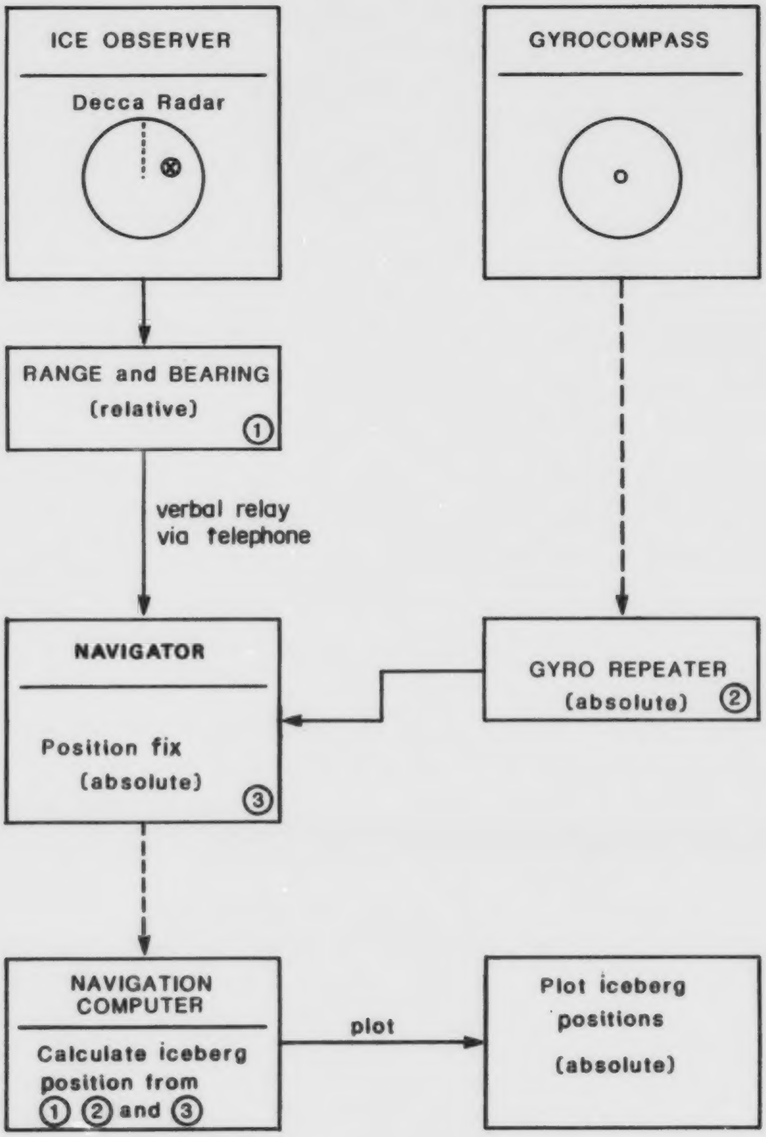
ICE OBSERVER
Decca Radar
GYROCOMPASS
RANGE and BEARING
(relative) ①
verbal relay
via telephone
NAVIGATOR
Position fix
(absolute) ③
GYRO REPEATER
(absolute) ②
NAVIGATION
COMPUTER
Calculate iceberg
position from
① ② and ③
plot
Plot iceberg
positions
(absolute)

Figure 9. Iceberg tracking and plotting.

into the navigation computer. From these data, the onboard computer calculated the absolute position of targets and reproduced them on a flat-bed plotter.

Each set of observations was plotted with a different colour to discriminate between targets and to allow better assessment of iceberg drift patterns. Bathymetric contours were drafted manually onto the plotting sheets to assess the grounding potential of icebergs. Resultant plots indicated trajectories of moving targets and positions of grounded icebergs.

Plotting sheets were renewed frequently as they became congested with information or as the vessel moved into another surveillance area. Fresh plotting sheets were initiated by plotting a few of the most recently collected positions to provide an overlap of the time series.

The accuracy of this procedure depended on the accuracy of the range and bearing and gyrocompass information and therefore was subject to the resolution of the range and bearing cursors of the radar screens. As a general practice, iceberg targets were logged by placing the range cursor so that it just touched the target whilst the bearing cursor was centered on the target. The accuracy of this method also depended on the radar range selected.

For more precise measurements of iceberg velocities or decelerations, the method used is less than ideal. At close ranges, the position of an iceberg centre could be in error by hundreds of metres depending on the size and shape of the iceberg and the position of the observation vessel relative to the iceberg.

Iceberg Dimensioning

Above water. Above-water iceberg shapes were documented in side view with 35 mm photography from the *Polar Circle*. Vertical and oblique aerial images of the above-water ice masses and their waterlines were acquired from the helicopter using both 35 mm and 70 mm cameras.

Photographs taken from the *Polar Circle* provided information for classification and identification of iceberg targets. Range and bearing (with respect to true north) were recorded together with general descriptions.

Lateral-view stereo photographs of icebergs selected for dimensioning were obtained from the *Polar Circle*. The equipment consisted of two Canon AE-1 35 mm cameras mounted 1.2 m apart on a hand-held frame. A Polaroid SX-70 camera was mounted at the centre point of the stereo baseline and all three cameras were triggered simultaneously. The procedure consisted of shooting stereo pairs of each iceberg from four quadrants (0°, 90°, 180° and 270°), generally beginning with the largest face, as the vessel circled the iceberg at a predetermined range. Coincident with the photography, a radar range to the iceberg was taken along with a gyro reference.

Aerial stereo photography involved the use of a Hasselblad 70 mm camera mounted on a bracket inside the helicopter. Photogrammetric analysis of photographs from several calibration flights during the program mobilization phase indicated little or no distortion due to the perspex of the helicopter "bubble" through which the photographs were taken.

Following the selection of an iceberg, it was overflown to select an optimum altitude for aerial photography. Based on an airspeed of about 60 kts, an automatic shutter timing interval was set on the camera which provided a minimum of 40% overlap between frames. Several rolls of both lateral-view and aerial film were processed onboard to confirm that the equipment and methodology were of acceptable standards.

For the purpose of contouring the above-water shape of the iceberg, Kenting Earth Sciences Limited was provided with the aerial stereo photographs which were enlarged by a factor of two for use in stereo instruments. Using flying height and camera focal length levelled to the waterline, the pictures were scaled to identifiable points between which the distances had been calculated and the resultant information compiled manually at 2.5 m intervals on a stereo plotter. The contour plots were supplied to Offshore Survey and Positioning Systems Limited (OSPS) of Vancouver, B.C., who digitized the contours to provide a three-dimensional display as well as area and volume estimates. The above-water information was then integrated with below-water information and was stored on nine-track magnetic tape. It is estimated that the above-water volume estimates based on the aerial stereo photographs are accurate to within approximately ±2%.

Below water. Below-water dimensioning of icebergs was undertaken by OSPS using the procedure illustrated in Figure 10 and summarized below.

The first task involved encircling the iceberg with a 1 inch diameter, nylon, Samson braid rope, to which were attached four Sonardyne acoustic transponders at roughly equal intervals - the intervals being calculated from

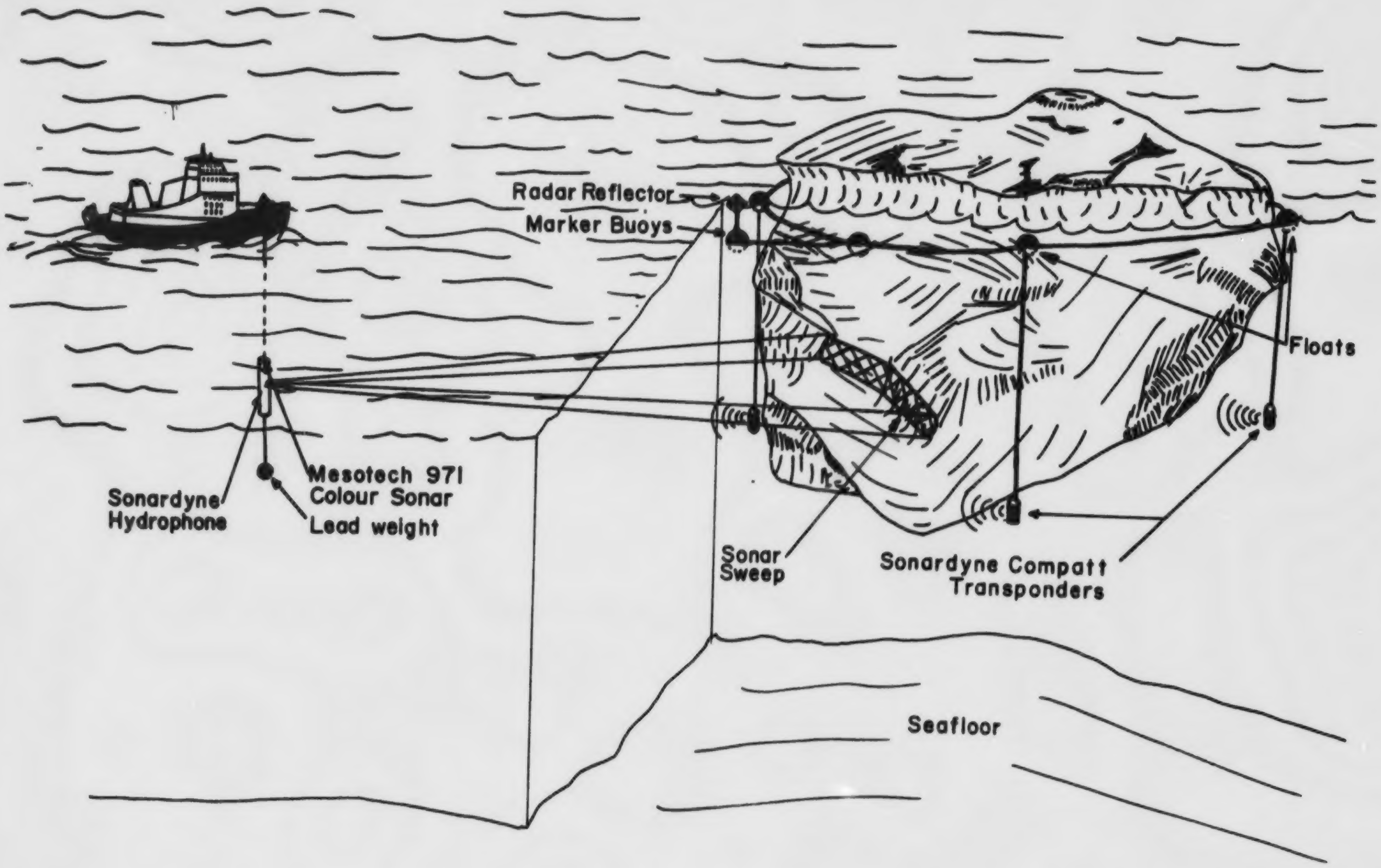
Radar Reflector
Marker Buoys
Floats
Sonardyne Hydrophone
Mesotech 971 Colour Sonar
Lead weight
Sonar Sweep
Sonardyne Compatt Transponders
Seafloor

Figure 10. Graphic illustration of underwater iceberg dimensioning.

measurement estimates acquired from oblique aerial Polaroid photographs. Alternatively, the iceberg girth was measured by means of a preliminary encirclement with the rope. The Sonardyne transponders were suspended at depths of 80-100 m by 3/4 inch nylon rope. Buoyancy was provided by Norwegian floats which were numbered for reference.

The Polar Circle moved around the iceberg paying out the rope and transponders. Normal practice was to start paying out on the upwind side to allow the rope to drift closer to the iceberg. Having encircled the iceberg and picked up the end buoy, a shackle and weight were attached to the rope and the vessel moved away causing the rope to tighten around the iceberg. When released, the shackle and weight prevented the noose from opening excessively. Under ideal conditions the procedure could be accomplished in 50-60 minutes; quite often, however, rolling or calving of the iceberg resulted in delays. With the equipment in place, the vessel was positioned between two transponders to begin the acoustic profiling procedure.

The profiling sequence conducted from the Polar Circle, consisted of lowering the Sonardyne hydrophone and the attached Mesotech 971 Color Sonar, in 5 m or 10 m increments. An 18 kg weight suspended below the hydrophone maintained it in a near-vertical position. At each depth interval, the hydrophone assembly collected range information simultaneously from the visible acoustic transponders and iceberg profile data in a horizontal swath. A compass, mounted in the scanning head, provided azimuth reference. All data collected were logged on floppy disc using an HP9826 computer.

On completion of all horizontal profiles from one position the Polar Circle was repositioned in the next quadrant and the sequence was repeated. Once profiling was complete, the equipment was recovered by releasing the end shackle and steaming around the iceberg, recovering the rope along the way.

Processing of the data involved converting the raw range and bearing data to Cartesian co-ordinate (x, y, z) format and editing to eliminate known sources of error. Collectively, the profiles were translated, rotated, and scaled allowing the individual sites to be aligned with respect to each other.

The adjacent overlapping profile data were superimposed to produce a composite profile, smoothed, then plotted as both individual slices and in a stacked format to produce a three-dimensional perspective view. Area and volume measurements were calculated for each profile, then incorporated with that for the above-water dimensioning to provide a perspective view of the entire iceberg as well as total area and volume estimates.

Three basic problems affect validity of the results. Firstly, the technique used to deploy and maintain the relative acoustic network was inadequate for icebergs with a circumference in excess of 500 m. The weight attached to the end of the transponder array was insufficient to hold the network tight against the iceberg and this was further complicated by small calving events which often necessitated readjustment of the transponder array.

Secondly, the absolute positions of the transponders in relation to the iceberg could not be defined accurately because of lack of aerial photography during the dimensioning process. Photographic documentation was not obtained during dimensioning because it was deemed unsafe by the Captain to have the helicopter operating from the ship while the vessel was so close to an iceberg and restricted in maneuverability.

Finally, vessel motion, both while maneuvering and while attempting to maintain station, caused disorientation of the transponder array, resulting in significant degradation of profile accuracy. It is estimated that the combination of these various errors yields an average uncertainty of about ±15% for underwater profiles and volumes derived from the acoustic data.

Iceberg Motions

C-CORE Motion Sensor Packages. C-CORE designed and built two complete motion sensor packages for use in the DIGS experiment. These packages were used to measure the three linear accelerations and three angular rotations of the icebergs chosen as likely candidates for interaction with the seabed.

To measure linear accelerations, each package was fitted with three orthogonally mounted Sundstrand QA 800 Servo-Accelerometers. The two horizontal ones (x,y axes) were scaled to ±1 g; the vertical one (z axis) was scaled to 0-2 g. These sensors have a maximum linearity error of 60 μg, a resolution of 5 μg, and a frequency response error of ±0.1% over 0-10 Hz.

To measure pitch and roll (angular rotations about x and y axes) of each package, two Penny and Giles 3910/60 Tilt Sensors were used. These have a range of ±30°, with a linearity error of ±0.15°, and a 3 Hz natural frequency. Being gravity referenced instruments, these tiltmeters also respond to linear accelerations. However, for the very small accelerations experienced by multi-million tonne icebergs, the resulting angular error is extremely small and can be ignored. It should also be noted that for small linear accelerations, the servo-accelerometers essentially record the gravitational components associated with the package orientation. As such, they provide a backup to the angular measurements made by the tiltmeters.

Each package was also fitted with an Endeco 86900128 Solid State Compass to measure magnetic bearing. The accuracy of the compass is ±1°, with a resolution of ±0.5°.

The six sensors for each package were mounted in a rigid frame, machined to provide orthogonal axes to within ±0.5°. The zero points and axis orientations were determined using a relative calibration procedure which relied on the accelerometers as the most accurate instruments available. Also checked by this means were the factory calibration factors for each sensor. The tilt of the calibration table applied a component of gravitational acceleration to the accelerometers. Agreement between the various sensors and of each sensor with its respective factory calibration factor was excellent. The factory calibrations of each compass were checked via rotations of the calibration table about its vertical axis.

The sensor clusters were flexibly mounted to an instrument plate within each package. Natural frequencies of the mounts in various directions were 7 to 15 Hz, giving a degree of shock protection to the sensors without compromising frequency response. The sensor outputs were filtered to -60 dB at 2 Hz, with -3 dB and negligible phase shift at 0.2 Hz.

The long-endurance capabilities of the packages for data acquisition were set in consideration of the random nature of iceberg scour and anticipated operational constraints. The filtered sensor signals and various reference voltages were sampled at 2 or 4 Hz (selectable), and converted to 12 bit + 1 sign bit digital equivalents. The digitized serial data were buffered, then periodically written on a magnetic tape cartridge. The same real-time data stream was sent via a Dataradio 4800 Radio Modem to the ship-based receiving unit for logging on a PDP 11/03 computer and tape drive. This telemetry link provided an important back-up to the internal data logger, as well as real-time operational information on the status of the iceberg and the instrument package.

The internal data loggers were designed and built by Seimac Limited, under contract to C-CORE. The target four-day endurance for the packages was achieved by incorporating a Ross Comp D161 Cartridge Tape Drive unit in each logger. Unfortunately, problems were encountered with the tape read capability of these data loggers such that the telemetry link alone was employed for actual data logging.

The flexibly mounted sensor clusters, data acquisition equipment, and power supplies/filter boards were installed on an aluminum plate mounted within box-type enclosures, along with two 12 VDC Sonnenschein Dryfit batteries (Figure 11). The two enclosure halves were sealed using an O-ring, and each bottom was fitted with four 5 cm long tapered stainless steel pins for securing the packages to the ice. Markings were applied to the enclosures to facilitate the determination of package orientation relative to the iceberg. A lattice-work cage was attached to each package by nylon rope, to facilitate recovery by helicopter. In view of the planned four-day endurance, the packages were

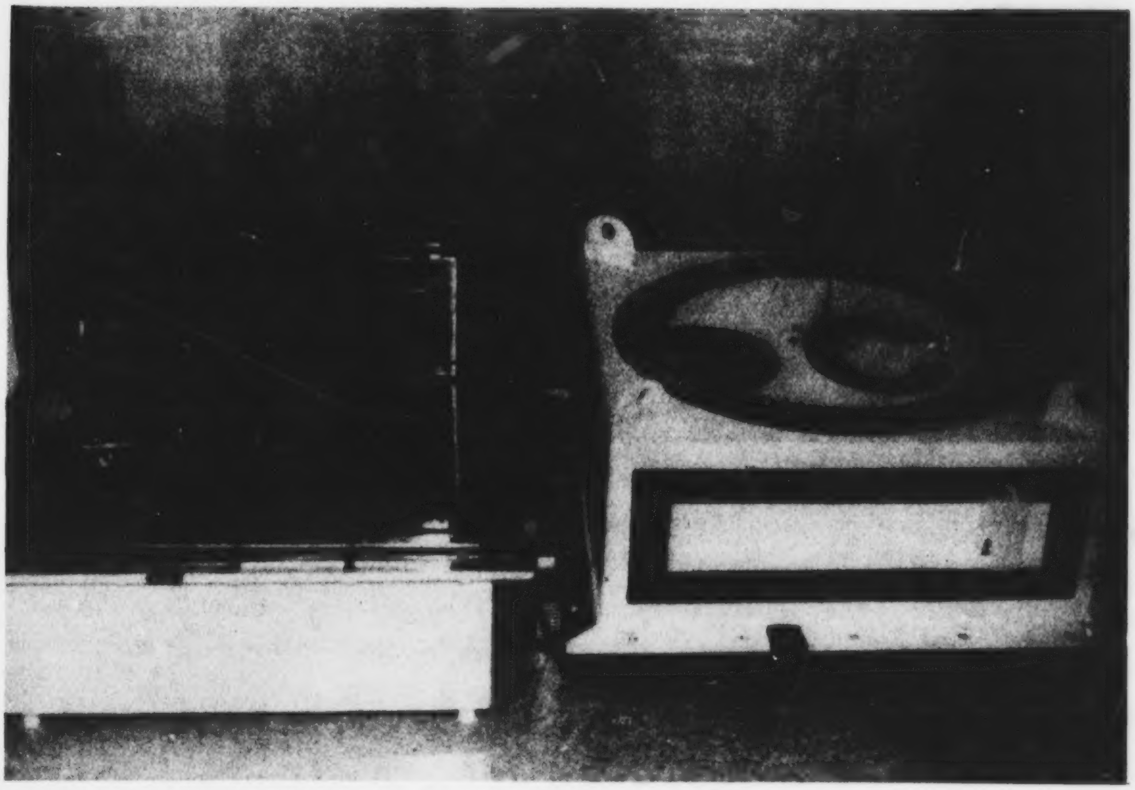

Figure 11. C-CORE motion sensor package.

also fitted with strobe lights, radar reflectors, and small radio transmitters, to safeguard against loss. The total mass of each package was approximately 90 kg, well below the buoyancy provided by the .66 x .66 x .51 m sealed box-type enclosures.

Deployment and Recovery of Packages. Five deployments and recoveries of the C-CORE motion sensor packages were achieved, over periods ranging from one to four days. In each case the package was powered up, checked and sealed, in the hold of the Polar Circle, then lifted onto the main deck. It was then connected via lanyards to the cargo hook of the helicopter (Figure 12). After careful lift-off, the package was flown to the target iceberg, and deposited on the ice in a roughly horizontal position (Figure 13). The package orientation on the iceberg was later determined from aerial photographs taken during the deployment. The packages were all retrieved by helicopter, either by employing a grapling hook or by hovering sufficiently close to enable direct lanyard hook-up.

The five package deployments on four different icebergs ("Bertha", "Gladys", "Julianna", and "Lucretia") yielded a total of about 150 hours of motion data. Three seabed-interaction events were captured as were numerous calving and rolling events. Table 2 lists deployment and recovery information for each C-CORE sensor package. As discussed, failure of the tape read capability of the Seimac data loggers necessitated use of telemetry to log motion data on the ship-borne computer. Unfortunately, transmission range limitations and frequent dropouts in the ship's AC power caused the actual data rate to be considerably less than the rate of sampling within the package. The ship's power fluctuations became so severe during the simultaneous deployments to "Julianna" and "Lucretia" that computer

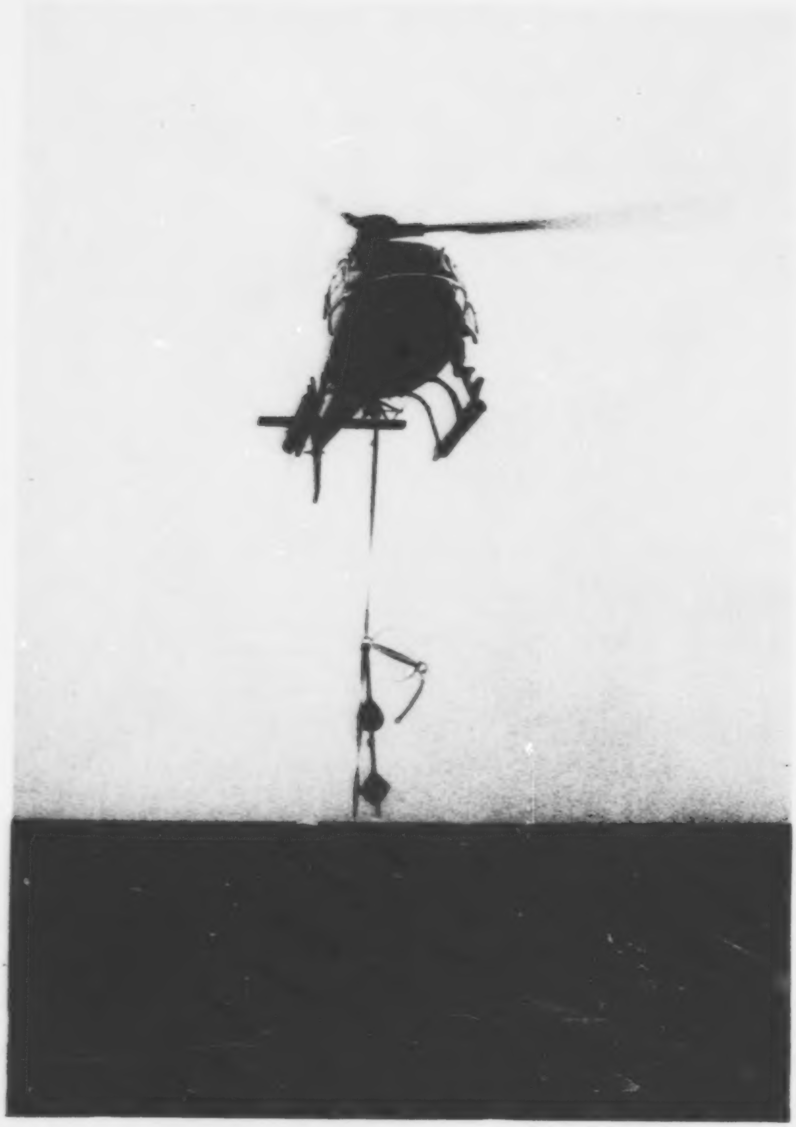

Figure 12. Helicopter lifts a C-CORE motion sensor package.

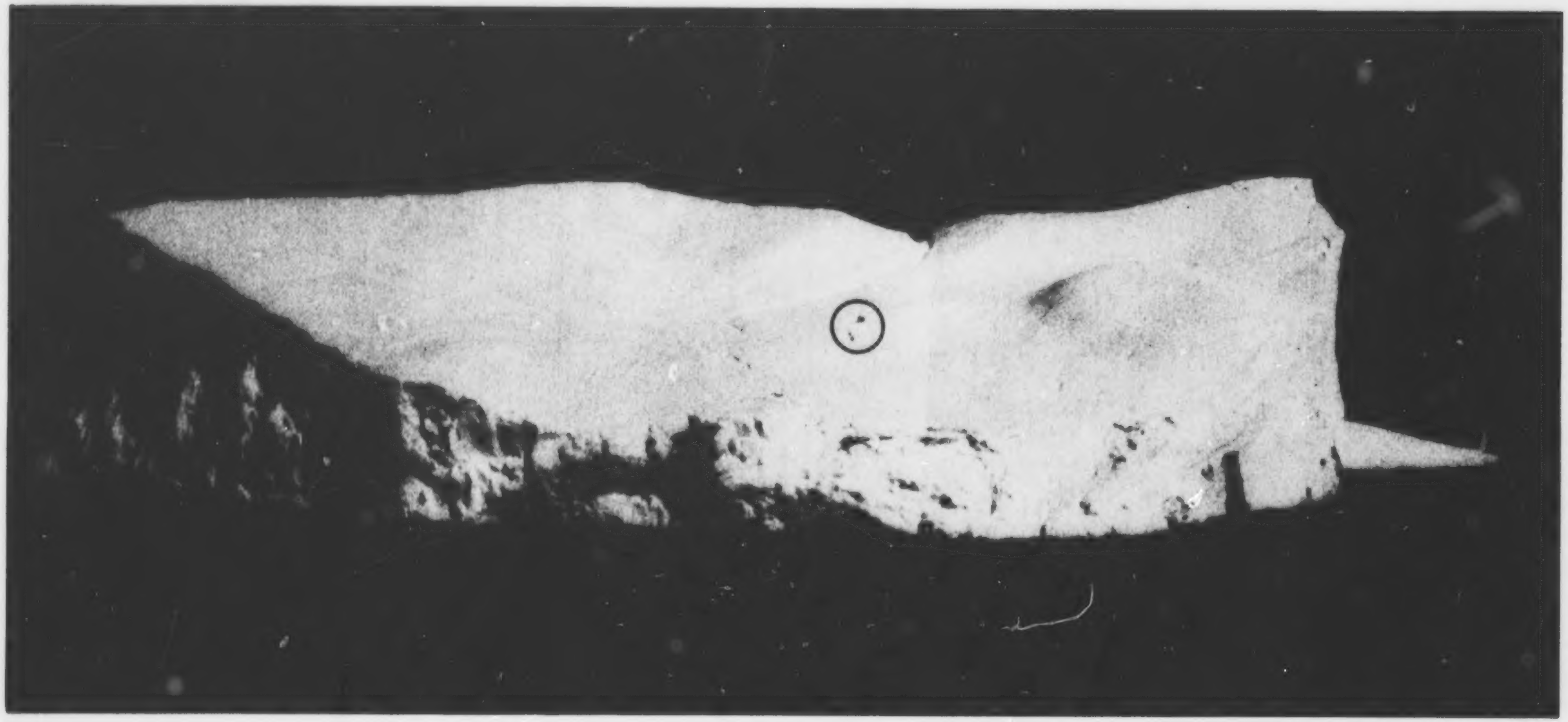

Figure 13. C–CORE package on 'Gladys'.

Table 2

C-CORE Motion Sensor Package Deployments

Deployment	Package	Iceberg	Date/time (GMT)	
			Deployment	Recovery
1	D	"Bertha"	4 Aug./2350	5 Aug./1905
2	D	"Gladys"	8 Aug./2233	9 Aug./2017
3	D	"Gladys"	9 Aug./2336	12 Aug./1830
4	D	"Lucretia"	19 Aug./1703	21 Aug./1700
5	C	"Julianna"	19 Aug./1740	21 Aug./2320

logging became untenable. Much of the data from these two deployments were logged on paper via a teletype and printer. Nevertheless, during all major events involving seabed interaction, an average rate of about 1 Hz of valid data was achieved.

Additional information on the design and use of the C-CORE sensor packages for both the DIGS experiment and the concurrent WIIM study may be found in Lever et al. (1986).

Atmospheric and Oceanographic Measurements

Moored Current Meters. Bottom current measurements were obtained by using two Interocean Type S4 current meters mounted on a specially designed tripod (Figure 14) about 1 m above the seafloor in water depths of 105 m and 168.4 m. The two meters were deployed in early August 1985 and were recovered three weeks later.

Ametek Straza Doppler Current Profiler. An Ametek Straza doppler current profiler (DCP) was provided for the DIGS experiment by the Bedford Institute of Oceanography (BIO) and operated under a directed contract by Seimac Ltd. from Dartmouth, N.S.

The system comprised an HP85 computer, electronics assembly, transducer junction box, and transducer assembly mounted on a complex boom and davit assembly.

The operating principle of the DCP is based on the doppler effect and measures relative motions of the water column by the volume reverberation and backscatter from tiny organisms and other particles in a series of depth categories.

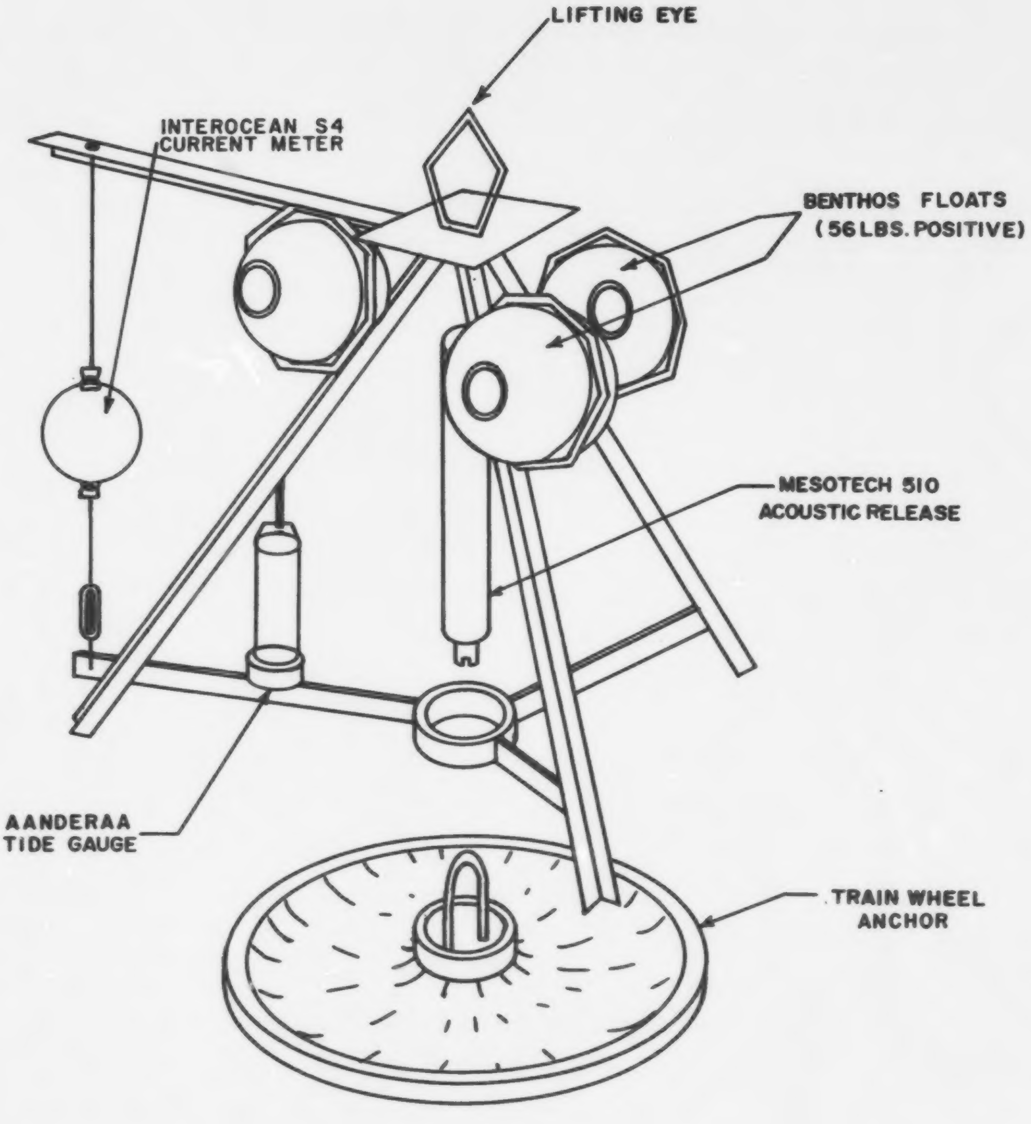
LIFTING EYE
INTEROCEAN S4 CURRENT METER
BENTHOS FLOATS (56 LBS. POSITIVE)
MESOTECH 510 ACOUSTIC RELEASE
AANDERAA TIDE GAUGE
TRAIN WHEEL ANCHOR

Figure 14. Current meter tripod configuration.

By oversight no raw DCP data were preserved. Post-cruise examination of the processed data on cassette tapes showed that they contain no usable information. This was later attributed to the failure of one pair of transducers, which went undetected in the field.

Current, Temperature and Depth Measurements. A Guildline Arctic Version current, temperature and depth (CTD) profiler was provided for the collection of physical oceanographic data. The unit unfortunately had technical problems that could not be corrected in the field and no data were collected.

Neil Brown Direct Reading Current Meter. The direct reading current meter (DRCM) was provided for back-up to the Ametek Straza DCP. Although it was not used for current profiling, it was used on several occasions to obtain current-temperature-depth data.

Tide Measurement. Two Aanderaa WLR-5 tide gauges, provided by BIO, were mounted with the current meters on the tripods (see Figure 14). At the end of the field program, the tide gauges were returned to BIO where the tapes were removed and the data were transcribed and processed.

Wave Measurement. Two Datawell 0.9 m waverider buoys were provided for the program. One buoy was moored in approximately 120 m water depth at 55°42'45"N, 58°12'11"W near moored current meter B on the north side of Makkovik Bank. The second buoy was used for the WIIM study (Lever and Diemand 1988) and was deployed and recovered daily in a free floating mode in the nearshore experimental area.

For the DIGS experiment, wave data were recorded on a Compac Pro desk-top computer interfaced to a DIWAR digital receiver. Data were recorded in real time and stored on diskette. Each block of data (26 min 40 sec) was processed in 200 second intervals with statistics filed and displayed on hard copy together with the wave spectrum.

For the WIIM study, waverider data were received with a Warep receiver and logged on a Seadata portable data logger.

Meteorology. Meteorological data were recorded manually every hour by two ice and meteorological observers onboard the Polar Circle. All observations were taken in accordance with Manual Marine Weather Observing (MANMAR) and Supplementary Aviation Weather Reporting Stations (SAWRS) specifications. Synoptic observations were transmitted to the Atmospheric Environment Service (AES) via either Goose Bay or Cartwright Coast Guard Radio after every third hourly observation (Table 3).

Table 3

Meteorological Conditions

OBSERVATION	Method MANMAR	SAWRS
Sky condition cloud		X
Cloud type	X	
Cloud amounts	X	X
Cloud heights	X	X
Ceiling height		X
Prevailing visibility	X	X
Ambient air temperature	X	X
Dew point temperature	X	X
Wind SPD/DIR - 2 min mean		X
Wind SPD/DIR - 1 min mean	X	
Wind gust		X
Mean sea level pressure	X	X
Altimeter setting		X
Pressure tendency	X	
Pressure change amount	X	
Weather and obstructions to vision	X	X
Sea surface temperature	X	
Sea wave characteristics	X	
Predominant and secondary swell characteristics	X	
Ice accretion characteristics	X	
Sea ice/iceberg characteristics	X	
Ship's course/speed made good	X	
Ship's lat/long	X	

Seabed Mapping and Profiling

Klein Hydroscan Sidescan Sonar. A Klein Hydroscan 100-kHz sidescan sonar system was used to provide high resolution documentation of seabed features. The towfish was deployed from the after-deck on a fixed sheave and the winch was remotely controlled from the main laboratory. Corrections for vessel speed, slant range and water column were achieved with a Klein Model 606 Processor. Data were recorded in analogue format on an HP 3968A instrumentation grade tape recorder, and produced as a real time display on wet paper records.

During normal operations the sidescan was operated at a 200 m range and towed 20 to 25 m above the seabed.

Huntec DeepTow Seismic System. A Huntec dual DeepTow Seismic (DTS) system, equipped with a 50-kHz sidescan sonar, was used to provide high-resolution shallow stratigraphic data and for general morphological mapping of the seabed. The system was configured to provide 540 J output at 6kV. The system was operated at 4kV (345 J) and triggered at a 3/8 s interval. Analogue records were graphically displayed on EPC 4600 recorders.

The record of acoustic stratigraphy was augmented by the Acoustic Reflectivity Unit (ARU) which calculates and displays the acoustic reflectivity of the seafloor and thus aids in the interpretation of data.

Analogue data from both the internal hydrophone and the external streamer were processed through an internal processor and Khron-Hite filter and recorded on magnetic tape.

Data from the 50-kHz sidescan sonar were collected with a Model 531T three-channel transceiver-recorder operating at a 375 m range. Sidescan sonar data were also recorded on analogue tape.

The Huntec towfish was deployed from the after-deck using a specially built gantry with the sheave coupled to a horizontally powered roller block. The electro-hydraulic winch for the Huntec DTS system could be controlled either directly at the winch or remotely from the main laboratory. For safety purposes the hydraulic power-pack was placed inside the main hold with hydraulic and control lines passed through watertight bulkhead connectors to the winch assembly.

Echo Sounder. Precision echo-sounding data were acquired with a Krupp Atlas-Deso 20 survey echo sounder. A 33-kHz transducer was mounted on a vertical boom deployed from the starboard side approximately at midships.

Digitization of echo sounder data by the Atlas-Deso 20 used a "stacking" technique plus an expectation window to suppress random and asynchronous interference. The Atlas-Deso 20 was interfaced to the navigation computer and digitized data were logged simultaneously with position fixes. Additionally, analogue data were acquired on strip-chart recordings for detailed measurements of seabed features.

The sounder was calibrated using a weighted cone and standard calibration techniques. The velocity of sound in water was fixed constant at 1,470 m/s.

High-Resolution Seismic Sparker System. Unfortunately, owing to problems with the sparker and the triggered capacitor bank, which could not be repaired in the field, this system yielded no data. As a result, all sub-bottom information was provided by the Huntec DTS system.

BRUTIV. The BRUTIV (Bottom Referencing Underwater Towed Instrument Vehicle) camera sled was supplied and operated under directed contract by CEY-X Ltd. of St. Andrews, New Brunswick. The sled was towed from the after-deck and was used for photographic documentation of seabed features.

After collecting video and still photographs on several lines, the tow cable parted resulting in temporary loss of the sled. Upon recovery it was discovered that the sled had sustained damage that could not be repaired in the field, which prevented its further use.

Remotely Operated Vehicle (ROV). An OSEL UFO remotely operated vehicle (ROV) was provided by Wolf Sub-Ocean Ltd. of St. John's, Newfoundland. The ROV was deployed from the port-side midships area of the shelter deck and was controlled from an operations van mounted near the main laboratory in the cargo hold.

During initial operation, a cable malfunction caused an electrical short, damaging a component which was not carried in the spares inventory. The problem was later rectified but other complications restricted operations.

The ROV had problems maneuvering against the strong currents on Makkovik Bank; therefore, operations were restricted to slack-water tidal periods. Photographic documentation of iceberg keel interaction with the seabed was impossible because of technical problems.

Observations from Submersible

Observations were made using the three-person Pisces IV submersible deployed from the Pandora II. Navigation during the first phase on Makkovik Bank was by means of a Syledis system giving an accuracy to within ±5 m. Navigation during the northern phase was entirely based on satellite navigation and frequently had errors in excess of 300 m. Seafloor sampling was achieved by a Leheigh corer, operated from the Polar Circle, and by small push cores held by the manipulator arm of the submersible. In all cases, Pisces dives were made in areas that had been surveyed previously with sidescan sonar to provide comparison between the acoustic data and direct visual observations. The individual dives are described later in the text.

Sediment Tracer Techniques

The tracer sand used for this experiment was a cesium silicate mineral called pollucite ($CsAlSi_2O_6$). Pollucite, a naturally occurring inert mineral, was chosen because of its detectability by neutron activation analysis which has a sensitivity of less than 0.1 ppm. It was both inexpensive and commercially available. It has a density of 2.7 to 2.75, in comparison to quartz which has a density of 2.65. The grain size distribution of the pollucite used during the DIGS experiment is shown in Table 4. The cesium content has an expected life in seawater of at least 18 months.

The sediment was deposited using a barrel deployment device (Figure 15), which was triggered to release upon contact with the seabed. At each site 20 kg of tracer sand were deployed along with an anchored buoy to act as an

Table 4

Grain size distribution of pollucite

Grain size (mm)	Weight (%)
1.000	22.06
0.710	13.64
0.500	11.63
0.355	9.11
0.250	7.71
0.177	6.81
0.125	5.53
0.0625	23.51

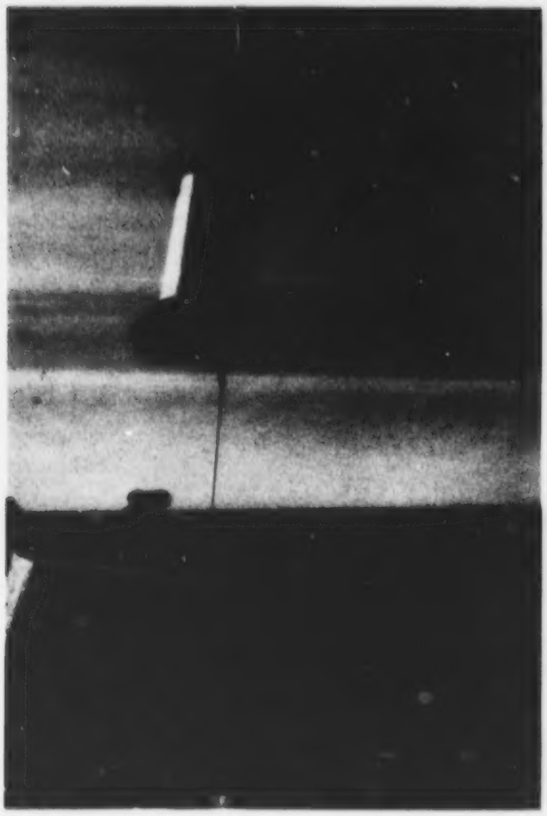

Figure 15. Deployment barrel for pollucite. The barrel is 60 cm high and 41 cm in diameter.

acoustic target. This simple technique worked well and left the tracer at the seafloor relatively undisturbed.

Subsequent seafloor sampling was carried out using the suction sampler mounted on the Pisces IV submersible which has a capacity of up to eight samples. Additional samples were obtained using small tube sampling devices (Barrie and Collins 1985). A sample of 1.0 g is needed for accurate neutron activation analysis. A 50 m interval sampling grid, centred on the tracer deployment location was established at each site.

Tracer sand was initially deployed at both current meter mooring locations. Additional pollucite was deployed in two freshly excavated iceberg scours, one near the "Gladys" grounding location and the other in a large scour code-named "Big Makk" observed during the Repetitive Mapping survey. The "Gladys" deployment was carried out with the barrel deployment device using a 100-kHz Datasonics transponder as a location buoy. The tracer in "Big Makk" was deployed from the Pisces IV submersible during Dive 12. In this case, 10 kg of tracer was deployed adjacent to a depth-of-disturbance rod placed in the scour trough.

CHAPTER 2

PHYSICAL AND ENVIRONMENTAL SETTING

PHYSIOGRAPHIC AND GEOLOGIC SETTING

The Labrador Shelf extends from latitude 51° to 61°N, encompassing an area of some 200,000 km^2 (Figure 16). It is flanked on the west by the Labrador Marginal Trough, which separates the shelf into an inner and outer region.

The Trough extends along the entire length of the Labrador Shelf with water depths in some areas exceeding 800 m. It marks the transition between erosion-resistant, Precambrian rocks to the west and less resistant, Cretaceous-Tertiary strata to the east.

The inner shelf, adjacent to mainland Labrador, lies in water depths generally less than 200 m. It is formed from Precambrian crystalline rocks which, in many areas, are exposed at the seabed, resulting in rugged, complex topography.

The outer shelf is comprised primarily of clastic sedimentary rocks of late Cretaceous and early Tertiary age which form a series of six large, flat-topped banks. Water depths over the banks generally range from 120 m to 300 m, however, depths as shallow as 85 m occur over parts of Makkovik Bank and Nain Bank. The banks are separated by a number of transverse topographic depressions, referred to as "saddles", which typically extend from the marginal trough to the continental shelf edge (see Figure 16).

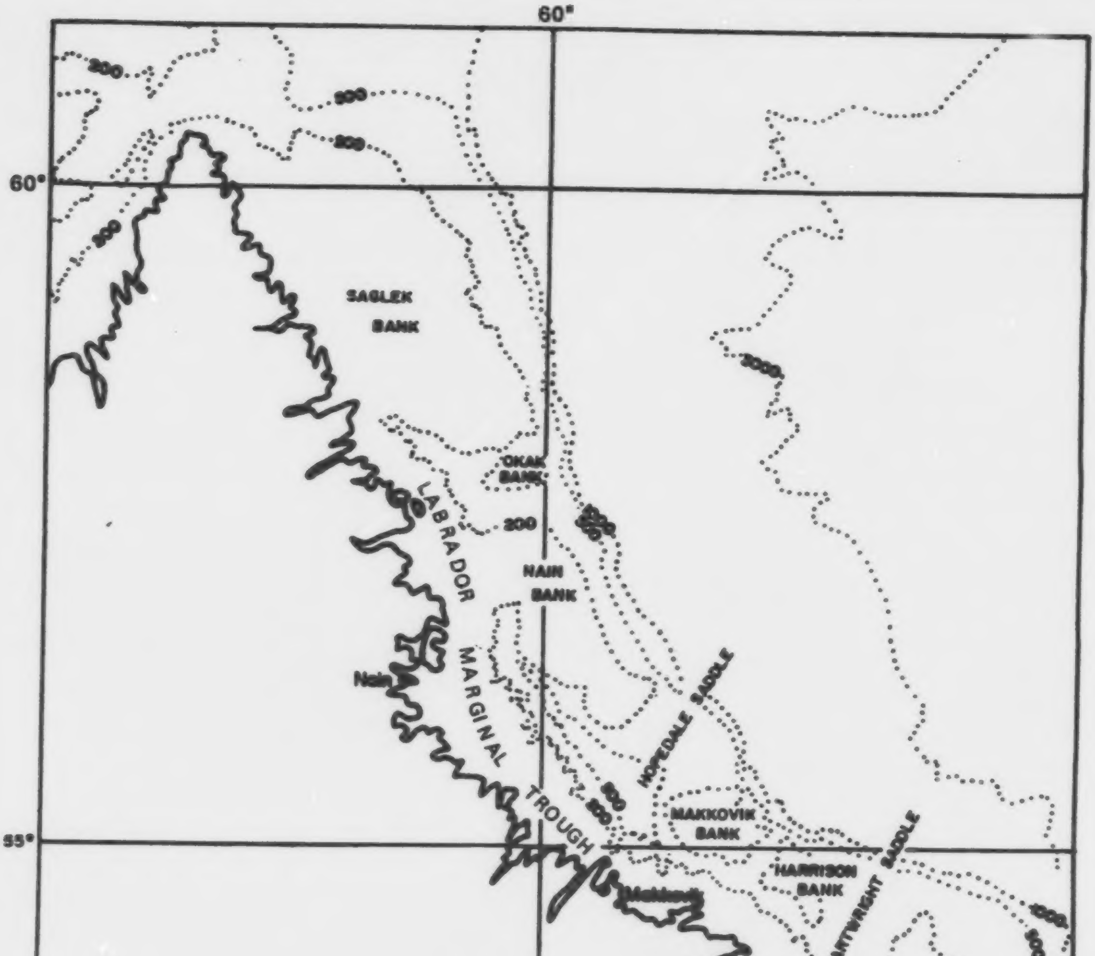
60°
60°
55°
50°
200
300
200
300
SAGLEK BANK
OKAK BANK
200
LABRADOR MARGINAL TROUGH
NAIN BANK
HOPEDALE SADDLE
Nain
MAKKOVIK BANK
HARRISON BANK
CARTWRIGHT SADDLE
Makkovik
3000
1000
500
200
200
HAMILTON BANK
Cartwright
Labrador
300
Isobaths in metres
SCALE
0 50 100 150 200
km
200
200
200

Figure 16. Physiography of the Labrador Shelf

It is generally agreed that at least three major episodes of glaciation have affected onshore Labrador. Work by Andrews (1963), substantiated by Prest (1970), Rogerson (1977), and Ives (1978) indicates that the most recent Wisconsinan glaciation was the least extensive of the three, probably not extending beyond the present Labrador coastline. Josenhans et al. (1986) recognize that, although less extensive than preceding events, the late Wisconsinan ice sheet did in fact extend into some offshore areas. This view partially supports that of Grant (1972), Fillon (1975), van der Linden et al. (1976), and Denton and Hughes (1981), who suggested that the glaciation may have effected the entire southern Labrador Shelf. Fillon and Harmes (1982), through examination of acoustic reflection profiles and cores, support the theory of a larger-scale ice sheet by inferring that in northern regions the ice may have extended as far east as the outer shelf, covering Saglek Bank and Hamilton Bank.

Despite disagreement over the chronology and extent of Pleistocene glaciations on the Labrador Shelf (see for example Rogerson 1977; Ives 1978; Josenhans et al. 1986, Fillon and Harmes 1982), it is certain that glacial action has played a role in present day shelf morphology and geology. Glacial ice advancing eastwards from Labrador is believed to have deepened the Labrador Marginal Trough (Grant 1972; McMillan 1973) and deepened and widened the saddles between the banks (Josenhans 1983) leaving extensive deposits of till and glaciomarine sediments over much of the shelf (Grant 1972; McMillan 1973; Fillon 1980; Josenhans 1983). These deposits are generally thin over the crystalline metamorphic rocks of the inner shelf. Topographical highs are blanketed by a cover about 10 to 40 m thick of reworked glacial tills (Josenhans et al. 1986).

On the outer shelf, glacial till is found mainly on the bank tops, the slopes leading into the saddles, and less commonly along the seaward limit of the banks (Josenhans et al. 1986). On the bank tops it is generally less than 50 m thick but increases to as much as 150 m in some localized areas along the western and northern parts of the banks.

At least three separate till units have been recognized throughout much of the region. Acoustically, these typically are homogeneous and unstratified, suggesting deposition beneath grounded ice (Josenhans 1983).

Post-glacial sediments are evident throughout the region. On some parts of the bank tops a veneer of fine muddy sand blankets the till. A layer of post-glacial silt extends eastward from the fringes of the outer shelf banks deep into the marginal trough and saddles.

Josenhans et al. (1986) divide the surficial Quaternary sedimentary cover into several units (Table 5). The lowermost unit is the Labrador Shelf Drift Formation which is comprised of a Lower Till (Unit 3a), which is divisible into as many as four undifferentiated till units, an Upper Till (Unit 3b), and the Hudson Strait Till (Unit 3c). The pro- and post-glacial marine sediments that overlie the tills are divided into the Qeovik Silt Formation (Unit 4), the Sioraq Silt and Gravel Formation (Unit 5c), the Sioraq Sand Formation (Unit 5b) and the Makkaq Clay Formation (Unit 5a). The distribution of these units on the Labrador Shelf is illustrated in Figure 17.

Makkovik Bank, the fourth largest of the six Labrador Shelf banks, has an area of roughly 11,000 km^2. It is bounded to the west by the Labrador Marginal Trough, to the north by Hopedale Saddle and to the south by a small unnamed

Table 5

Correlation between surficial geological units identified in different studies on the Labrador and Scotian shelves

		Labrador Shelf			Scotian Shelf
	Josenhans et al. (1986)	van der Linden et al. (1976)	Fillon and Harmes (1982)	Barrie and Piper (1982)	King (1970) Scotian Shelf
HOLOCENE	Unit 5 pro-& post-glacial marine sediments				
	5a Makkaq Clay	Goose Clay	Unit I	(Ponded Sediments)	LeHave Clay
	5b Sioraq Sand	Groswater Unit			Sambro Sand
	5c Sioraq Silt & Gravel	Cartwright Sand & Gravel	Unit II	Upper Basin Fill Unit	
PLEISTOCENE				Conformable Cover	
	Unit 4 Qeovik Silt	Lower Part of Goose Clay	Units V, VI, VII & VIII	Lower Basin Fill Unit	Emerald Silt
	Unit 3 Labrador Shelf Drift Formation	Cartwright Sand & Gravel Glacial Drift			Scotian Shelf Drift
	3c Hudson Strait Till		Unit III Unit IV		
	3b Upper Till				
	3a Lower Tills				
TERTIARY	Unit 2 Bedrock	Bedrock			Bedrock
PRE-TERIARY	Unit 1 Acoustic Basement				

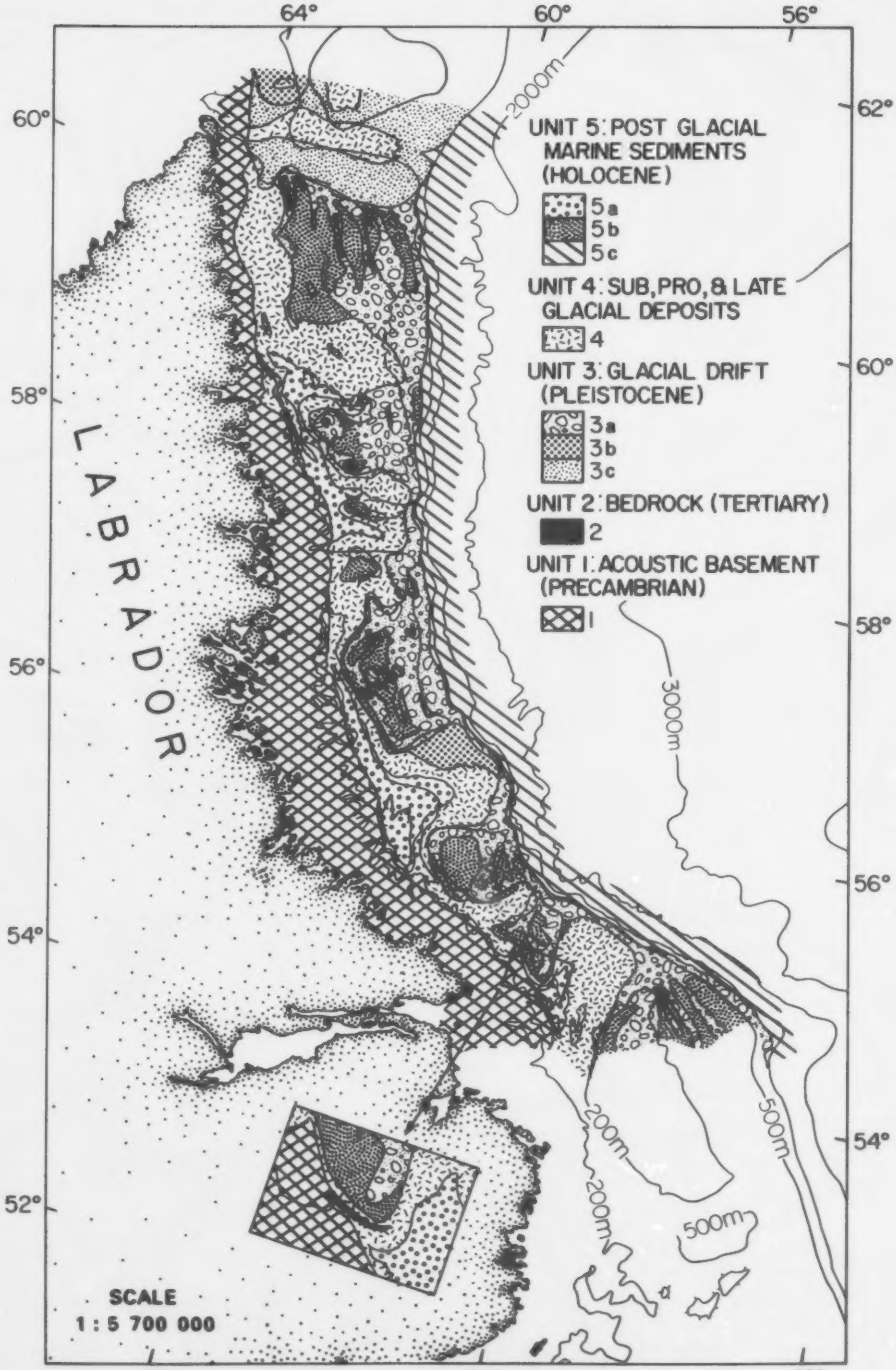
64°
60°
56°
60°
62°
58°
60°
56°
58°
54°
56°
52°
54°
2000m
3000m
500m
200m
200m
500m
UNIT 5: POST GLACIAL MARINE SEDIMENTS (HOLOCENE)
5a
5b
5c
UNIT 4: SUB, PRO, & LATE GLACIAL DEPOSITS
4
UNIT 3: GLACIAL DRIFT (PLEISTOCENE)
3a
3b
3c
UNIT 2: BEDROCK (TERTIARY)
2
UNIT 1: ACOUSTIC BASEMENT (PRECAMBRIAN)
1
LABRADOR
SCALE
1 : 5 700 000
60°
56°
52°

Figure 17. **Surficial geology of Labrador Shelf (after Josenhans et al. 1986)**

saddle (Figure 16). The minimum water depth on Makkovik Bank is 85 m on the Bank's western margin. The detailed bathymetry of the Bank is presented on Chart 1.

The Labrador Shelf Drift Formation is generally less than 50 m thick on the top of Makkovik Bank but may increase to as much as 150 m along the Bank margin (NORDCO 1984). On the Bank top, where the Lower Tills are exposed at the surface, they are usually capped by a thin surface lag.

The contact between the Lower Tills (Unit 3a) and Upper Till (Unit 3b) is always sharp, smooth, and laterally continuous suggesting erosion by an intervening glacial advance (Josenhans et al. 1986). The Upper Till is not evident on the top of Makkovik Bank but instead overlies the more extensive Lower Tills along the western Bank edge pinching out before the Bank top. The Upper Till surface is usually iceberg scoured with an undulating relief of about 4 m. This topography is interpreted to have formed by iceberg scouring at the margin of the ice sheet during glacial retreat (Josenhans et al. 1986). Samples of the Upper Till indicate a homogeneous, poorly sorted, sandy mud with gravel and boulders. The unit is slightly overconsolidated with average shear strengths of about 20 kPa, water content of 25% to 30% dry weight, bulk density of 1.8 to 1.9 g/cc, liquid limit of 34%, and plastic limit of 16% (Josenhans et al. 1986).

Qeovik Silt (Unit 4) overlies the Labrador Shelf Drift Formation. It has a conformable depositional style which mimics the underlying till surface (Josenhans et al. 1986). The unit is much less competent than Labrador Shelf Drift, being characterized by shear strengths of 4 to 18 kPa, water content of 20% to 60% and bulk densities ranging between 1.3 and 1.9 g/cc (Josenhans et al. 1986). It occurs around the periphery of the Bank and extends deep into the surrounding trough. In areas of less than 230 m water depth, the surface layer has been reworked by iceberg scouring. This reworking becomes increasingly evident with decrease in water depth up the bank slope. Reworking by icebergs in waters deeper than 230 m is interpreted to represent relict scouring activity (Todd 1984; Todd et al. in press; Josenhans and Zevenhuizen 1984).

On some parts of Makkovik Bank, the Lower Tills are overlain directly by Sioraq Sand (Unit 5b). It is derived by winnowing from the underlying till and ice rafted debris, appearing as a patchy veneer of fine to muddy sand with some gravel. The unit exhibits highly variable geotechnical properties (Josenhans et al. 1986) and consists predominantly of sand-sized material (Gilbert and Barrie 1985). The detailed surficial geology of Makkovik Bank is illustrated on Chart 2.

METEOROLOGIC AND OCEANOGRAPHIC SETTING

In a normal August, six to eight weak, low pressure disturbances track east-northeastward through the Newfoundland and Labrador region. Most of these systems continue across the Labrador Sea passing south of Greenland, but about 30% to 40% curve northward and move into the Davis Strait region (eg., Bursey et al. 1977). These frontal systems are relatively benign during the summer months. The low pressure systems are followed by periods of generally fair weather associated with subsidence in cells or ridges of higher atmospheric pressure.

The most frequent wind direction during August is from the north to northwest for Hopedale and the north Labrador

Coast and north Labrador Sea marine areas and from the south-southwest to south-southeast for Cartwright and the south Labrador Coast and south Labrador Sea marine areas (Atmospheric Environment Service 1984). Makkovik Bank, lying mid-way along the Labrador coast, would be expected to have, on average, about equal probability of winds from the north and the south during August. Mean wind speed during August for the Makkovik Bank area is 14.6 kts (27.0 km/hr) and gales (winds of 34 knots or more) usually occur about 2% to 3% of the time.

The wave climate of the ice-free period over Makkovik Bank, which normally extends from the end of June until near the end of December, is not well known. Normally, the frequency distribution of significant wave heights in August shows only a slight increase in occurrence of higher waves than in July, when sea states are lowest. The increasing intensity of cyclonic weather disturbances during the fall months results in significantly higher average sea states beginning in September (Atmospheric Environment Service 1984). Along the mid-Labrador coastal region, median significant wave height during summer is typically 1.0 to 1.5 m, whereas during late autumn it is about 2.0 to 3.0 m (Atmospheric Environment Service 1984).

Makkovik Bank is situated between two southward geostrophic current flows produced by sharp density gradients (Smith 1931). The inshore flow follows the contours of the Labrador Marginal Trough. This flow exists because of a low density water mass adjacent to the coast with colder and lower salinity water properties than on Makkovik Bank. The offshore flow follows the continental slope and is produced by a density gradient between the cold, low salinity water on the Labrador Shelf and the warmer, more saline water of the Labrador Sea.

The currents around the edge of Makkovik Bank are much stronger than on the Bank itself, where the currents are relatively weak and variable (NORDCO Limited 1980). The current is composed of tidal components, direct wind effects, inertial effects, low frequency oscillations, and internal density adjustments. Spectral analysis of the data show that the energy is mainly concentrated in two broad frequency ranges; a low frequency band, and a tidal and inertial band (Fissel and Lemon 1982). The low frequency variations have the greater contribution to the current flow. The low frequency component has a period of between 4 and 5 days (NORDCO Limited 1979).

On Makkovik Bank, the tidal current has semi-diurnal and diurnal components that are comparable in magnitude. The M_2 constituent is of the order of 7 to 10 cm/s and the K_1 constituent is about 6 cm/s (NORDCO Limited 1979). The tidal ellipse has been found to be circular indicating no preferred tidal current direction (Fissel and Lemon 1982). The tidal currents change relatively little with depth with respect to amplitude and degree of circular polarization.

The mean current speed on Makkovik Bank is about 14 cm/s, whereas the mean southward velocity is of the order of a few centimetres per second because of the oscillatory nature of the flow. From current measurements by NORDCO Limited in 1979, it was noted that the highest speeds at all depths occurred during times when the winds increased. From observations made in 1980 (NORDCO Limited 1980), the maximum current speeds at depths 25 m, 55 m, and near bottom were 77 cm/s, 47 cm/s, and 33 cm/s respectively (Fissel and Lemon 1982).

Water masses from various sources are present on the Labrador Shelf. Smith et al. (1937) have provided the standard description of the oceanography of the Labrador Sea area. A shallow layer of relatively warm, low salinity water derived from local runoff, ice melt and from Hudson Strait prevails near the coast during the summer months. At greater depths and inshore of the banks, cold, low salinity water from the Canadian Arctic exists. East of the banks the water is relatively warm and saline as a result of contributions from the West Greenland Current. This water mass is frequently present over the banks and in the saddles to a depth of 300 m. Seaward of this water mass is the even warmer saline water mass of the Labrador Sea.

In a normal year, pack ice clears from the Makkovik Bank area about the first of July but in unusually severe years, ice has persisted until the beginning of August (Sowden and Geddes, 1980). The 1985 ice season was relatively severe on the east coast with final clearing of the Bank occurring in the last week of July, shortly before the DIGS experiment began. Normally, the first incursion of pack ice occurs over the Bank in the fourth week of December.

Icebergs drifting southeastward with the Labrador Current are found in highest concentrations during the late spring. Gustajtis and Buckley (1977) indicate the average density of icebergs in spring is more than 20 per 0.25° latitude-longitude square in the vicinity of Makkovik Bank. Relatively rapid deterioration during the warm season results in concentrations of about 2 to 10 icebergs per 0.25° square during an average summer and one to five in an average fall on the Bank.

CHAPTER 3

ICEBERG OBSERVATIONS AND RELATED DATA

METEOROLOGIC AND OCEANOGRAPHIC DATA

Winds and Weather

The meteorologic observation program aboard the *Polar Circle* is described in Chapter 1. Data from the primary meteorological observations are presented in a tabular format along with time series plots and histograms in Appendix 3. A brief discussion of these data follows.

The time series plots of mean sea level (MSL) pressure observed aboard the *Polar Circle* show that the Makkovik Bank region was affected by five low- and high-pressure systems during the first three weeks of August 1985. Using the mean wind speed as a measure of the strength of the average pressure gradient over the region, the intensity of these weather systems appears to have been slightly weaker than usual, as may be inferred from an examination of surface weather charts for the period. The scalar mean wind speed was 13 kts (24 km/h) while the August climatological scalar mean speed for the area was 14.6 kts (27.0 km/h). Exceedence of observed wind speed compared with the climatological norm (Atmospheric Environment Service 1984) is plotted in Figure 18.

The lower than normal frequency of winds in excess of 30 kts may be, in part, an artifact of the observational period: mean speeds are likely to be higher toward the end

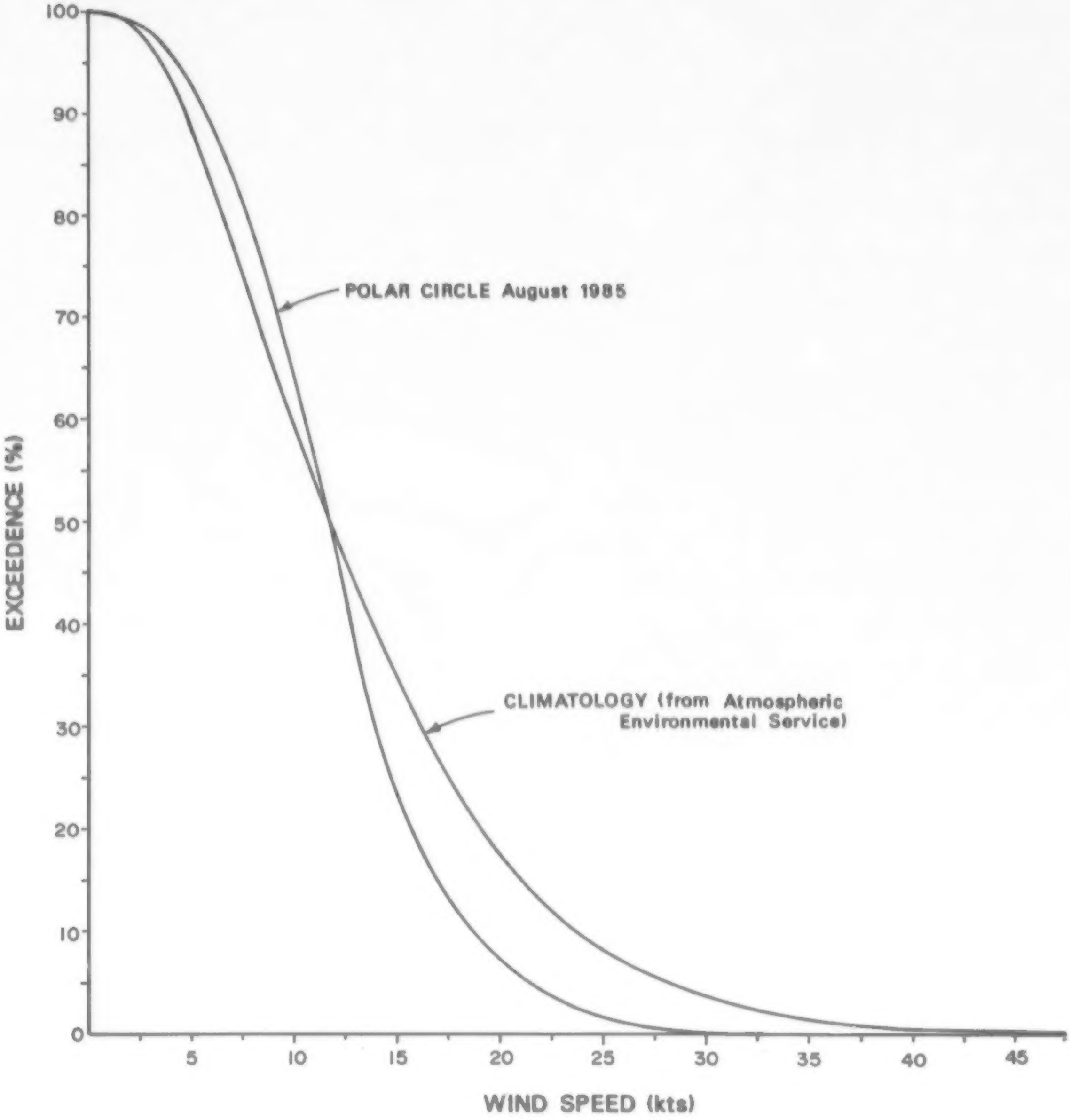

Figure 18. Percent exceedence of wind speed.

of the month as a consequence of the normal increase in intensity of weather disturbances toward the end of summer.

The 1985 measurements show winds were from the west to north nearly 40% of the time and about 35% of the time from the east-southeast to south-southwest.

Evidence of a more frequent occurrence of a relatively dry flow off Labrador and across the cool waters to the north of the Makkovik Bank is seen in the summary statistics for visibility. Table 6, which was derived from the data in Appendix 3, compares the visibility observations from the Polar Circle with the climatological statistics for the South Labrador coast marine area (Atmospheric Environment Service 1984), which includes Makkovik Bank.

Surface air temperatures recorded from the Polar Circle during the experiment appear to be near the climatological norm for the period. The highest temperature observed was 17°C and the lowest was 3°C.

Waves

Sea wave and swell observations were made visually every three hours along with the standard marine synoptic weather observations (MANMAR). These estimates were supplemented by measured wave data from a Datawell Waverider buoy which was deployed on the northwest section of Makkovik Bank at latitude 55°42'45"N, longitude 58°12'11"W on August 3, 1985. One-dimensional spectra observations were made at half-hour intervals, however, the data set is incomplete primarily because of ship movement beyond the range of signal reception.

Table 6

FREQUENCY OF VISIBILITY OBSERVATIONS

Visibility	MV *Polar Circle* August 1985 (%)	Climatology* August (%)
<0.5 naut mi (<0.9 km)	7.1	11.0
<1.1 naut mi (<2.0 km)	8.4	14.0
<2.2 naut mi (<5.4 km)	9.1	18.2
<5.4 naut mi (<10.0 km)	19.5	28.5
≥5.4 naut mi (≥10 km)	80.5	71.5

---

* Atmospheric Environment Service 1984.

Time series plots, scatter diagrams and histograms of primary wave parameters are given in Appendix 4. The appendix also contains a listing of root mean square wave heights (in metres) tabulated by wave period for each measurement.

Exceedence of significant wave height for all measurements obtained from the Waverider buoy during the DIGS experiment is plotted in Figure 19. The 50% exceedence level was 1.3 m and the 10% value was 2.3 m. These may be compared with the estimated offshore wave climatology for the region which shows that the 50% and 10% values are approximately 1.7 m and 3.3 m respectively. The maximum significant wave height recorded by the Waverider buoy during the experiment was 3.4 m. While the data set is discontinuous, these statistics tend to support the earlier suggestion that the winds over Makkovik Bank during August 1985 were lighter than normal for this period.

Currents and Tides

Bottom currents were measured on the western side of Makkovik Bank by an Interocean S4 current meter placed in a bottom stand at Mooring 1 (Chart 3). The currents were measured at about 1 m above bottom in a water depth of 120 m for 17 days. The data show a strong tidal current with periods of diurnal and semi-diurnal frequency. At this depth the tidal current was usually aligned in an east-west direction. The mean velocity was south-southwest at 3.6 cm/s. The current had a mean speed of 9.4 cm/s and a maximum of 33.2 cm/s which occurred on August 15. The higher speeds, above 25 cm/s, occurred on August 4, 15, 16, and 17. A detailed summary of these data is provided in Appendix 5.

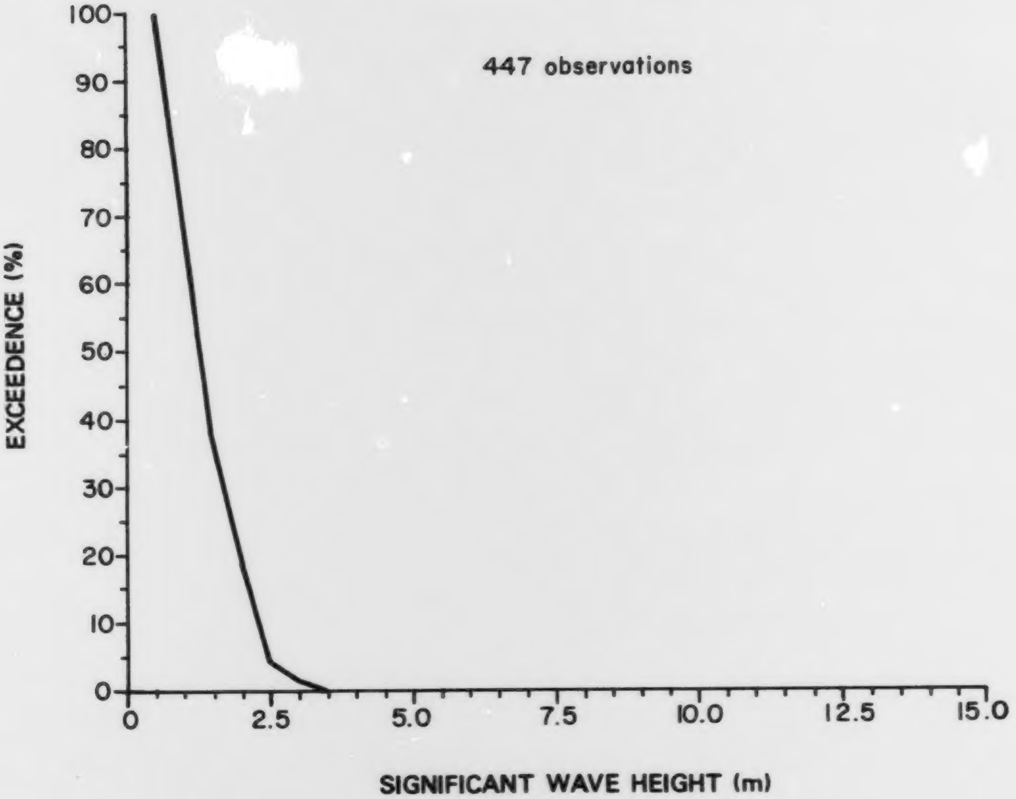

Figure 19. Percent exceedence of significant wave height.

Unfortunately, no velocity profiles were acquired because of problems with the Ametek Straza Doppler Current Profiler as discussed in Chapter 1.

Tidal measurements were made with two bottom mounted Aanderaa tide gauges at Moorings 1 and 2 (Chart 3). The 20-day records show the tides to be mainly semi-diurnal. The minimum range for the period was about 0.45 m on August 10; the maximum range recorded was nearly 2.0 m on August 19 with the moon in perigee three days after the new moon. The tide traces are presented in Appendix 5.

Water Properties

Temperature and salinity profiles (see Appendix 6) were obtained with a Neil Brown DRCM profiler aboard the Polar Circle. Significant differences in the traces are seen in the near-surface waters, whereas little variation is seen below 30 m. Appendix 6 also contains time series plots of bottom temperature measurements at Mooring 1 (depth 120 m) and Mooring 2 (180 m). Although temperatures remained near -1.60°C at both stations, the time series at the deeper location (Mooring 1) showed greater variability.

Sea Ice and Icebergs

During the DIGS experiment sea ice was not a consideration on Makkovik Bank as it had cleared from the area during the last week of July, shortly before the start of the field program. An operational flight conducted on July 29 by the Atmospheric Environment Service (AES) indicated the presence of a large number of icebergs along the Labrador coast.

Numerous icebergs during the month of August provided an opportunity to assess their size and trajectories in an effort to define those likely to ground. Chart 4 illustrates the drift tracks of icebergs based on radar sightings during the field program. The highest concentration of icebergs occurred around the periphery of the Bank, primarily along the northern and eastern edges. This distribution partially reflects the amount of time spent in these areas by the survey vessel. Icebergs associated with the Bank periphery illustrate a consistent drift orientation generally parallel to isobaths, suggesting strong influence by bathymetry-controlled currents. The iceberg population on the Bank top indicates a random drift pattern suggesting a varied current regime as described in Chapter 2.

The iceberg density for the study period is estimated from the radar plots to be about three to four icebergs per square 0.25° latitude-longitude (773 km^2). This observation compares favourably with Gustajtis and Buckley (1977) who estimate two to ten icebergs per 0.25° square for an average summer on Makkovik Bank.

SUMMARY OF DATA ON ALL ICEBERGS INVESTIGATED

Throughout the field program all data on iceberg locations were filed on data tape and hard copies were prepared for the various time frames. The iceberg drift tracks extracted from these data are presented on Chart 4. The trajectories for the 11 "code-named" icebergs are presented in greater detail on Chart 5.

All iceberg plots, photographs, colour video tapes, and associated data tapes are archived at the Atlantic Geoscience Centre (AGC).

Although all icebergs seen on ship's radar were tracked, only those selected for additional investigation (e.g., draft measurement) were "code named". A brief chronological description and a summary of the data collected on each named iceberg is given in the following sections. This compilation was made from several sources and incorporates analysis of photographic and other records. A table summarizing the observations and data collected accompanies the description of each iceberg. Also, a summary of all iceberg deterioration observations is given in Appendix 7. All times are given in GMT.

Above-water measurements were estimated from Polaroid photographs taken from the Polar Circle using the height measured from the helicopter's radar altimeter as a known dimension. The mass of each iceberg reported in this section was calculated using the formula: $M = 3 \times L \times W \times H$ where L and W are maximum waterline length and width, respectively, and H is maximum height (Robe and Farmer 1975).

Iceberg "Anastasia"

Data collected for iceberg "Anastasia"

Data collected	August 2	August 4
Height(m)		35
Width (m)	90	
Length (m)	220	
Draft (m)		110 (approx.)
Mass (10^6 tonnes)	2.1	
Photographs		
Slides		8
Polaroid	1	
Video		approx. 10 min
Wave height(m)		
Minimum	0	1
Maximum	1.5	1.5
Wind speed (kts)		
Minimum	5	14
Maximum	14	18
Grounded		Until 1645 GMT.
Drift track: 3-5 August		

2 August. "Anastasia" was located by helicopter.

3 August. Radar tracking of icebergs continued. The ship stood by in the area to plot trajectories for observation of grounded icebergs and to track the general flow regime.

4 August. Draft measurements indicated 105 to 107 m on one side, 120 m on the other and suggested that the iceberg was grounded.

Preparations were made for C-CORE motion sensor package deployment. Before deployment and without prior warning by calving, "Anastasia" rolled, at about 1645 GMT. After this roll the iceberg was again free-floating. It first moved to the southeast, then to the northeast, as indicated on Chart 5. Numerous photographs were taken of this iceberg before, during, (Figure 20) and after its roll. In addition, the roll was recorded on videotape which is archived at AGC.

A number of survey lines run over the initial iceberg location using the 50-kHz and 100-kHz sidescan sonars and the Huntec DTS system failed to provide any conclusive evidence of seabed disturbance. A sidescan mosaic was constructed for the area between icebergs "Anastasia" and "Deborah". The mosaic is discussed in Chapter 4.

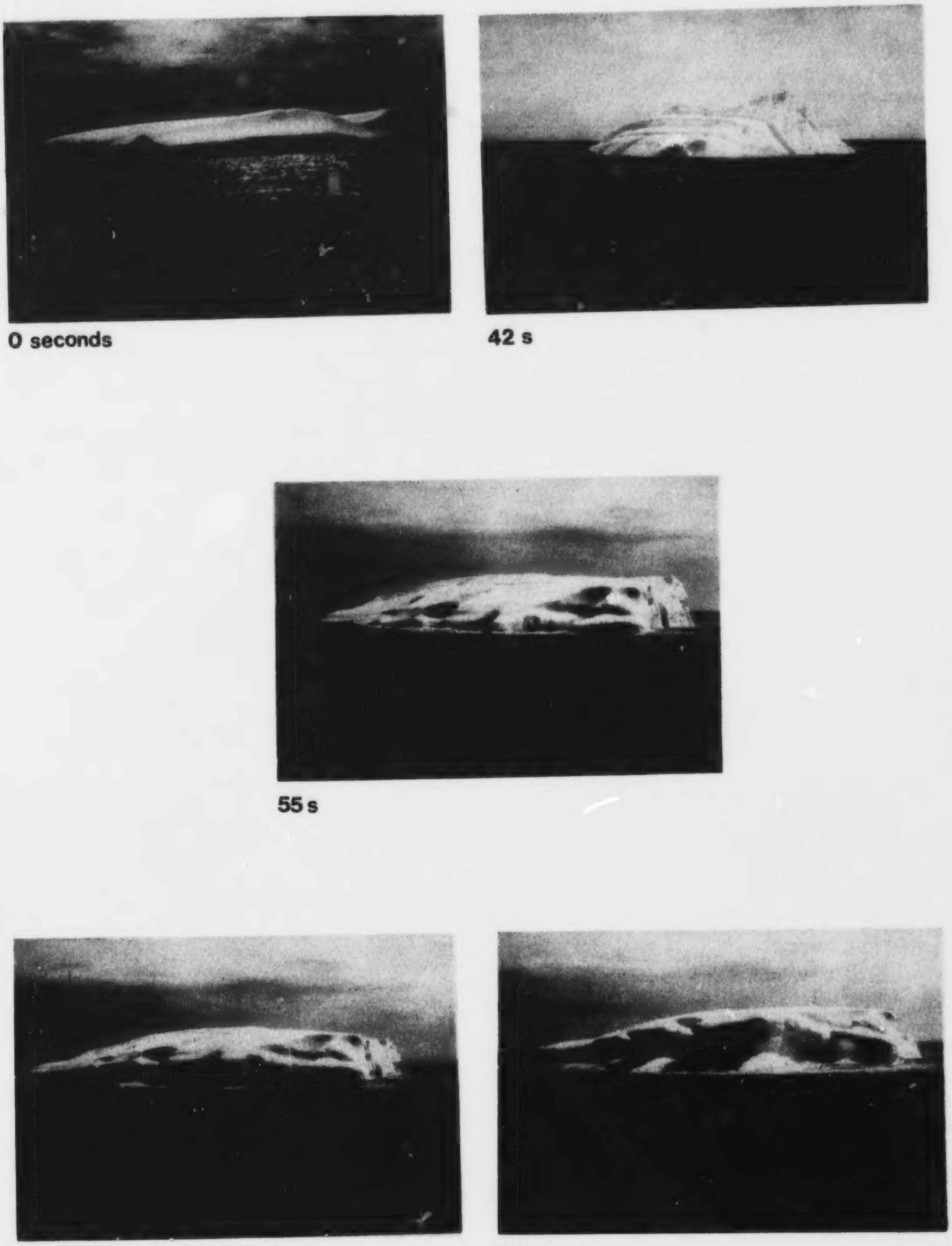

0 seconds

42 s

55 s

60 s

68 s

Figure 20. "Anastasia" roll sequence.

Iceberg "Bertha"

Data collected for iceberg "Bertha"

Data collected	August 4	August 5	August 6
Height (m)		31	
Width (m)	80	135	
Length (m)	140	160	
Draft (m)		107	115
Mass (10^6 tonnes)		2.0	
Photographs			
Colour		7	25
Slides		2	5
Aerial		14	
Polaroid	1	1	5
Stereo pairs		X	*
Profiles			
Above-water		X	
Below-water			X
Wave height(m)			
Minimum	1	0.5	0
Maximum	1.5	1.5	1
Wind speed (kts)			
Minimum	14	3	5
Maximum	18	17	16
Grounded	X	until 1030 GMT	

Drift track: 3-6 August

* Waterline stereos

Note: changes in width, length and draft reflect the results of calving and melting over the period of observation.

4 August. At 2350 GMT, the C-CORE motion sensor package "D" was deployed on "Bertha".

5 August. "Bertha" was found to be grounded in 107 m of water. Preparations were made for underwater dimensioning early in the day; however, at about 1030 GMT "Bertha" calved, rolled approximately 30°, yawed approximately 90°, and floated free (see Appendix 7). The free-floating iceberg drifted to the northwest, as shown on Chart 5. Although loud cracks could be heard on numerous occasions, the iceberg remained stable for the rest of the day. A second attempt to obtain the underwater profile of this iceberg was aborted when the profiling rope became tangled in the ship's propellor. "Bertha's" circumference was measured as 420 m.

The motion sensor package stopped transmitting at about 1500 GMT and was retrieved at 1905 GMT.

Numerous photographs were taken throughout the day including a set of aerial stereo photographs taken at 1614 GMT which were subsequently used for the determination of above-water shape.

6 August. During the night and early morning a series of survey lines were run over the "Bertha" grounding site and drift path using sidescan sonar (50-kHz and 100-kHz), sub-bottom profiler and BRUTIV. The seabed data indicated a series of four or five pit-like features which were later investigated by the Pisces IV submersible. These pits are believed to have formed during the roll/free-float event on August 5, which is described in more detail later in this chapter.

Because of difficulties with rope handling, underwater profiling was delayed until 1530. The draft was estimated as 115 m at this time. Between the stereo photography flights on August 5 and the completion of underwater dimensioning, a calving event at about 0945 GMT removed much of one end of the iceberg resulting in a small tilt of approximately 2°.

At 1704 GMT "Bertha" underwent another maior calving and rolling event. A photographic record of the entire event was obtained (see Appendix 7).

Iceberg "Cordelia"

Data collected for iceberg "Cordelia"

Data collected	August 7
Height (m)	60
Width (m)	160
Length (m)	240
Draft (m)	177
Mass (10^6 tonnes)	6.9
Photographs	
Colour	2
Slides	3
Polaroid	4
Wave height(m)	
Minimum	0.1
Maximum	1
Wind speed (kts)	
Minimum	5
Maximum	15

Drift track: 7 August

7 August. The draft of this large free-floating tabular iceberg was measured by OSPS using the profiler. Height was measured by radar altimeter, and other linear dimensions were measured from photographs using height as a known dimension. Water depth was 250 m in the area.

There was a calving event at about 1200 GMT (see Appendix 7) and temperatures were obtained from four growlers. No further investigations were carried out on this iceberg because radar plots indicated a trajectory parallel to the northeastern Bank edge (Chart 5) making "Cordelia" an unlikely grounding candidate.

Iceberg "Deborah"

Data collected for iceberg "Deborah"

Data collected	August 7
Height (m)	70 (approx.)
Draft (m)	112
Photographs	
Colour	1
Slides	1
Polaroid	3
Wave height(m)	
Minimum	0.1
Maximum	1
Wind speed (kts)	
Minimum	5
Maximum	15

Drift Track: 7-9 August

7 August. This large pinnacled iceberg was located on the north central Bank edge in about 140 m of water. Its draft was measured by OSPS using the profiler. Height was obtained using radar range and angular height measured by sextant. Initial radar information suggested the possibility of grounding, however, following a re-evaluation of the iceberg trajectory (Chart 5), a decision was made to leave the area. Later in the program a series of survey lines were run between this position and that of "Anastasia" and a mosaic of the area assembled. The mosaic is described in detail in Chapter 4.

Iceberg "Erica/Hermione"

Data collected for iceberg "Erica/Hermione"

Data collected	August 8	August 13
Height (m)		52
Width (m)		200
Draft (m)	132	132
Photographs		
Colour		3
Slides	2	1
Polaroid	X	1
Wave height(m)		
Minimum	1	1
Maximum	2	5
Wind speed (kts)		
Minimum	15	16
Maximum	25	26
Grounded	X	X

Drift track: 9-13 August

8 August. "Erica" was grounded in 132 m of water when found and is thought to be iceberg "Hermione", later identified on August 13. This conclusion is based on morphological similarity and the fact that they had identical locations. Photographs were taken of the iceberg, however, no further investigations were carried out because of the presence of more promising candidates to the south.

13 August. Dimensions were taken from the Polaroid photograph. The iceberg was still aground in 132 m of water (see Chart 5 for location). It was decided to search for a free-floating iceberg likely to scour.

Iceberg "Frieda"

Data Collected for iceberg "Frieda"

Data collected	August 5	August 7	August 8	August 9
Height (m)	40			
Width (m)	160			
Length (m)	200			
Draft (m)			123	
Mass (10^6 tonnes)	3.8			
Photographs				
Colour			3	3
Slides			3	4
Aerial		12	X	
Polaroid	1	1	1	
Wave height (m)				
Minimum	0.5	0.1	1	0
Maximum	1.5	1	2	2
Wind speed (kts)				
Minimum	3	5	15	7
Maximum	17	15	25	15

Drift track: 8-11 August

8 August. Both "Frieda" and "Gladys" were tabular icebergs within 1 km of one another on the southeastern corner of Makkovik Bank (Figure 21). Water depth in the area was about 147 m and "Frieda's" draft was measured at 123 m. A major calving event at about 1430 GMT resulted in a measurable tilt of the iceberg (see Appendix 7). Sediment samples were obtained from the top of the iceberg late in the evening (Figure 22).

9 August. About 0900 GMT a major calving event resulted in production of two fragments constituting separate radar targets (see Appendix 7). These targets were tracked for as long as they were within range (see Chart 4).

10 August. At 1000 GMT "Frieda" split in half (see Appendix 7). The two ram fragments released August 9 were still visible on radar at about 10 km distance. That is, within 25 hours, "Frieda" had split into four major pieces.

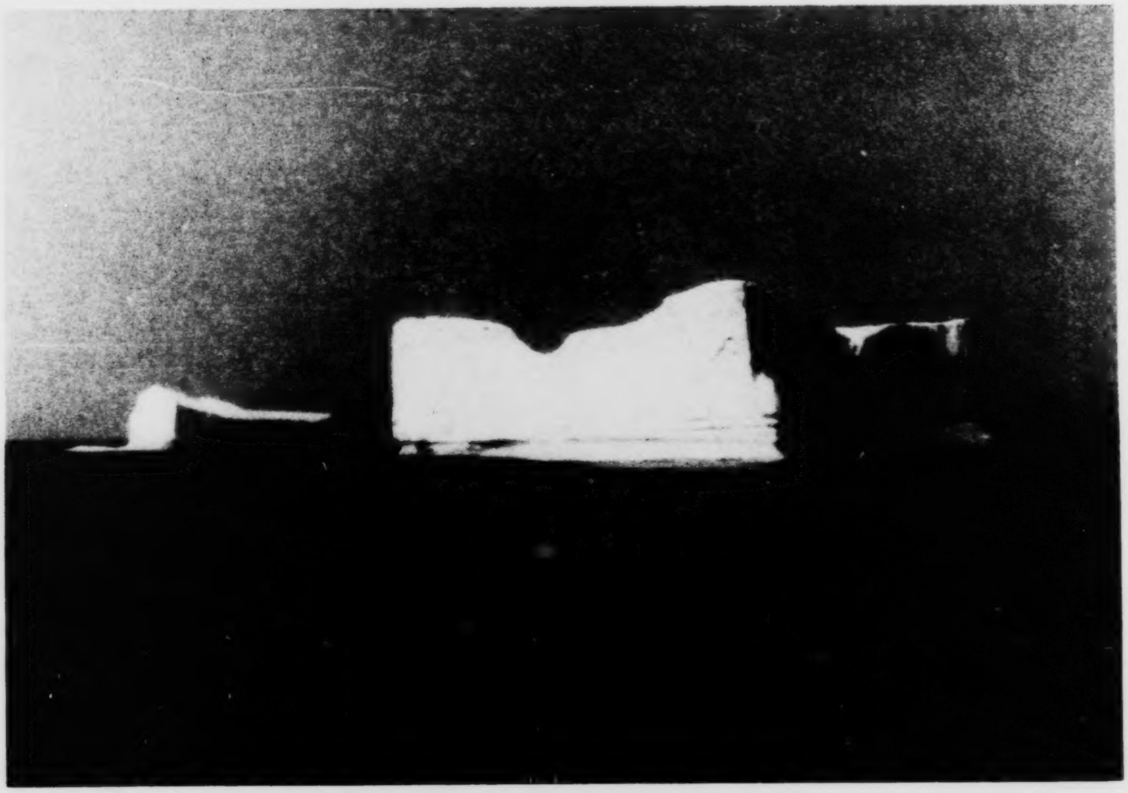

Figure 21. Icebergs 'Frieda' and 'Gladys'.

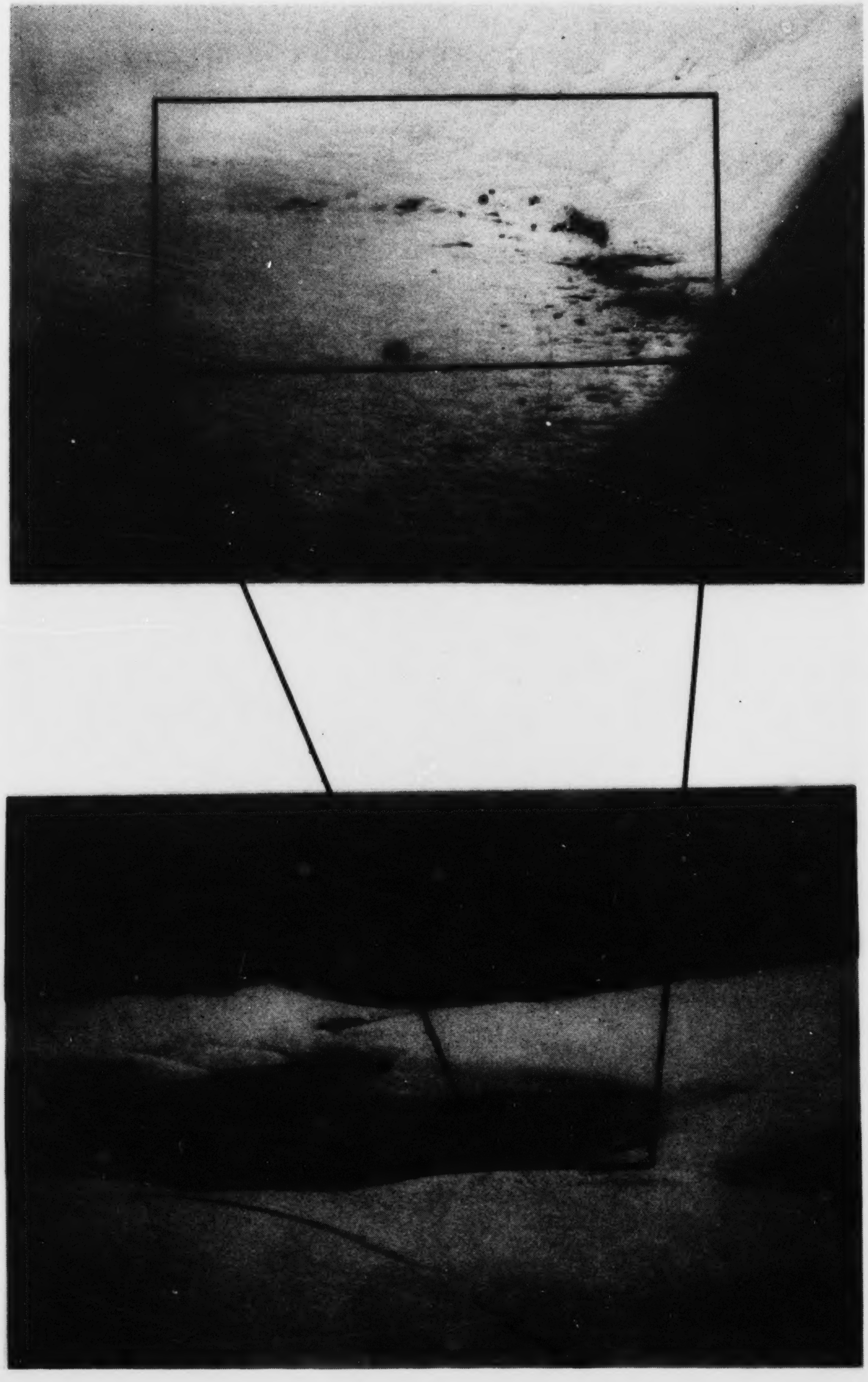

Figure 22. Sediment on iceberg "Frieda".

Iceberg "Gladys"

Data collected for iceberg "Gladys"

Data collected	August 5	August 7	August 8	August 9	August 10	August 11
Height (m)	70		60			
Width (m)	170		170		230	
Length (m)	250		250		300	
Draft (m)			132/142[a]	142	134	134
Mass (10^6 tonnes)	8.9		7.7			
Photographs						
Colour			3	7	11	6
Slides						
Aerial		11	25		12/9[b]	
Polaroid	2	1	1			4
Stereo pairs			X		X/X[b]	*
Profiles						
Above-water			X		X	
Below-water						X
Wave height (m)						
Minimum	0.5	0.1	1	0	1	0
Maximum	1.5	1	2	2	1	1.5
Wind speed (kts)						
Minimum	3	5	15	7	5	10
Maximum	17	15	25	15	11	17
Grounded (after split)					X	X
(still aground on August 22)						
Drift track: 8-13/22 August						

* - Waterline stereos.

a - Before/after roll.

b - Two halves after split.

Note: Changes in height, width, length, draft and mass reflect the results of calving and melting over the period of observations.

8 August. It was thought that "Frieda" and "Gladys" had recently split from a single iceberg. Evidence to support this included 1) a general morphological similarity between the two, 2) their close proximity and 3) the presence in both of them of a distinctive yellow banding.

"Gladys" was triangular in shape with deep crevasses running parallel with one side. From the above-water dimensions obtained from scaled photographs the mass was calculated as 8.9 million tons on August 5, decreasing to 7.7 million tonnes on August 8 as a result of calving and melting.

Measurements of the draft of the iceberg ranged from 120 m to 132 m in about 147 m of water suggesting that the iceberg was not grounded. A later draft measurment (at 2048 GMT after a minor roll) of 142 m suggested that "Gladys" might be grounded, but the iceberg continued to move (see Chart 5) and no scour was observed on sidescan records covering the observed trajectory (Figure 23).

Motion sensor package "D" was deployed on "Gladys" at 2233 GMT in anticipation of the iceberg grounding. Aerial stereo photographs were taken after this.

9 August. Underwater dimensioning was begun and a circumference of 750 m obtained. A major calving event around 1530 GMT (see Appendix 7) resulted in the abandonment of profiling efforts when a cascade of ice pushed the line away from the iceberg resulting in the shearing of the profiling rope. A draft measurement was made at 2130 GMT indicating that "Gladys" was possibly aground in 142 m of water.

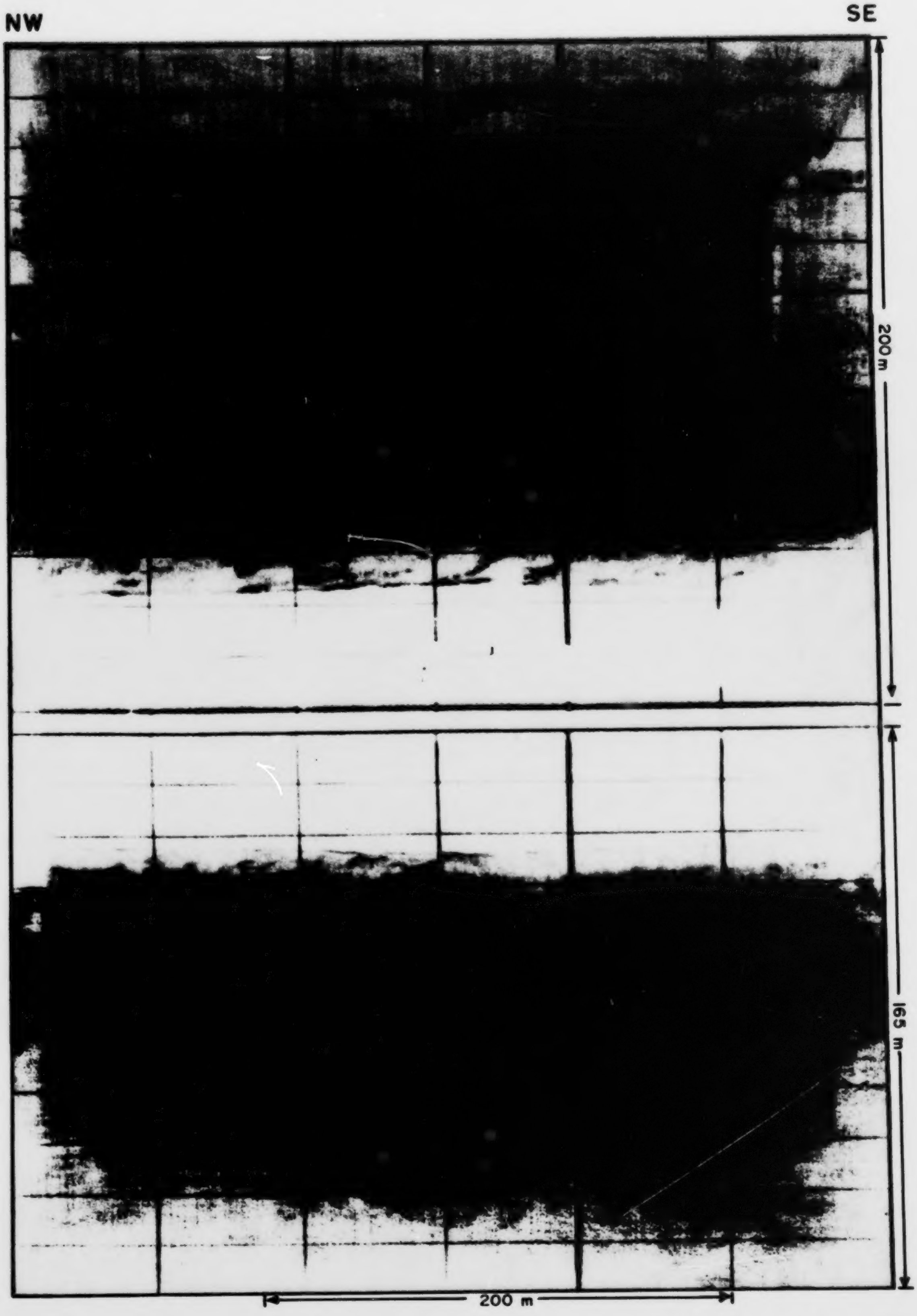
NW
SE
200 m
165 m
200 m

Figure 23. A sidescan sonogram from line 42 illustrating the acoustic image received from iceberg 'Gladys'. Available data indicate no evidence of seabed disturbance.

A problem with the telemetry unit necessitated recovery of the motion sensor package at 2017 GMT, with redeployment at 2336 GMT.

10 August. About 1300 GMT "Gladys" underwent a moderate calving event resulting in a roll of about 5 to 10°.

At about 1320 GMT "Gladys" split, resulting in a large number of growlers and two sizeable icebergs (Figure 24 and Appendix 7). The C-CORE package was located on the larger of the two main fragments which grounded solidly in 134 m of water after rolling through about 30°. The other main fragment drifted away, first to the northwest and then to the southeast (see Chart 5). A complete description of the "Gladys" splitting event, including a photographic sequence, is contained in Appendix 7.

The pre-splitting calving events interfered with attempts to measure the below-water profile of the original iceberg. Aerial stereo photographs of the two main fragments of "Gladys" were taken at about 2100 GMT. At about the same time a small calving event resulted in the production of a number of sediment-laden growlers, probably originating from the grounded keel (see Appendix 7).

11 August. Below-water dimensioning was carried out from approximately 1220 to 1850 GMT. Calving events are described in Appendix 7.

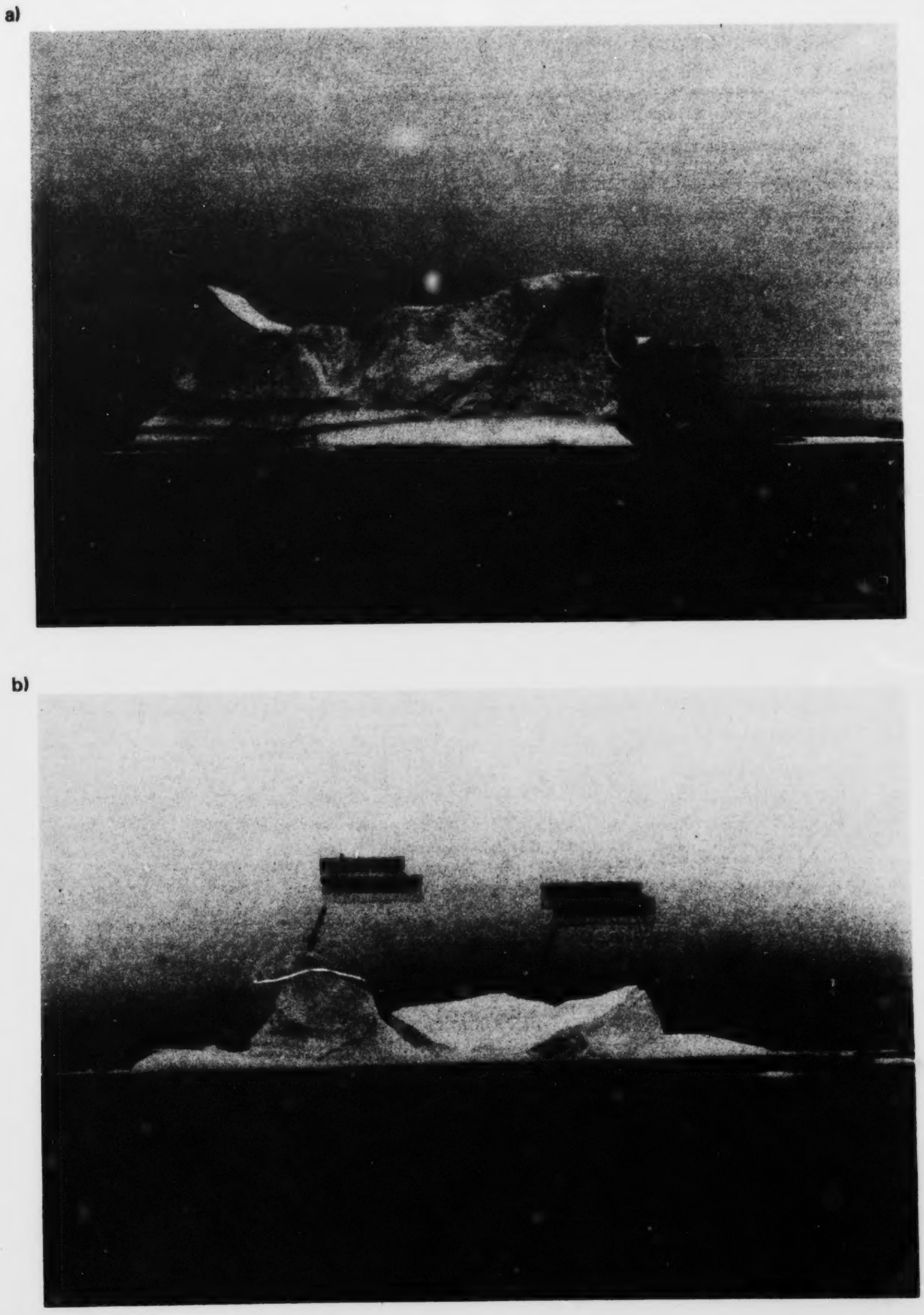

Figure 24. "Gladys" before and after split.

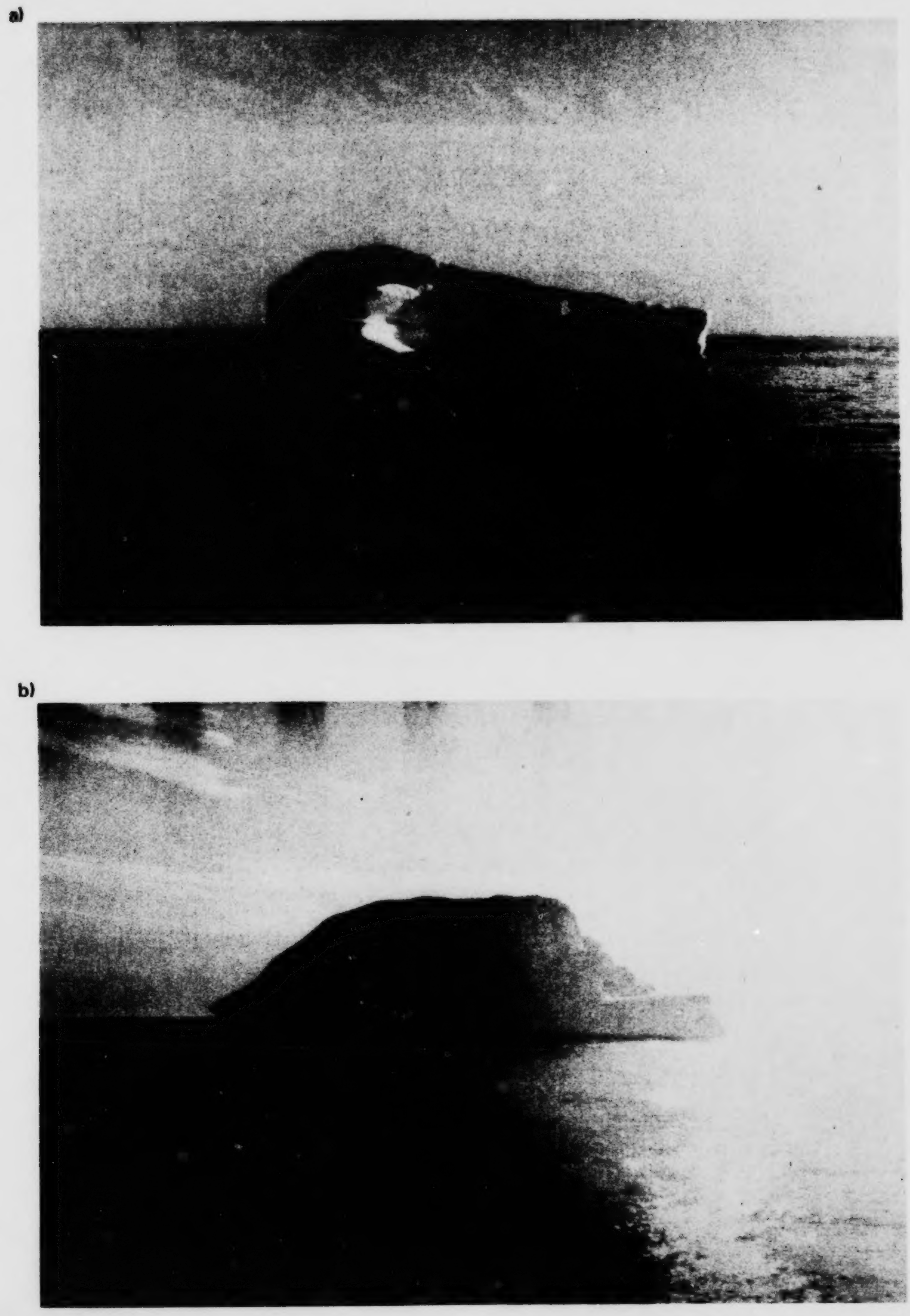

Figure 28. Surface photographs of "Bertha".

12 August. No major change in the orientation of the iceberg resulted from the numerous calving events throughout the day (see Appendix 7). The C-CORE instrument package stopped transmitting at 0910 GMT and was retrieved at 1830 GMT.

Numerous survey lines were run using sidescan sonar and Huntec DTS allowing the assembly of a sidescan composite of the area which is discussed later in the text. Attempts to gain video information using the ROV met with limited success because of strong currents and mechanical complications.

13 August. At about midday, survey lines were run between the "Gladys" grounding site and the Datasonics beacon northwest of the site using the Huntec DTS and 100-kHz sidescan sonar.

22 August. Polar Circle returned to the "Gladys" site in hopes that the iceberg had drifted free and that survey lines could be run in the area. Unfortunately, the iceberg was still grounded in its original position, and the scour/pit could not be surveyed. Pandora II was informed of the situation as they had planned a submersible dive for this location. A comparison of aerial photographs taken at this time with those taken when the iceberg was first grounded revealed that significant deterioration had taken place, but with little effect on the overall orientation of the iceberg.

Iceberg "Isadora"

Data collected for iceberg "Isadora"

Data collected	August 13
Draft (m)	115
Photographs	
Slides	2
Wave height (m)	
Minimum	1
Maximum	5
Wind speed (kts)	
Minimum	16
Maximum	25

Drift track: 12-14 August

13 August. The iceberg was encountered in 160 to 170 m of water, but a draft measurement indicated that it was unlikely to ground. The iceberg was in the shape of a small, high plateau surrounded on three sides by an extensive, low apron. A sounding was taken from the lowest side. No further work was carried out on this iceberg because of deteriorating weather conditions.

Iceberg "Julianna"

Data collected from iceberg "Julianna"

Data Collected	Aug. 2	Aug. 3	Aug. 16	Aug. 18	Aug. 19	Aug. 20	Aug. 21
Height (m)	67	70		75	68		
Width (m)		250			260		
Length (m)		360			290		
Draft (m)			147			170+	
Mass (10^6 tonnes)		19			15		
Photographs							
Colour			2	X			
Slides			2		3		2
Aerial		26			7		
Polaroid	1	1			2		
Stereo pairs		X			X		
Profiles							
Above-water					X		
Below-water						X	
Wave height(m)							
Minimum	0	0		1	1	0	
Maximum	1.5	1		2	1.5	1.5	
Wind speed (kts)							
Minimum	5	6		3	5	3	
Maximum	14	16		12	16	14	
Grounded			X	X	X	X	

Drift track: 7 and 16-18 August

Note: Changes in height, width, length, draft and mass reflect the results of calving and melting over the period of observation.

16 August. Operations resumed early in the day, although visibility had not improved sufficiently to permit helicopter flying. Two large icebergs were identified by radar on the northwest corner of Makkovik Bank. The drafts of both were measured. "Julianna", a large tilted tabular iceberg, was thought to represent the reduced remains of a very large iceberg sighted during a reconnaissance flight on August 2 (see Appendix 7). An extrapolated trajectory is presented on Chart 5.

18 August. Simultaneous operations were undertaken on both "Julianna" and "Lucretia" (see below).

19 August. The C-CORE motion sensor package "C" was deployed on "Julianna" at 1740 GMT, and aerial stereo photographs were taken at 2100 GMT.

20 August. The circumference was measured at about 650 m. Underwater profiling suggested that "Julianna's" draft exceeded 170 m, and that the iceberg was probably aground. A check of the iceberg trajectory charts show that "Julianna" had not moved since intensive investigation began on August 18.

Polar Circle kept position near both "Julianna" and "Lucretia" during the night to monitor signals from both sensor packages. "Lucretia" moved slowly out of range.

21 August. "Julianna" rolled through 10° at about 0115 GMT. There were several small calving events later in the morning. The iceberg remained grounded throughout the day. The C-CORE sensor package stopped transmitting at 1900 GMT and was retrieved at 2300 GMT.

A series of survey lines was run in the vicinity of "Julianna" with Ametek Straza data collected simultaneously. Unfortunately, the water was too deep to acquire corrected sidescan data suitable for mosaicing purposes.

Iceberg "Kit Kat"

Data collected for iceberg "Kit Kat"

Data collected	August 16
Height (m)	65 (approx.)
Width (m)	260
Draft (m)	105
Photographs	
Slides	2
Polaroid	2

Drift track: 16 August

16 August. This iceberg was the second encountered to the northwest of Makkovik Bank along with "Julianna" (see Chart 5). The water depth in the area was about 500 m, so no further work was initiated and attention was focussed on "Julianna".

Iceberg "Lucretia"

Data collected for iceberg "Lucretia"

Data collected	August 18	August 19
Height (m)	60	57
Width (m)		260
Length (m)		340
Draft (m)		155
Mass (10^6 tonnes)		15
Photographs		
Colour		3
Slides	1	1
Aerial		7
Polaroid		4
Stereo pairs		X
Profiles		
Above-water		X
Wave height(m)		
Minimum	1	1
Maximum	2	1.5
Wind speed (kts)		
Minimum	3	5
Maximum	12	16
Drift track: 19-21 August		

18 August. The height of this very large tabular iceberg was measured by helicopter to be about 60 m. Its large size and initial easterly trajectory suggested that it might scour along the northwestern edge of Makkovik Bank (see Chart 5).

19 August. C-CORE's motion sensor package was deployed on "Lucretia" at 1703 GMT. Aerial stereo photographs were taken at 2145 GMT and the draft was measured at 2203 GMT.

21 August. "Lucretia" underwent a large calving event at about 1500 GMT leading to a 20° roll. Unfortunately, the iceberg remained in very deep water, moving eastward along the edge of the Bank at about 1 km/h (see Chart 5). The C-CORE instrument package was retrieved at 1700 GMT.

DETAILED ICEBERG OBSERVATIONS

Four icebergs were investigated extensively: "Bertha", "Gladys", "Julianna", and "Lucretia". For each, aerial stereo photographs taken during the cruise were analysed by Kenting Earth Sciences Limited to yield above-water contour maps. For icebergs "Bertha", "Gladys" and "Julianna", underwater acoustic data were converted to contour maps by Offshore Survey and Positioning Systems (OSPS).

The motion data acquired by the C-CORE sensor packages are provided later in this Chapter, both as compressed time-series plots and as expanded plots of specific iceberg-seabed interaction events of interest.

Iceberg Shape and Volume

The above-water contour maps were digitized and transferred to nine-track magnetic tape by OSPS, together with their below-water profile data. Table 7 identifies the dates and times of aquisition of these data.

Because of difficulties with the transponder array and the large, deteriorating icebergs encountered, the underwater profiles initially prepared by OSPS were found to have significant alignment errors. These errors resulted in derived vertical profiles that were considerably more jagged than the source horizontal profiles. Consequently, OSPS was requested to smooth the underwater data. The smoothed data are contained on magnetic tape and were used for the dynamic modelling of each grounding event.

It was intended that the position of the OSPS transponder floats on the aerial photographs be used to

Table 7

Original iceberg shape data files

Iceberg file	Date, time (GMT) of source measurement
"Bertha" (above-water)	05/08/85, 1614
"Bertha" (below-water)	06/08/85, 1530-1700
"Gladys" (above-water before split)	08/08/85, 2300
"Gladys" (below-water after split)	11/08/85, 1220-1850
"Gladys" (above-water after split)	10/08/85, 2100
"Julianna" (above-water)	19/08/85, 2100
"Julianna" (below-water)	20/08/85, 1614
"Lucretia" (above-water)	19/08/85, 2145

Note: all "Gladys" below-water measurements refer to the the grounded portion of the iceberg.

align data on above- and below-water shape. Unfortunately, the position of the transponder array around each iceberg could not be ascertained and the position of the above-water data related to the below-water data for each iceberg was estimated manually using the profiles themselves, numerous photographs, and calculations of the centres-of-gravity of above- and below-water portions separately. The resulting composite-shape data files were written with the same format as the originals onto the end of the magnetic tape, archived at AGC.

Iceberg "Bertha", shape and volume. The three-dimensional perspectives and waterline contour of "Bertha" are shown in Figures 25 and 26, respectively, and Appendix 8, with ship and aerial photographs of this iceberg shown in Figures 27 to 29.

Both above- and below-water dimensioning of "Bertha" took place after the iceberg floated free of the seabed. For a free-floating iceberg of uniform ice density, ρx_i, in seawater of density, ρ_W, the ratio of above-water volume, V_a, to total volume, V_t, may easily be determined:

$$V_a / V_t = 1 - \rho_i / \rho_w \qquad (1)$$

Volume estimates were supplied by OSPS (calculated by averaging adjacent horizontal profiles and multiplying by their vertical separation distances). Volume error estimates of ±2% for V_a and ±15% for V_b, as discussed in Chapter 1, have been applied.

For iceberg "Bertha":

volume above, V_a = 199,000 m^3 ± 4,000m^3
volume below, V_b = 1,160,000 m^3 ±170,000m^3
total volume, V_t = 1,360,000 m^3 ±170,000m^3

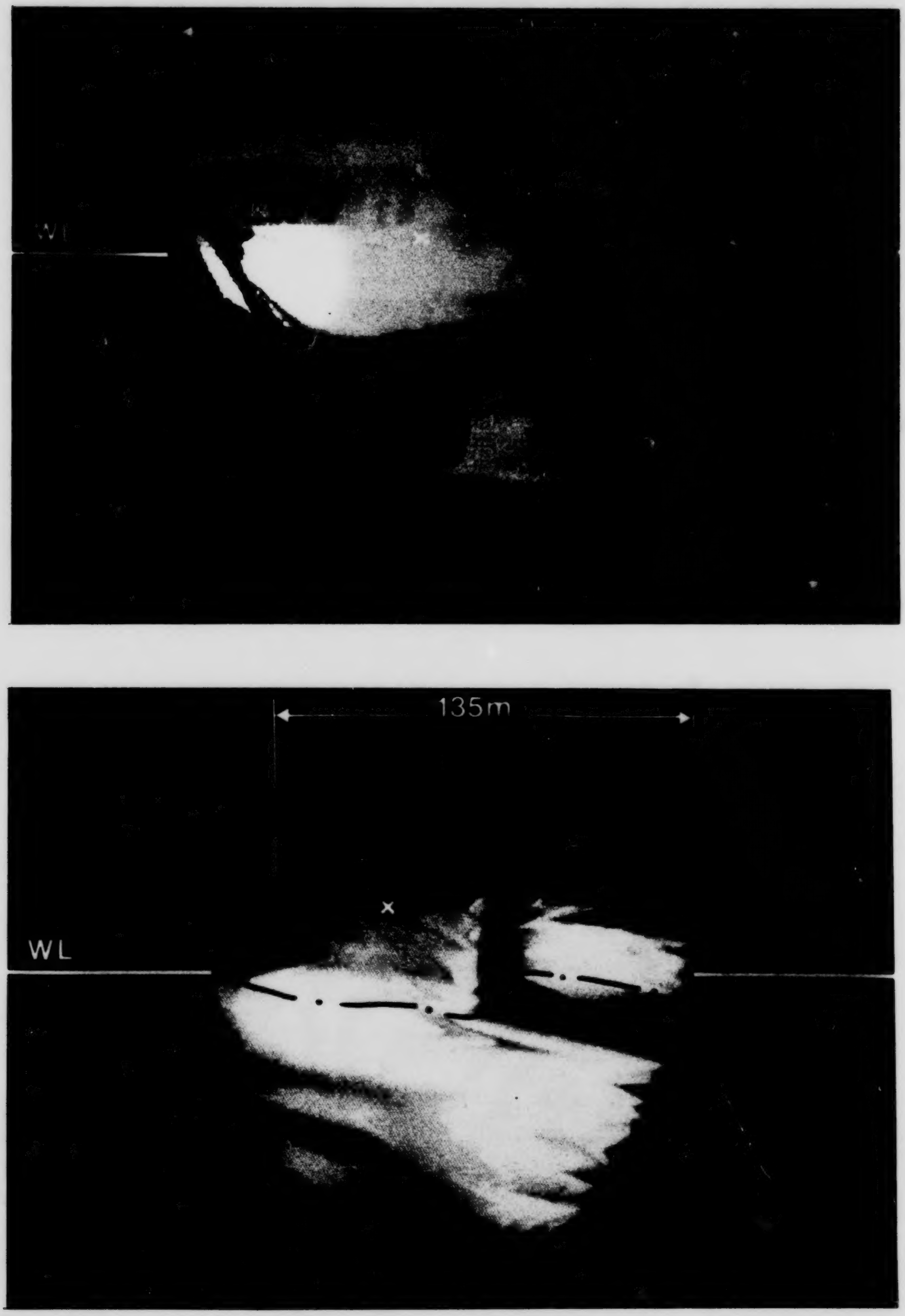

Figure 25. Computer generated perspectives of "Bertha", above- and below-water.

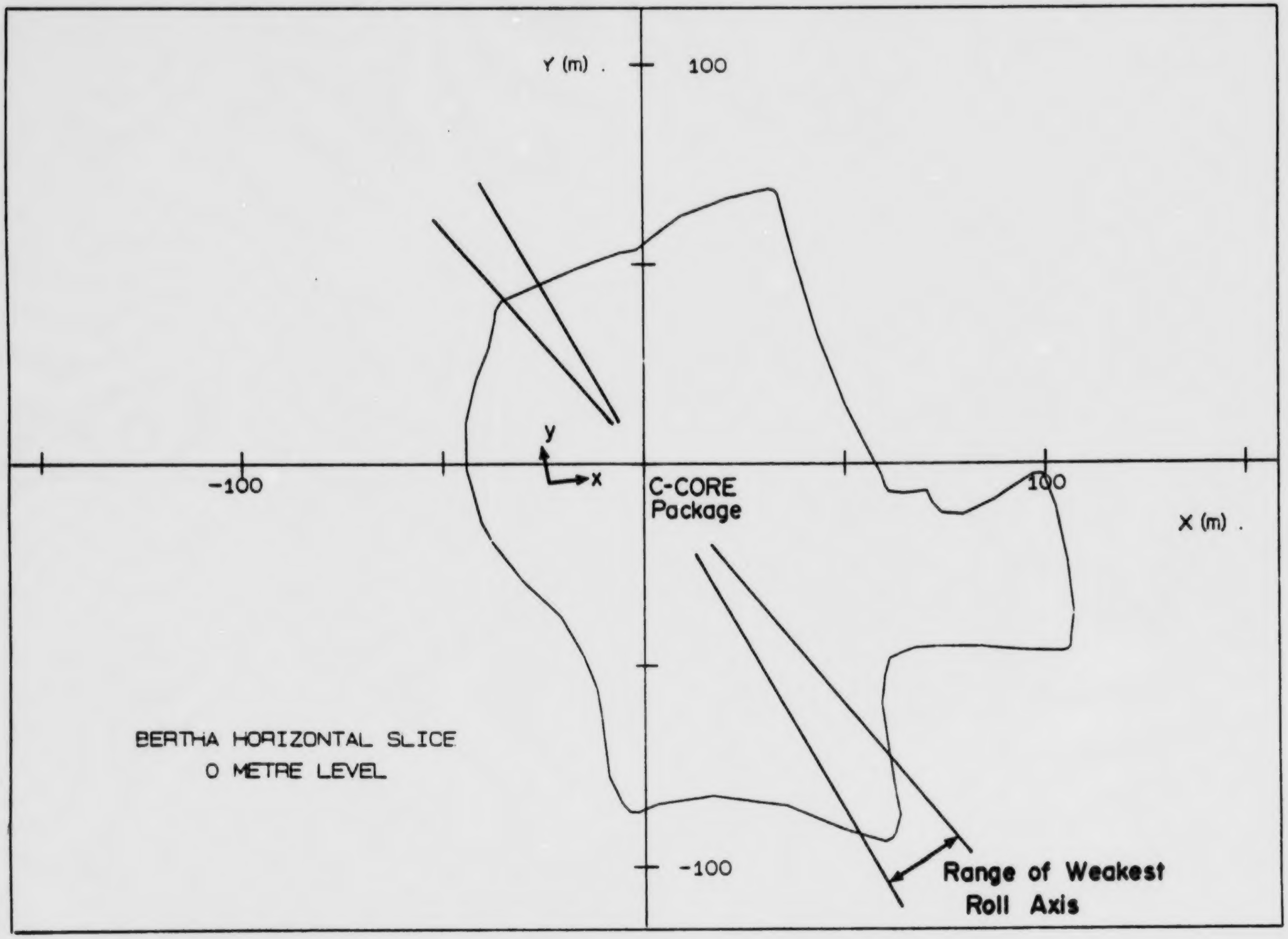
Y (m)
100
-100
100
X (m)
-100
y
x
C-CORE
Package
BERTHA HORIZONTAL SLICE
0 METRE LEVEL
Range of Weakest
Roll Axis

Figure 26. 'Bertha' waterline contour, showing axis conventions for shape data and C-CORE motion package. Package height above waterline is 13 ± 1 m

a)

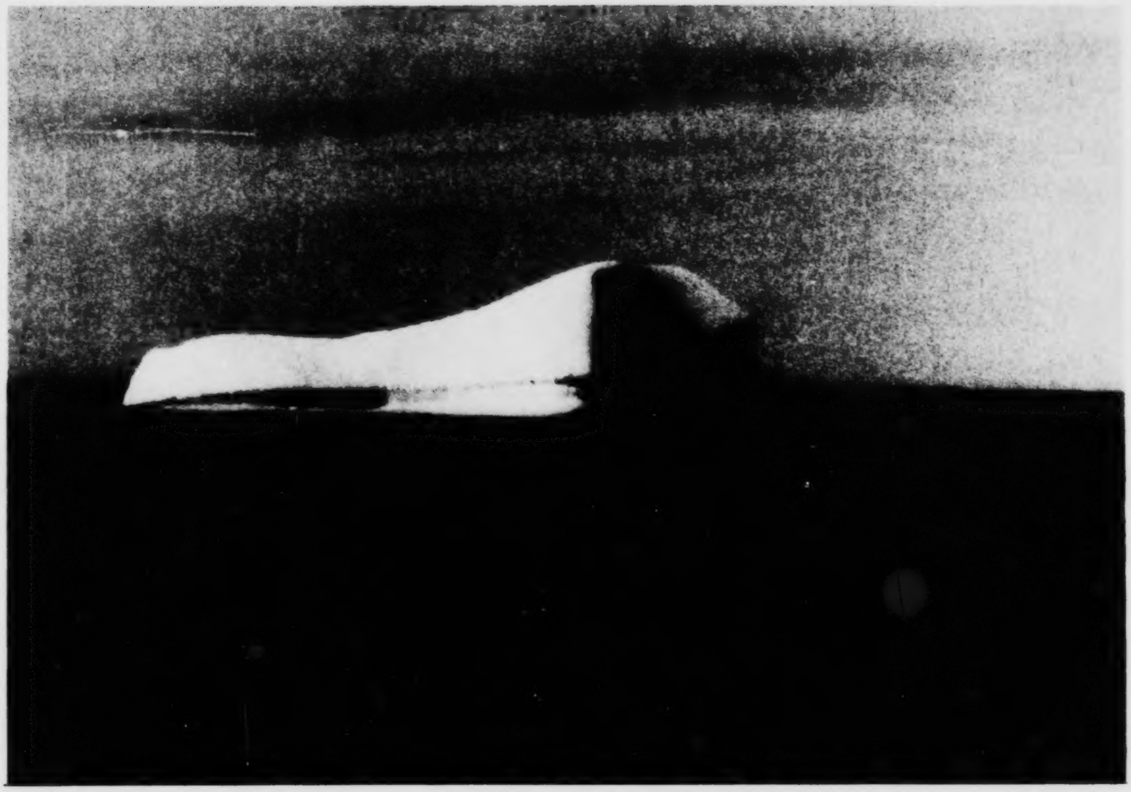

b)

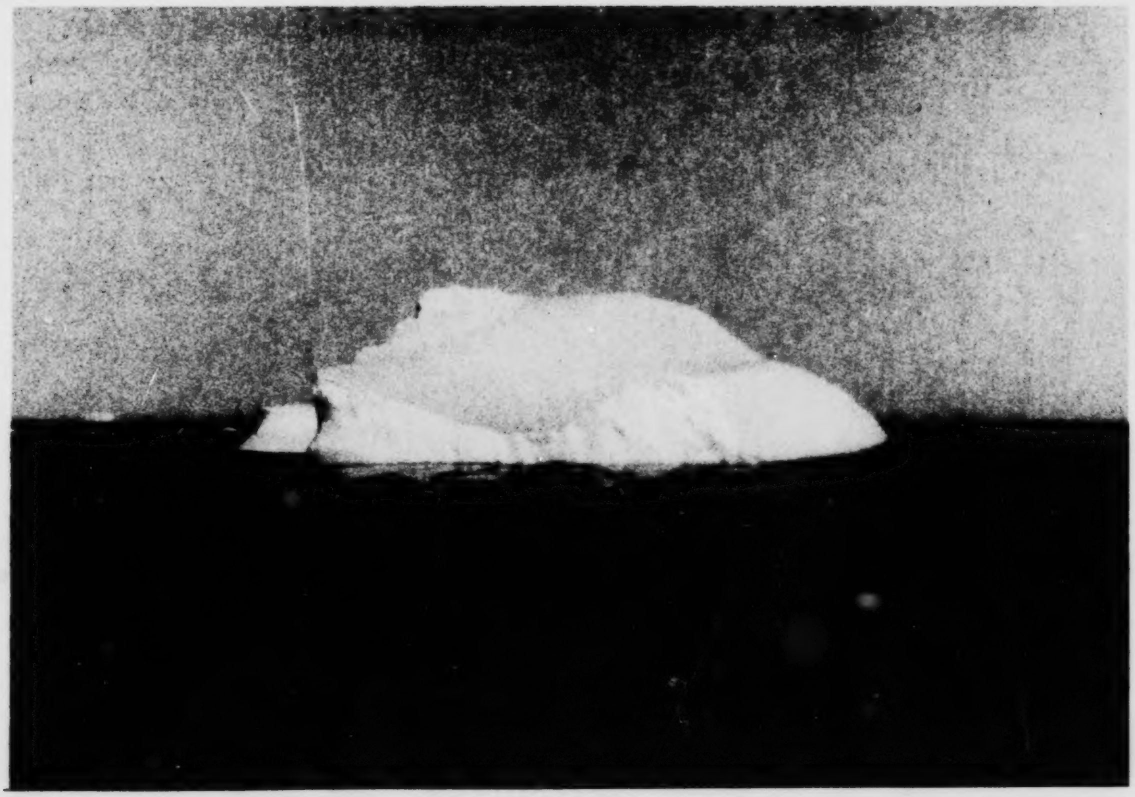

Figure 27. Surface photographs of 'Bertha'.

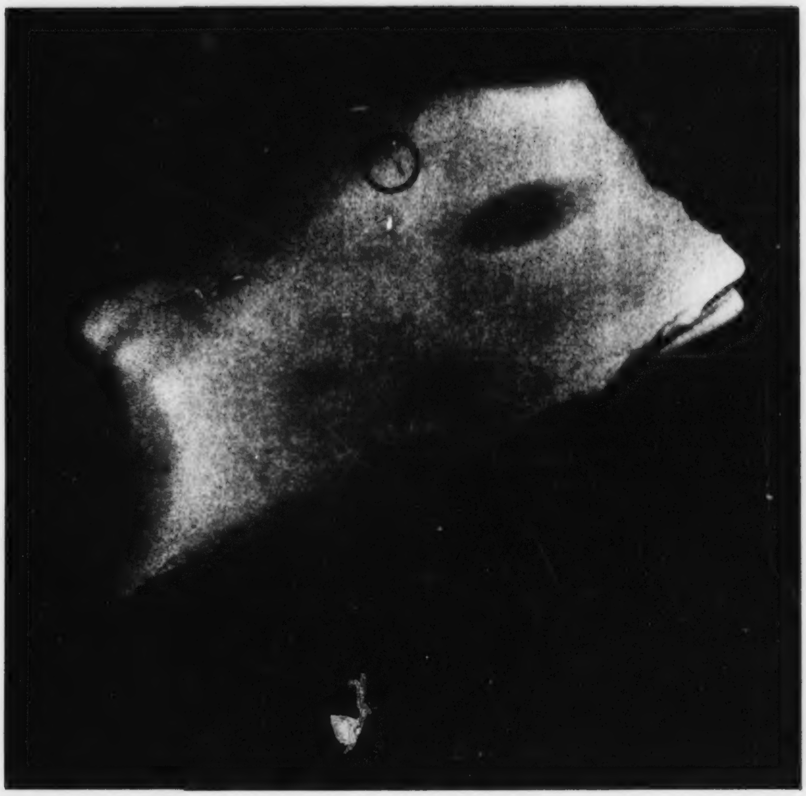

Figure 29. Aerial photograph of 'Bertha',showing position of C-CORE package.

For our purposes, seawater may be assumed to have a uniform density of 1.025 tonnes/m^3. Evidence from deep cores in glaciers suggest that ice density approaches 0.917 tonnes/m^3 at depths greater than 150 to 200 m (Danish Hydraulic Institute 1979). These high densities result from the hydrostatic pressure of the overlying ice; a phenomenon which should be replicated for deep draft icebergs. Furthermore, lower density surface layers are ablated during the journey south. Ice taken from the surface of a grounded iceberg near St. John's, Newfoundland, was found to have an average ice density of 0.904 tonnes/m^3 (El-Tahan et al. 1984). Thus, an average ice density of 0.90± .01 tonnes/m^3 may be assumed.

Based on the measured above-water volume, equation (1) thus yields an estimate of the below-water volume of 1,430,000 ± 120,000 m^3. This value of V_b compares favourably with the value based on the underwater shape data, namely 1,160,000 ± 170,000 m^3.

The discrepancy between these two below-water volume estimates may be explained by the fact that the above- and below-water shape measurements were not made simultaneously. A significant calving event took place at 0945 GMT on August 6, between the times of the aerial stereo photography and below-water profiling of "Bertha". Thus, the measured above-water volume would be expected to exceed that needed for equilibrium with the measured below-water volume.

For comparative purposes, the separate above- and below-water volume measurements may be used, together with equation (1), to yield total volume estimates for "Bertha" at the separate times the two source shape measurements were made. Based on the measured above-water volume, the estimated total volume at 1613 GMT on August 5 was

1,630,000 ±120,000 m^3. Based on the measured below-water volume, the estimated total volume at about 1600 GMT on August 6 was 1,320,000 ± 200,000 m^3. That is, "Bertha" lost an estimated mass of 280,000 ±210,000 tonnes in the 24 hours between above- and below-water profiling operations. Although the error on this estimate is high, it is encouraging to note that mass loss is indeed predicted, giving a degree of confidence in the "Bertha" shape measurements.

Iceberg "Gladys", shape and volume. The above-water shape of iceberg "Gladys", as photographed on August 8, before the iceberg split on August 10, is shown in Figures 30-32, with three-dimensional perspectives presented in Appendix 8. Based on a computed above-water volume of 1,040,000 ± 21,000 m^3 and an assumed average ice density of 0.90 ±.01 tonnes/m^3, the mass of the free-floating "Gladys" before splitting is found to be 7,680,000 ±590,000 tonnes (see equation (1)). As noted previously, underwater profiles were not obtained for "Gladys" prior to splitting.

Ship and aerial photographs of the portion of "Gladys" that remained free-floating after the split on August 10 are shown in Figures 33 and 34, respectively. No photogrammetric analysis was performed on these stereo images because this portion of "Gladys" did not scour the seabed.

Ship and aerial photographs of the portion of "Gladys" that grounded solidly after the split on August 10 are shown in Figures 35-36 and 37, respectively. Below-water profiles based on aerial stereo photographs taken on August 10 were combined by OSPS with under-water profile data acquired on August 11. The three-dimensional shape and waterline contour of the grounded portion of "Gladys" are shown in Figures 38 and 39 respectively.

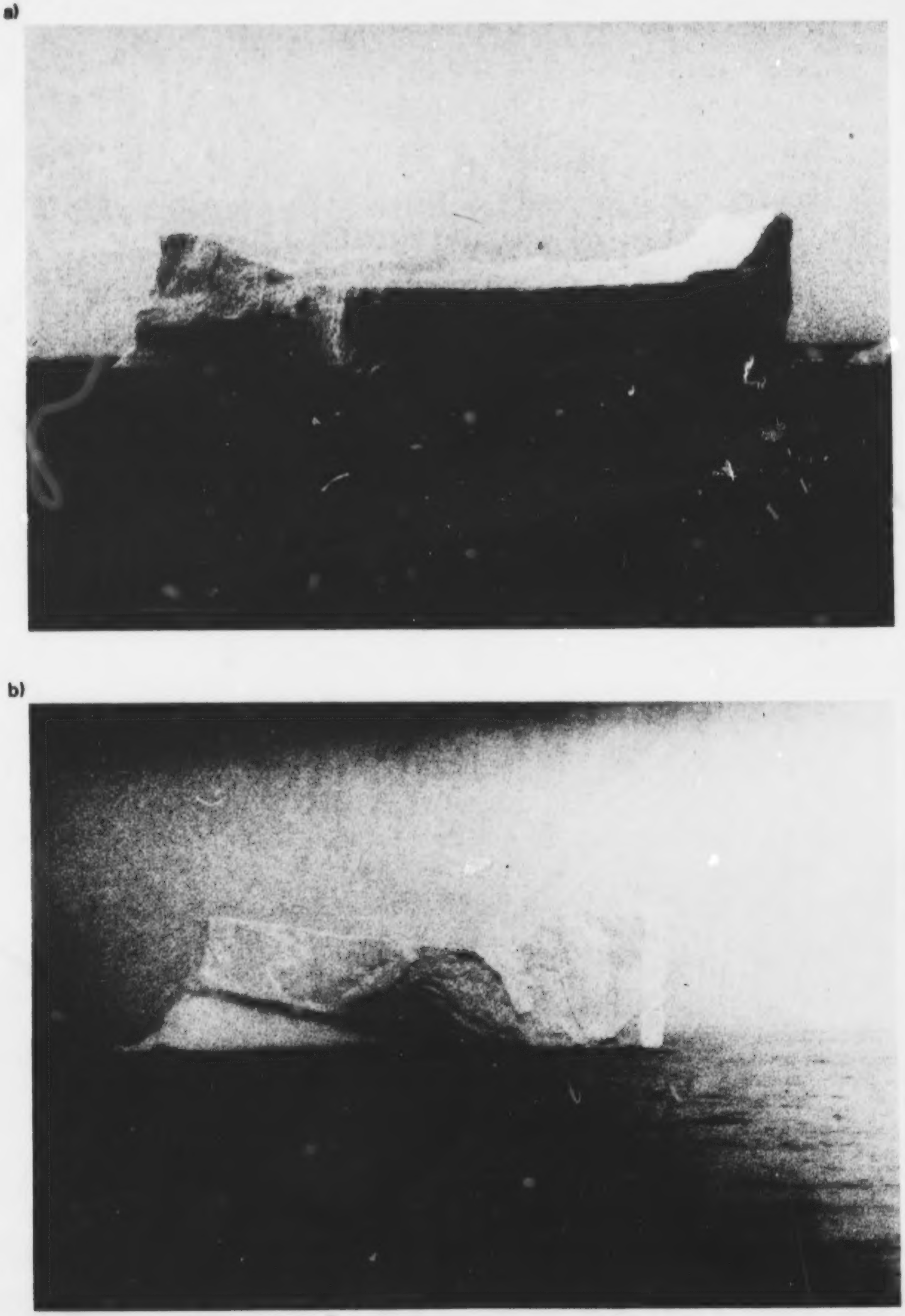

Figure 30. Surface photographs of "Gladys", before split.

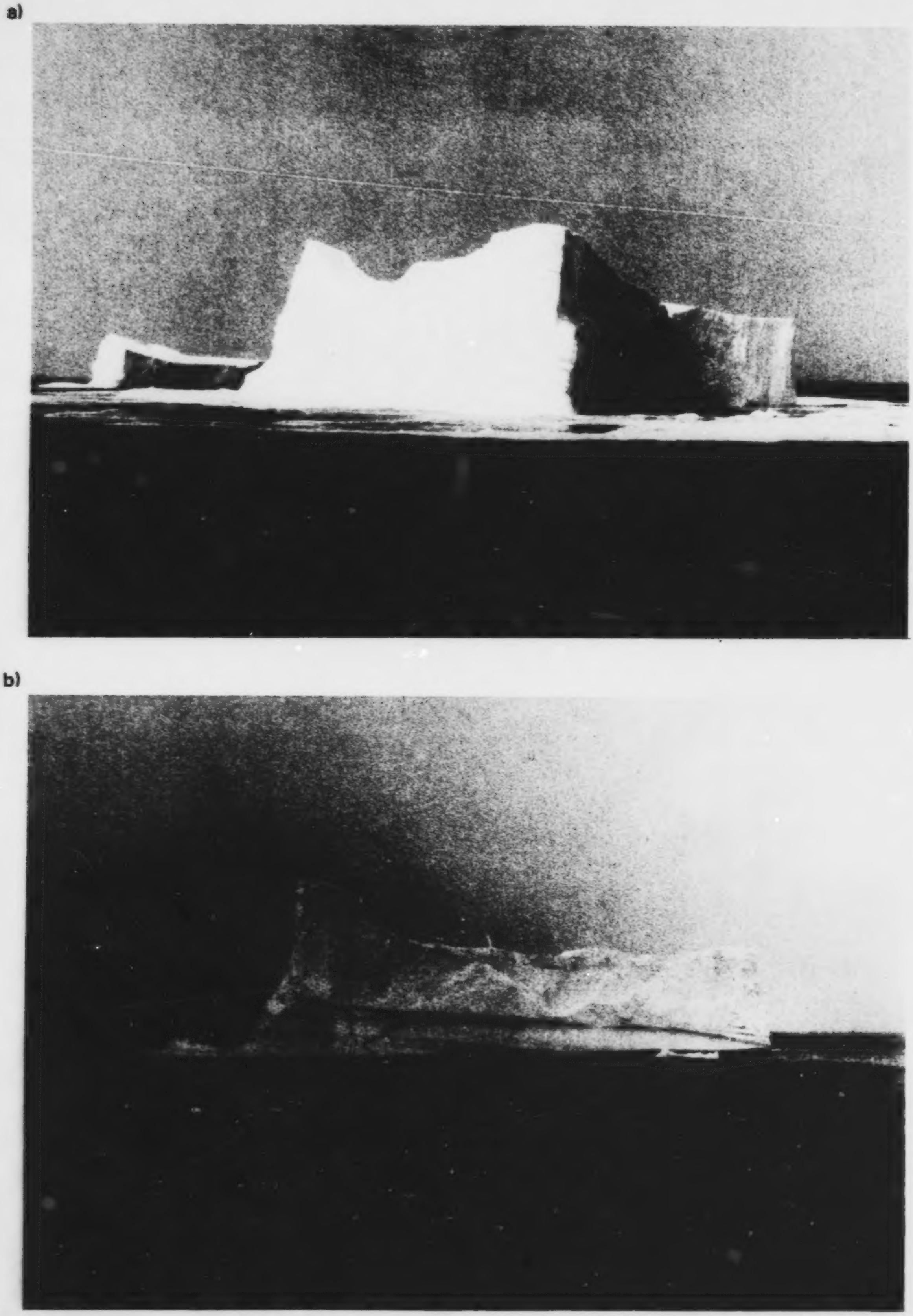

Figure 31. Surface photographs of "Gladys" before split.

Figure 32. Aerial photograph of 'Gladys', before split.

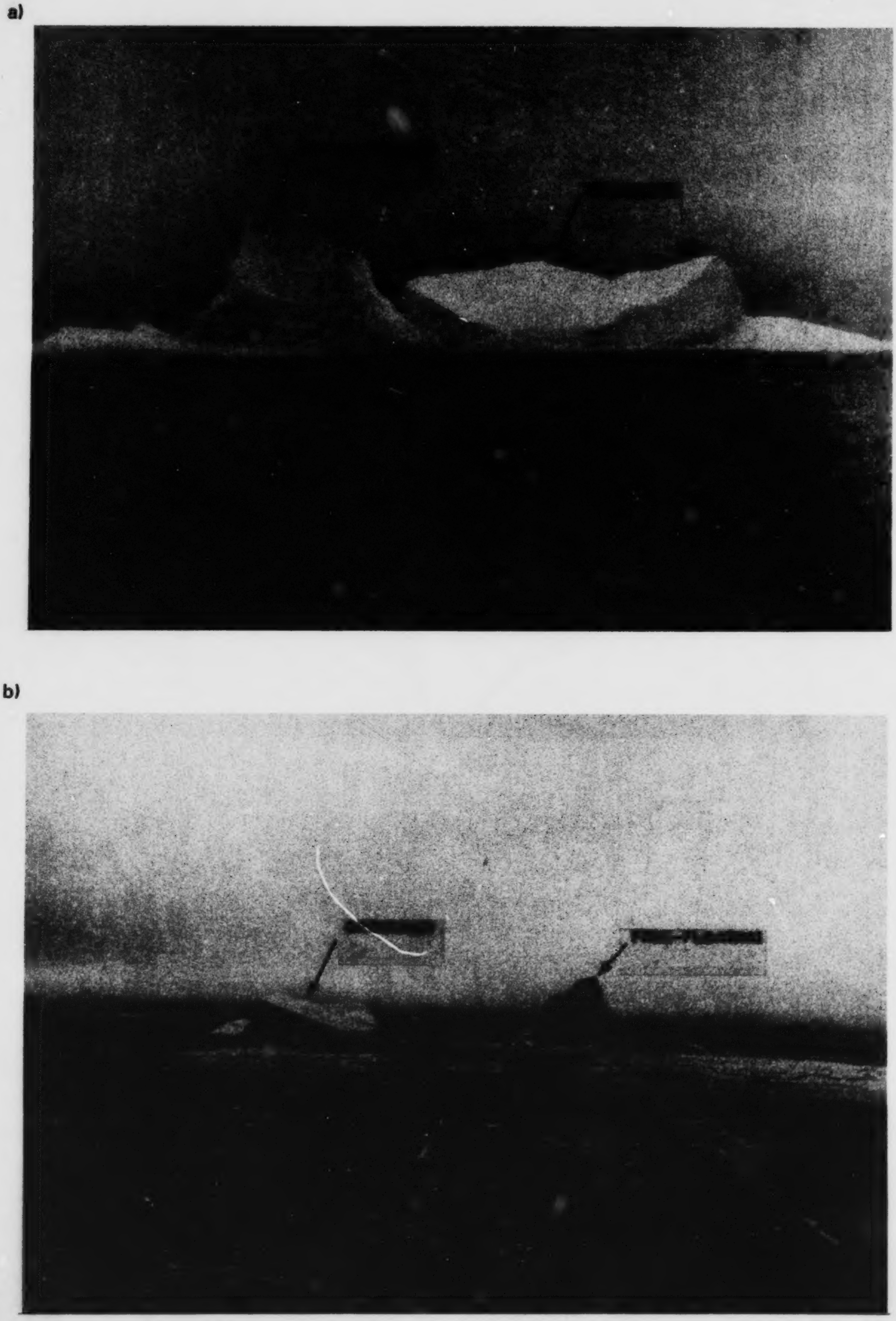

Figure 33. The two major pieces of iceberg 'Gladys' after the split on August 10.

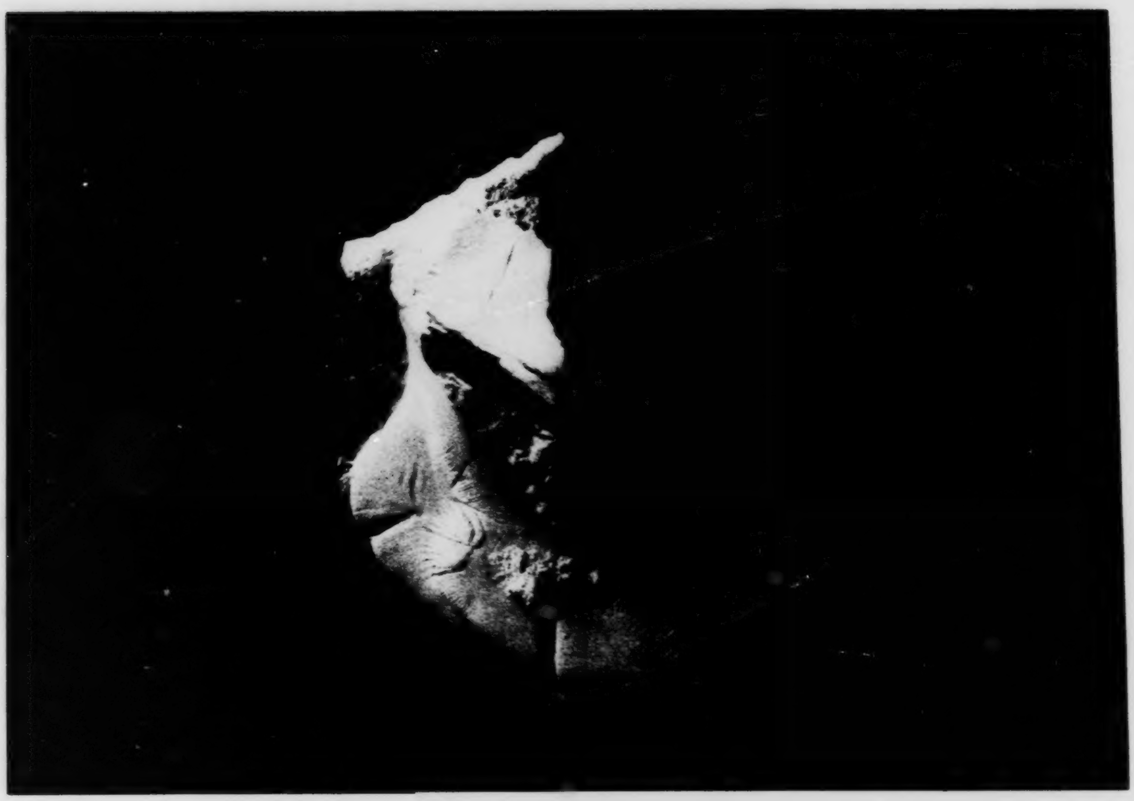

Figure 34. Free-floating portion of "Gladys" after split.

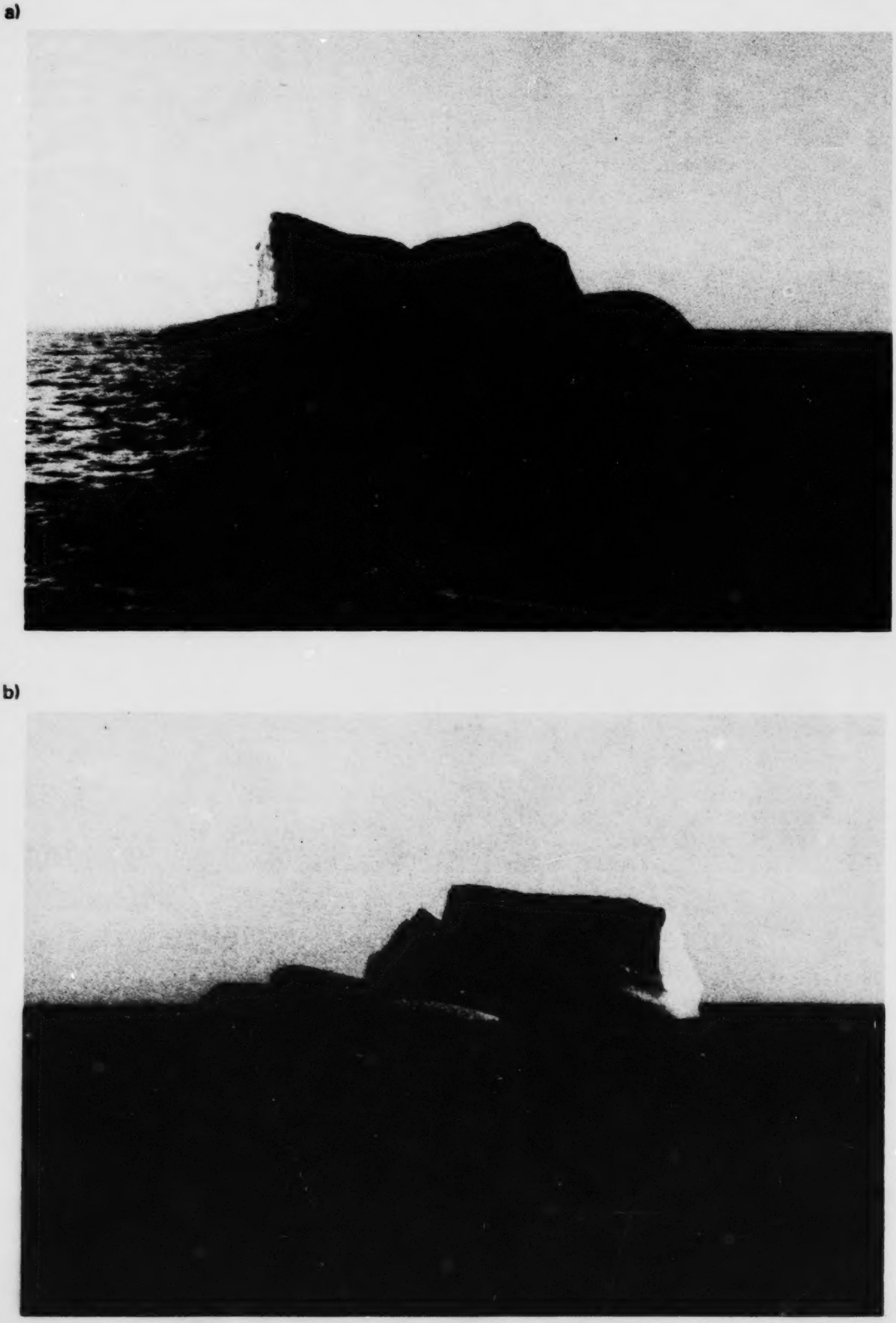

Figure 35. Surface photographs of grounded portion of "Gladys" after split.

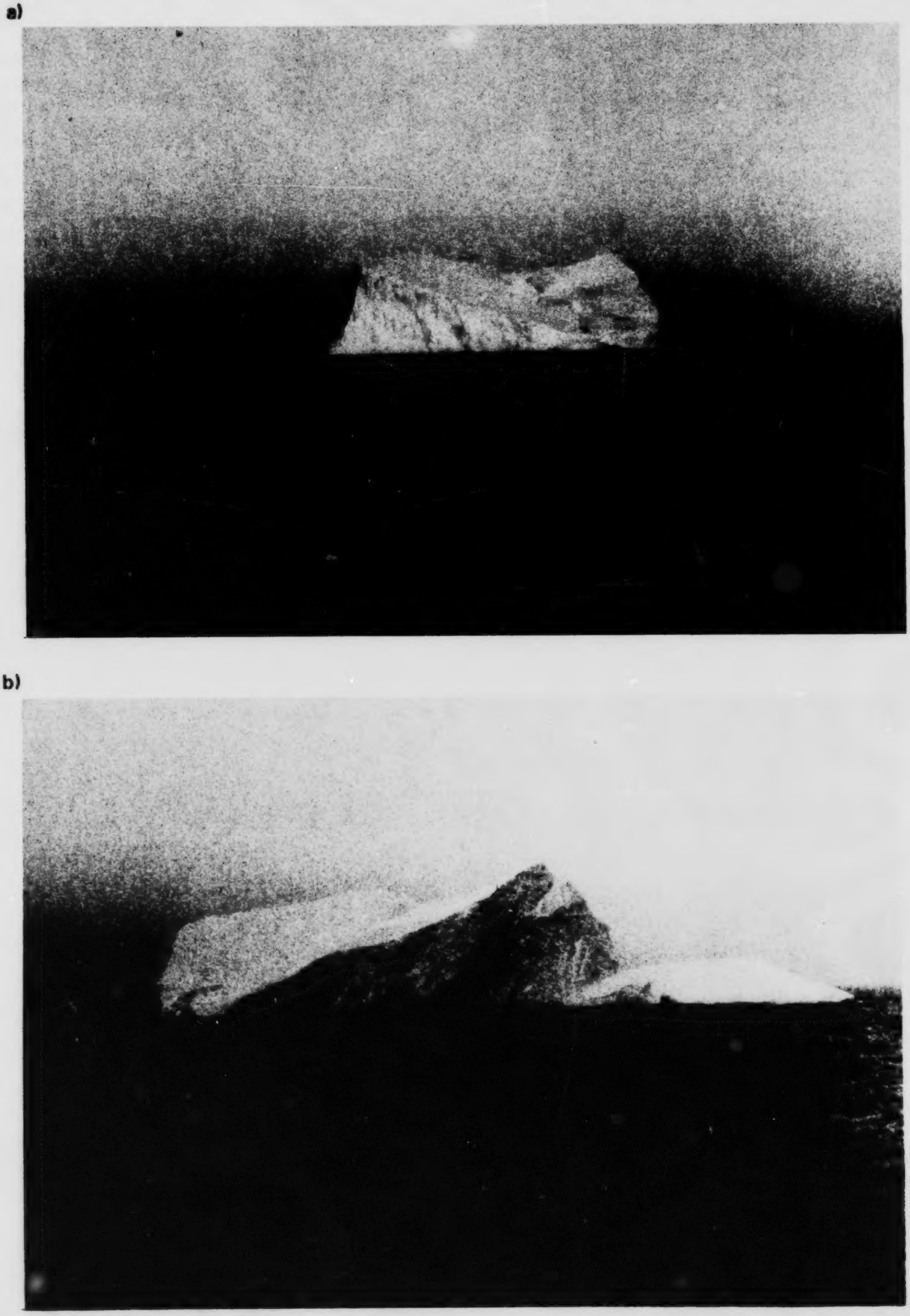

Figure 36. Surface photographs of grounded portion of "Gladys" after split.

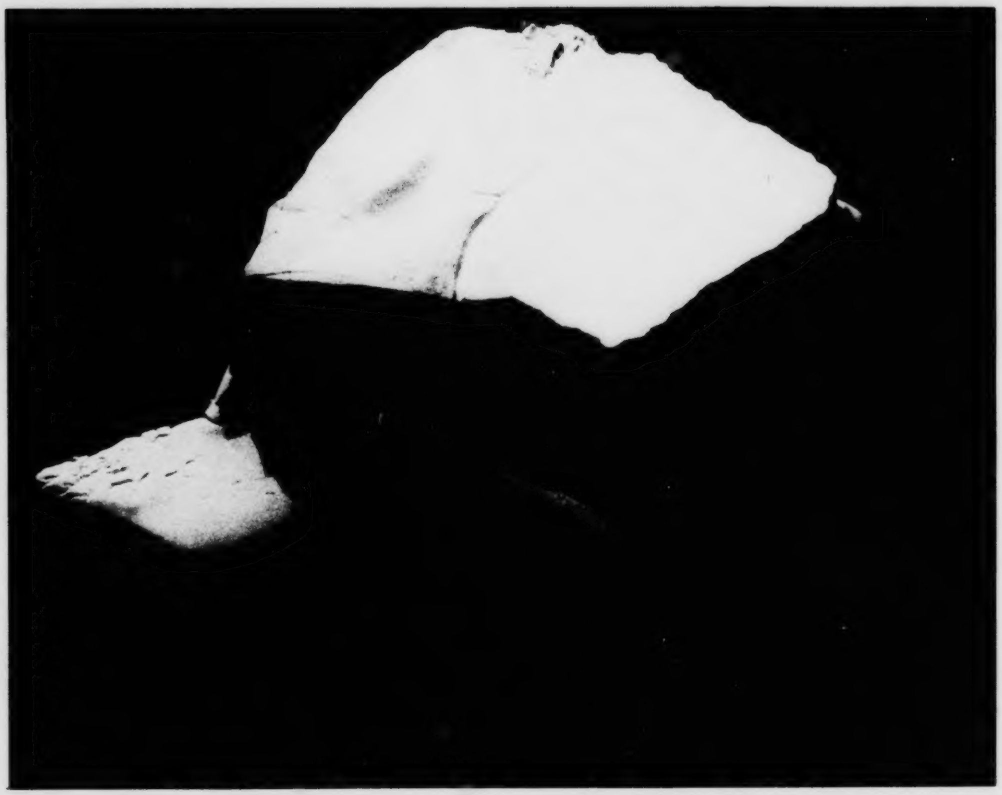

Figure 37. Aerial photograph of grounded portion of "Gladys" after split.

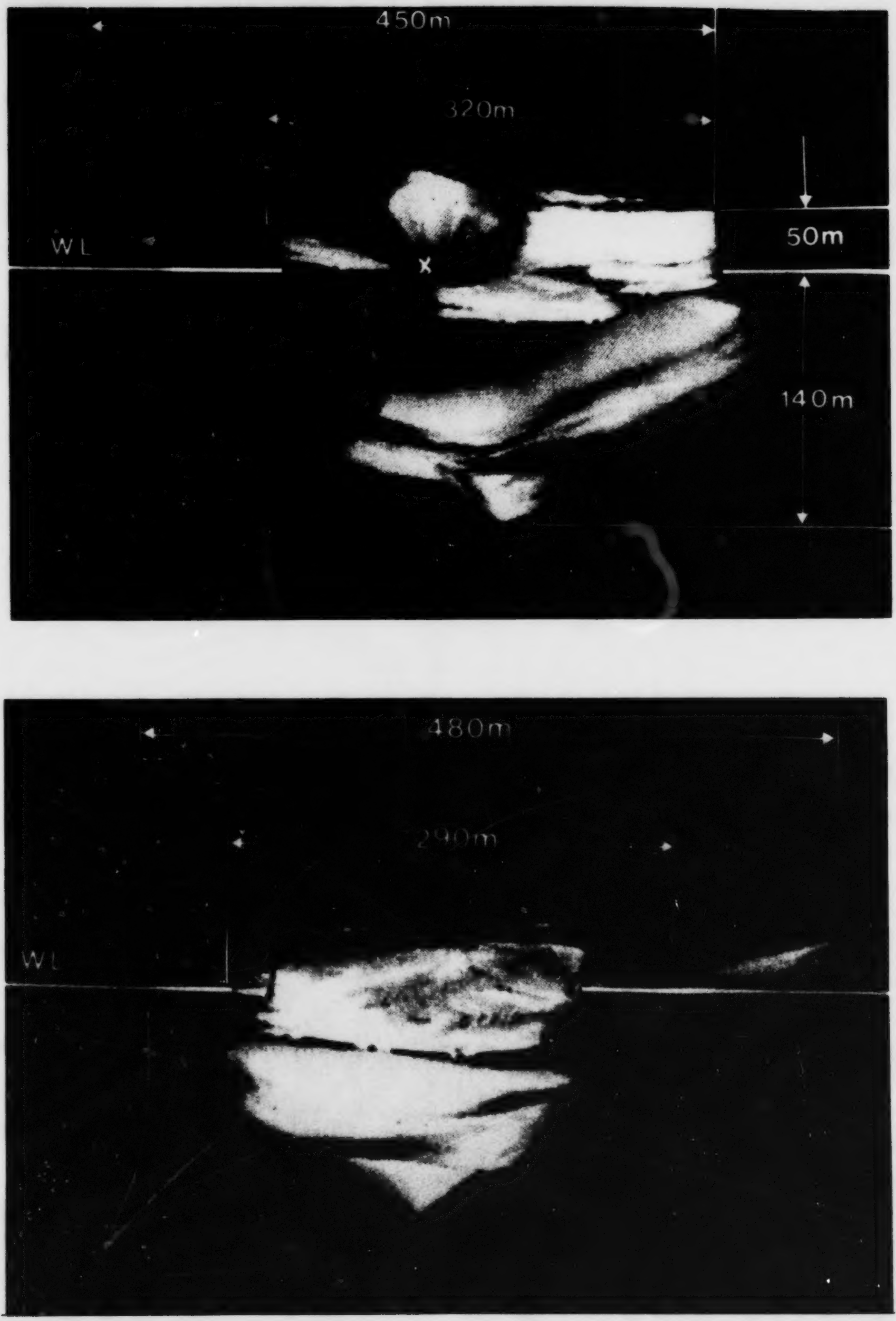
450m
320m
WL
50m
140m
480m
290m
WL

Figure 38. Computer generated perspectives of grounded portion of "Gladys", above- and below-water.

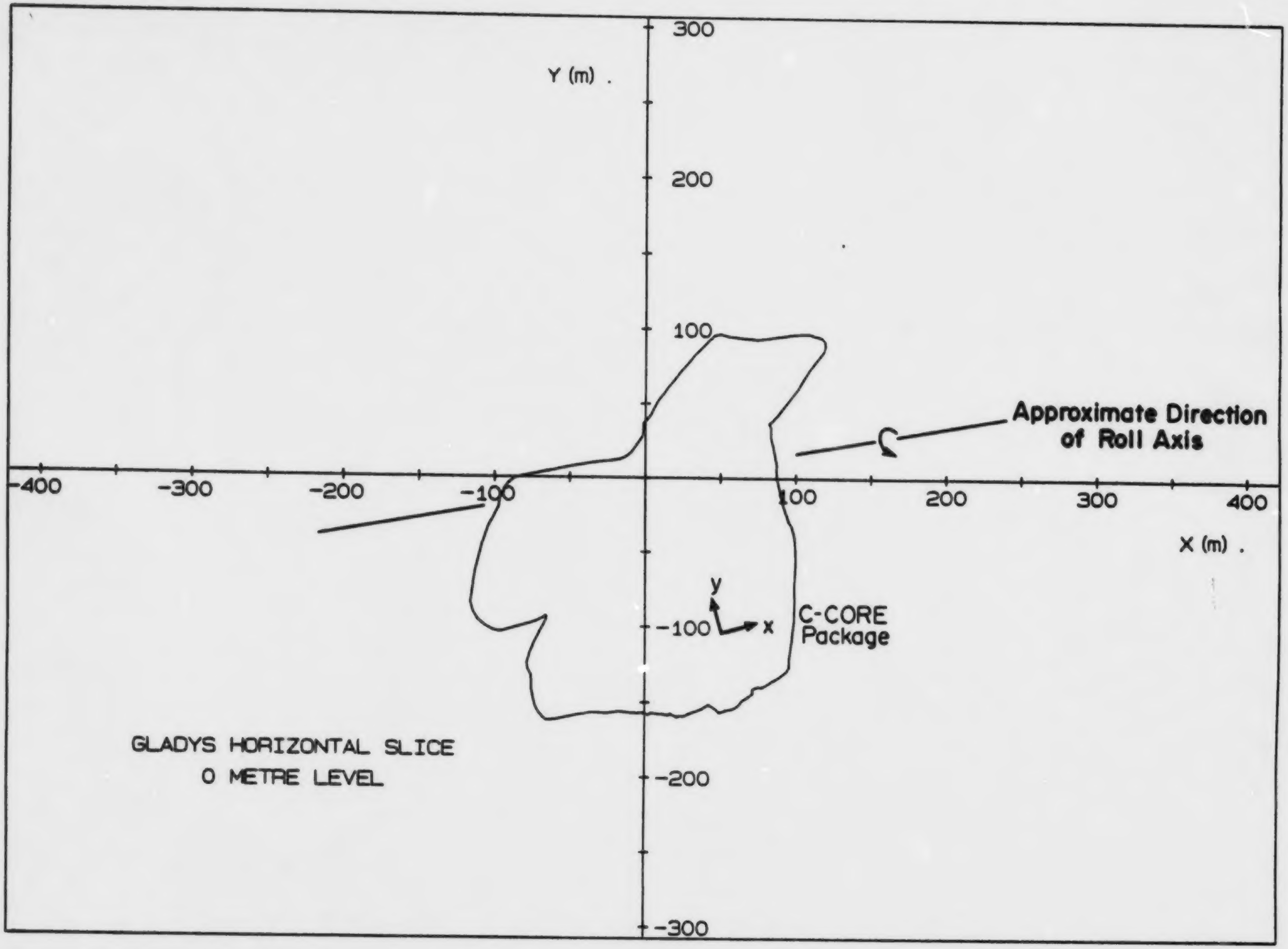

Figure 39. Waterline contour for grounded portion of 'Gladys', showing axis conventions for shape data and C-CORE motion package. Package height above waterline is 23±1 m.

Although "Gladys" was known to be aground in 134 m of water when the data were acquired, the OSPS underwater profiles extend only to a depth of 110 m. In addition, many of the source profiles available contain missing segments (one- to three-quarters of entire profile) and some source profiles are absent altogether. Where profiles were incomplete or absent, OSPS interpolated between vertically adjacent profiles. The keel from a depth of 90 m to 110 m in fact contains few measured data; these profiles have been largely constructed by repeating missing segments from the 90 m contour.

It should also be pointed out that several minor calving and rolling events took place between the above- and below-water dimensioning operations.

The volume estimates for "Gladys" are as follows:

volume above, $V_a = 794{,}000\ m^3 \pm 16{,}000\ m^3$
volume below (to 110 m depth), $V_b = 5{,}500{,}000\ m^3 \pm 830{,}000\ m^3$
volume total (to 110 m depth), $V_t = 6{,}300{,}000\ m^3 \pm 830{,}000\ m^3$
volume total (to 140 m depth), $V_t = 6{,}500{,}000\ m^3 \pm 830{,}000\ m^3$

Since the measured shape of "Gladys" was available only to a depth of 110 m, the keel was later extended to 140 m depth by manually adding horizontal profiles (at 5 m intervals) to the shape data file contained on magnetic tape. The total volume of this keel extension was 197,000 m^3. The shapes of the profiles added were chosen to allow for a smooth variation of the keel with depth, starting from the last measured profile at 110 m (see Appendix 8).

The keel extension raised the below-water volume of "Gladys" to 5,700,000 ± 830,000 m^3. For this underwater volume, and assuming an average ice density of 0.90 ±.01 tonnes/m^3, an above-water volume of at least 790,000 ±140.000 m^3 would be needed for the iceberg to be in contact with the seabed, and V_a would need to be higher than this for the iceberg to exert a downward force on the seabed. Since the measured above-water shape was 790,000 ±16,000 m^3, the iceberg shape data do not provide for any downward seabed contact force. The difficulties posed by these data in the simulation of the August 10 split/roll seabed contact event are discussed in Chapter 5.

Iceberg "Julianna", shape and volume. The ship and aerial photographs of "Julianna" are presented in Figures 40-42, with associated three-dimensional perspectives in Figure 43. The waterline contour is presented in Figure 44. "Julianna" was aground in just over 170 m of water. Because of the large size and deep draft of the iceberg, underwater profiling was at 10 m rather than 5 m intervals. The calculated volumes are as follows:

volume above, V_a = 1,403,000 m^3 ±28,000 m^3
volume below, V_b = 7,300,000 m^3 ±1,100,000 m^3
total volume, V_t = 8,700,000 m^3 ±1,100,000 m^3

Assuming an average ice density of 0.90 ±.01 tonnes/m^3, the mass of "Julianna" based on total volume is 7,800,000 ± 1,000,000 tonnes. Because the iceberg was in contact with the seabed, the above- and below-water volumes are used to calculate the vertical seabed load (see Chapter 5).

Iceberg "Lucretia", shape and volume. The ship and aerial photographs of "Lucretia" are shown in Figures 45-47, with associated above-water three-dimensional perspectives in

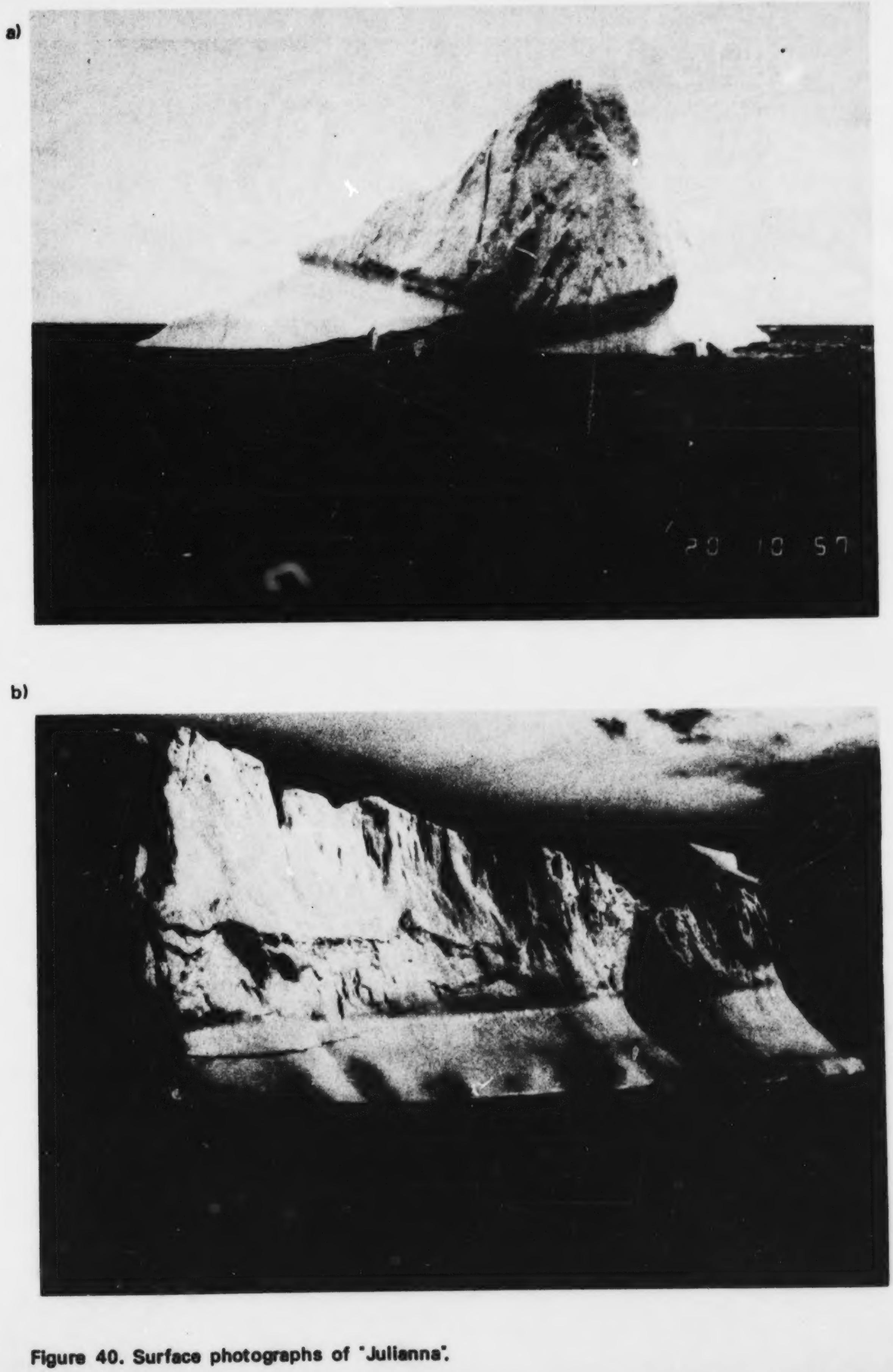

Figure 40. Surface photographs of "Julianna".

a)

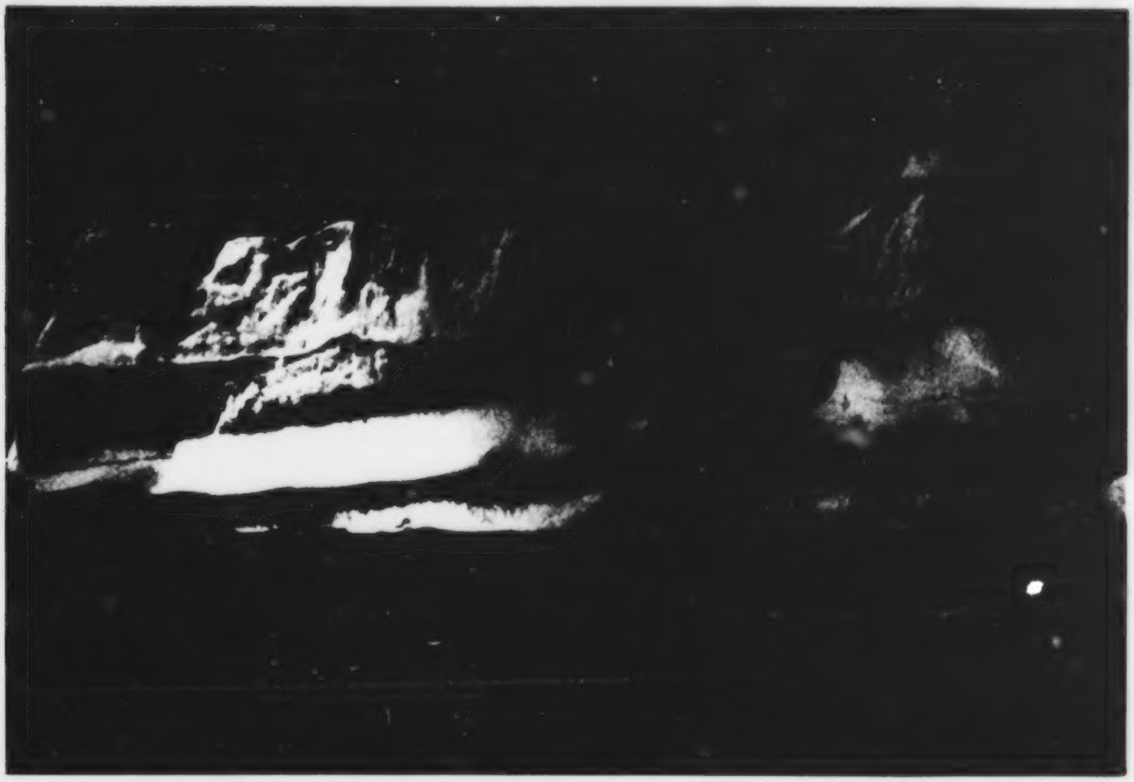

b)

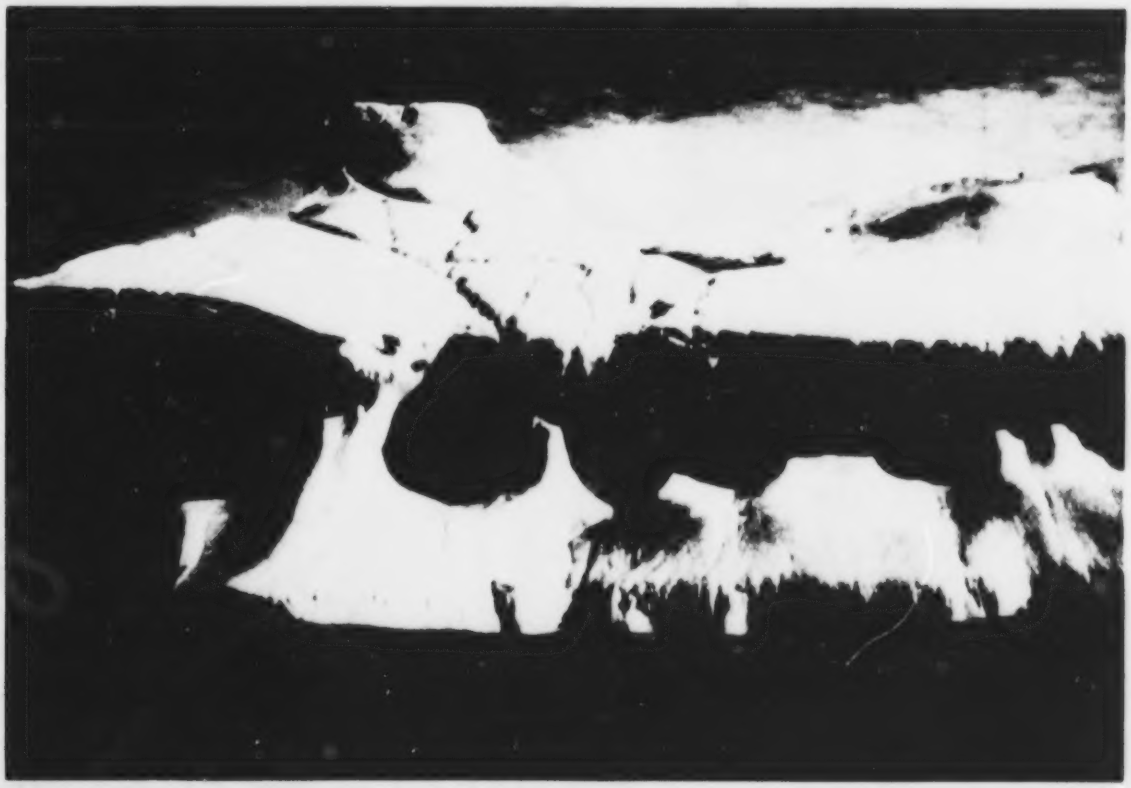

Figure 41. Surface photographs of "Julianna".

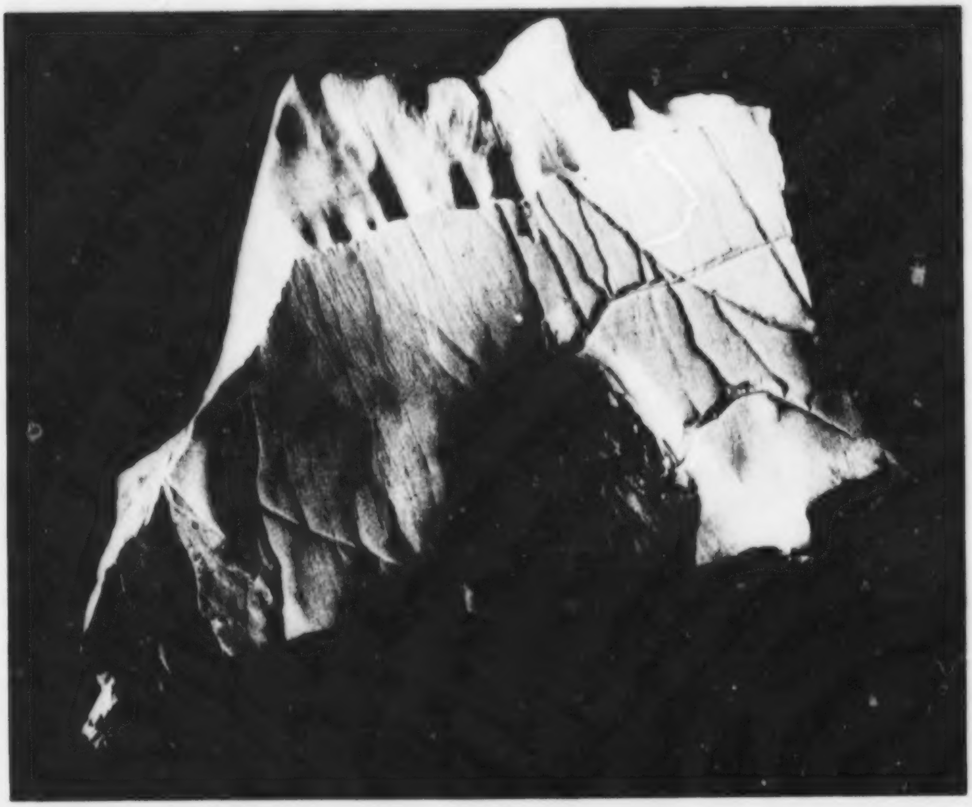

Figure 42. Aerial photograph of 'Julianna'

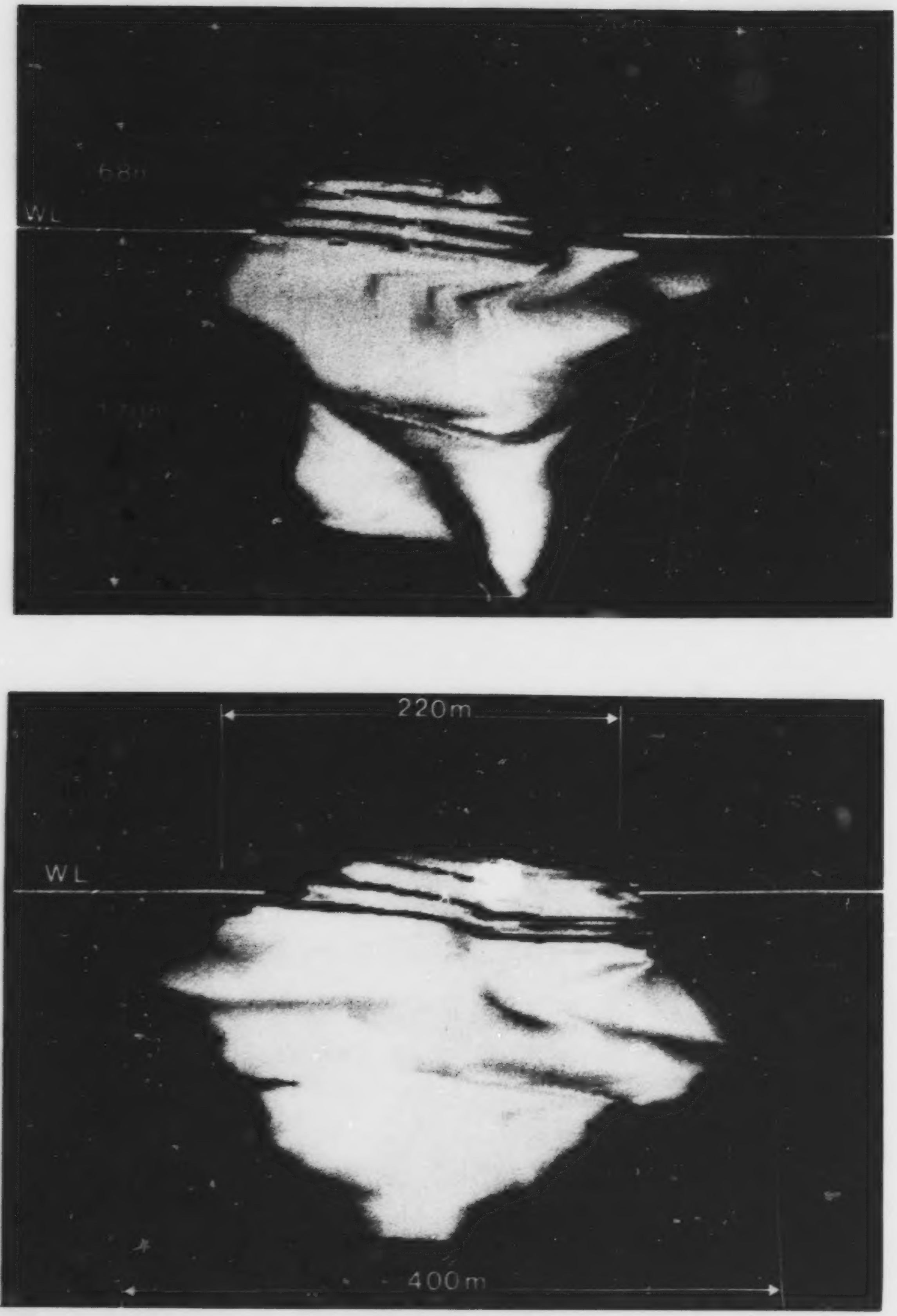
68m
WL
220m
WL
400m

Figure 43. Computer generated perspectives of "Julianna", above- and below-water.

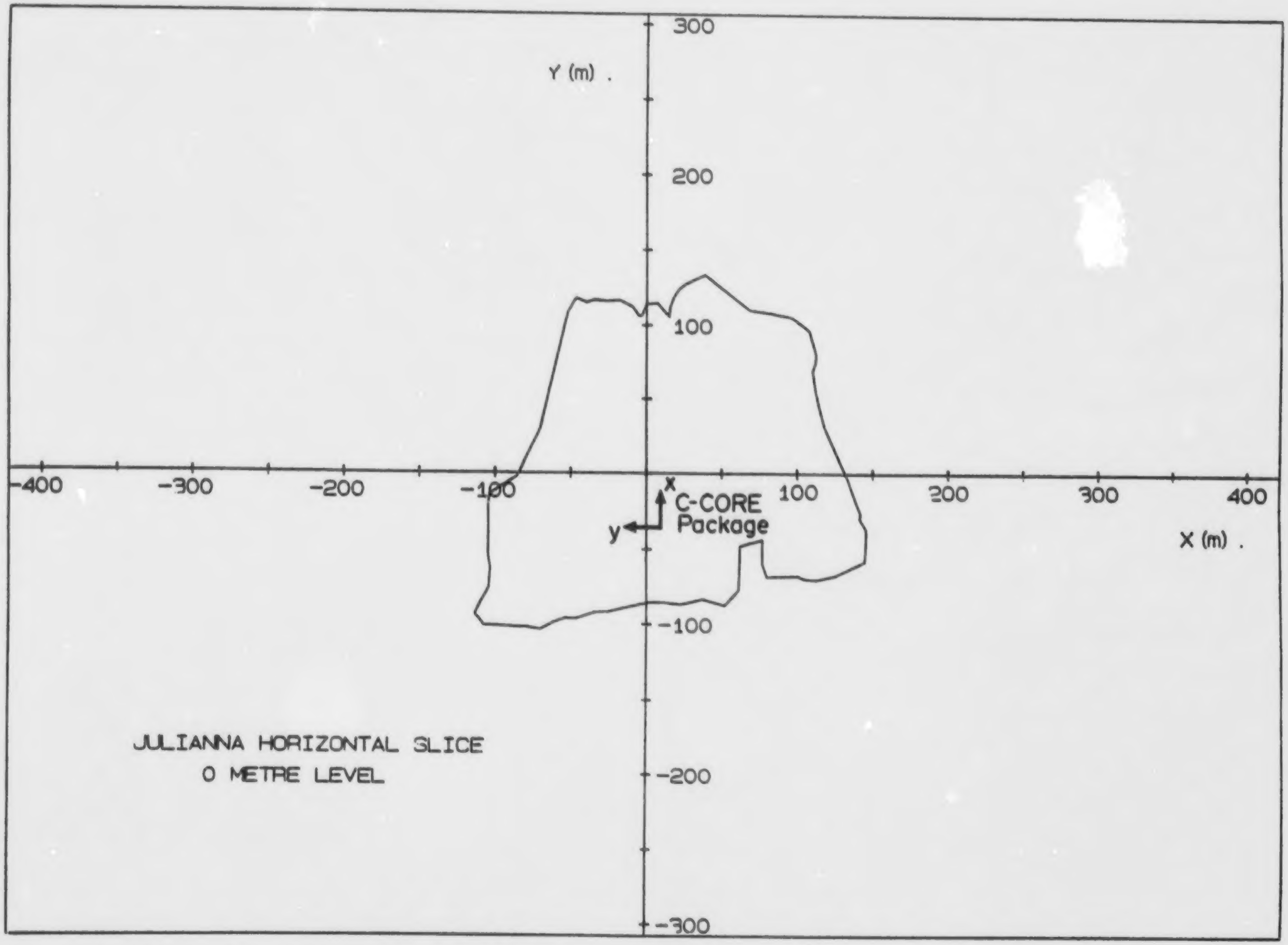

Figure 44. 'Julianna' waterline contour, showing axis conventions for shape data and C-CORE motion package. Package height above waterline is 55±1 m.

a)

b)

Figure 45. Surface photographs of 'Lucretia'.

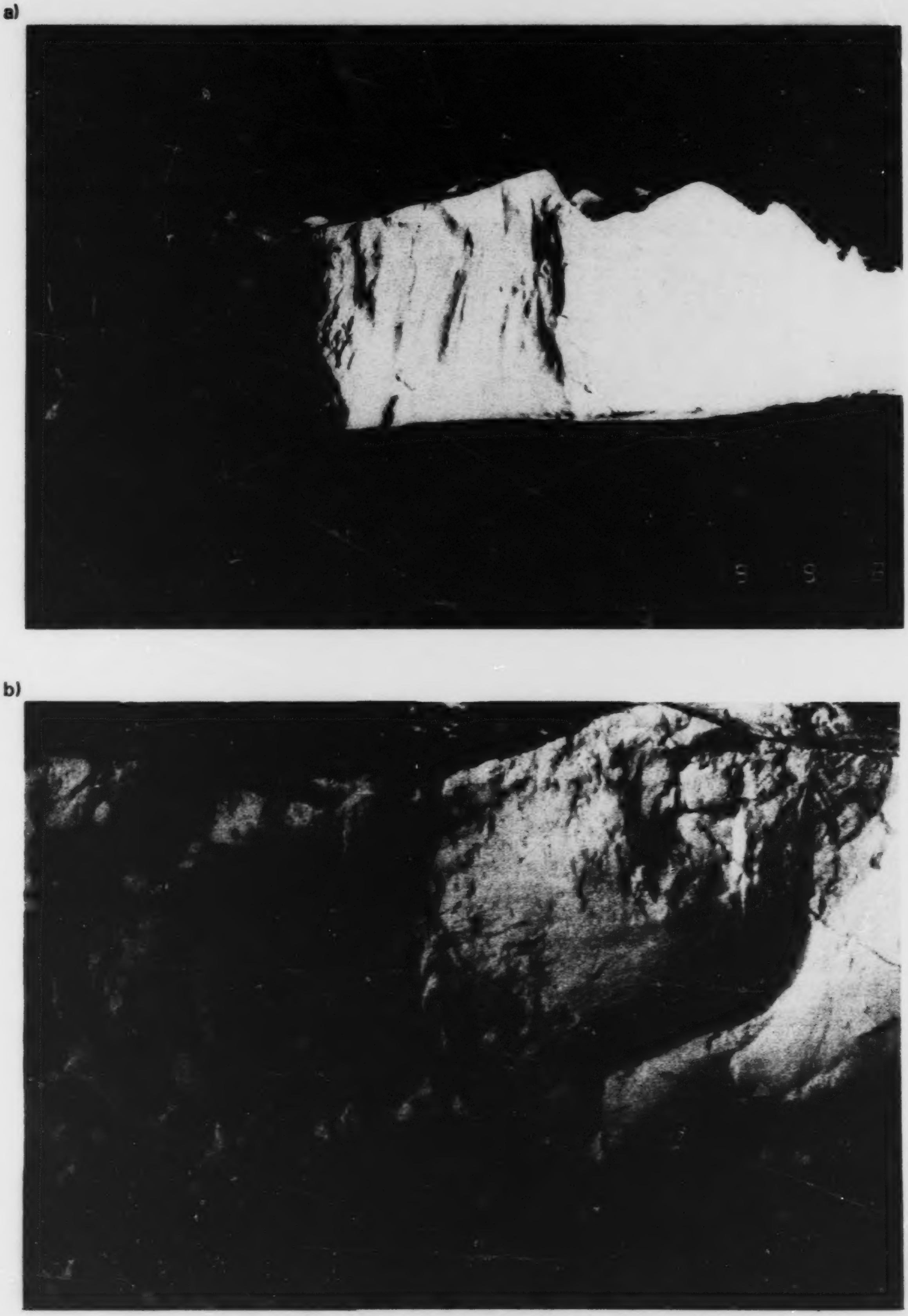

Figure 46. Surface photographs of "Lucretia".

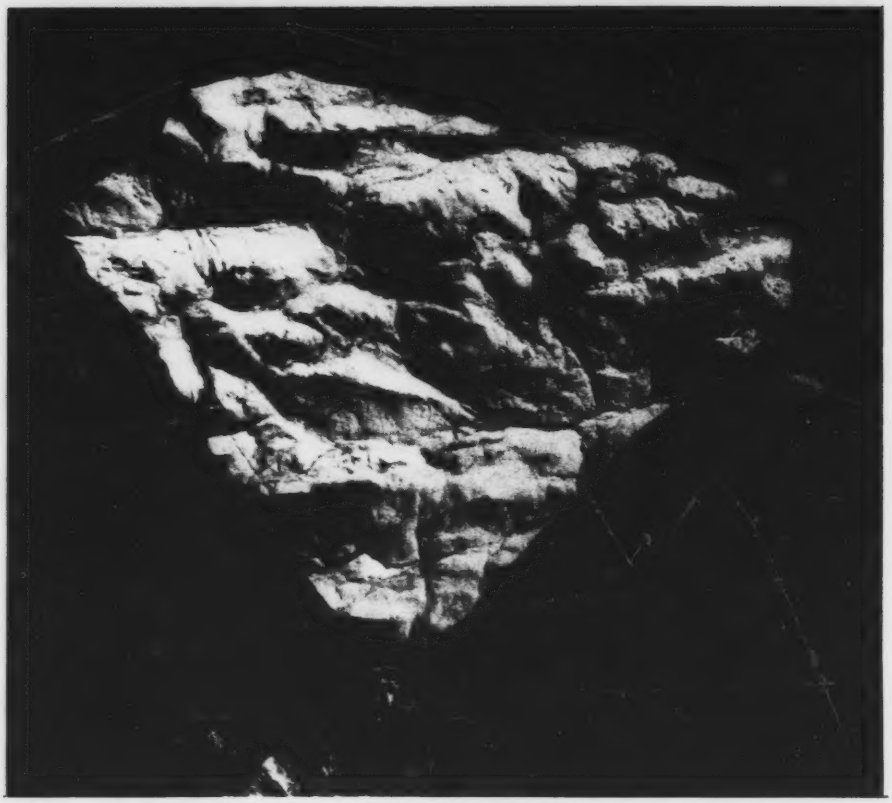

Figure 47. Aerial photograph of "Lucretia".

Appendix 8. The above-water volume calculated from the above-water shape data is 2,228,000 ± 45,000 m^3. Assuming an average ice density of 0.90 ±.01 tonnes/m^3 and using equation (1), a total mass of 16,400,000 ±1,300,000 tonnes is estimated for this iceberg. The waterline contour of "Lucretia" is shown in Figure 48.

Iceberg Motions

As discussed in Chapter 1, during each deployment of the C-CORE packages, the digitized output of the motion sensors was transmitted to the Polar Circle for onboard logging. Two factors affected the quality of the data. Firstly, the analogue-to-digital converters on the internal Seimac data loggers experienced significant unsteady fluctuations (typically ±10% of mean level). Secondly, the marginal communications link between the transmitting and receiving telemetry units resulted in multiple retransmissions of the same data packet, which in turn produced gaps in the digital time series being logged. Thus, the desired 4 Hz data rate was only achieved for relatively short bursts of 1- 1.5 s, followed by 1-4 s gaps.

Fortunately, this reduced data rate was adequate to follow the relatively slow motions (50 - 70 s periods) exhibited by the large icebergs investigated. Furthermore, the effect of the data logger A/D fluctuations could be minimized by averaging the 4 Hz data within each packet, thereby yielding a fairly reliable set of sensor readings every 1 - 4 s.

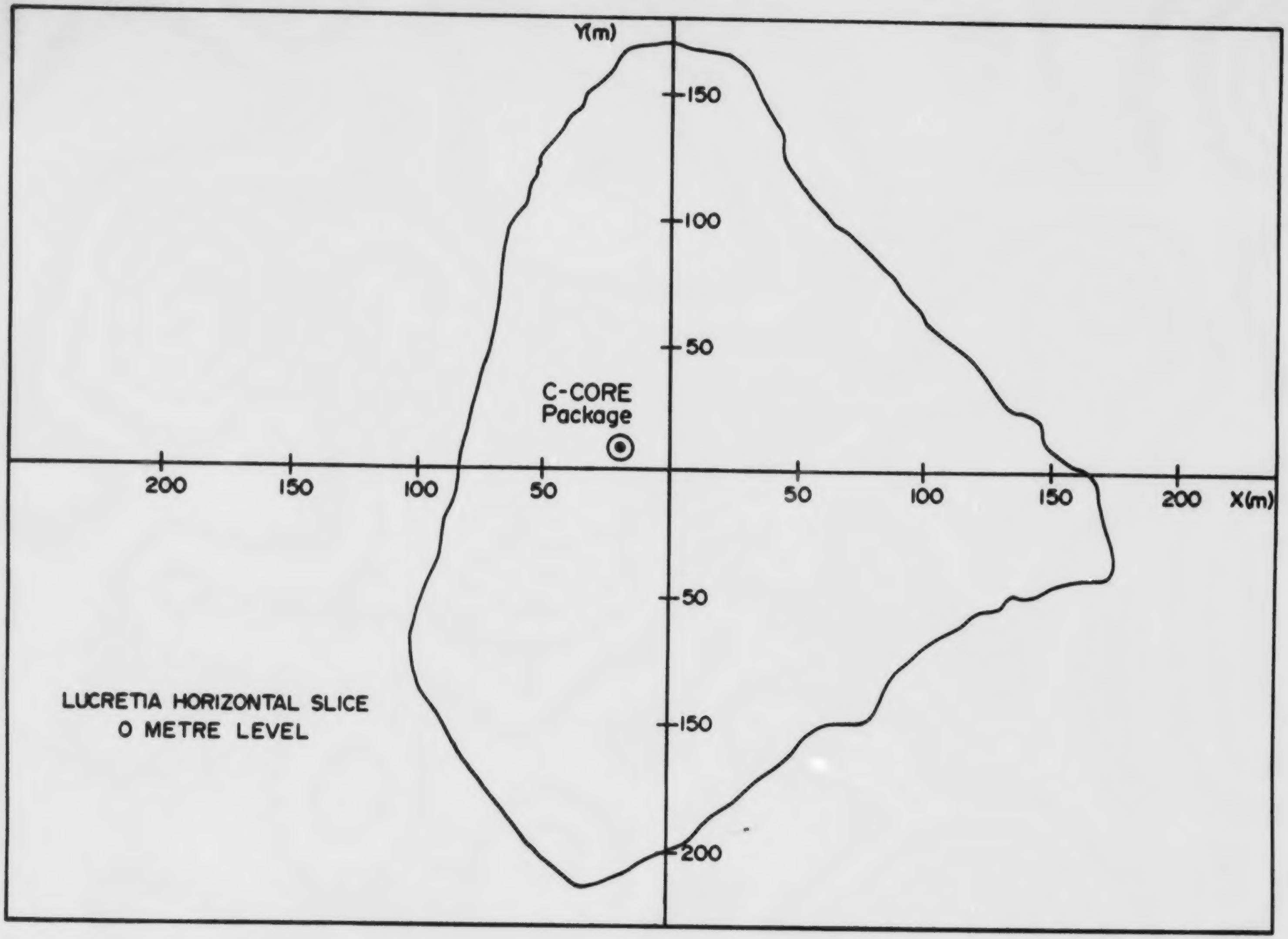
Y(m)
150
100
50
C-CORE
Package
200
150
100
50
50
100
150
200
X(m)
50
150
200
LUCRETIA HORIZONTAL SLICE
O METRE LEVEL

Figure 48. 'Lucretia' waterline contour, showing axis convention for shape data.

The motion data tapes logged on the Polar Circle were subsequently analysed by C-CORE. Checks were implemented in software to ensure the quality of the data packets. As the data stream contained samples of reference voltages within each sensor package, it was possible to correct for the long-term drift of the analogue-to-digital converters. A magnetic tape containing the output in physical units of each motion sensor for all five deployments is available on AGC open file.

Figure 49 shows the physical interpretation of the six motion signals. AX, AY, AZ represent the total acceleration (including gravitational components) along the three orthogonal axes x,y,z of the instantaneous package orientation. TX represents the angle between the instantaneous x axis and the horizontal plane, measured in the x-z plane. TY represents the angle between the instantaneous y axis and the horizontal plane, measured in the y-z plane. Both TX and TY are positive when their respective axes are above the horizontal plane. The compass reading is the angle between magnetic north and the projection of the x-axis onto the horizontal plane.

Figure 50 shows a typical compressed time series plot of all six sensor outputs in physical units. Note that time shown is in hours GMT. At the beginning of each plot, the period between the start of logging and deployment on the iceberg is clearly evident. Once deployed, the sensors yield reasonably steady values (exclusive of the A/D fluctuations previously mentioned), until the iceberg changes orientation through calving, rolling, etc. As each deployment is discussed in turn below, the important seabed interaction events will be identified, and detailed plots presented.

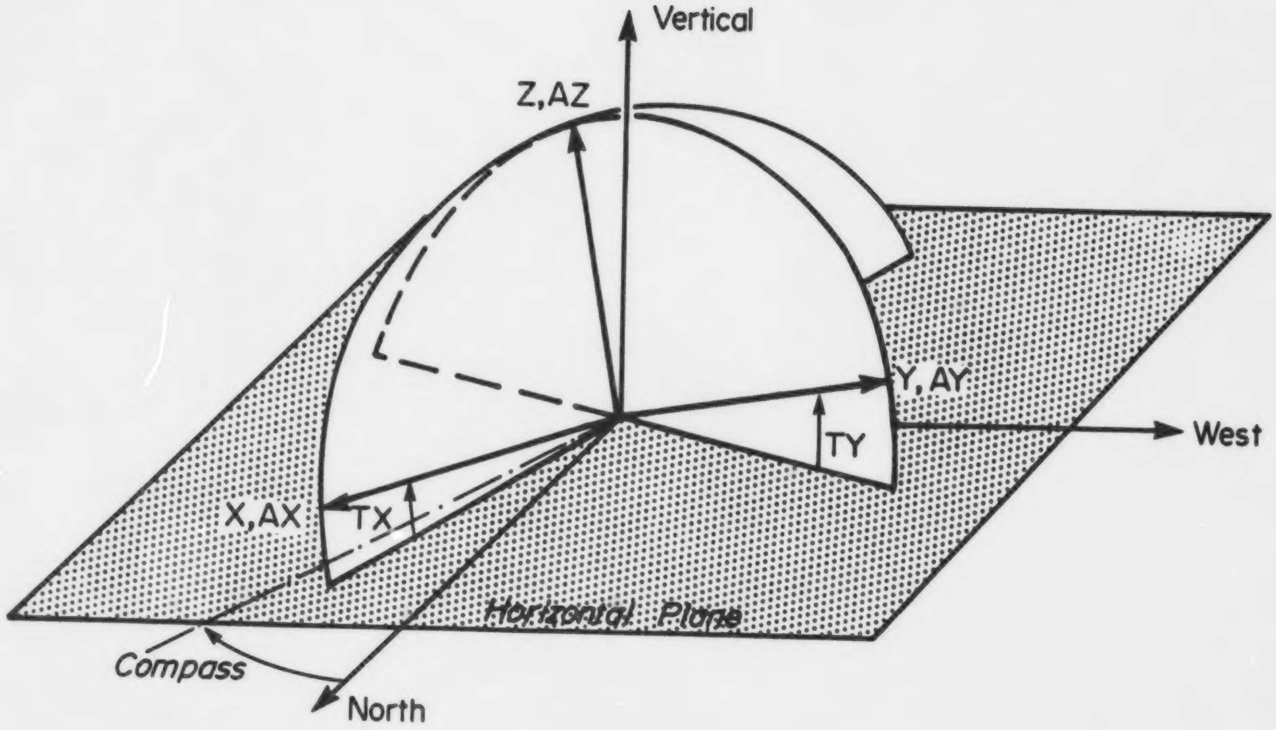
Vertical
Z,AZ
Y, AY
West
TY
X,AX
TX
Horizontal Plane
Compass
North

Figure 49. Sensor package measurement convention.

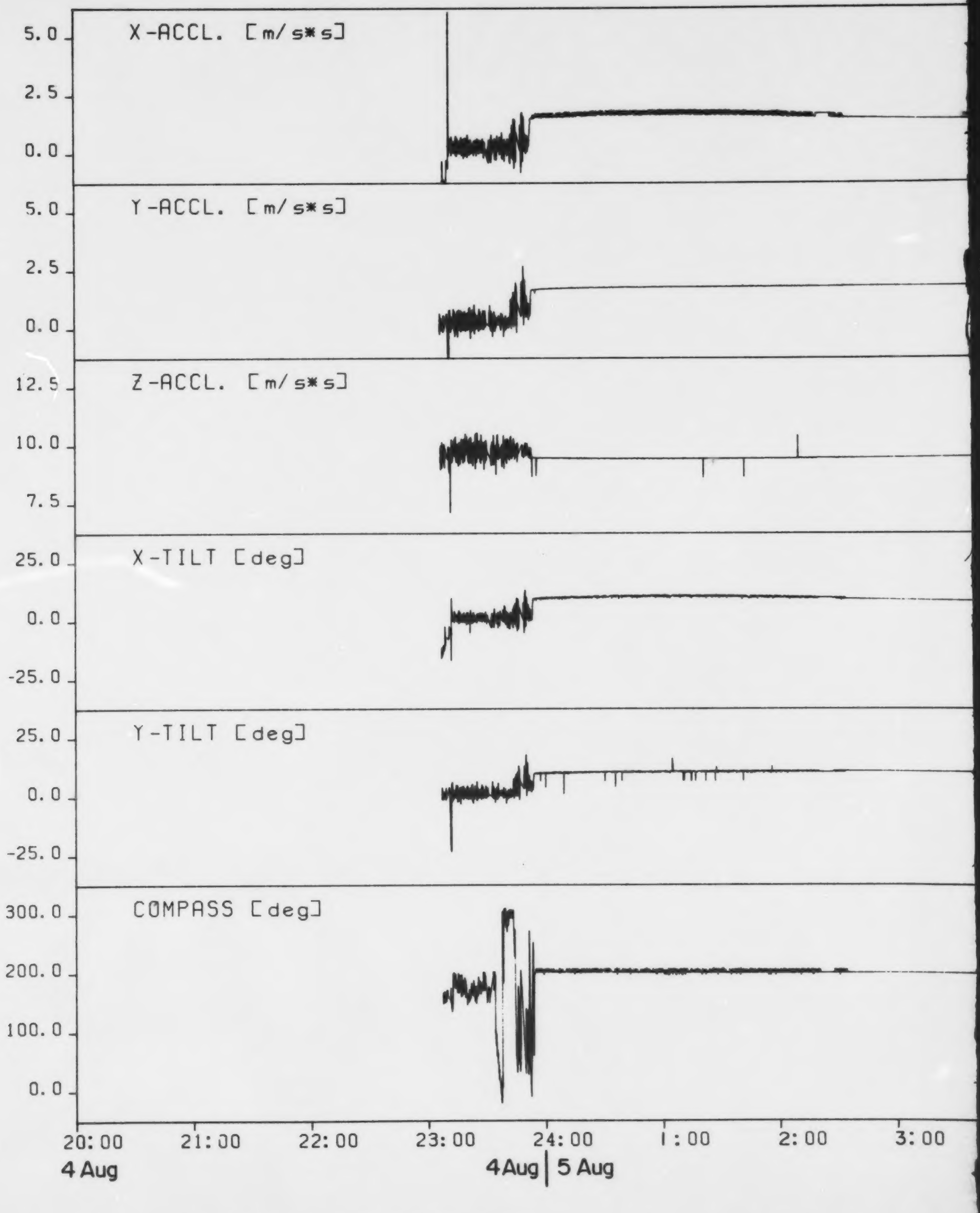

Figure 50. Compressed time series plot, iceberg "Bertha".

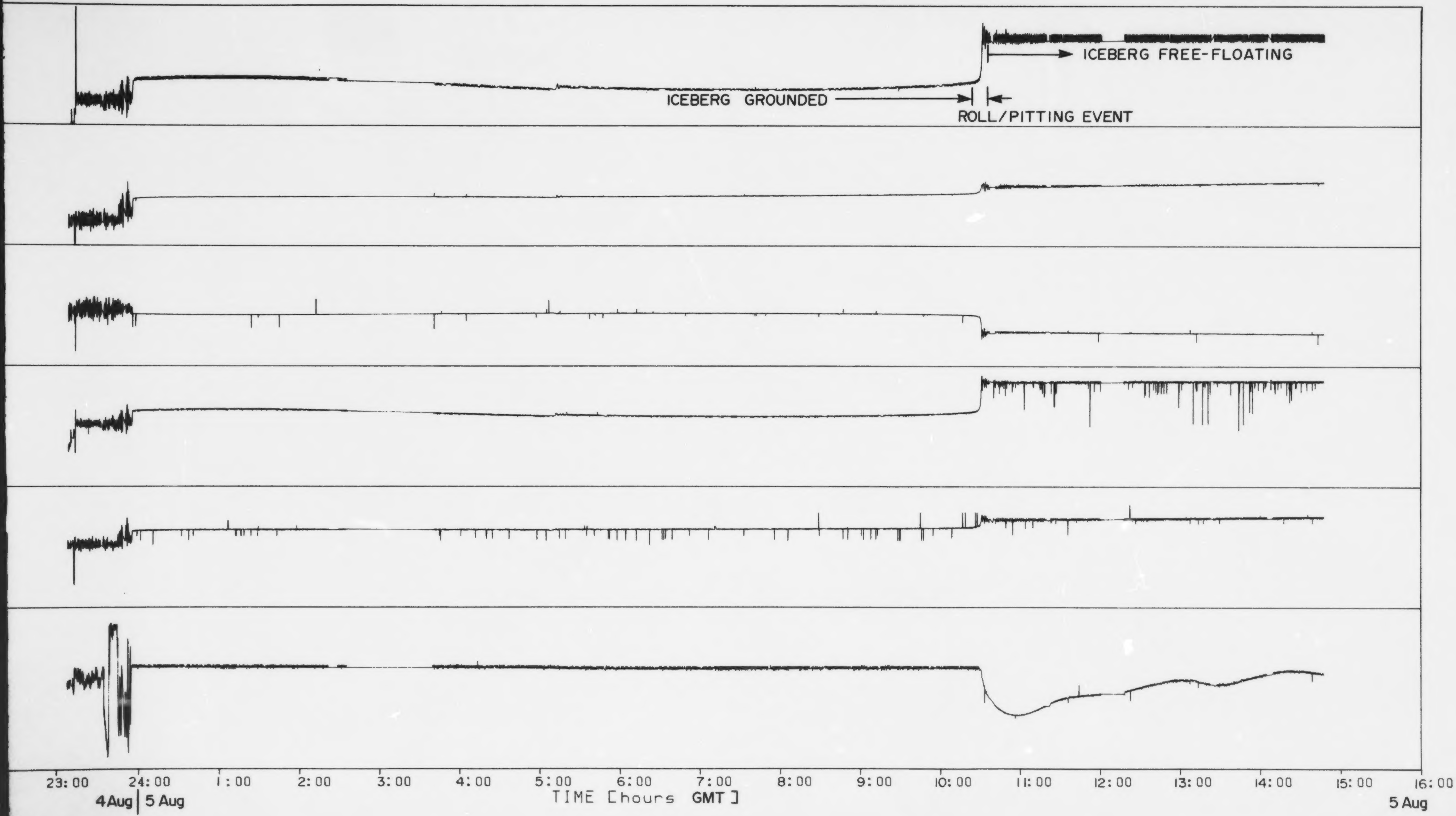

plot, iceberg "Bertha".

Deployment D-1, "Bertha". C-CORE package "D" was deployed on the grounded iceberg "Bertha" at approximately 2350 GMT on August 4. The short period oscillations and excursions at the beginning of the record prior to 2350 GMT represent motion of the sensor package while in transit to the iceberg (see Figure 50). The package continued to transmit data until 1448 GMT on August 5. One major event was captured during this period of time, shown starting at 1030 GMT on August 5. As noted previously, at 1030 GMT, August 5, "Bertha" was observed to calve, roll about 30°, yaw about 90° and float free of the seabed. This behaviour is confirmed by the data in Figure 50, in which changes in steady X-tilt of 20°, steady Y-tilt of 5°, and compass readings of 120° are seen. The occurrence of high tide at 0110 GMT and low tide at 0710 on August 5 are also evident on the X-acceleration and X-tilt curves in Figure 50, since the iceberg was grounded during this period.

Detailed motion plots of the "Bertha" calve/float-free event are shown in Figures 51-53. Note that the time is expressed in seconds, with 0 representing 1024 GMT on August 5. Although the general behaviour of the iceberg is quite readily apparent, fluctuations as a result of voltage variations in the conversion from analogue to digital format obscure some of the detail. The calving which triggered the events is difficult to identify, but probably took place at 350 + 50 s. The roll behaviour which followed included several large oscillations, which dampen out with time. The linear accelerations associated with this behaviour are very small (less than approximately 0.05 m/s^2). The accelerometers readings thus essentially represent the gravitational components along three orthogonal axes, and as such provide the same information regarding this primarily rotational event as the tiltmeters (see Figures 51, 52).

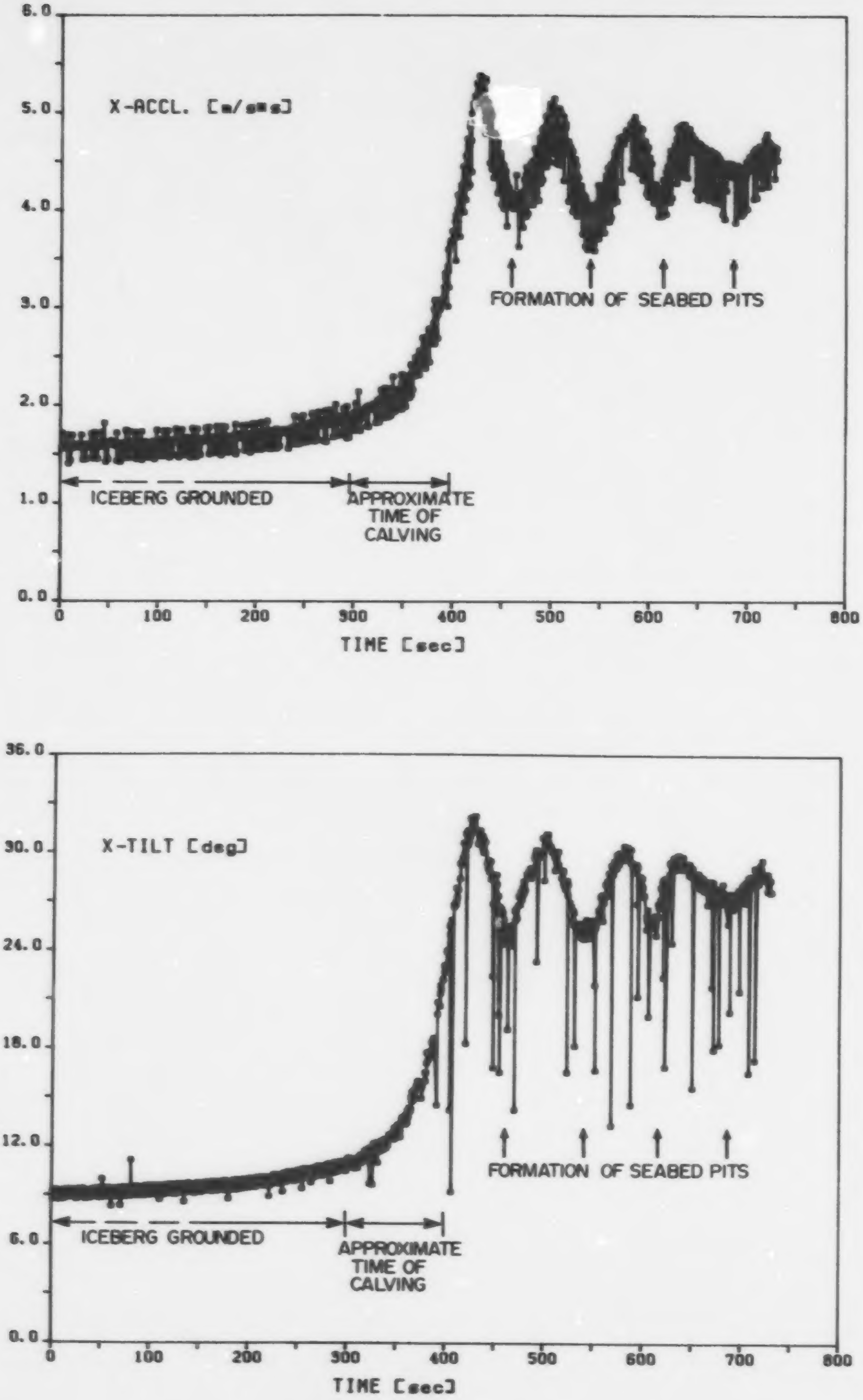

Figure 51. 'Bertha' roll/pitting event, X-acceleration and X-tilt. Time 0 represents 1024 GMT on August 5.

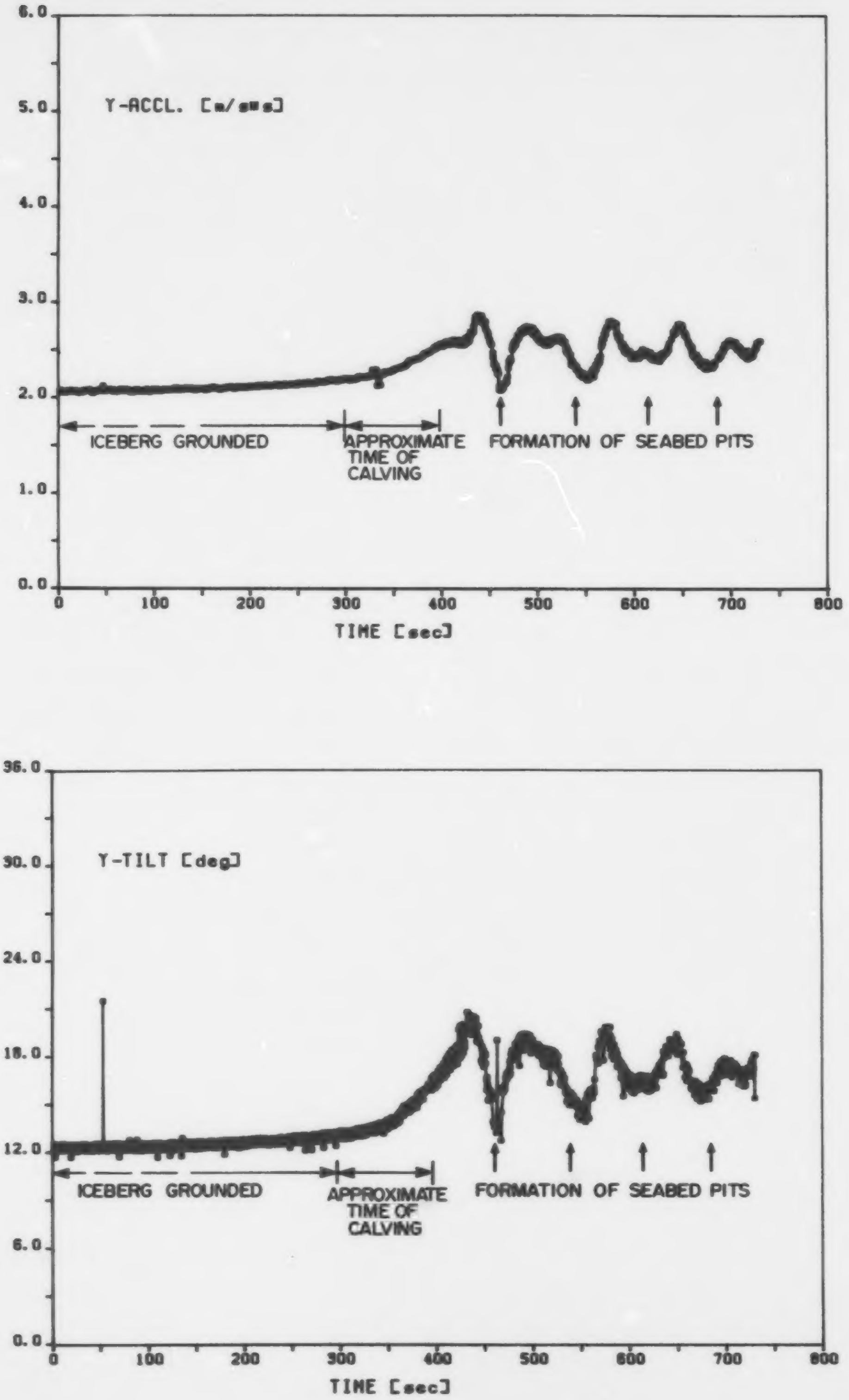

Figure 52. "Bertha" roll/pitting event, Y-acceleration and Y-tilt. Time 0 represents 1024 GMT on August 5.

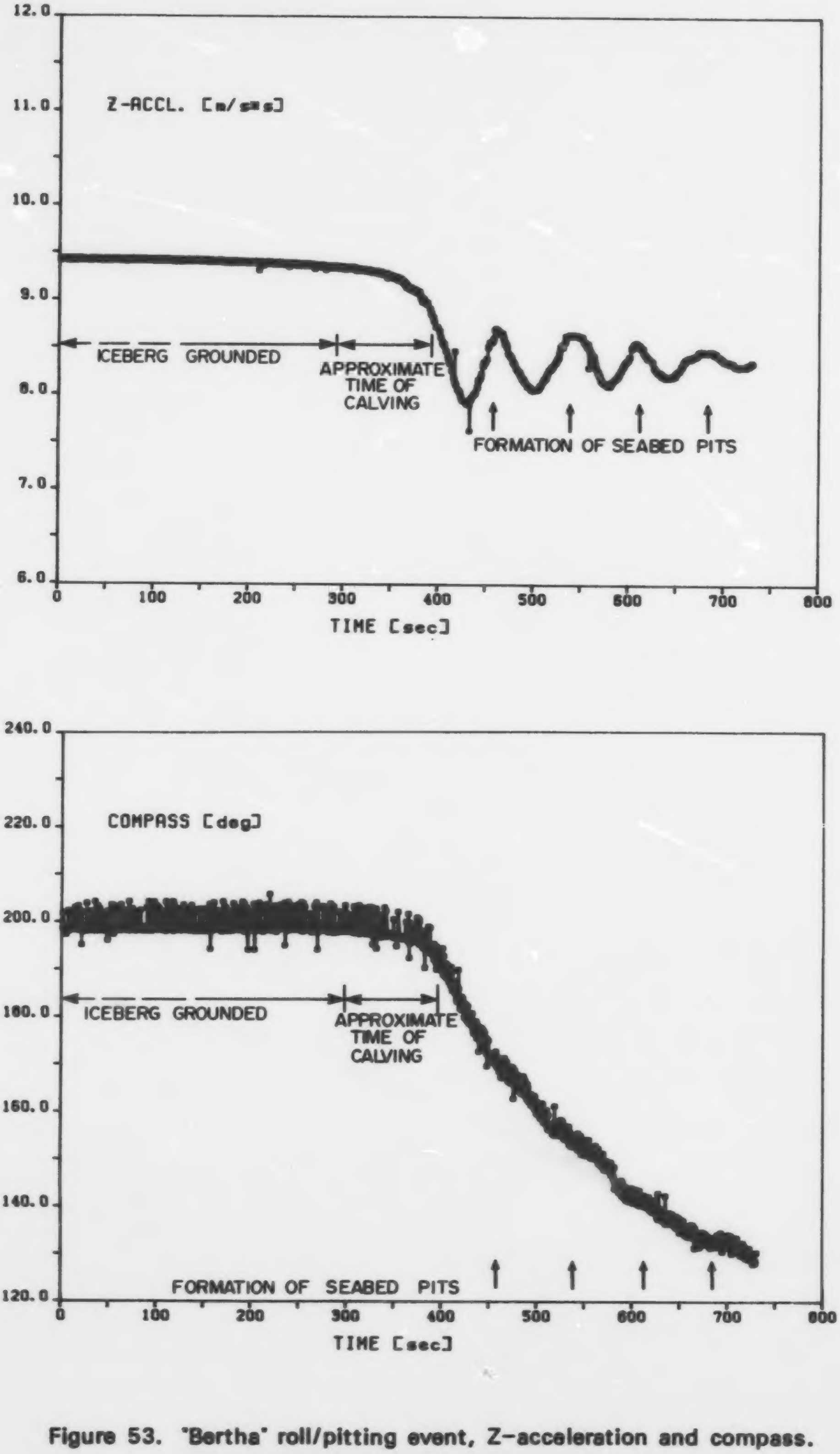

Figure 53. 'Bertha' roll/pitting event, Z-acceleration and compass. Time 0 represents 1024 GMT on August 5.

Based on visual evidence obtained by the submersible (see Chapter 4), "Bertha" produced a grounding pit followed by four discrete impact marks. Using these motion data and the iceberg profile data presented in Chapter 3, the "Bertha" seabed interaction event is reconstructed in Chapter 5.

Deployment D-2. C-CORE package "D" was deployed on "Gladys" at 2233 GMT on August 8 and it continued to transmit data until about 0840 GMT on August 9. As seen on Figure 54, one event is clearly identifiable at 0424 hours on August 9. Unfortunately, this occurred during the night and thus was not observed by the team onboard Polar Circle. Sidescan data recorded over the trajectory of "Gladys" during this period, however, reveal no new scour features. Hence, no further work has been conducted on this event.

It is interesting to note the long term variation in compass reading for this free-floating iceberg. A trend of approximately 5 deg/hr with a ± 40 deg variation superimposed, was apparently generated by the wind and current forces during the observation period.

Deployment D-3. C-CORE package "D" was redeployed on "Gladys" at 2336 GMT on August 9 and it continued to transmit data until 0910 GMT on August 12. The compressed time series data plot for this deployment are shown in Figure 55. The split of "Gladys" into two parts is seen at about 1320 GMT on August 10, preceeded at 1300 GMT by a large calving event. The sensor package was on "Gladys" and recorded the motion of the piece which grounded during its roll and subsequent contact with the seabed. Because no fresh seabed disruption could be discerned on the sidescan records covering the path of "Gladys" before the split, the calving event at 1300 GMT apparently did not result in seabed contact and thus is not considered further.

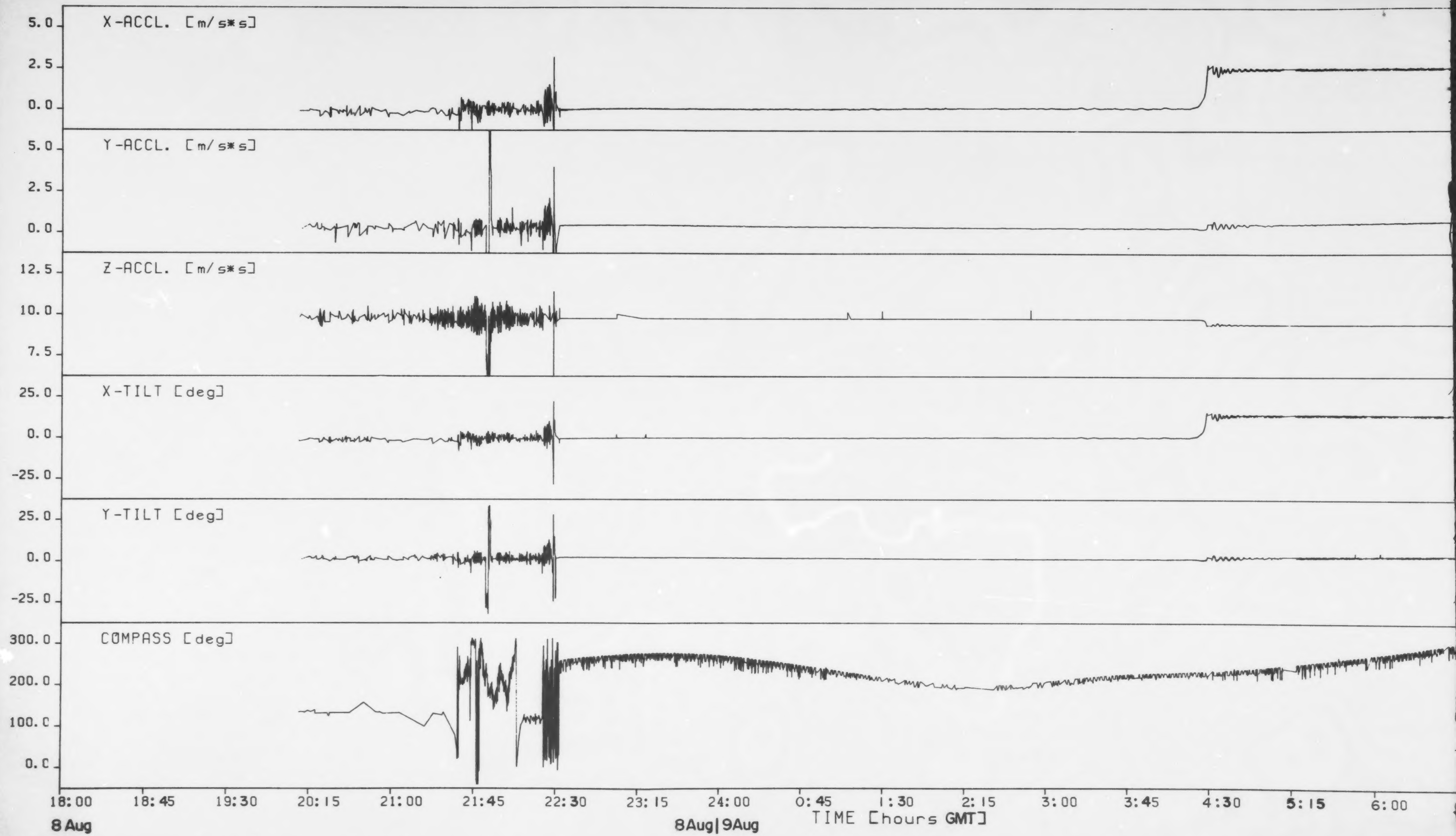

Figure 54. Compressed time series plot, iceberg "Gladys", deployment D-2.

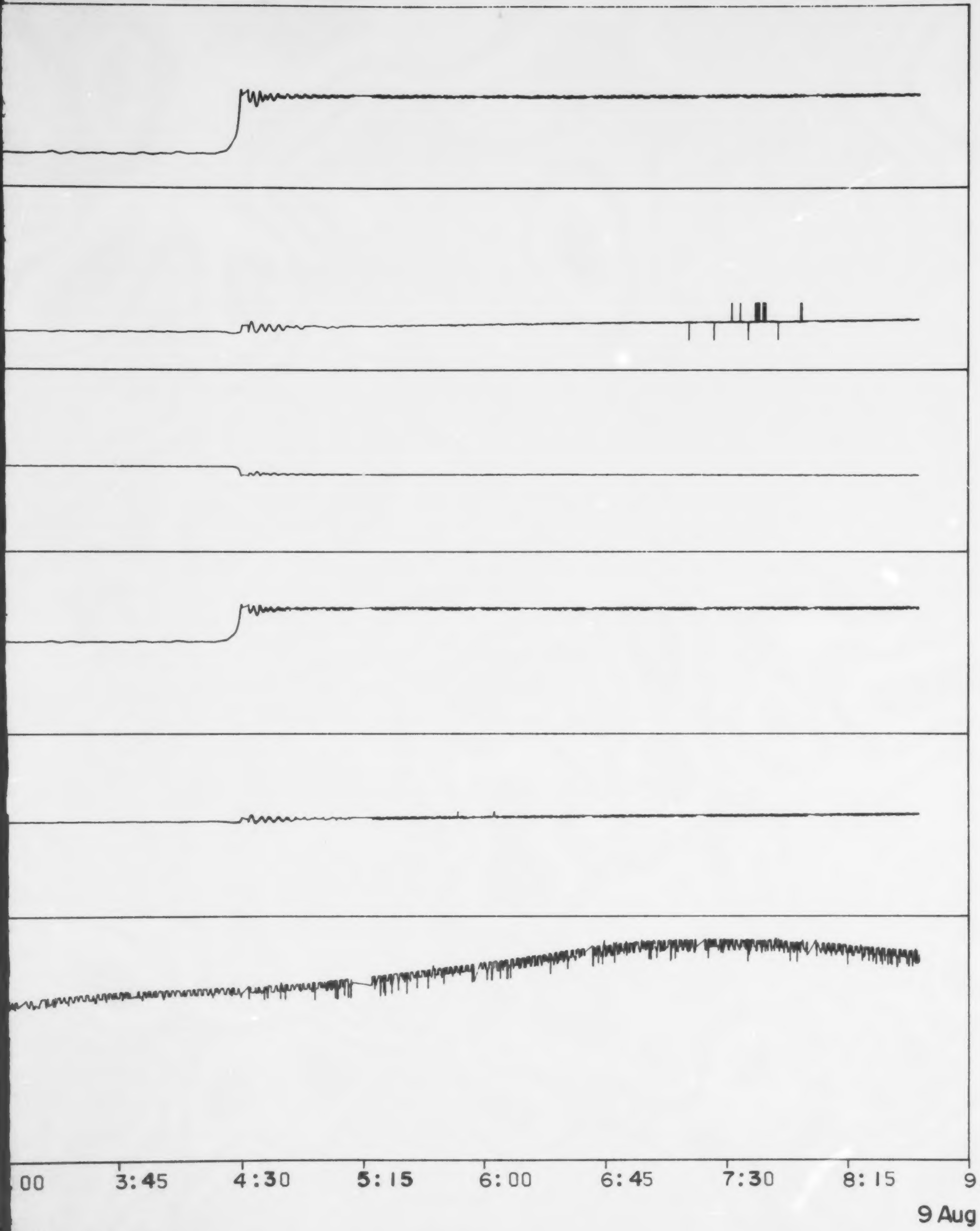

.00
3:45
4:30
5:15
6:00
6:45
7:30
8:15
9.00
9 Aug

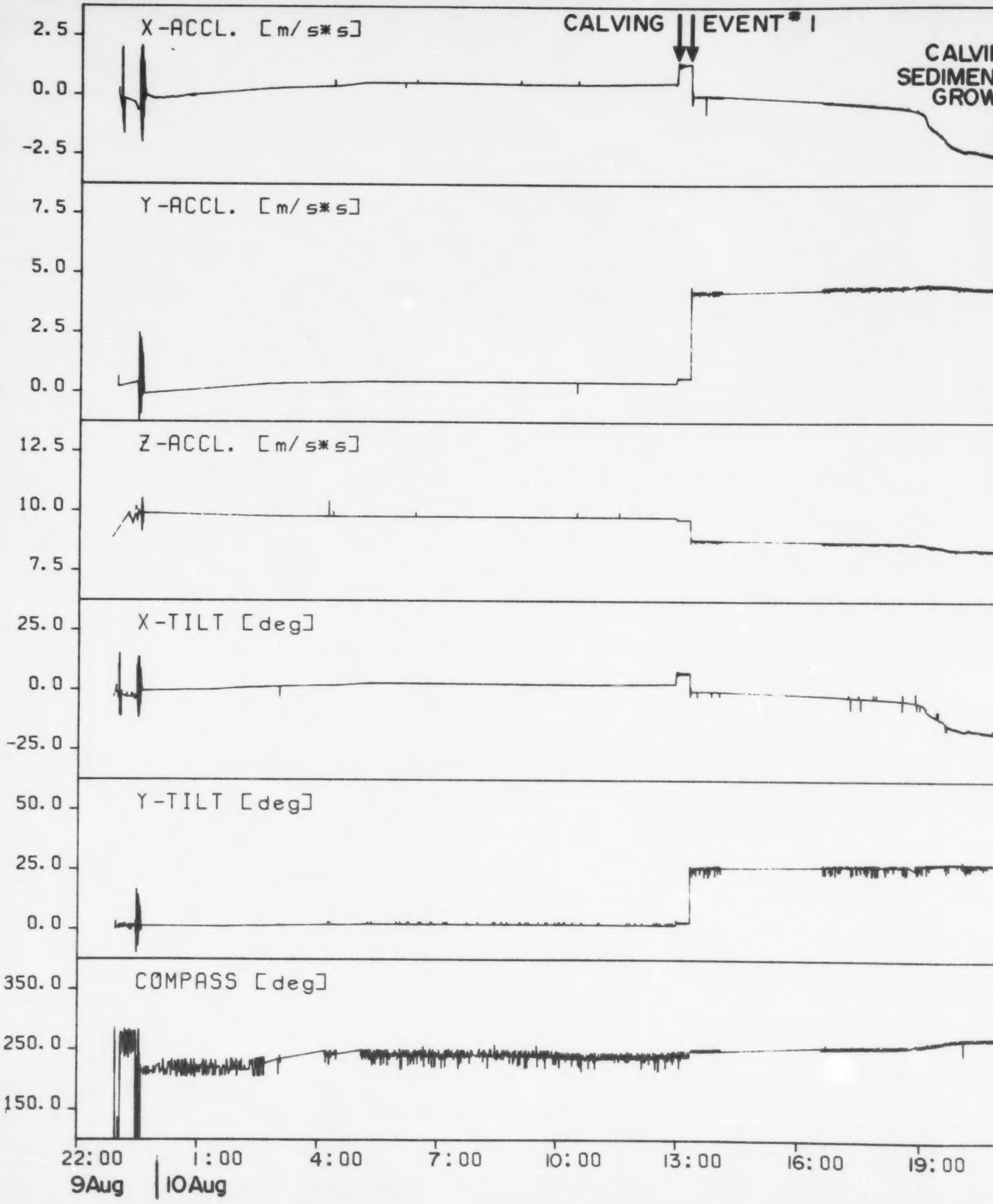

Figure 55. Compressed time series plot, iceberg "Gladys", deployment D-3.

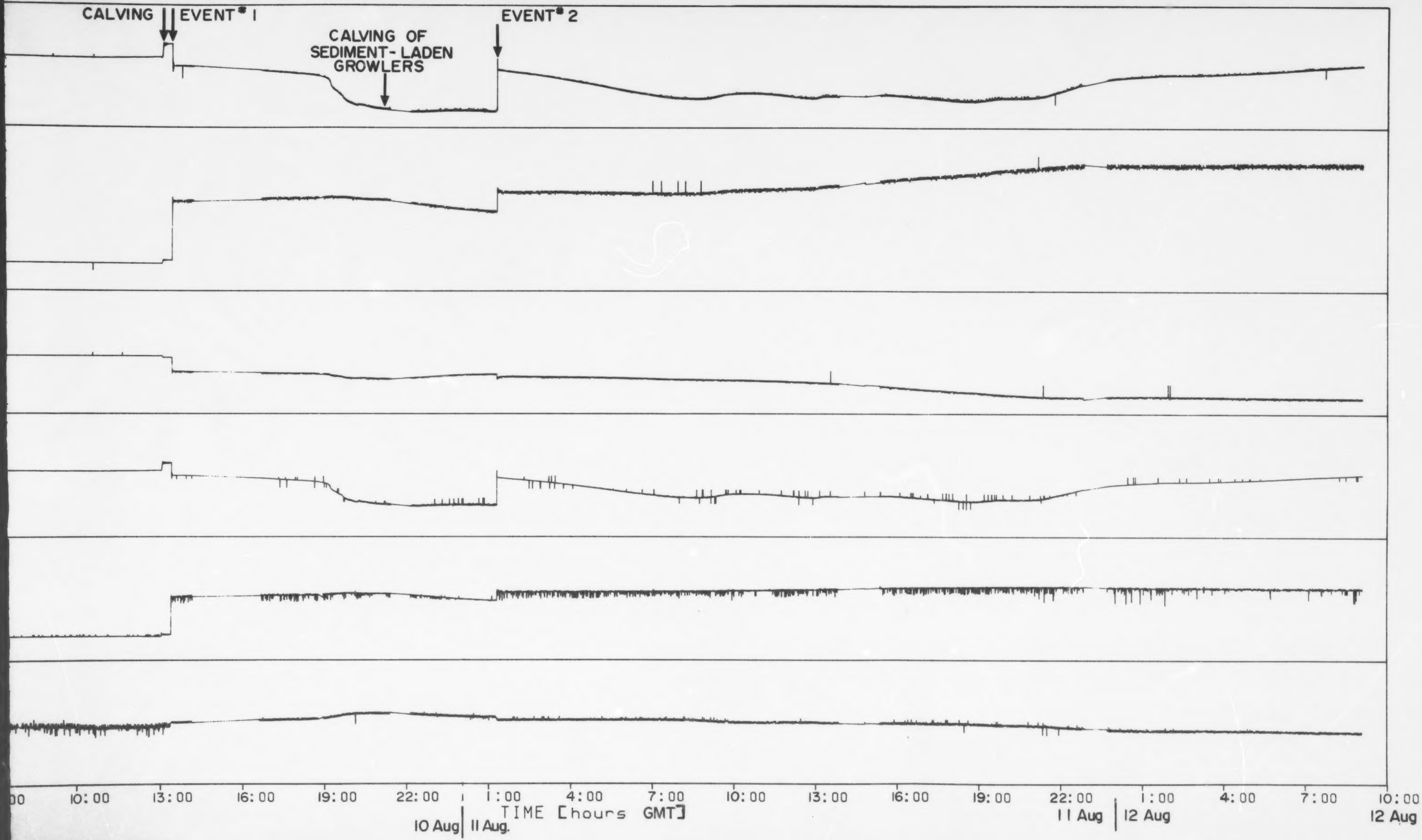

rg "Gladys", deployment D-3.

Detailed motion plots of the "Gladys" split/roll event ("Gladys" event #1) are shown in Figures 56-58. Because this event was very abrupt, the time scale has been expanded considerably, with 0 representing 1319 GMT on August 10. Beginning at about 68 s, an increase of 22° on Y-tilt and a decrease of 7° on X-tilt are seen over a period of only 17 s. At 85.25 s, the iceberg is still rolling rapidly, yet the next data packet, at 89.5 s, shows an abrupt increase in X-tilt and a reduced rate of increase in Y-tilt. It is thus believed that "Gladys" struck the seabed between these two time intervals; a period of about 4.25 s. The motion traces after seabed contact indicate that the iceberg oscillated about its grounded keel, with these oscillations essentially dying out beyond 300 s. The dynamics of this dramatic split/roll seabed interaction event is treated in Chapter 5.

Once in contact with the seabed, "Gladys" experienced additional adjustments in orientation. As noted in Chapter 3, "Gladys" was observed to calve a number of sediment-laden growlers at about 2100 GMT on August 10. It is felt that this represented ice released from the keel/seabed interface. As seen on Figure 55, this calving was preceeded by a slow decrease in X-tilt of about 15° beginning at 1900 GMT. Note that the main split/roll event at 1320 GMT was experienced primarily on Y-tilt, but that X-tilt did decrease during the event. It is likely that the further reduction of X-tilt was a combination of soil and keel ice accommodation associated with the high stresses generated during impact leading to ice failure at the seabed interface.

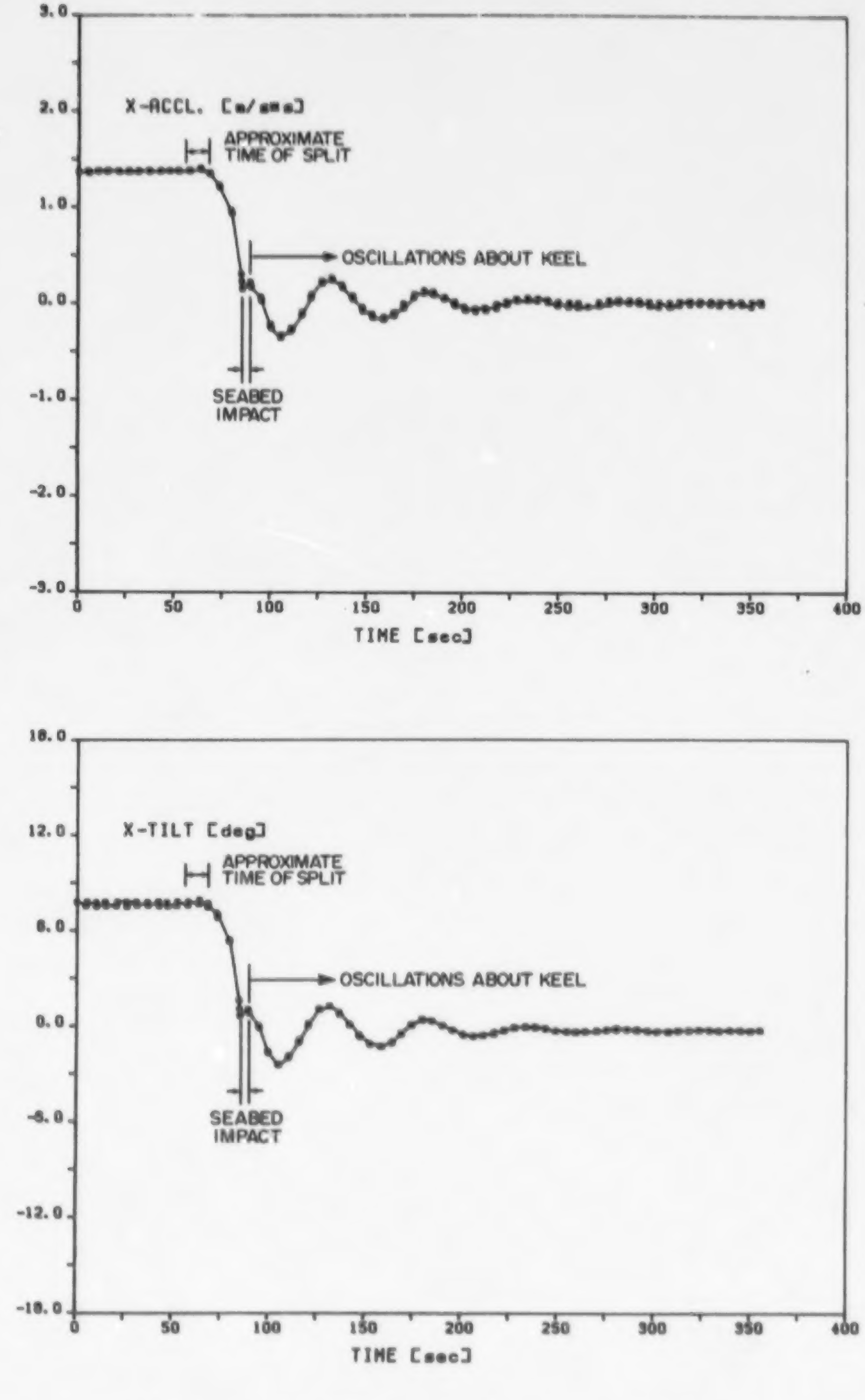

Figure 56. 'Gladys' split/roll event, X-acceleration and X-tilt. Time 0 represents 1319 GMT on August 10.

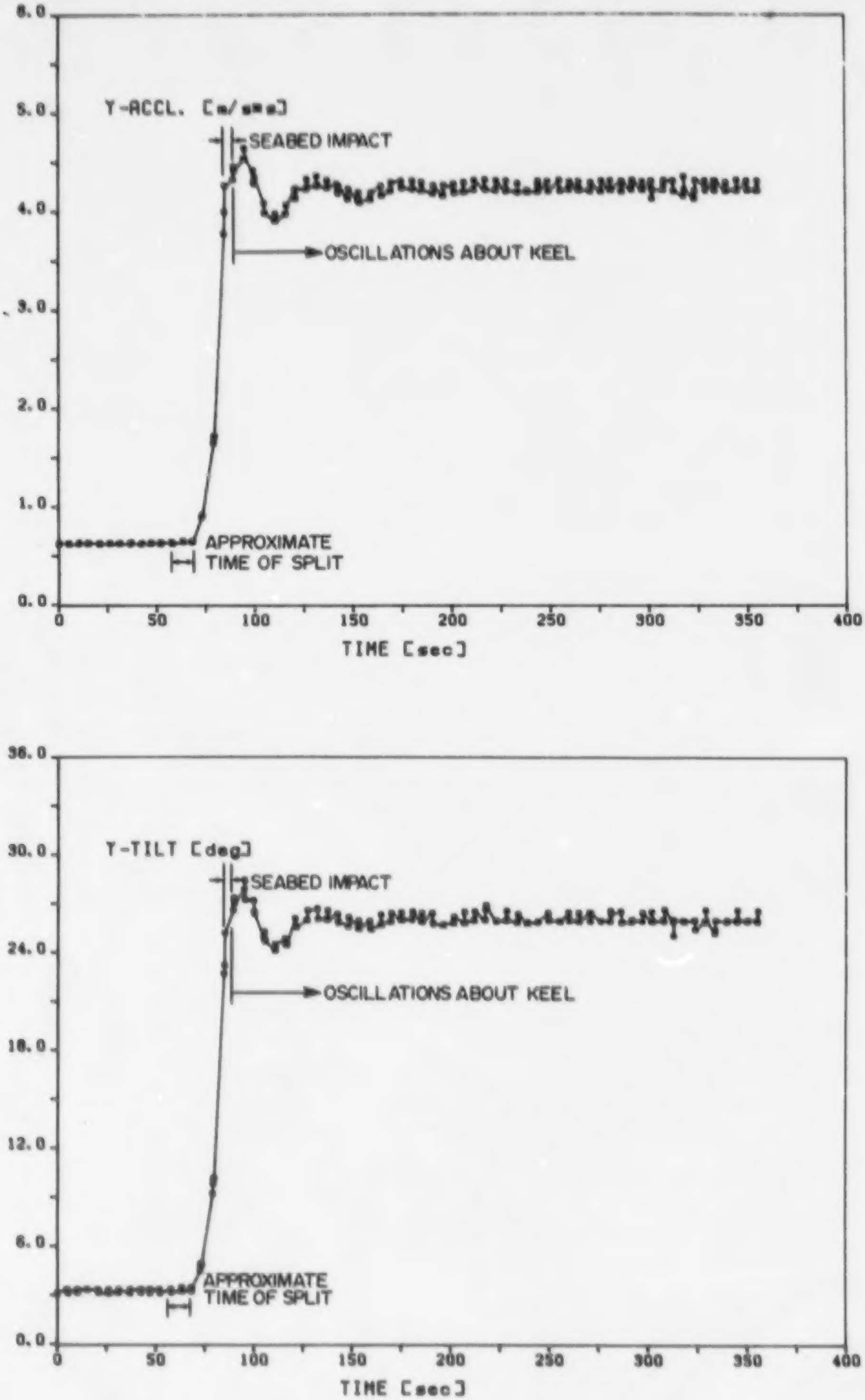

Figure 57. 'Gladys' split/roll event, Y-acceleration and Y-tilt.
Time 0 represents 1319 GMT on August 10.

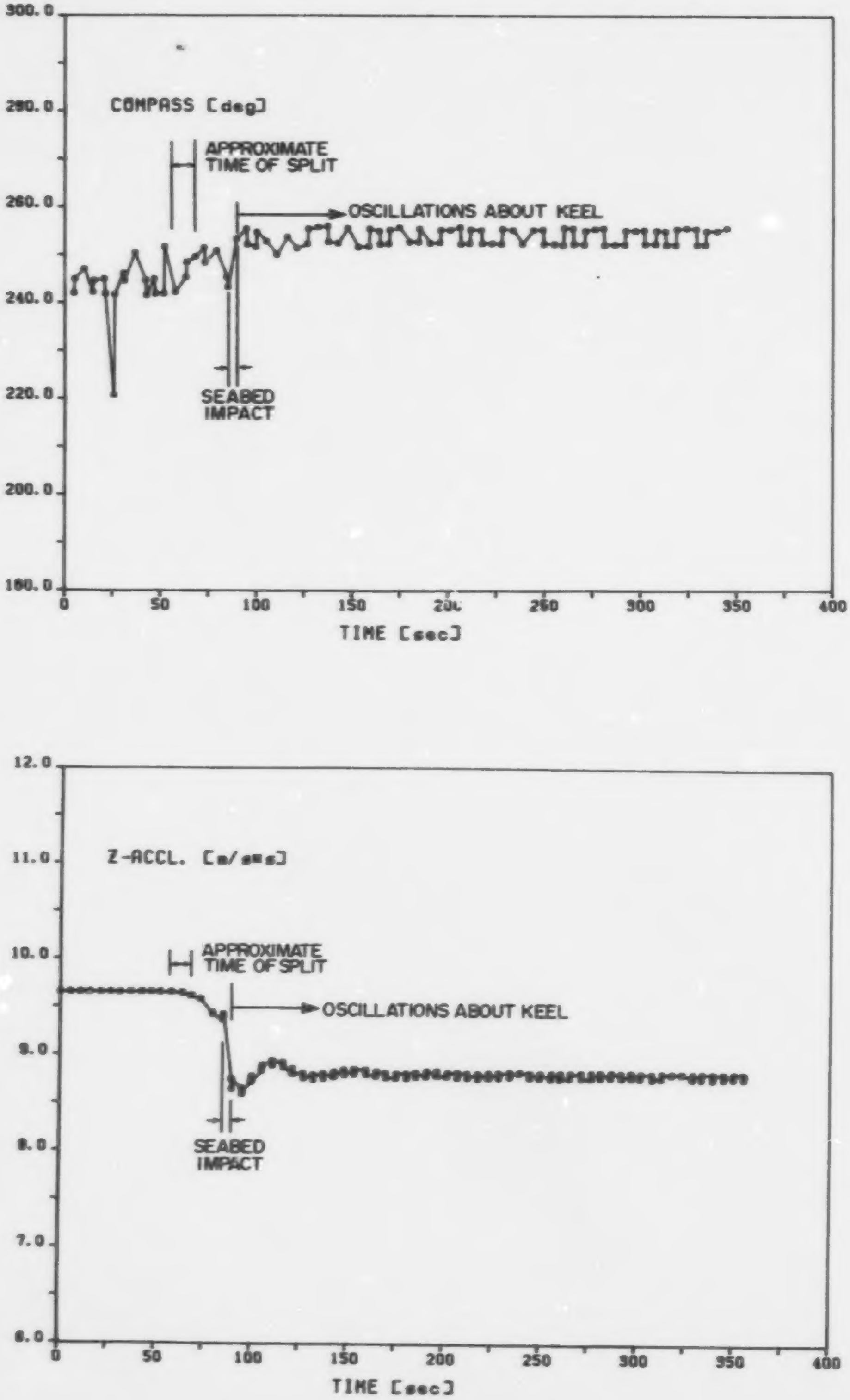

Figure 58. "Gladys" split/roll event, Z-acceleration and compass. Time 0 represents 1319 GMT on August 10.

A second adjustment in orientation of "Gladys" may be seen on Figure 55, at 0117 GMT on August 11. This "Gladys" event #2 occurred at dusk, and no calving was noted by observers onboard the Polar Circle. Figures 59-61 show this event on an expanded time scale, with 0 representing 0116 GMT on August 11. It can be seen that the adjustment was primarily along X-tilt, and was very abrupt with some overshoot but no post-event oscillation. In contrast to event #1 and the subsequent keel accommodation, X-tilt in this event increased.

Unfortunately, conclusive evidence is not available to dismiss the possibility of ice failure during this abrupt event #2. However, a repeat of the calving of sediment laden growlers would likely have been observed even at dusk. It is likely that event #2 represents additional soil failure associated with the large static contact forces.

The overall behaviour of "Gladys" following the main split/roll event, including event #2, is discussed in Chapter 5. In addition to numerous minor calving events, the observed adjustments in orientation of the iceberg between the times of aerial photography and underwater profiling affected the quality of the overall shape determination and the dynamic analysis of event #1.

Deployment D-4. C-CORE package "D" was deployed on "Lucretia" at 1703 GMT August 19 (see Figure 62). At 1748 GMT on August 19, the package was rotated approximately 180° to centre the compass away from the 0-360° transition point. Although numerous ship's power interruptions caused large gaps in the logged data, computer logging continued until about 0442 GMT on August 21. At that time, the data were logged on paper by a printer until the package was recovered at 2320 GMT on August 21. As "Lucretia" remained in deep

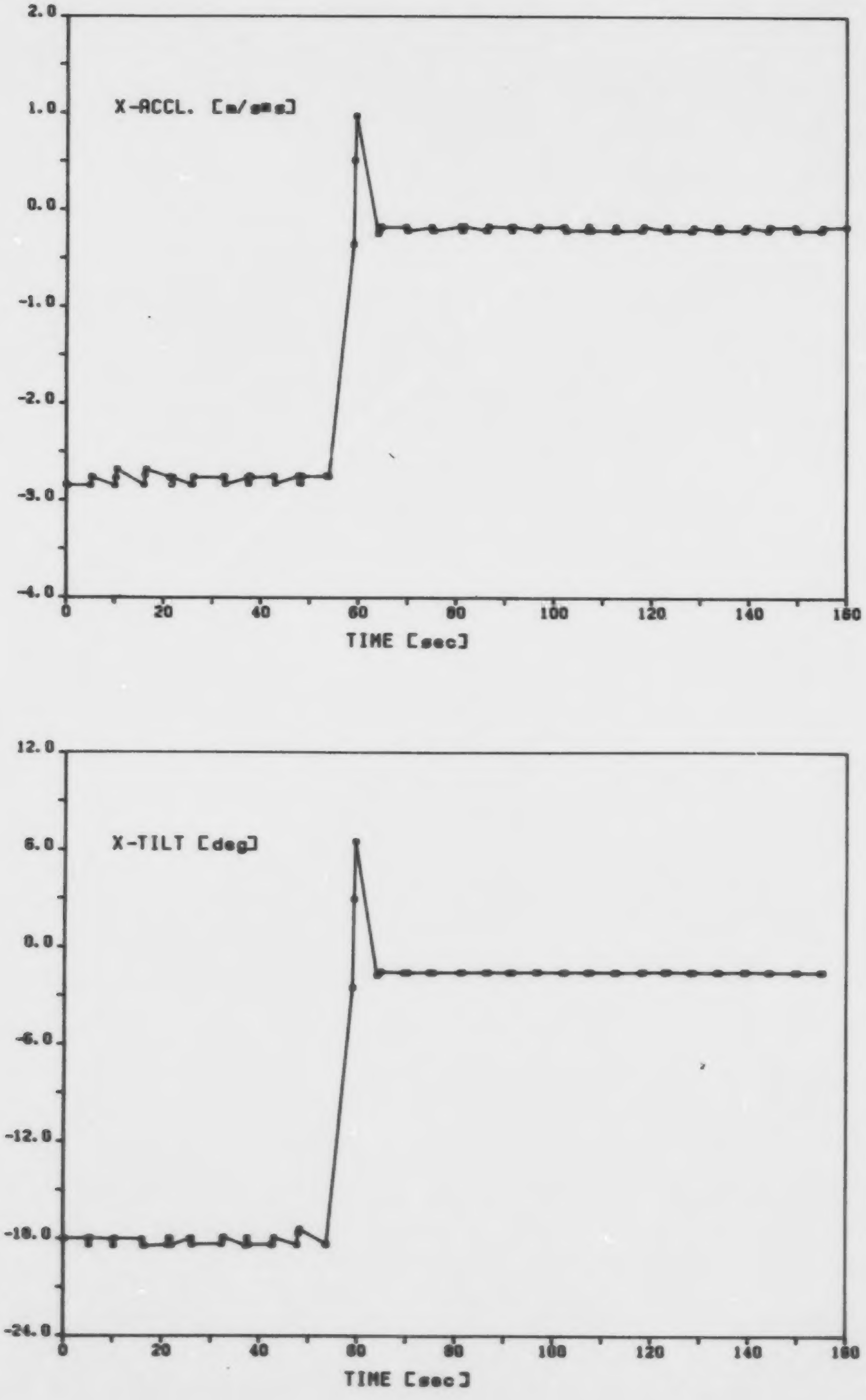

Figure 59. 'Gladys' event #2, X-acceleration and X-tilt. Time 0 represents 0116 GMT on August 11.

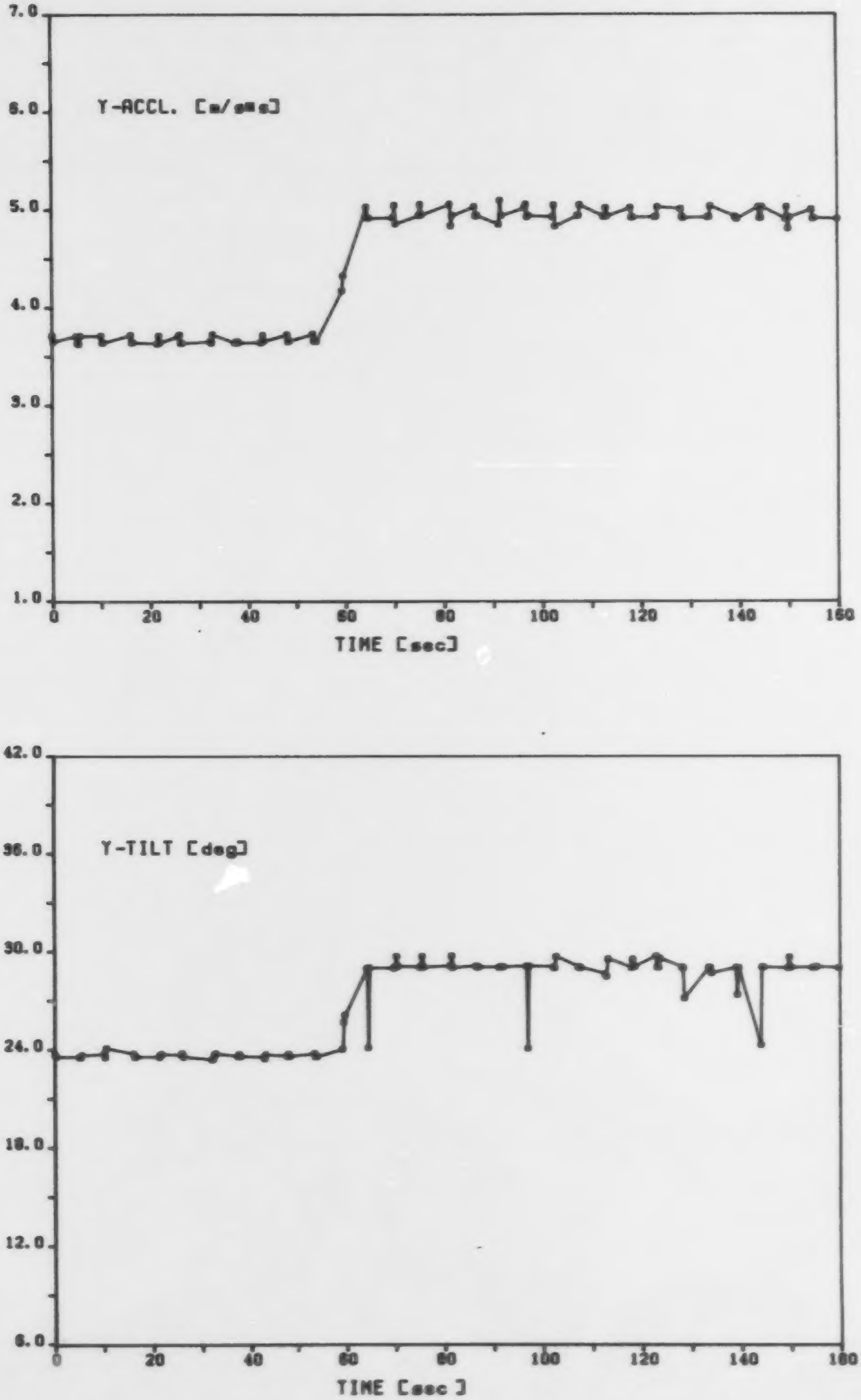

Figure 60. 'Gladys' event #2 Y-acceleration and Y-tilt. Time 0 represents 0116 GMT on August 11.

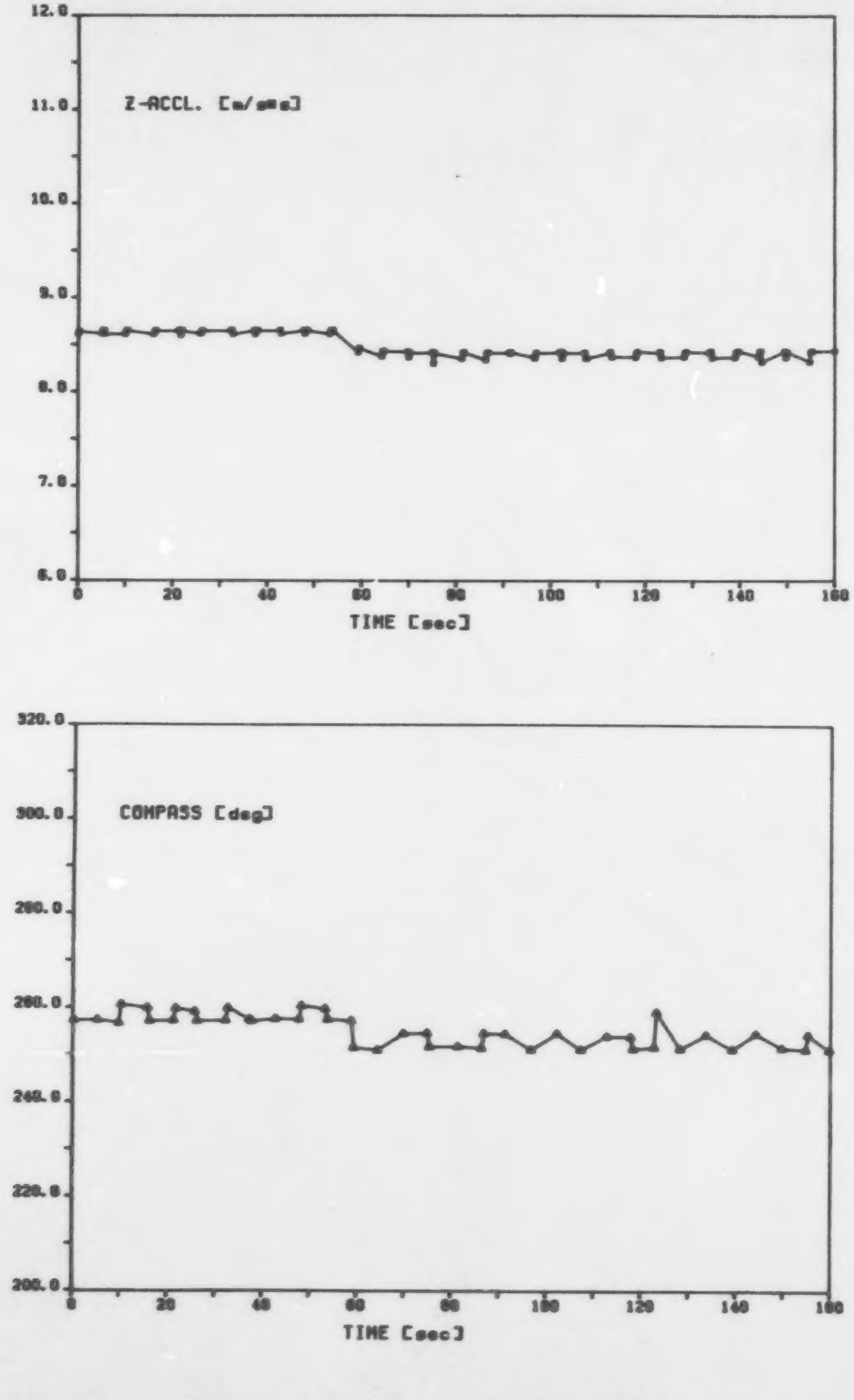

Figure 61. "Gladys" event #2, Z-acceleration and compass. Time 0 represents 0116 GMT on August 11.

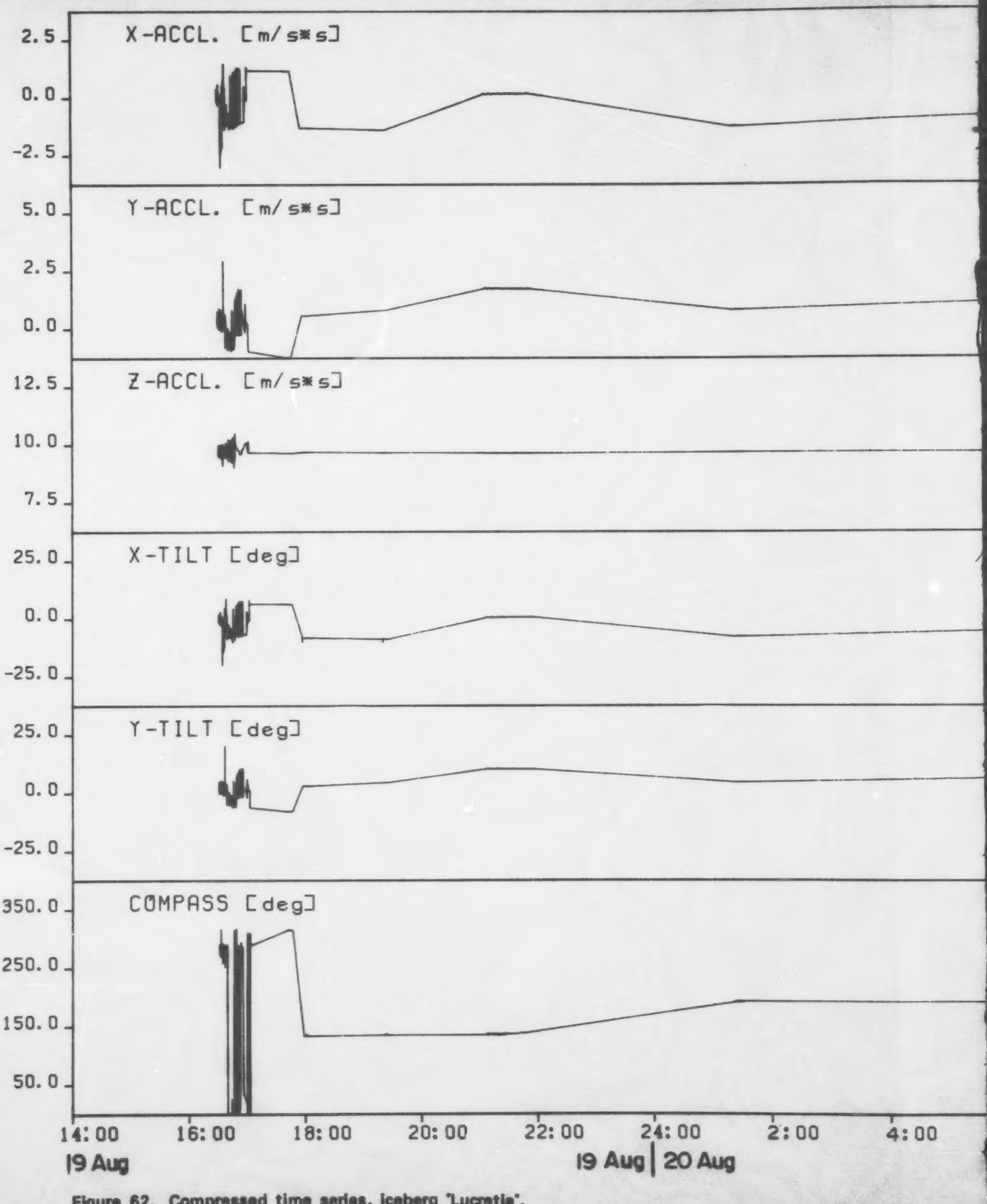

Figure 62. Compressed time series, iceberg "Lucretia".

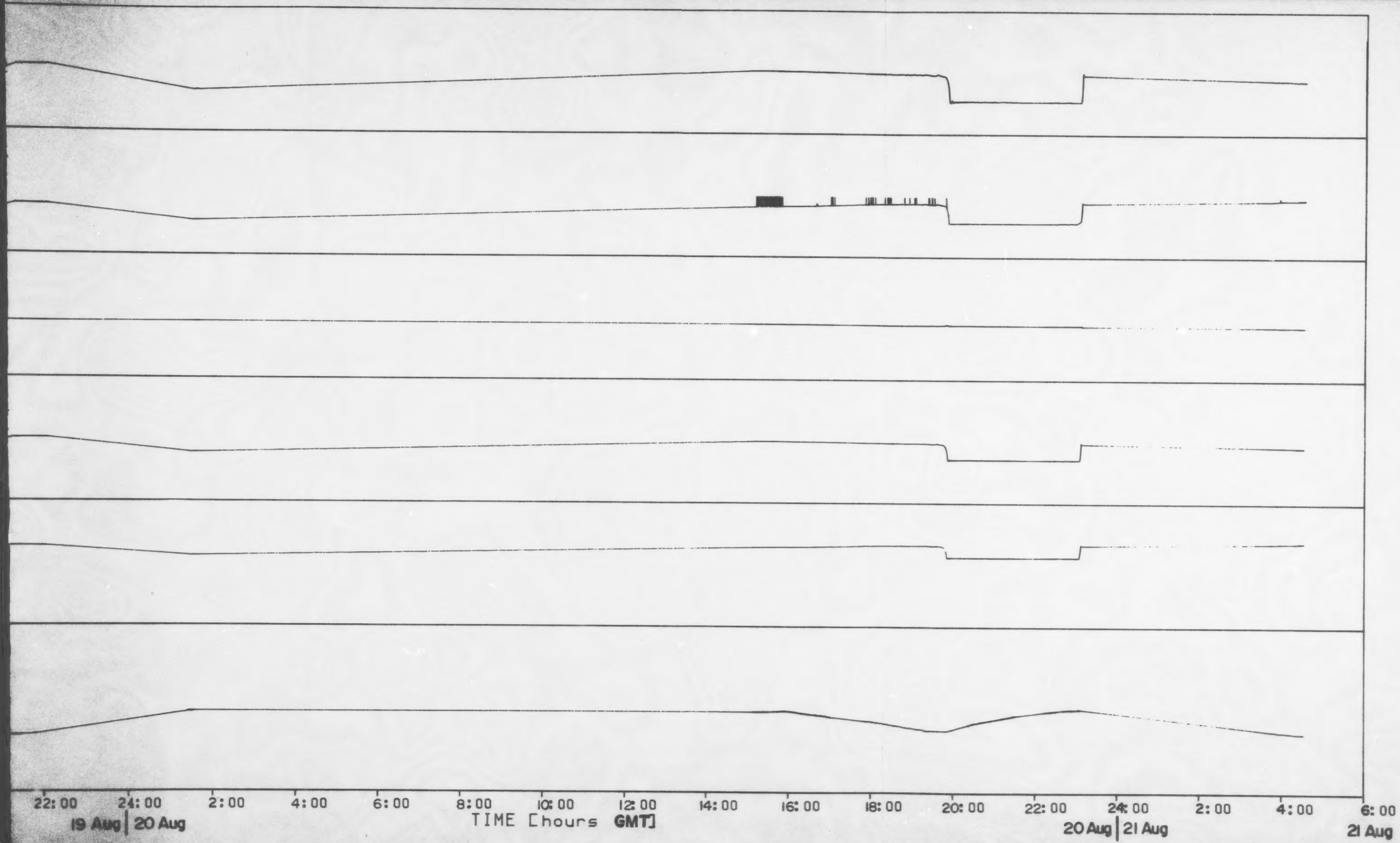
22:00
24:00
2:00
4:00
6:00
8:00
10:00
12:00
14:00
16:00
18:00
20:00
22:00
24:00
2:00
4:00
6:00
19 Aug | 20 Aug
TIME [hours GMT]
20 Aug | 21 Aug
21 Aug

water throughout its observation period, no seabed interaction events were observed, and hence no further analysis was conducted on data from this deployment.

Deployment C-5. C-CORE package "C" was deployed on the grounded iceberg "Julianna" at 1740 GMT on August 19 (see Figure 63). Computer logging continued until about 0442 GMT on August 21, at which time the data were logged on paper by a printer until transmission ceased at approximately 1900 GMT on August 21. Although several small calving events were observed during this observation period, "Julianna" remained solidly grounded with little change in orientation. Although no dynamic seabed interaction events were observed for "Julianna", an analysis is presented in Chapter 5 whereby static vertical seabed load is determined based on buoyancy considerations.

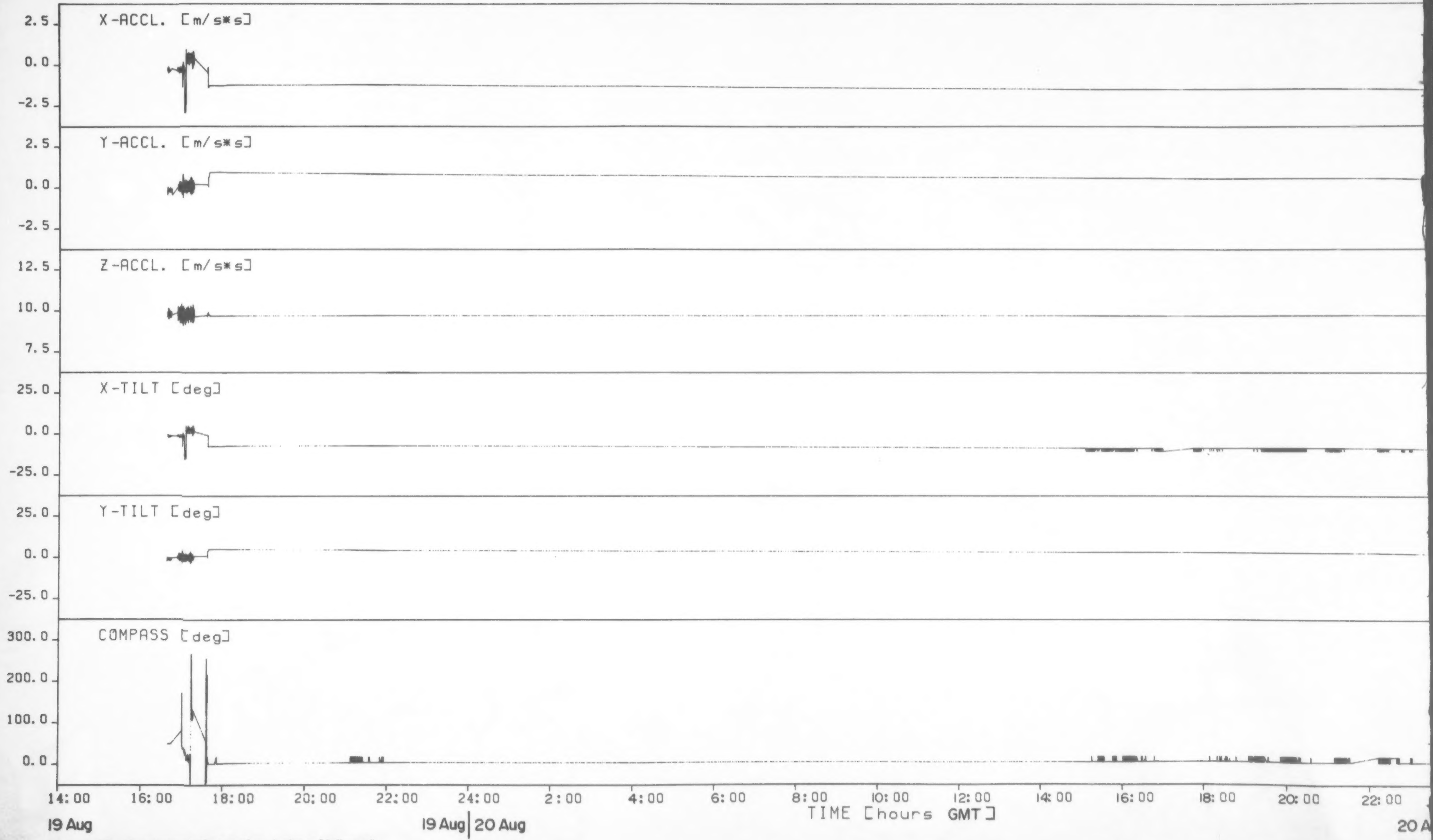

Figure 63. Compressed time series, iceberg 'Julianna'.

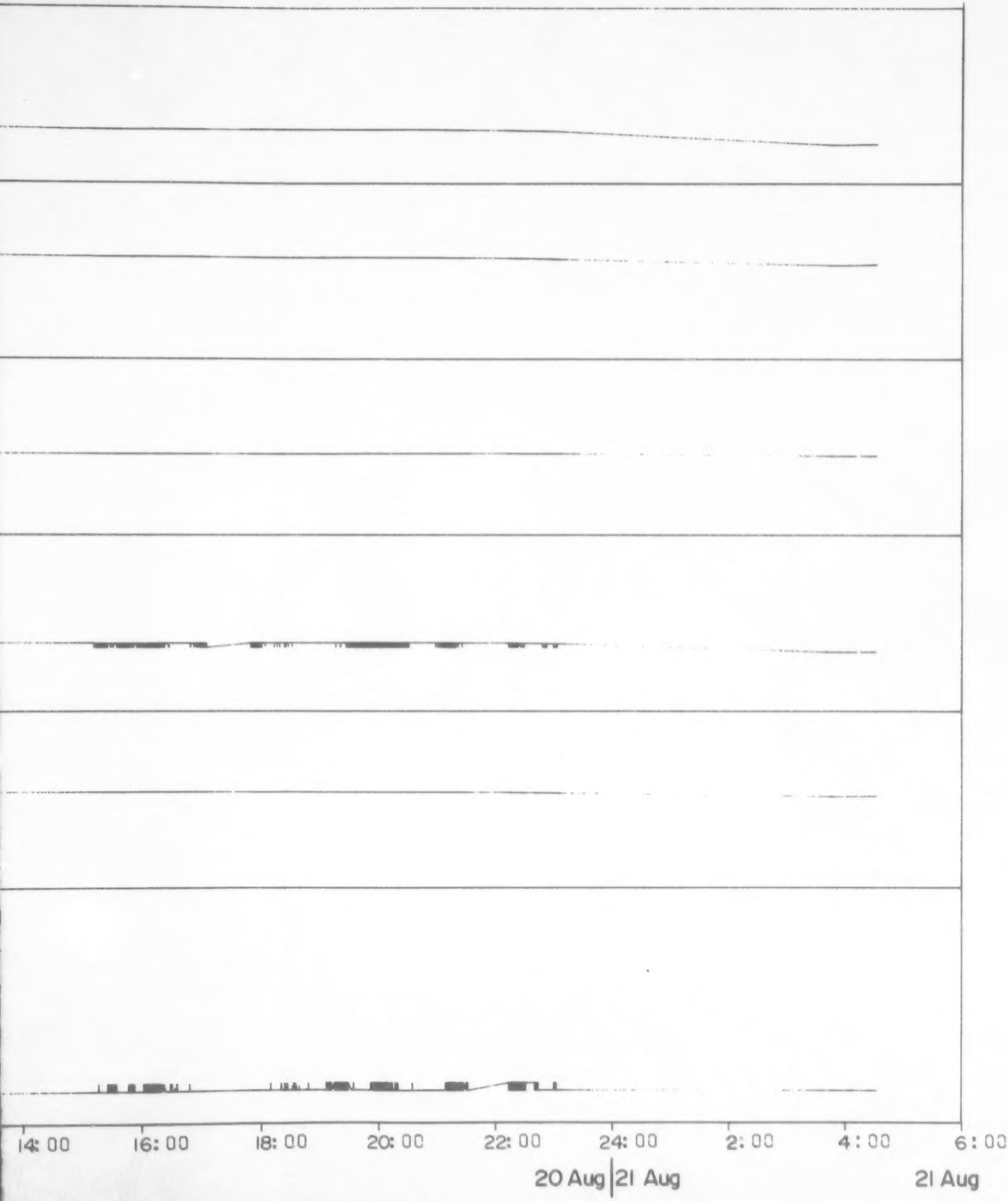
14: 00
16: 00
18: 00
20: 00
22: 00
24: 00
2: 00
4: 00
6: 00
20 Aug
21 Aug
21 Aug

CHAPTER 4.0

ICEBERG SCOUR AND SEDIMENT TRANSPORT OBSERVATIONS

OBSERVATIONS FROM SUBMERSIBLE

This section describes visual observations of both new and old scours made from the Fisheries and Oceans Canada research submersible Pisces IV. During some of these dives new features of iceberg scours were recorded in detail for the first time. Newly documented features include cohesive, blocky and fractured berms with relief as great as 6 m; irregularly shaped pits within the scour troughs, now recognized as ice meltout features, and indicating the breaking off of iceberg ice from the scouring keel; small-scale ridge and groove microtopography, generated by irregularities in the trailing keel surface; flat-topped mounds in a depressed area of one scour ("Big Makk") which may represent a zone of redeposition beneath the scouring keel; small conical mounds, interpreted as sand volcanos, which may represent extrusion of liquefied sediment during scour.

These descriptions have been condensed from detailed dive logs which are reproduced in Appendix 9. The dives in this section are described in chronological order except for two dives on the "Big Makk" scour and two dives on the western edge of Makkovik Bank. These dives are combined in two sections for the sake of readability. A map showing the location of all dives made on Makkovik Bank during the DIGS experiment is given in Figure 64. Dives conducted on Saglek Bank, Hudson Strait and on the Southern Baffin Island Shelf, although not done as part of the DIGS experiment, are included for their relevance to the study.

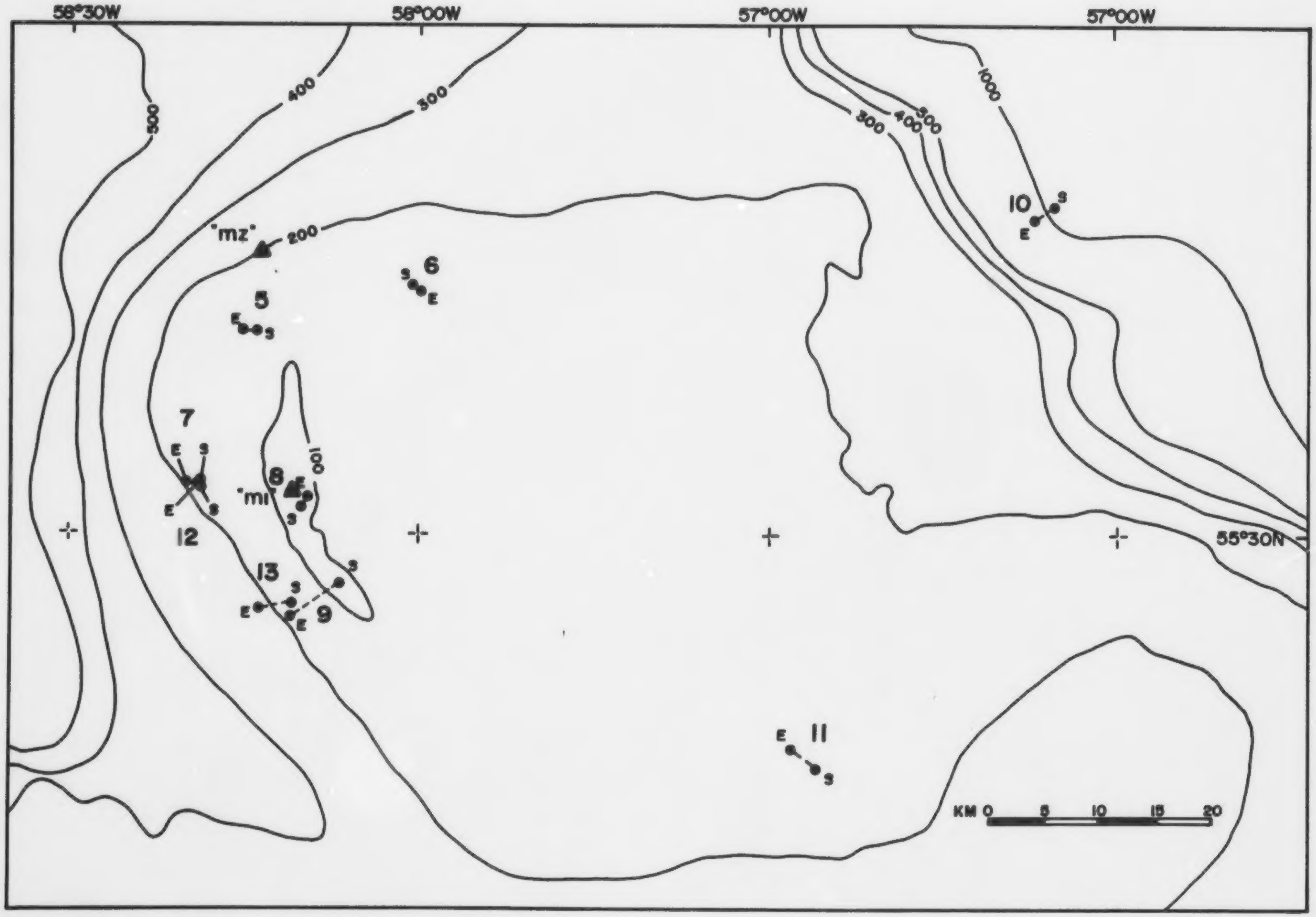
58°30W
58°00W
57°00W
57°00W
55°30N
500
400
300
200
100
300
400
500
1000
"mz"
"mi"
5
6
7
8
9
10
11
12
13
E
S
KM 0 5 10 15 20

Figure 64. *Pisces IV* dive locations, Makkovik Bank.

Although described in detail in this section, specific scour features are not illustrated here. Photographs of those features, together with possible interpretations of their origins, are discussed more fully in Chapters 5 and 6 under specific headings.

Makkovik Bank, "Bertha" Grounding Site

This dive (location number 5) surveyed the scour mark that iceberg "Bertha" made two weeks earlier in 107 m water depth (Figures 65 and 66). The seabed around the site had a well-developed gravelly lag surface above the Upper Till (Josenhans et al. 1986) with considerable and varied biogenic cover. In some areas, localized sand or gravel ripples were also present. These bedforms and the well-developed lag surface indicate a dynamic current regime.

Ungrounding of the iceberg produced four aligned but separate impact marks which could clearly be seen on the 100-kHz sidescan data (see Figures 65 and 66).

Small-scale ridge and groove microtopogaphy seen on the sidescan sonograms was observed from the submersible in the troughs of the last three impact marks. In one impact mark (B3 in Figure 66) lineations were observed as two distinct sets at nearly 90°, centred on a boulder embedded in a small pit. The event started from a pit which lacked linear grooves, but had well-developed berms up to 1.5 m in height. Apparently, wallowing of the grounded iceberg displaced the surficial sediment and underlying glacial till from below the keel to form the berms. The sediments in the trough of the pit were apparently remoulded and compacted. Within the

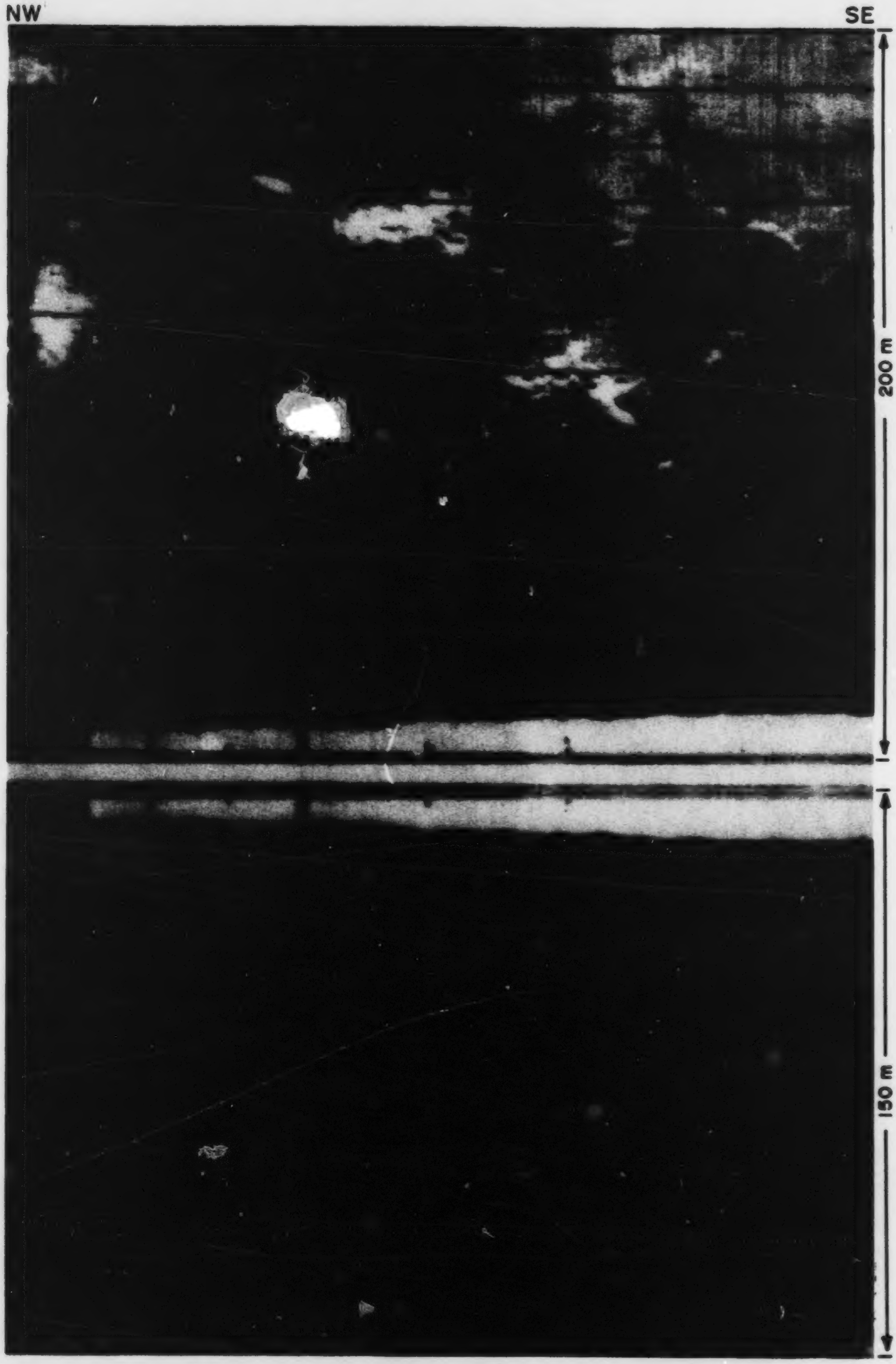
NW
SE
200 m
150 m

Figure 65. A sidescan sonogram from Line 9A showing the "Bertha" pits.

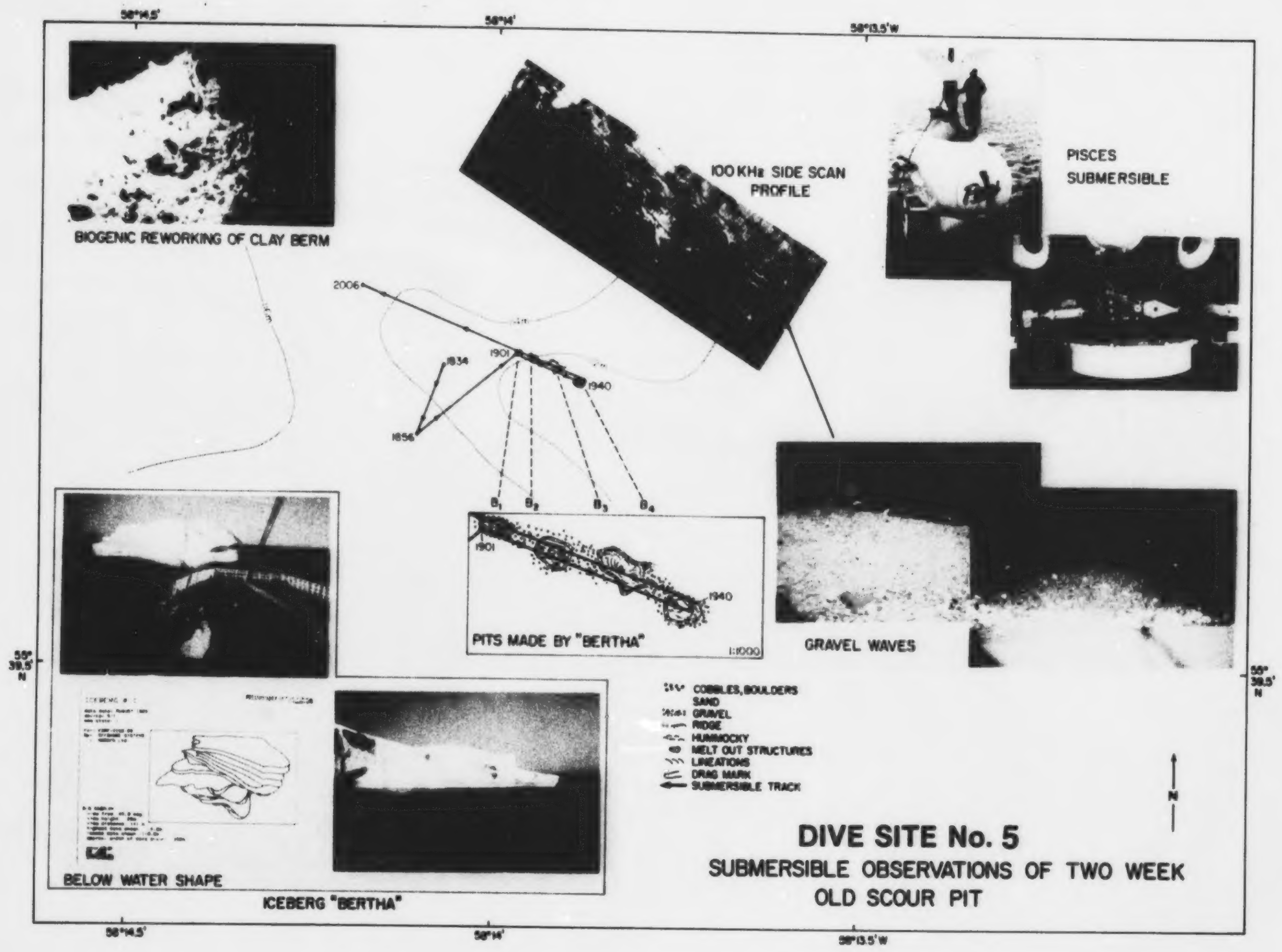
58°14.5'
58°14'
58°13.5'W
55° 39.5' N
BIOGENIC REWORKING OF CLAY BERM
100 KHz SIDE SCAN PROFILE
PISCES SUBMERSIBLE
2006
1901
1834
1856
1940
B1
B2
B3
B4
PITS MADE BY "BERTHA"
1:1000
GRAVEL WAVES
BELOW WATER SHAPE
ICEBERG "BERTHA"
COBBLES, BOULDERS
SAND
GRAVEL
RIDGE
HUMMOCKY
MELT OUT STRUCTURES
LINEATIONS
DRAG MARK
SUBMERSIBLE TRACK
N
DIVE SITE No. 5
SUBMERSIBLE OBSERVATIONS OF TWO WEEK OLD SCOUR PIT

Figure 66. Makkovik Bank, iceberg "Bertha" grounding site (Dive number 5).

pit trough, a boulder was observed partially buried in the seabed and rimmed by ice. When disturbed by the manipulator arm of *Pisces*, the ice floated to the surface. It is likely that the ice was broken from the iceberg keel.

Makkovik Bank, "Anastasia" Grounding Site

Dive number 6 on Makkovik Bank was made to investigate the seabed feature made during the grounding of iceberg "Anastasia" in 118 m of water. The presumed grounding site was passed over but not recognized during the dive and two old iceberg pits were investigated instead.

The seabed in this region consists of a pale yellow-green fine sand veneer of Sioraq Sand over undivided Labrador Shelf Drift. Fields of subdued, large, symmetrical ripples up to 0.5 m in amplitude and with wavelengths of about 0.75 m are common. A shelly, gravelly lag is usually found in the ripple troughs. Crest orientation was inconsistent. Frequently, smaller ripples with amplitudes of less than 5 cm and wavelengths of 5 to 10 cm were developed on one or both flanks of the large symmetrical ripples. Their crests are generally at high angles to the symmetrical ripple crests and are oriented normal to the north-south flowing current observed throughout the dive. Coarse sand lag was observed in the troughs of the small ripples.

Two iceberg pits were examined. They consisted of irregular berms in a U-shaped configuration with pit diameters of about 15 to 20 m. The berms were formed of blocky, cohesive, pebbly, bouldery clay. The clay matrix was heavily burrowed by benthic organisms and the surface was characterized by numerous small cavities 5 to 10 cm wide, and irregular white encrustations which may have been algae. The berms stood about 2 m above the seabed and were discontinuous so that the U-shaped nature of the pits was not immediately obvious. The pit troughs were not appreciably lower than the surrounding seabed and contained ripples suggesting that some degree of infilling has occurred. Concentrations of encrusted boulders and cobbles were always associated with the base of the berms, and, in the second pit, the crest of the interpreted head wall berm was capped with boulders.

Outcroppings of the near-surface pebbly clay were observed during the dive. One outcrop occurred as a scarp face, apparently offset along the surface of a micro-fault, and was sampled. In this outcrop, a cylindrical area of paler clay was observed in cross-section on the scarp face. Similar clay outcrops are associated with a 10 m deep iceberg pit on the Grand Banks (Barrie et al. 1986).

Makkovik Bank, "Big Makk," Repetitive Mapping Mosaic

Dives 7 and 12 (Figure 67) in 150 m depth investigated a scour ("Big Makk") that had been surveyed earlier by 100 kHz sidescan sonar, and which appeared as a fresh feature on the sonogram (Figure 68). The scour was about 315 m long and 50 m wide with negligible incision depth and slight positive relief at the southwestern end. Maximum berm height was 3.5 m at the eastern end and minimum berm height was less than 1 m along the southern lateral berm. The seabed surrounding the scour consists of a well developed gravel lag with occasional patches of sand. Underlying this lag are normally consolidated, silty, pebbly clays of the Qeovik Silt Formation. Gravel ridges, which correspond to old, winnowed scour berms, are characterized by concentrations of

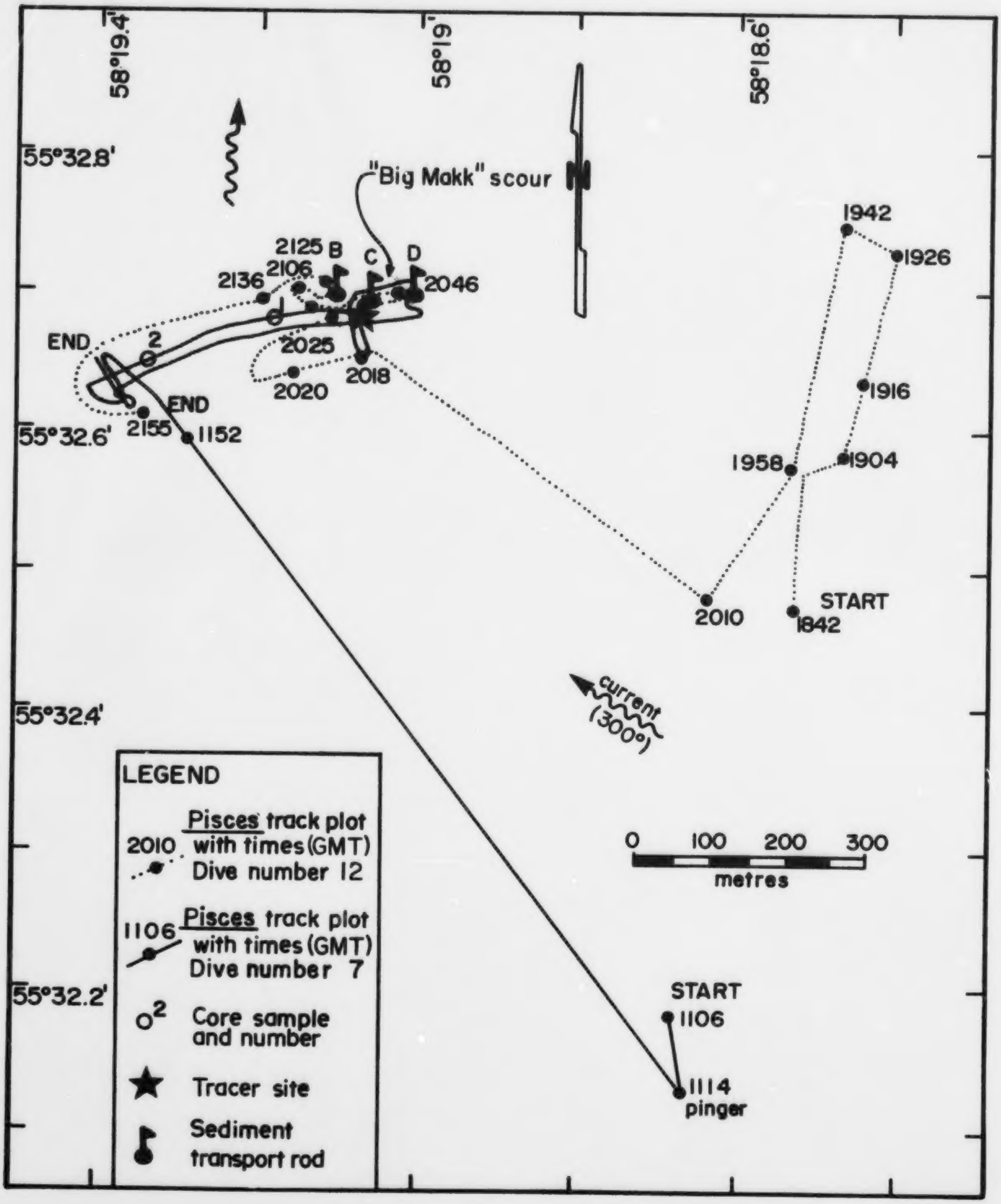
58°19.4'
58°19'
58°18.6'
55°32.8'
55°32.6'
55°32.4'
55°32.2'
"Big Makk" scour
2125 B
2106
2136
C
D
2046
END
2
2025
2020
2018
2155
END
1152
1942
1926
1916
1958
1904
2010
START
1842
current (300°)
0 100 200 300
metres
START
1106
1114
pinger
LEGEND
2010 Pisces track plot with times (GMT) Dive number 12
1106 Pisces track plot with times (GMT) Dive number 7
o2 Core sample and number
★ Tracer site
Sediment transport rod

Figure 67. 'Big Makk' site, Repetitive Mapping area, Makkovik Bank.

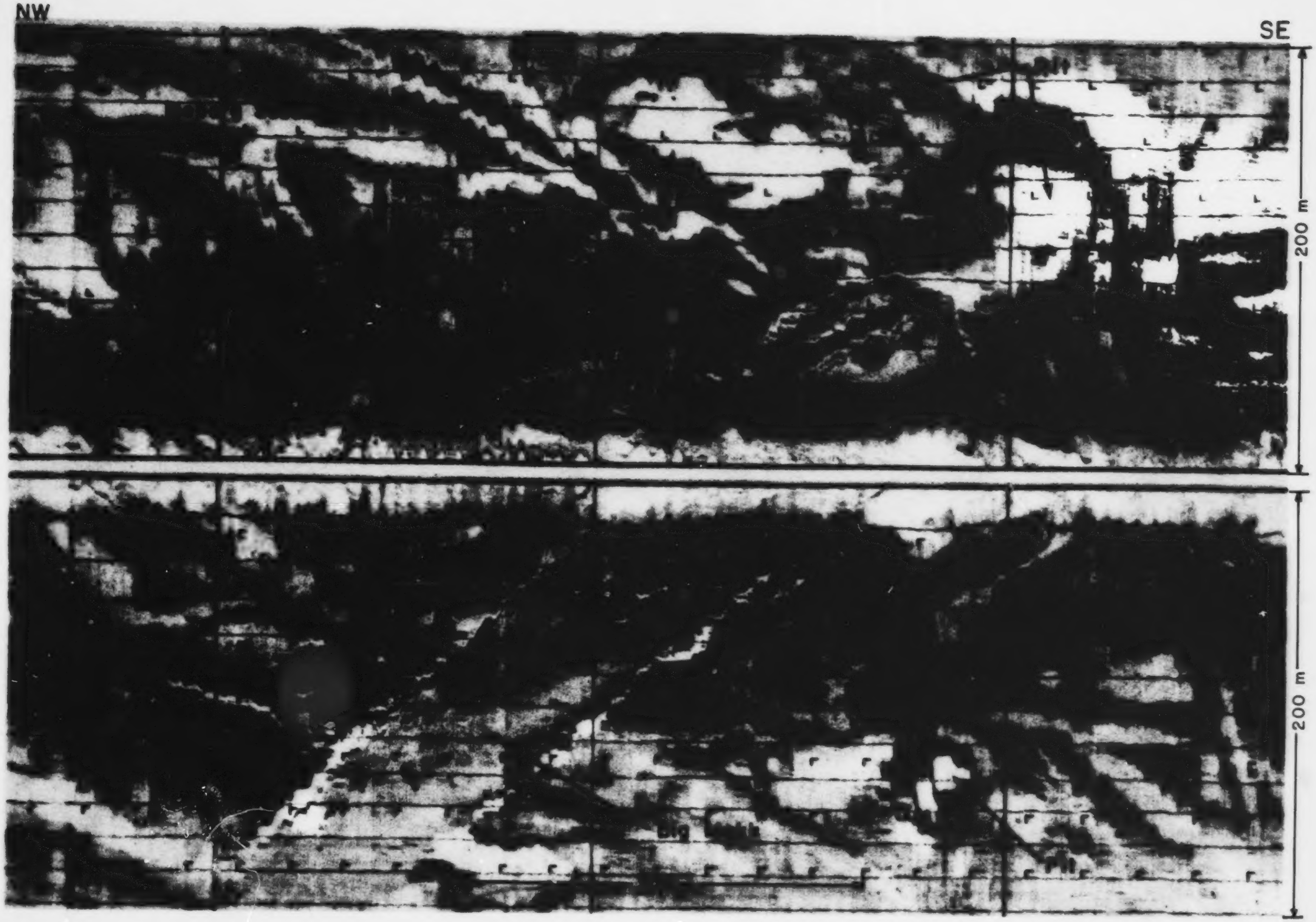
NW
SE
200 m
200 m
Big Makk

Figure 68. A sidescan sonogram from Line 55 of the Repetitive Mapping Site's 'Big Makk'. Note how fresh it appears compared to the surrounding ice-related features.

heavily colonized boulders and cobbles. Seabed relief is about 2 m. As interpreted from sidescan data the feature consists of steep berms of material which had apparently been extruded from below the iceberg. Linear grooves and ridges with amplitudes everywhere of less than 5 cm occur in the troughs and are parallel to the berms. Also within the trough were pits in which boulders were generally found. These pits may have resulted from ice breaking off from the scouring keel, becoming incorporated in the seabed and subsequently melting.

The eastern half of the scour consists of a large depressed area (about 20 m wide and 100 m long as measured from the sonogram) generally 0.5 to 0.75 m below the trough floor. Within this area, numerous flat-topped, irregular shaped mounds occur. The floor of the depressed area between the mounds is characterized by concentrations of gravel and shell debris, similar to the unscoured seafloor outside the scour. Possibly in this region the scouring keel was not incising the seafloor but rather depositing a thin, discontinuous layer of reworked sediment derived from the erosive part of the scour, above undisturbed seabed. Several conical mounds of unconsolidated material, including pebbles and shell debris, less than 0.5 m high are developed on top of the striated scour surface in this region and in the depressed areas between the flat-topped mounds. Clearly, they formed after passage of the scouring keel and may be sand volcanos, the surface expression of localized sub-scour liquefaction processes.

A feature of this scour was the presence outside the scour berms of isolated mounds, about 1 to 2 m^3 in volume. These mounds had some evidence of erosion on their surfaces as seen by the exposure of pebbles and cobbles protruding from the silty clay matrix. Their origin remained unexplained until a later dive (Number 13 on Saglek Bank) on a fresh scour during which similar but less eroded mounds of sediment outside the scour berm were observed. The blocks may have formed by the extrusion of cohesive seafloor sediment from below the iceberg. It is possible that the compacted sediment projected, unsupported, beyond the berm crest. Failure of the unsupported masses may then have formed isolated blocks 1 to 3m away from the berm crest outside the scour.

The iceberg that formed the "Big Makk" scour is inferred to have moved from southwest to northeast because of the presence of a sloping ramp and absence of a berm at the southwest end, and the presence of a high berm at the northeast end; the latter is probably indicative of iceberg lift off. The lead-in ramp is elevated between 0.5-0.75 m above the general seabed and slopes into the main portion of the scour trough at between 10° to 15°. Material to generate this positive relief feature presumably came from the displacement of silt and clay beneath the keel against the direction of movement of the iceberg.

To determine the rate of erosion or deposition within the scour three sediment disturbance rods were deployed. Two rods (B and C) were deployed on the berm crest and one rod (D) was deployed in the scour trough (see Figure 67). Future inspection either by manned submersible or by remotely controlled vehicle will allow determination of the amount of erosion or deposition since deployment. Although the scour berms and sediment blocks showed clear evidence of erosion and disintegration causing reduced berm height, there was no evidence of infill within the scour trough.

Western Makkovik Bank, Shallow Tracer Sand Site

At the shallower of the two current meter sites in 100 m water depth a sediment tracer site was established during dive 8 (see Figure 64). The submersible was used to relocate the site and to collect sediment samples for analysis of the pollucite deployed two weeks earlier. At the beginning of the dive a series of large symmetrical ripples with sharp to rounded crests was observed developed in depressions with their crests at seabed level. These large bifurcating ripples with wavelengths of 3 m and amplitudes of 0.5 m were located in linear groups resting on the substrate of glacial till and surrounded by flat, unrippled seabed. Ripple crest orientation was generally southeast to northwest. Between groups of ripples, patches of a white crusty mat, possibly of algae and similar to that observed at the "Anastasia" grounding site (Appendix 9), were encountered. When broken from the seabed the material floated.

Inspection of the current meter mooring showed no evidence of interference of flow around its legs. The tripod was sitting on two legs and the central anchor wheel. The pollucite tracer sand site was located adjacent to the current meter and was sampled at five locations (see Appendix 9). The subsea float deployed with the tracer was not located.

Western Edge of Makkovik Bank

Dives 9 (Figure 69) and 13 were intended to traverse and visually groundtruth a 70 kHz sidescan mosaic which extends over the shallowest part of the western bank edge and into deeper water (138 m) where a fresh scour had been observed

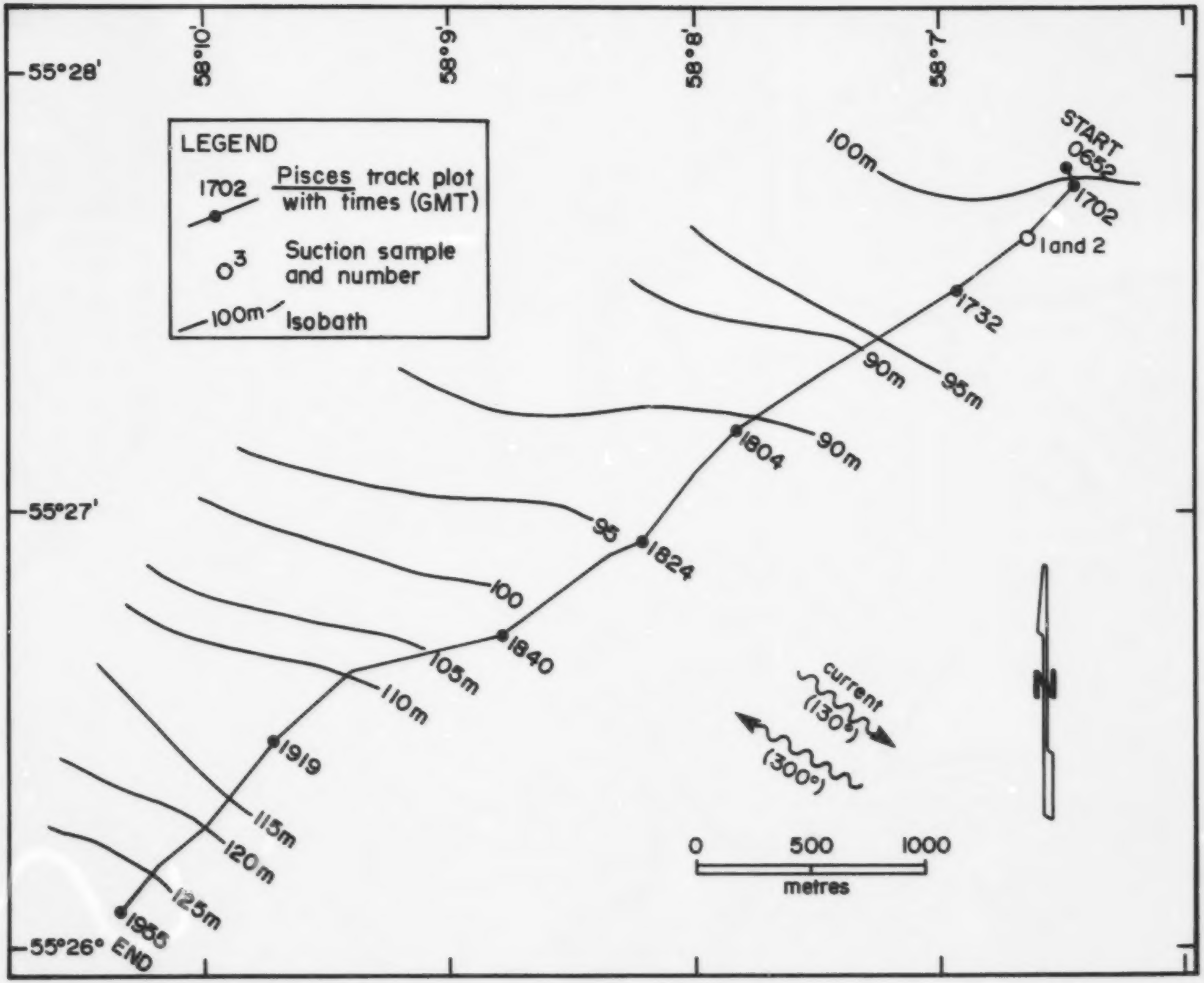
55°28'
55°27'
55°26°
58°10'
58°9'
58°8'
58°7'
LEGEND
1702
Pisces track plot with times (GMT)
O3
Suction sample and number
100m
Isobath
START 0652
1702
1 and 2
1732
1804
1824
1840
1919
1955
END
100m
95m
90m
90m
95
100
105m
110m
115m
120m
125m
current (130°)
(300°)
N
0
500
1000
metres

Figure 69. Western edge, Makkovik Bank (Dive number 9)

on BRUTIV photographs collected two years earlier. In addition, relict beach ridges were searched for.

The first dive began at 100 m water depth on a gravelly boulderly lag with occasional 100 to 200 m wide patches of biogenically reworked, smooth fine sand. Within these fine sand patches were fields of coarse, large, symmetrical ripples. The ripples typically had wave lengths of 60 to 80 cm and crest heights of <0.5 to 30 cm and although they showed considerable variations in grain size they were consistently coarser than the surrounding fine sand. In cross section, individual ripples are symmetrical with perfectly flat stoss and lee slopes. The shape of the ripple fields were generally oval in planform with lengths of 60 to 100 m and widths of 20 to 40 m. These bedforms were devoid of benthic organisms and had extremely sharp crests. Considering the high rate of reworking by bottom dwellers observed in this area these features may possibly have been formed within a few days prior to our visual inspection. The traverse over the bank top in areas shallower than the inferred late Wisconsinan low stand of sea level at -110 m did not appear appreciably different than the deeper areas; there were no apparent relict beach ridges and the local current regime appeared strong enough to explain the features seen.

On the western margin of Makkovik Bank, at 115 m, the surface veneer of fine sand increased in thickness and distribution. This area may be one of deposition of sandy material that is winnowed from the bank top. Seabed relief is smooth and iceberg scour ridges were rare, recognized only by linear mounds of pebbles and cobbles protruding a few centimetres above the surrounding gravel lag.

The dive investigated an area of exposed stiff, pebbly clay devoid of gravel lag, which may have been an area of iceberg impact. However, no berms were visible and the interpreted impact only removed the gravel lag without affecting the stiff underlying material. Iceberg scour berms with more noticeable relief were noted where the underlying substrate changed from overconsolidated older tills to the less consolidated more easily remoulded upper till. The dive terminated at 123 m depth in an area of numerous eroded scours some of which had berm slopes of up to 20° or 30°.

The second dive (Figure 70) began in 109 m water depth over a field of coarse sand ripples. Bottom currents were less than 8 cm/s (0.25 kt) to the north. Wavelengths within the ripple field were 1.5 to 2 m and ripple heights were 30 to 40 cm. From the beginning of the dive to a depth of 125 m, the dive traversed areas of coarse sand ripples which were situated in larger areas of fine sand. Subdued scour ridges started to become apparent at 125 m depth and increased rapidly in relief and frequency in deeper water. A "fresh" scour was seen at a depth of 137.5 m. This feature was asymmetric with no berm on the upslope side and a berm with up to 6 m of relief on the downslope side. The berm had steep walls with slopes of up to 45°. The axis of the scour had a contour parallel orientation of 330°. Angular blocks of extruded sediment were observed on the outer margin of the berm.

The transition from surrounding seabed to the upslope scour margin was recognized by a marked textural change from the typical lag gravel of the undisturbed seabed to a smooth lineated clay surface within the scour trough. The scour incised the gravel lag by less than 5 cm. It is possible an asymmetric ice keel generated this one-sided scour. The

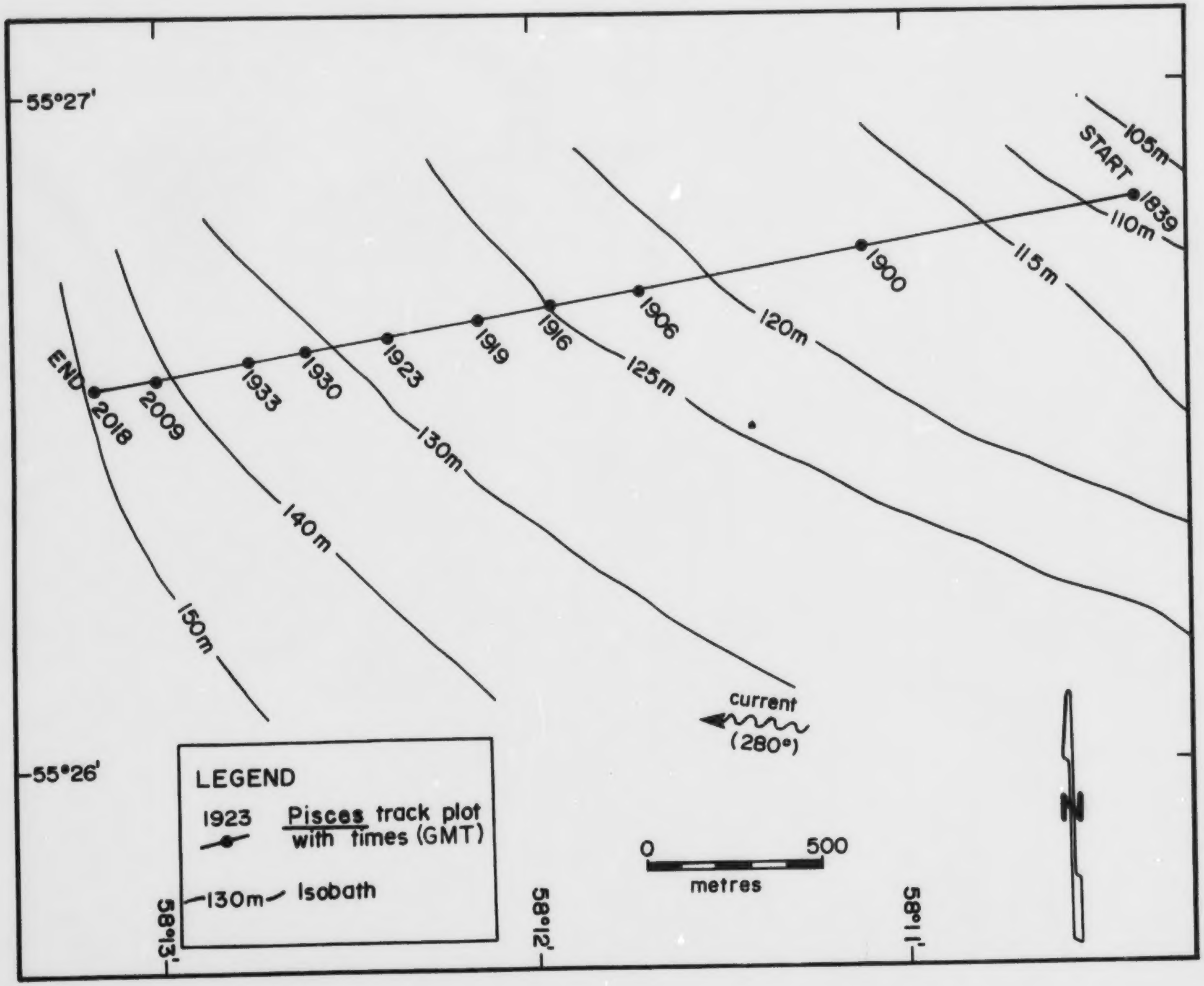
55°27'
55°26'
58°13'
58°12'
58°11'
105m
110m
115m
120m
125m
130m
140m
150m
START
1839
1900
1906
1916
1919
1923
1930
1933
2009
2018
END
current
(280°)
0
500
metres
N
LEGEND
1923
Pisces track plot with times (GMT)
130m
Isobath

Figure 70. Western edge, Makkovik Bank (Dive number 13, a continuation of Dive number 9).

keel probably conformed to the local seabed slope, although it must have penetrated more than 5 cm of the seabed on the downslope side to have excavated enough material to plough up the 6 m high berm.

The berm crest was followed for about 200 m and considerable change in height and slope was noted. Berm height varied between 1 and 6 m. The lack of biogenic cover and the angularity of the sediment blocks suggests that the scour was made within the last year. It must be less than three years old because no fresh scour mark was seen in 1983 when the same area was surveyed with the BIO 70-kHz sidescan sonar and with the BRUTIV camera sled.

The 1983 survey clearly identified a fresh scour mark at 152 m and one objective of the dive was to investigate this feature to determine the amount of erosion or change it had undergone in three years. Unfortunately, the dive had to be aborted before reaching this target because of thick fog at the surface.

Southeastern Makkovik Bank, "Gladys" Grounding Site

Dive number 11 was made to observe the surficial geology in the vicinity of the "Gladys" grounding site. The actual site was not visited because the iceberg was still aground at the time of the dive. The seabed near the site consists primarily of fine sand which partially buries boulders and ice scour features. As this area is the shallowest part of southeastern Makkovik Bank, the potential for iceberg grounding and scouring should be high, as suggested by the iceberg tracking observations. However, only one scour feature was observed in more than 1 km traversed with the submersible.

Boulders seen along the survey track (Appendix 9) appeared to be of one lithology and to have been recently deposited as no benthic organisms encrusted their exposed surfaces. Because the submersible course was along the drift paths of "Gladys" and "Frieda", it is probable that the fresh boulders were dropped from one of these icebergs.

The tracer sand deposited earlier from the Polar Circle was not relocated. For safety reasons the submersible could not approach iceberg "Gladys" and the pit it excavated.

Saglek Bank

Dive number 14 was conducted on the southwestern portion of the region covered by a sidescan mosaic (Figures 71 and 72) made in 1979. The purpose of the dive was to investigate and sample the pronounced north-south trending curvilinear scour (A) and a large iceberg pit (B) in a water depth of 172 m. The large scour seen on the 70-kHz sidescan system was successfully located but its sharply defined acoustic nature was not confirmed visually. Instead the scour was found to have very subdued relief and featureless berms. The depth of the trough was 2 m and berm height was 2 m for a total relief of 4 m. Berm slope angles ranged between roughly 10° to 15°. Seabed material consists of a blanket of unconsolidated silt which covers patches of buried boulders. Some confusion occurred over the submarine's location when it became apparent that it was at the intersection point of several large scours. Coring of the trough and flank of the large northwest-southeast trending scour (C) was successful.

The large iceberg pit (B) was found to have a depth from trough to berm crest of 6 m and successful coring of the

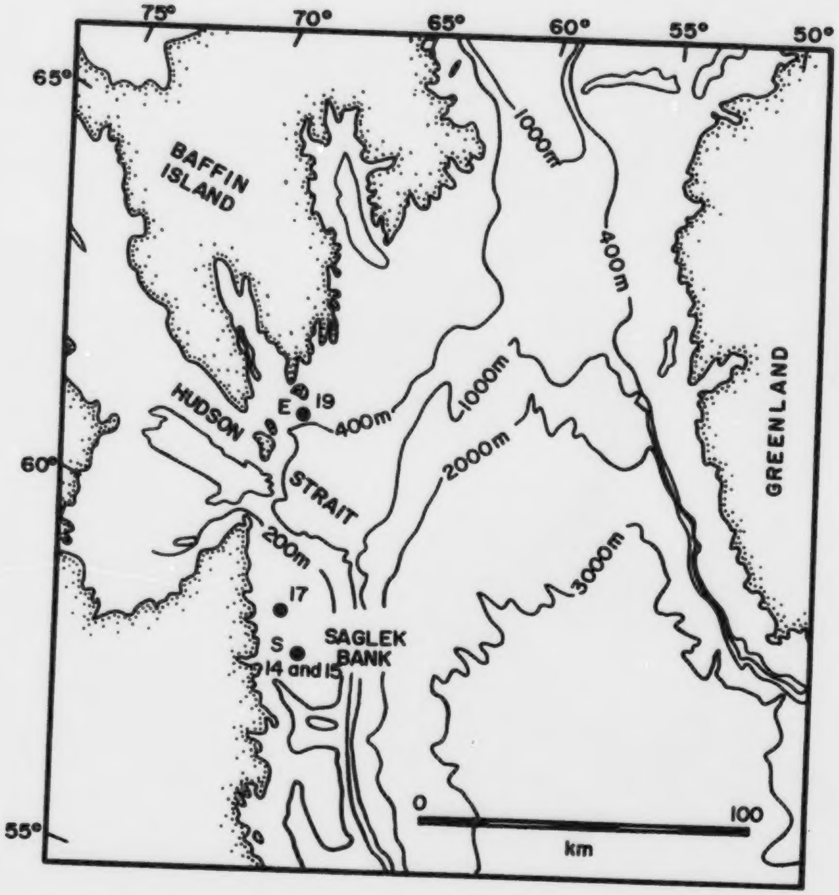
75°
70°
65°
60°
55°
50°
65°
60°
55°
BAFFIN ISLAND
HUDSON STRAIT
GREENLAND
SAGLEK BANK
1000m
400m
400m
1000m
2000m
3000m
200m
E
19
17
S
14 and 15
0
100
km

Figure 71. Pisces dive locations on Saglek Bank and southeast Baffin Island Shelf.

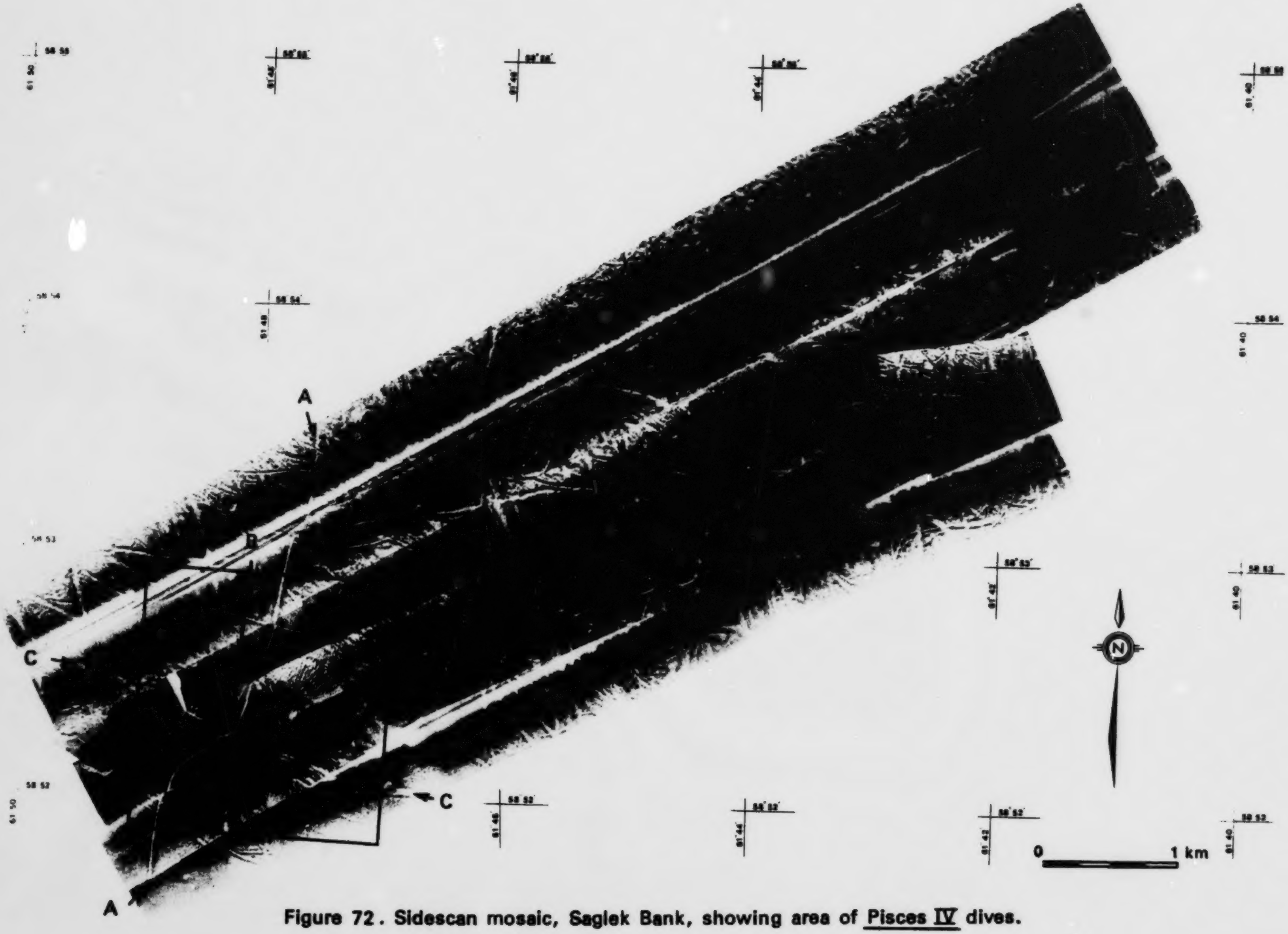
58°55'
58°54'
58°53'
58°52'
61°50'
61°48'
61°46'
61°44'
61°42'
61°40'
A
B
C
C
A
N
0
1 km

Figure 72. Sidescan mosaic, Saglek Bank, showing area of Pisces IV dives.

berm crest and pit trough was completed in relatively cohesive silts. The pit is asymmetric with a northeast-southwest linearity and steep (approximately 30°) inner berm walls except at the southwestern end where slopes of 5° to 10° were encountered.

Dive number 15 was a continuation of dive number 14 (Figure 73), and was also conducted in the area of the Saglek East sidescan mosaic. An upslope traverse across geologic units 5a and 4 was made (see Table 5) from relatively undisturbed to intensely scoured seabed.

Although numerous intersecting scours can be seen on the mosaic, individual scours could not be discerned from the submersible and the intensely scoured surface, beginning at a depth of about 170 m, was characterized by hummocky terrain with relief generally of about 2 m. This terrain was difficult to traverse because the submersible alternately traversed up and down slopes with fairly steep (20° to 30°) angles.

It was impossible to distinguish between surficial geologic units and for most of the dive surficial sediments and surface morphology remained constant. At 153 m depth, surficial silts appeared to be slightly coarser than at lower depths although the change was not consistent. Numerous buried boulders were observed throughout the dive except at a depth of about 164 m where they were sparse. The boulders were mostly draped by a thin veneer (5 to 10 cm thick) of silt and were hard to distinguish. However, whenever the submersible's skids touched the seabed they nearly always grated on boulders.

Dive number 17 (Figures 71 and 74) investigated a scour in 120 m water depth believed to have been made by iceberg

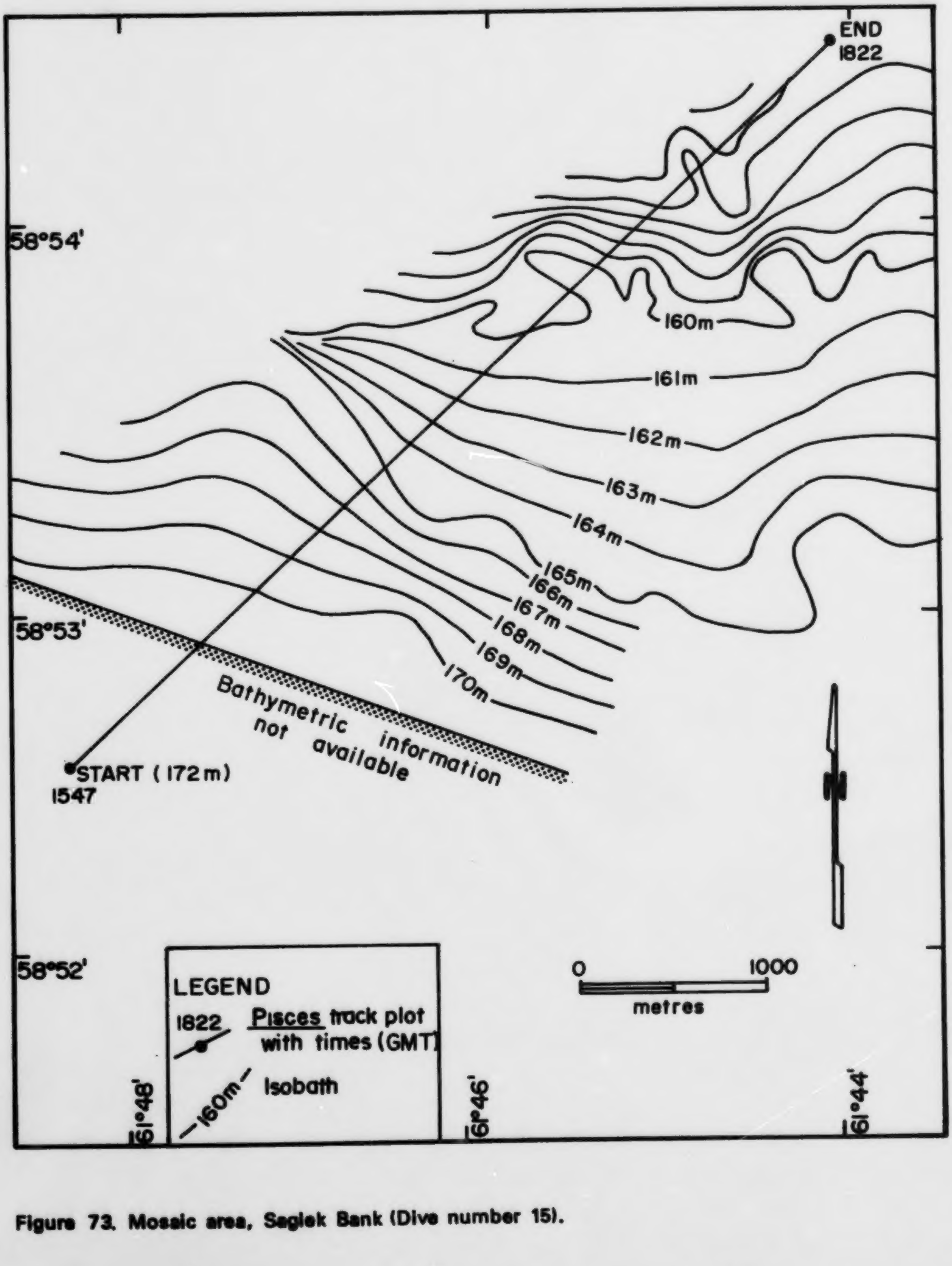
END
1822
160m
161m
162m
163m
164m
165m
166m
167m
168m
169m
170m
58°54'
58°53'
58°52'
Bathymetric information not available
START (172m)
1547
0
1000
metres
LEGEND
1822
Pisces track plot with times (GMT)
160m
Isobath
61°48'
61°46'
61°44'

Figure 73. Mosaic area, Saglek Bank (Dive number 15).

"Caroline" in 1979, and to investigate another, much fresher scour that had been observed on 100-kHz sidescan data that were collected during this cruise. The sidescan data showed that this fresh scour had cut across the "Caroline" scour. The scours appeared markedly different (Figure 74). The fresh feature had linear grooves in its trough, parallel to the berms. In several places individual boulders or cobbles were observed at the beginning of a small scale ridge, resembling "crag-and-tail" features characteristic of sub-glacial deposition. Raised blocks of material on the berm crest were clearly visible on the sidescan data, appearing as localized acoustic shadows. This difference in acoustic character between the two scours suggested that visual identification of the fresh scour would be possible. High resolution subsurface data indicated that both scours were cut into the glaciomarine Qeovik Silt (Josenhans et al. 1986).

On this traverse, Pisces followed the "Caroline" berm until the fresh scour was located. The submersible then moved across the fresh scour and back onto the "Caroline" berm, which was followed as far as the terminal pit. Pisces then traversed back to the fresh scour and surveyed that feature to the end of the dive.

South Baffin Island Shelf

Dive number 19 (Figure 71) was intended to investigate a conical seabed feature discovered in 1981 and interpreted to be a mud volcano developed above a major unconformity between Precambrian and Tertiary rocks (Woodworth-Lynas 1983). Because of uncertainties in exact positioning of the ship the cone was not found. However, two iceberg scours

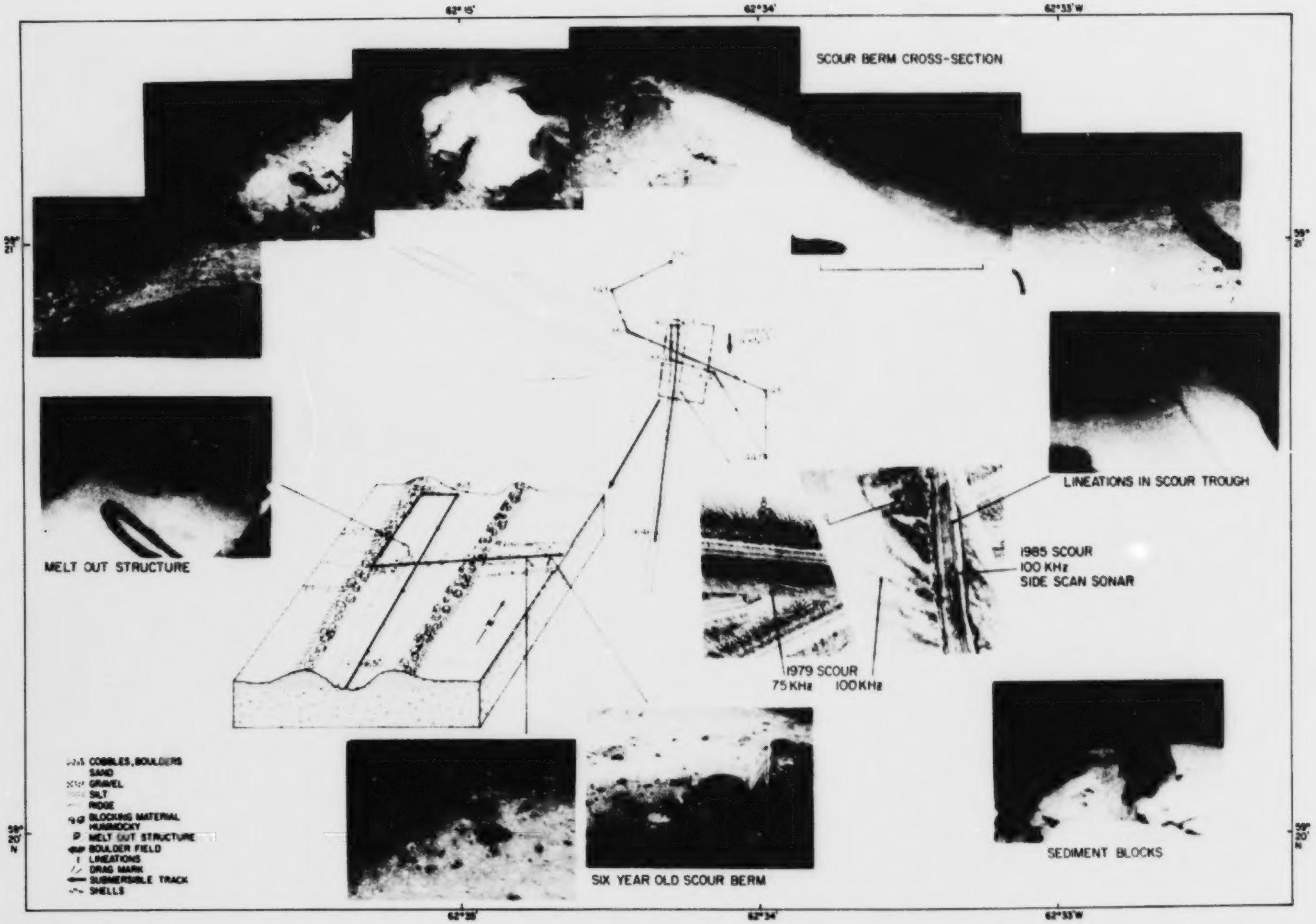

62° 15'
62°34'
62°33'W
59° 21'
59° 20' N
SCOUR BERM CROSS-SECTION
LINEATIONS IN SCOUR TROUGH
1985 SCOUR
100 KHz
SIDE SCAN SONAR
1979 SCOUR
75 KHz
100 KHz
MELT OUT STRUCTURE
SIX YEAR OLD SCOUR BERM
SEDIMENT BLOCKS
COBBLES, BOULDERS
SAND
GRAVEL
SILT
RIDGE
BLOCKING MATERIAL
HUMMOCKY
MELT OUT STRUCTURE
BOULDER FIELD
LINEATIONS
DRAG MARK
SUBMERSIBLE TRACK
SHELLS

Figure 74. Iceberg 'Caroline' scour, Saglek Bank (Dive number 17).

were investigated in a water depth of 230 m, one of which appeared recently formed.

The seabed in this area consists of large areas of boulders, cobbles, and gravel, generally well colonized by encrusting algae, sponges, and benthic fauna. Boulders rest on a surface of fine to medium-grained, well sorted sand. Undulose topography of about 1 m relief characterized the seabed. Boulders are concentrated in ridges which probably represent the winnowed remnants of old iceberg scour berms.

The first scour encountered had subdued berms of less than 2 m consisting of uncolonized boulders and cobbles resting in a bioturbated pale clay matrix, mostly covered by a thin veneer of sand. Berm width was about 3 m. The trough was flat-bottomed and faint lineations with negligible relief (few centimetres) were seen beneath a thin sand veneer. Broken shell debris and uncolonized gravel clasts also rested in the trough. Scour depth was negligible, probably no greater than 0.5 m.

The berms crests were preferentially reworked by bottom currents. Gravelly lag was developed in places and small patches of current-generated sand ripples were also found.

The second scour had a berm height of 4 m with steep inner slopes. Current-generated sand ripples and uncolonized gravel lag characterized the crest and inner berm flanks. The trough was characterized by a thin pebble armour developed directly on clay which was exposed in patches. A 5 m high mound was found apparently within the trough and the maximum total relief from scour berm crest to the deepest part of the trough was 7 m.

DESCRIPTION OF SIDESCAN MOSAICS

A total of four locations, in addition to the Repetitive Mapping site, were surveyed during the field program (Chart 3), with 1:10,000 scale track plots prepared for each (Charts 6, 7, 8, 9, 10). Due to a number of constraints it was decided to produce only four mosaics and associated interpretations. Data quality and coverage for the iceberg "Julianna" location were inferior to the other sites and, therefore, no post-survey analysis was performed. Information acquired from the remaining four locations is presented in the following sections. The nomenclature of surficial geological units has been taken from Josenhans et al. (1986) as outlined in Table 5.

Repetitive Mapping Mosaic

Bathymetry. The Repetitive Mapping mosaic extends over a portion of the steeply inclined western flank of Makkovik Bank (see Chart 3). Water depths range from a minimum of 85 m (the shallowest point on the Bank) near the eastern end of the mosaic, to a maximum of 207 m at the southwest corner (Chart 11). The shallowest point is situated on a north-south trending ridge that crosses the area roughly 3 km from the eastern end of the mosaic. This ridge forms the western boundary of the bank in this area. The ridge is a flat-topped feature with water depths averaging 88 m to 90 m over much of its surface. On the eastern flank of the ridge, the seabed slopes at 1:100 (0.57°) towards the east, decreasing to 1:425 (0.13°) on the bank top. The seabed on the bank top is flat except for microtopographic variations associated with iceberg scours and small bedforms.

West of the ridge, the seabed falls away into the Labrador Marginal Trough. The average slope is 1:77.5

(0.74°) towards the west. Two small morainic ridges cross the mosaic area in a north-south orientation part way down the slope. Minimum water depths on these ridges are 107 m and 122 m respectively (Chart 11). Meso- and microtopographic variations, related primarily to iceberg scours, become increasingly pronounced down-slope.

Surficial Geology. Four separate surficial geologic units are recognized on the Repetitive Mapping mosaic. These are the Lower Tills and Upper Till units of the Labrador Shelf Drift Formation, the muddy glaciomarine Qeovik Silt and patches of Sioraq Sand. All four units are widely recognized on the Labrador Shelf (Josenhans et al. 1986). Brief descriptions of their character and distribution within the mosaic area are given below. Chart 12 illustrates the distribution of units and includes a geologic profile.

The Lower Tills unit of the Labrador Shelf Drift Formation underlies the entire mosaic area. The total thickness of the unit cannot be defined on the high-resolution sub-bottom profiler records collected. It is exposed at or near the seabed over the majority of Makkovik Bank in water depths of less than roughly 105 m. On the Huntec DTS profiles the till has a homogeneous character and lacks coherent reflectors. The upper surface of this unit is generally smooth to gently undulating across the bank top. Deeper down on the western flank of the bank the upper surface is much rougher, possibly as a result of iceberg scouring. This rough topography was not observed by Josenhans et al. (1986) who noted that the upper surface of the Lower Tills is always smooth, possibly as a result of erosion by the ice sheet which deposited the Upper Till.

In water depths greater than roughly 105 m within the mosaic area, the Lower Tills is overlain by a discontinuous layer interpreted as the Upper Till unit of the Labrador Shelf Drift Formation. On average, the Upper Till unit is 3 to 5 m thick. Exceptions to this include two morainic accumulations, with relief of as much as 13 m, occurring part way down the western flank of the bank in roughly 120 and 130 m of water (Chart 12 and Figures 75 and 76). On the Huntec DTS profiles the character of the Upper Till is similar to that of the Lower Tills except that it is slightly more acoustically transparent. Earlier work by Josenhans et al. (1986) suggests that the 160 m contour represents the shallowest observed occurrence of Upper Till. The presence of this unit in 100 to 105 m of water in the mosaic area considerably extends its previously interpreted distribution.

A thin (1 m to 4 m), discontinuous layer overlies both the Upper Till and Lower Tills on the western flank of Makkovik Bank (Figure 77). This unit is markedly more acoustically transparent than either till unit and has been interpreted by Josenhans et al. (1986) as a proglacial, poorly sorted muddy sand of the Qeovik Silt Formation. They described Qeovik Silt as generally characterized by continuous, coherent reflectors and a conformable depositional style, but this character is not evident in much of the mosaic area because most of the unit is heavily scoured (Chart 12). However, in deeper water just west of the mosaic area the Qeovik Silt has a more typical, well layered, conformable character.

Between 100 and 120 m water depth on the western flank of Makkovik Bank, the Qeovik Silt has a surface veneer of sand. This veneer is too thin to be recognized on the DTS profiles but is evident on the sidescan mosaic (Chart 12) because of its light tone and the presence of sand waves.

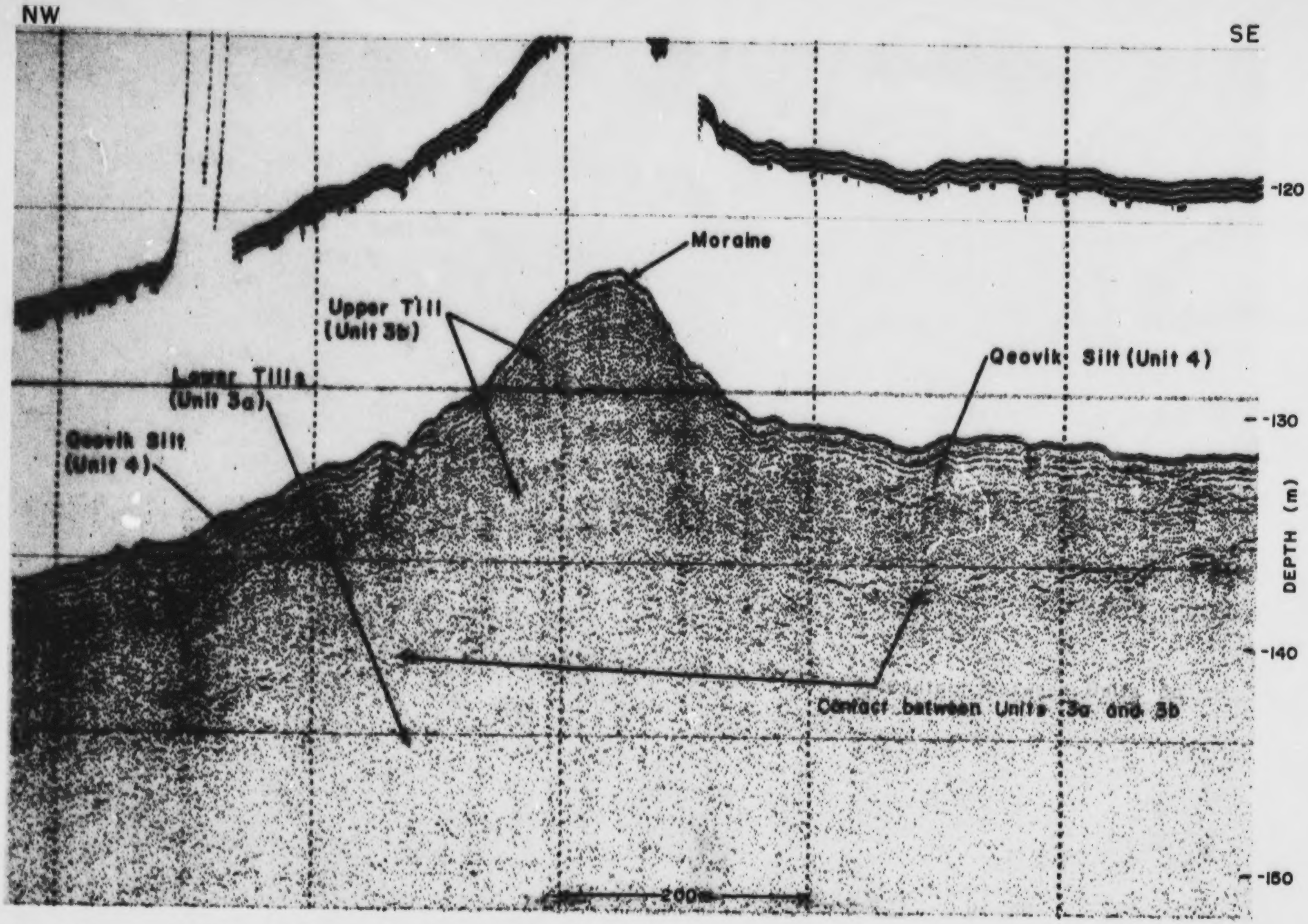

Figure 75. A DTS profile from part of Line 65 from the Repetitive Mapping site illustrating Units 3a, 3b and 4 and one of two moraines identified on the site.

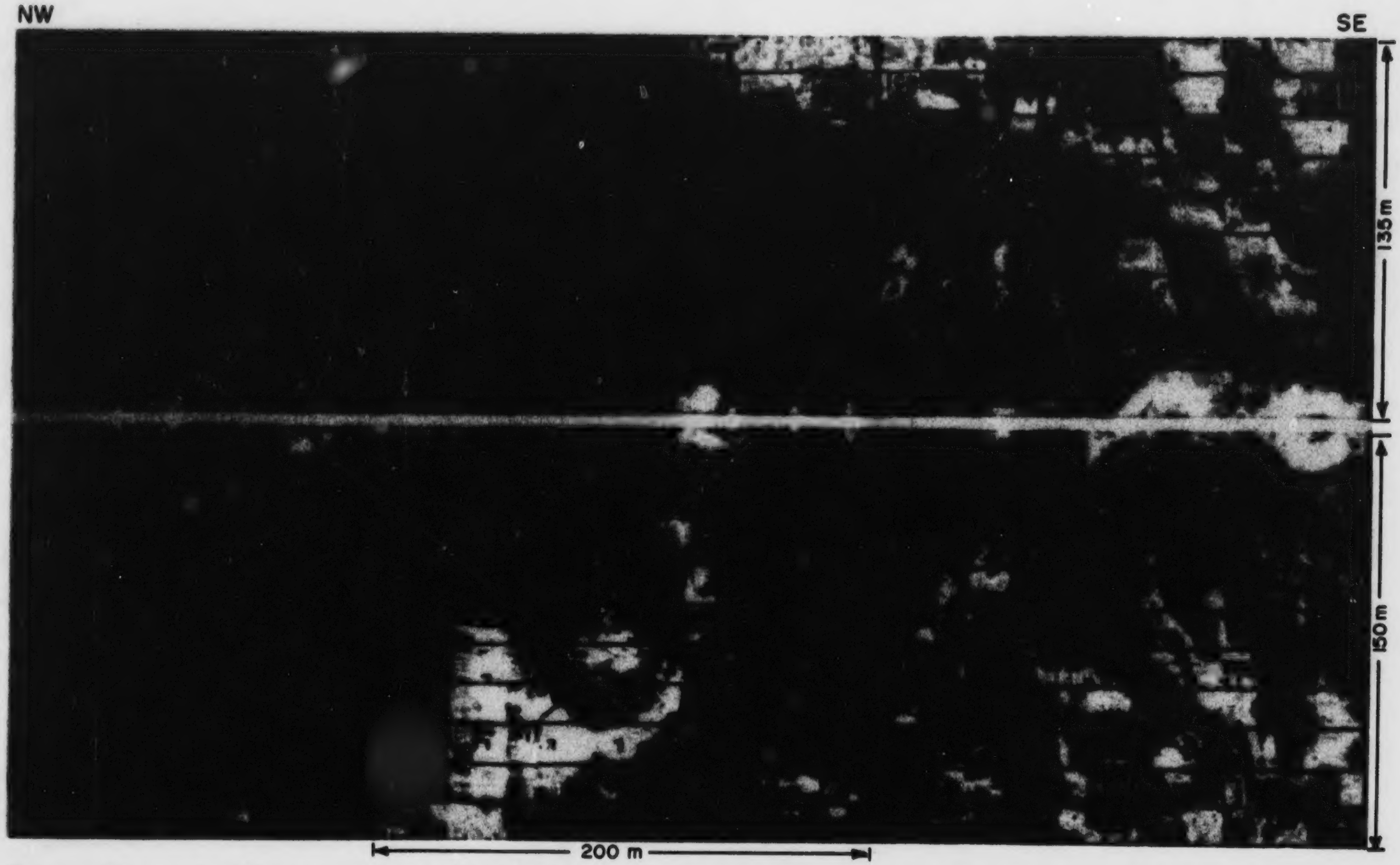

Figure 76. A sidescan sonogram (100-kHz) of part of Line 65 from the Repetitive Mapping site illustrating an iceberg scour traversing Qeovik Silt (Unit 4) and Upper Till (Unit 3b) terminating as a pit.

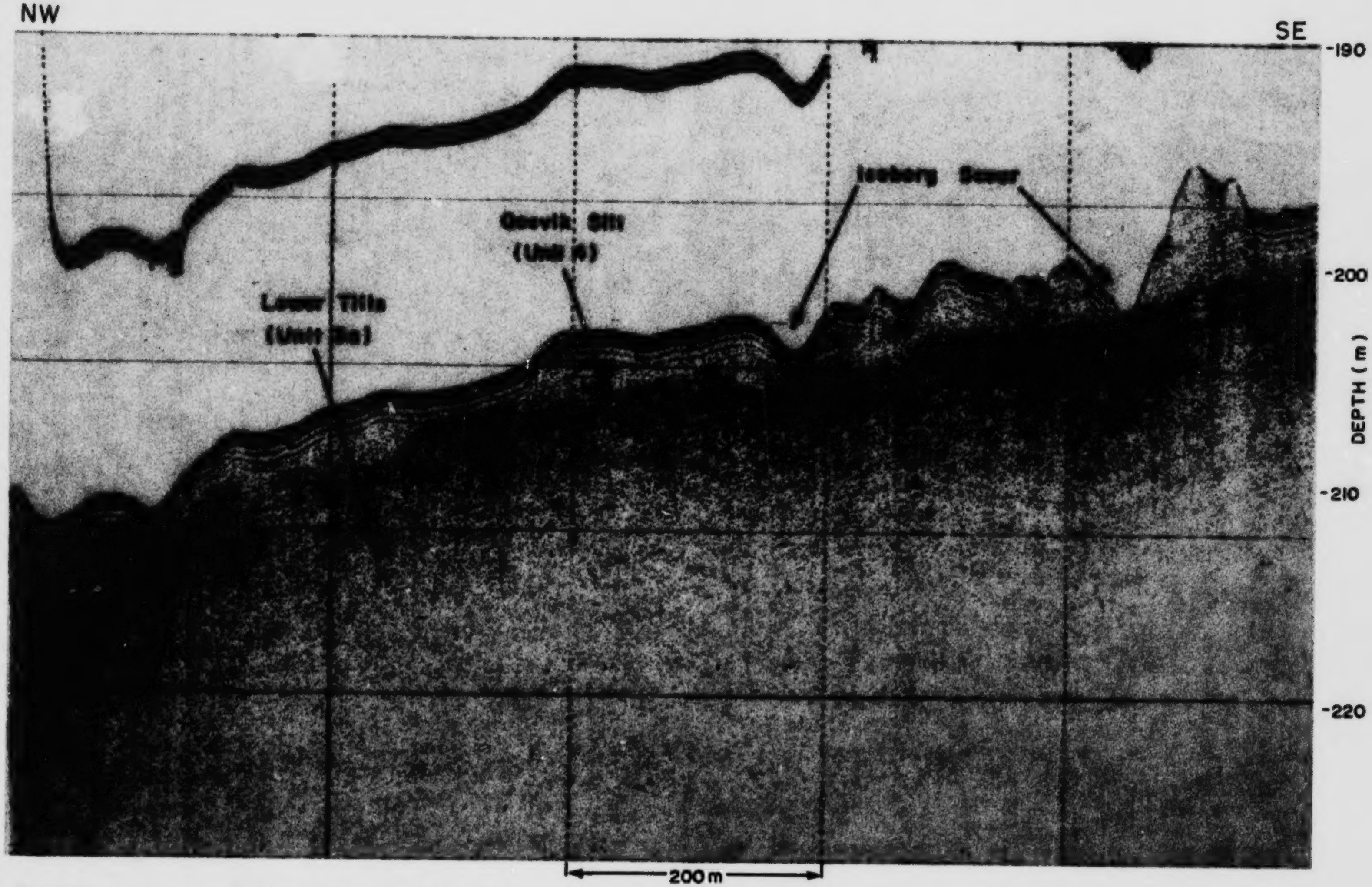

Figure 77. A DTS profile of part of Line 57 from the Repetitive Mapping site showing Units 3a and 4 and the scoured character of the surficial unit. Note the large scour which penetrates through to the Lower Tills.

East of the shallow ridge marking the brink of Makkovik Bank, the Lower Tills unit is overlain by a thin (1 to 2 m) layer of Sioraq Sand. This unit is characteristically a fine, well sorted sand (mean grain size = .177 mm) (Gilbert and Barrie 1985) with some gravel. The sand is believed to have been derived from reworking of the Lower Tills by scouring icebergs and input of new material by ice rafting (Josenhans et al. 1986). The sand is presently being transported and reworked by the prevailing currents (Gilbert and Barrie 1985).

Bedforms. Small-scale, wave-formed ripples were documented on submersible dives carried out southeast of the Repetitive Mapping mosaic area (Dive Locations 8, 9 and 13). Larger symmetrical ripples are readily apparent on the 100-kHz sidescan sonograms (Figure 78) over much of the mosaic area in water depths of less than 120 m. These bedforms have wavelengths of 0.5 to 2.0 m, heights of up to 30 cm, and are generally symmetric in cross-section and straight crested. Although variable from area to area the crests of many ripples are consistently oriented N140°E. These bedforms are present over most of Makkovik Bank. Observations from the submersible indicate that the megaripples are composed of medium-to coarse grained, well-sorted sand. Small discrete fields of large symmetrical ripples have sharp boundaries and the basal surface of the ripples is generally 10 to 20 cm below the level of the surrounding fine sand seabed. Starved, large, symmetrical ripples, (i.e., individual ripples separated by flat areas of basal lag gravel) were observed in places.

Just off the western flank of the Bank, a field of relatively large bedforms is evident in the sandy veneer blanketing the Oeovik Silt (Chart 12). These are straight-crested features oriented N125°E with crest to

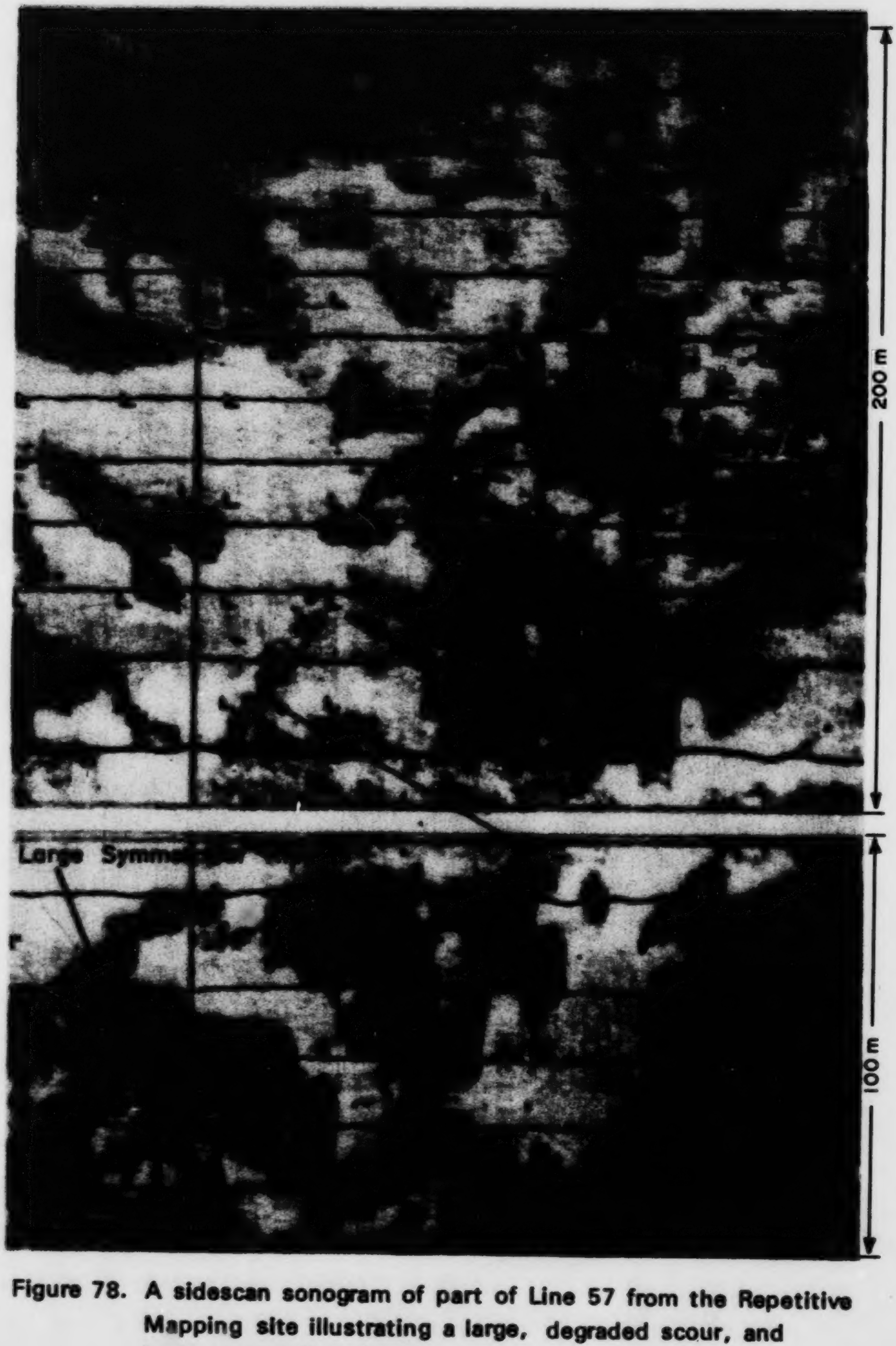
Large Symme
200 m
100 m

Figure 78. A sidescan sonogram of part of Line 57 from the Repetitive Mapping site illustrating a large, degraded scour, and large symmetrical ripples.

crest spacing on the order of 70 to 100 m. The height of these features is probably less than 0.5 m because they are not evident on the Huntec profiles. Given their relative dimensions they are probably best classified as sand waves within the scheme outlined by Amos and King (1984).

The above mentioned bedforms and their significance is more completely addressed later in this chapter.

Iceberg Scours and Other Ice-related Features. The seabed within the Repetitive Mapping mosaic area has been heavily reworked by icebergs. A total of 296 scour and pit features have been documented and measured (Appendix 10). Where possible, attempts have been made to correlate scours on sidescan sonograms with those evident on corresponding DTS records. The resulting data are summarized here.

On the western flank of Makkovik bank, below 120 m water depth the predominant scour orientation is N124°E (Figure 79), or roughly 40° to the regional bathymetric contours. On the bank top, in less than 120 m water depth, a dominant N130°E orientation exists along with a secondary orientation of N70°E (Figure 80).

An analysis of scour widths within each geologic unit reveals the following:

Unit 5b, average scour width = 17.1m;
Unit 3a, average scour width = 18.0 m;
Unit 3b, average scour width = 20.75 m; and
Unit 4, average scour width = 21.7 m.

From the distribution of measured scour widths (Figure 81), the average scour width is 21 m. The maximum width

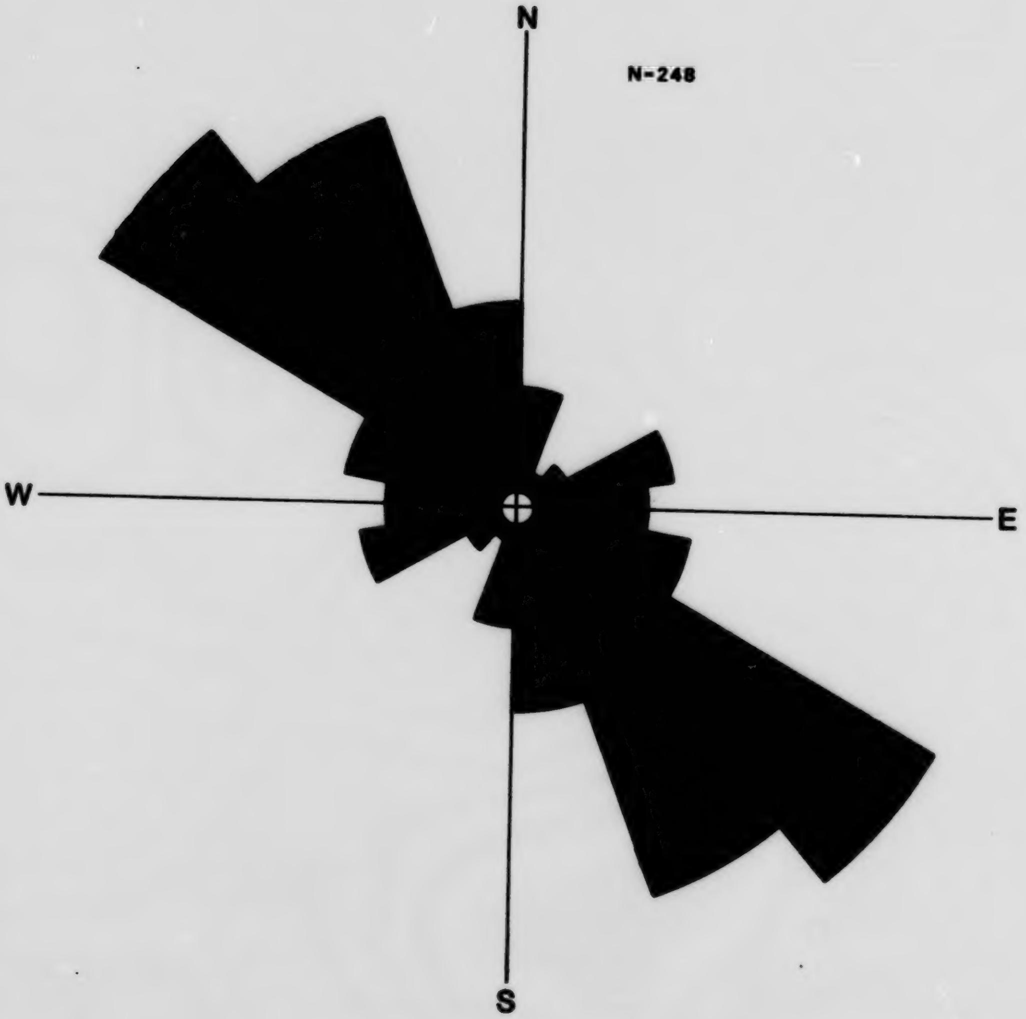

Figure 79. Iceberg scour orientations - Repetitive Mapping site >120 m water depth.

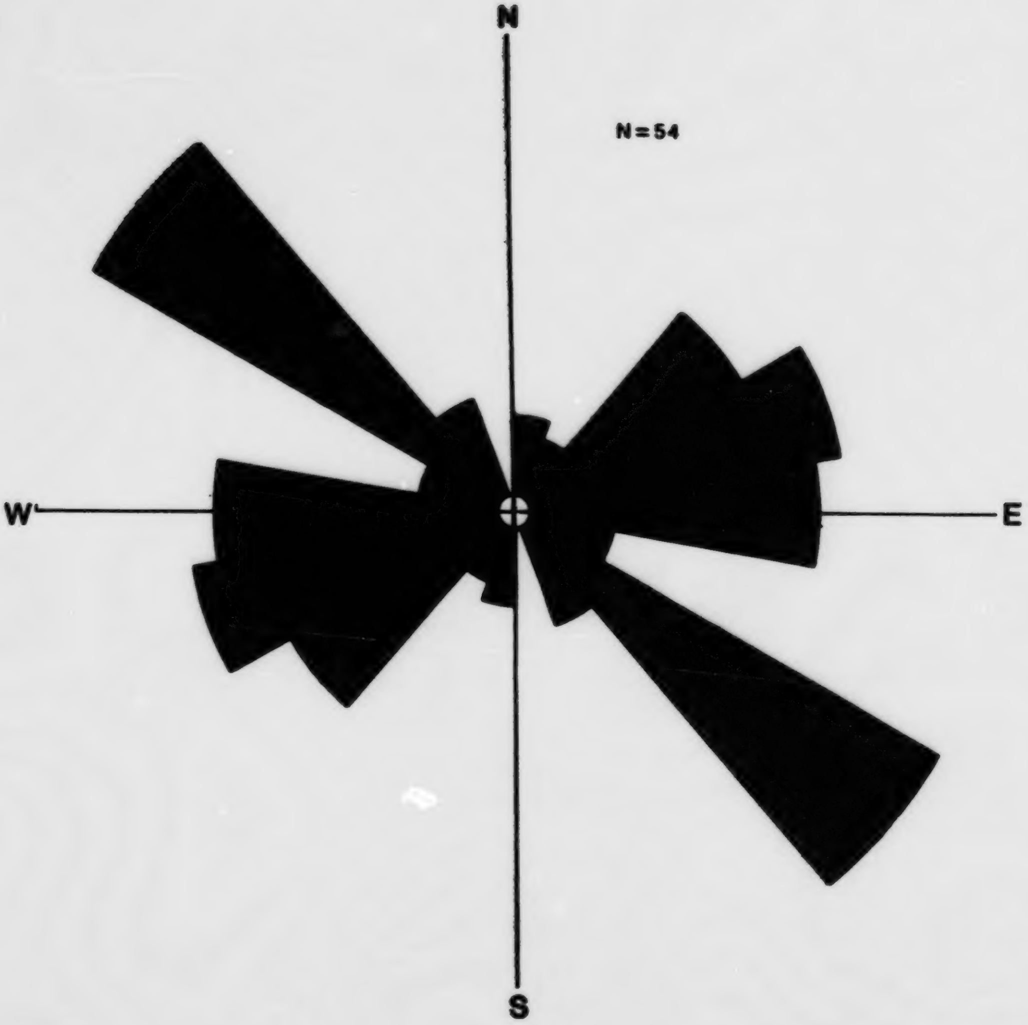

Figure 80. Iceberg scour orientations – Repetitive Mapping site <120m water depth.

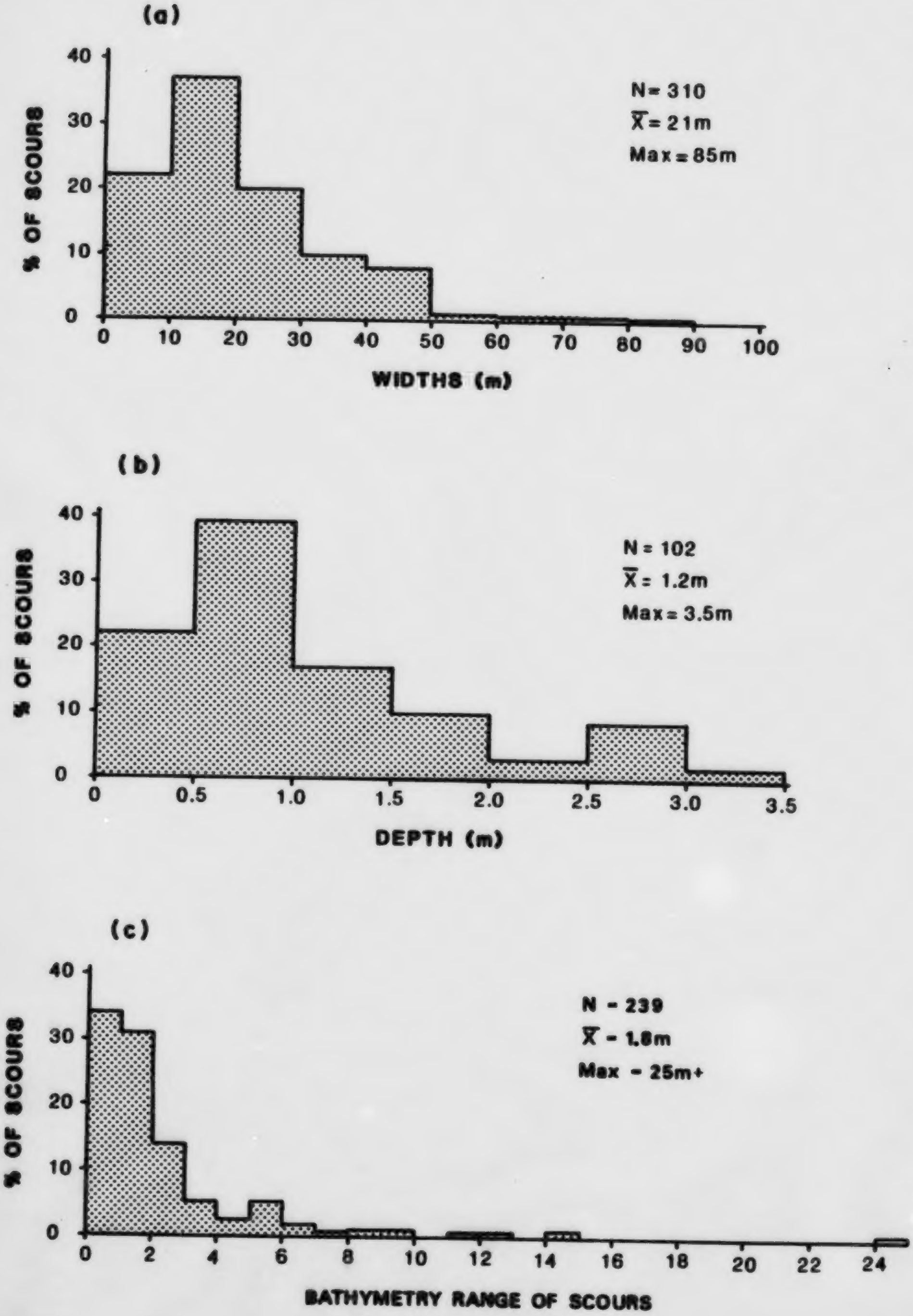

Figure 81. Histograms illustrating iceberg scour dimensions – Repetitive Mapping site; a) scour width; b) scour depth; c) bathymetry range of scours.

measured was 85 m. In contrast, the average pit width for each geologic unit is as follows:

Unit 5b, 40 m;
Unit 3a, 18 m;
Unit 3b, 30.7 m;
Unit 4, 49.1 m.

For the purposes of this compilation, a pit has been defined as any ice-related feature with a length-to-width ratio of less than 2:1. The maximum recorded pit width on the mosaic is 125 m.

Figure 81 illustrates the distribution of scour depths for the mosaic area as measured from the DTS profiles. The scour depths measured for each geologic unit are as follows:

Sioraq Sand, average scour depth is 0.71 m;
Qeovik Silt, average scour depth is 1.25 m;
Lower Till average scour depth is 0.64.

The average scour depth (all geologic units and water depths) is 1.2 m with the maximum measured depth being 3.5 m.

Individual scours may traverse significant (up to 25 m) ranges in water depth (see Appendix 10). Figure 81(c) illustrates the range in water depth traversed as a function of a percentage of the total population. One scour (scour # 80 - see Appendix 10) traverses across a bathymetric range of at least 25 m and extends beyond the southern margin of the mosaic area. The depth of scour #80 ranges from 0.7 to 1.2 m. The average upslope/downslope vertical range is 1.8 m. There is a positive correlation between scour length and bathymetric range.

"Bertha" Mosaic

Bathymetry. The "Bertha" mosaic site is located on the northwestern edge of Makkovik Bank (Chart 3). Water depths range from a minimum of 102 m near the southeastern end of the mosaic to a maximum of 135 m at the northwestern end of the mosaic (Chart 13). On the bank top (southeastern end of mosaic) the seabed is relatively smooth and flat with local slopes averaging 1:100. Northwest of the shallowest point the seabed slopes uniformly towards N45°W at 1:150. Over this portion of the mosaic, the seabed is rough with undulations on the order of 1 to 3 m in height and 50 m to 100 m in wavelength.

Surficial Geology. Two surficial geologic units are exposed within the "Bertha" mosaic area. Undivided Labrador Shelf Drift Formation (Josenhans et al. 1986) underlies the entire mosaic area (Figure 82). This unit has a moderate grey level and incoherent internal character with a single, discontinuous internal reflector evident on the DTS profiles (see Figure 82). Its upper surface is generally rough, probably the result of scouring by icebergs, except on the bank top where it is relatively smooth. In water depths of less than about 106 m, the surface of the unit, where exposed at the seabed, has been reworked by currents to produce a thin lag of coarse sand and gravel (see Chart 14).

At the northwest end of the mosaic the Labrador Shelf Drift is overlain by a northwest-thickening cover of Qeovik Silt (see Figure 82). This unit is more acoustically transparent than the underlying till but lacks the internal stratification normally associated with it (Josenhans et al. 1986), possibly as a result of reworking by iceberg scouring. On the sidescan mosaic (Chart 14) the Oeovik Silt appears darker in colour and smoother than the Upper Till

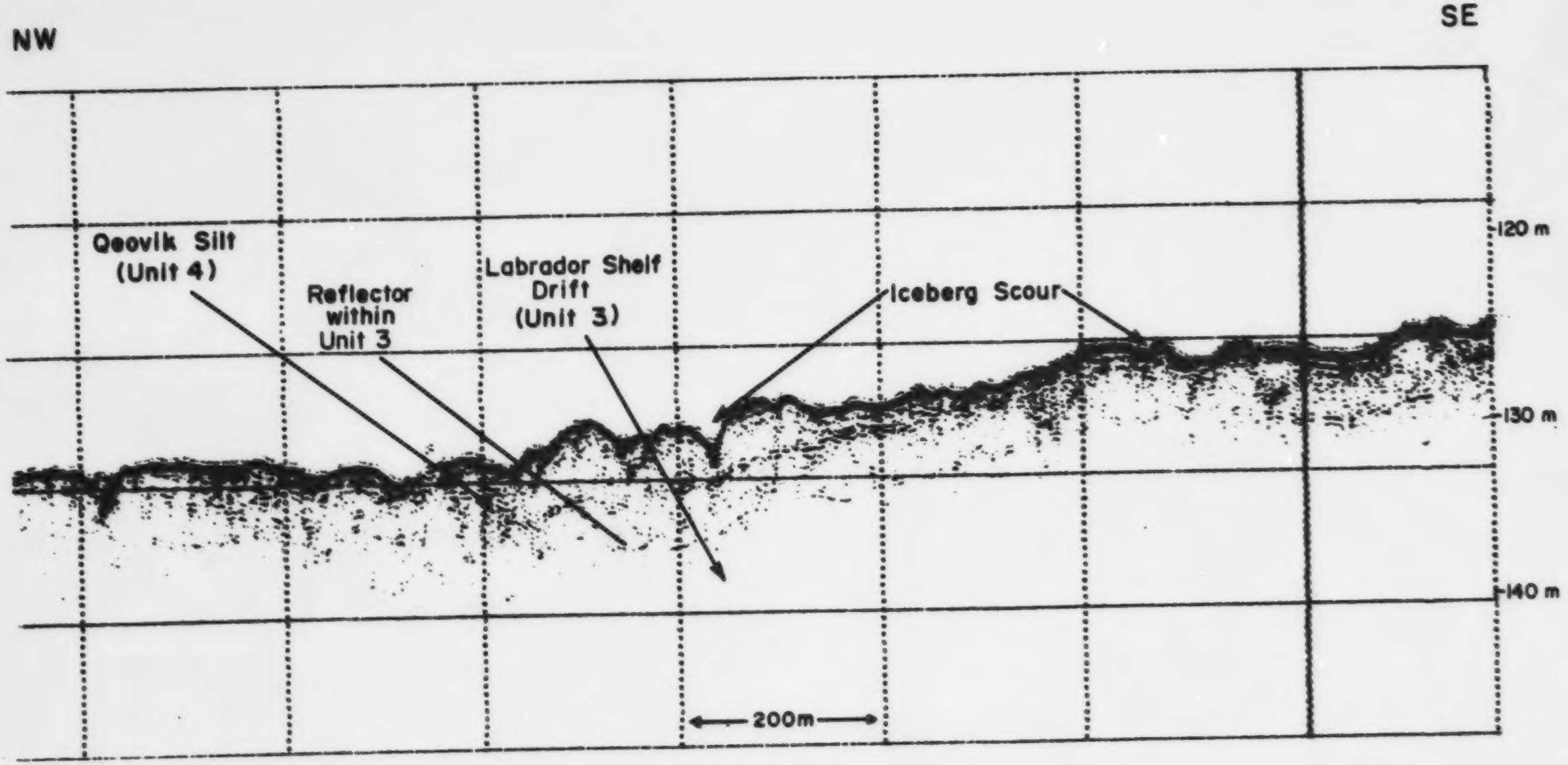

Figure 82. A DTS profile of part of Line 9 from the iceberg 'Bertha' site illustrating the two units identified and the heavily scoured seabed.

unit, and shows no evidence of a sand veneer. Seabed photographs taken by BRUTIV show a coarse, well-sorted, surficial gravel lag developed on the surface of this unit.

Bedforms. The predominant bedforms evident on the "Bertha" mosaic are large, symmetric ripples. These features appear well defined on the sidescan sonograms (Figure 83) and on the BRUTIV seabed photographs. They are two-dimensional megaripples (Amos and King 1984) with straight to bifurcated crests. Crest orientation is predominantly N145°E (indicating contour-parallel flow) and the wavelength is between 1.0 and 2.0 m. Photographs of these features show them to consist of well-sorted, coarse to pebbly sand. In most cases, the underlying gravel lag is exposed in the troughs between individual ripples. Individual patches of large, symmetrical ripples are generally elongate in a northeast-southwest orientation (see Figure 83). These ripples are not observed below 110 m (Chart 13).

Iceberg Scours and Other Ice-Related Features. A total of 145 iceberg scours and pits have been documented and measured within the "Bertha" mosaic area (Appendix 10). All measurements were made from a 1:5,000 scale preliminary mosaic. Where identifiable, scours on sidescan sonograms were correlated with those on DTS records.

The predominant scour orientation (Figure 84) is N103°E, or roughly 60° to the trend of the bathymetric contours. Average scour widths for geologic units 3 and 4 are 16.8 m and 19.9 m respectively. The widest scours measured in each unit are 53 m and 54 m respectively (Figures 85a and 85b). Average pit widths are 31.7 m for Unit 3 and 30.0 m for Unit 4. For classification purposes a pit was defined as any ice-related feature with a length-to-width ratio of less than 2:1. The maximum amount of upslope and downslope

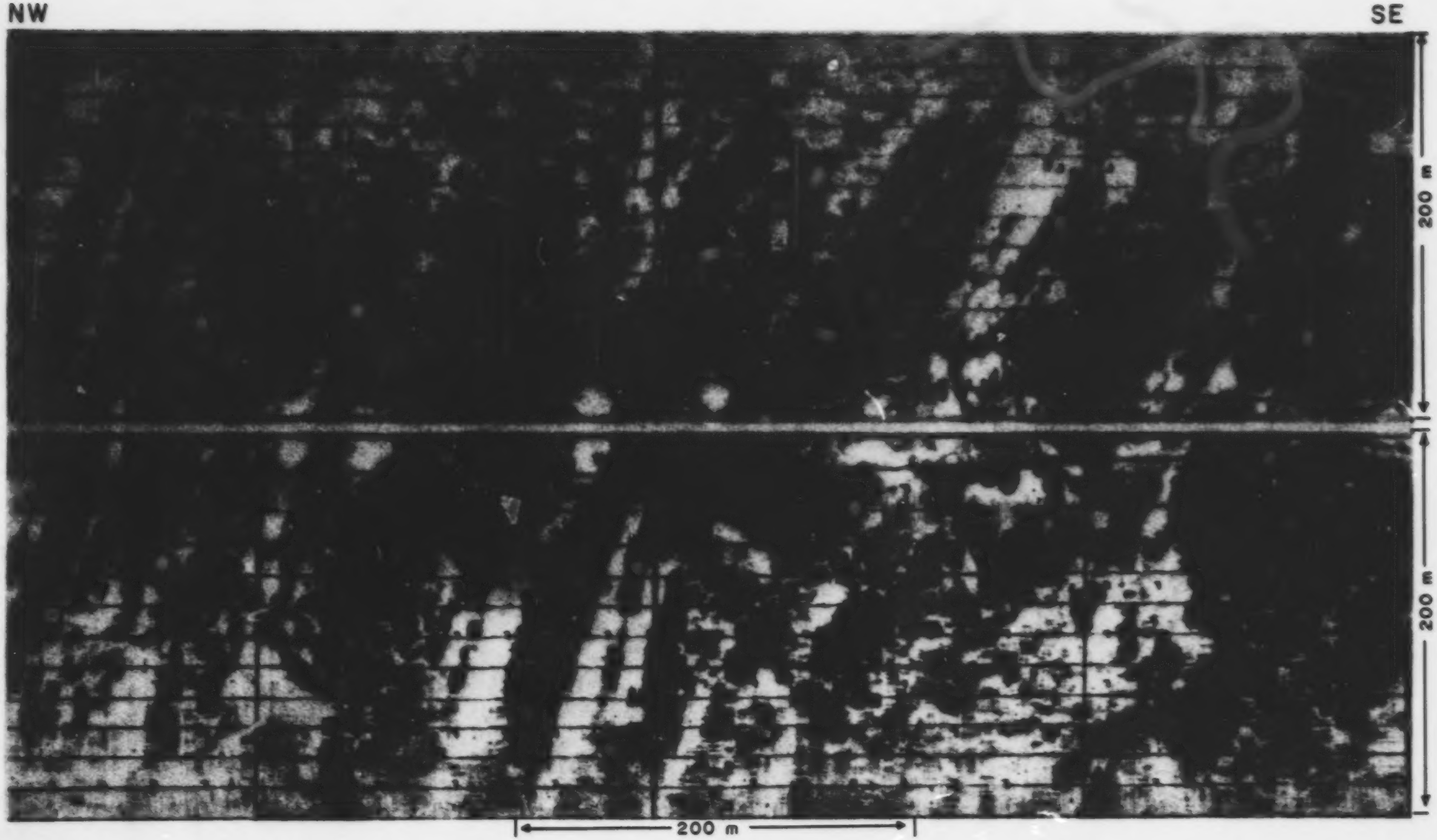
NW
SE
200 m
200 m
200 m

Figure 83. A sidescan sonogram of part of Line 13 from the Iceberg 'Bertha' site showing a number of iceberg scours.

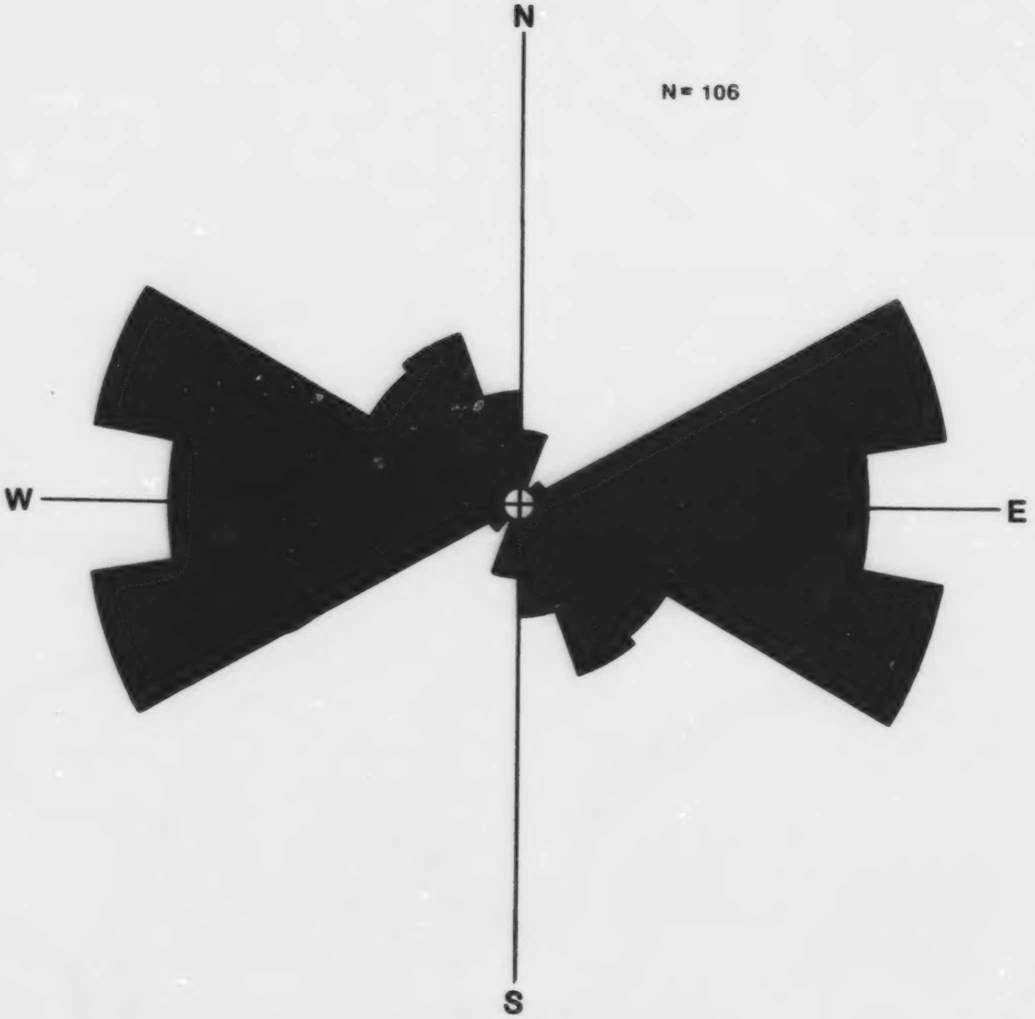

Figure 84. Iceberg scour orientations - Iceberg "Bertha" site.

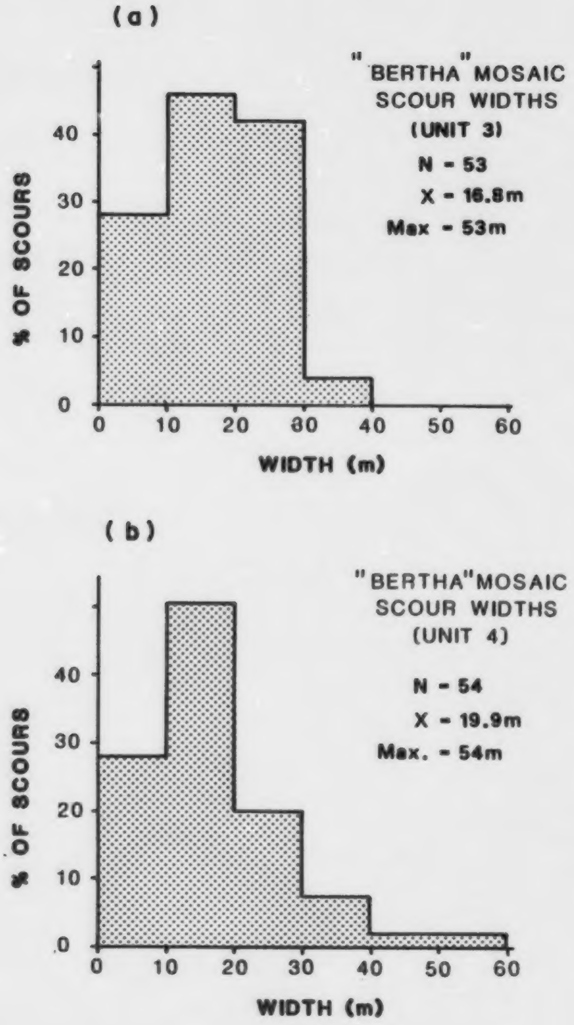

Figure 85. Iceberg scour dimensions – iceberg "Bertha" site; a) scour widths (unit 3); and b) scour widths (unit 4).

vertical range documented is 3 m. Average measured scour depths are 0.7 m for Unit 3 and 0.9 m for Unit 4.

"Anastasia/Deborah" Mosaic

Bathymetry. The "Anastasia/Deborah" mosaic site is located on the south side of an east-west trending ridge which forms the northern margin of Makkovik Bank (see Figure 75). Isobaths are oriented roughly N70°E and the seabed slopes uniformly towards the southeast from a depth of 120 m to 144 m. The average seabed slope is 1:70 (0.8°) except over the northwest corner of the site where the seabed is relatively flat across the top of the ridge (Chart 15).

Over the northwestern half of the mosaic, where Labrador Shelf Drift is exposed at or near the surface, the seabed is relatively rough. To the southeast, the seabed is flat except where interrupted by iceberg scours.

Surficial Geology. Two surficial geologic units are present within the "Anastasia/Deborah" mosaic area. Labrador Shelf Drift (Josenhans et al. 1986) underlies the entire area (Chart 16) and is exposed at or near the seabed over the northwestern half of the mosaic. This unit lacks internal reflectors on the DTS profiles except for the presence of short, poorly defined layers (Figure 86). There are insufficient data to allow division of this unit into the Upper Till or Lower Tills of Josenhans et al. (1986). The upper surface of the unit is generally flat to gently undulating where exposed at the surface. Surface roughness is caused by intense iceberg scouring. These scours are readily evident on the sidescan mosaic (Chart 16 and Figure 87). Where buried by overlying sand, the till surface varies from smooth to very rough.

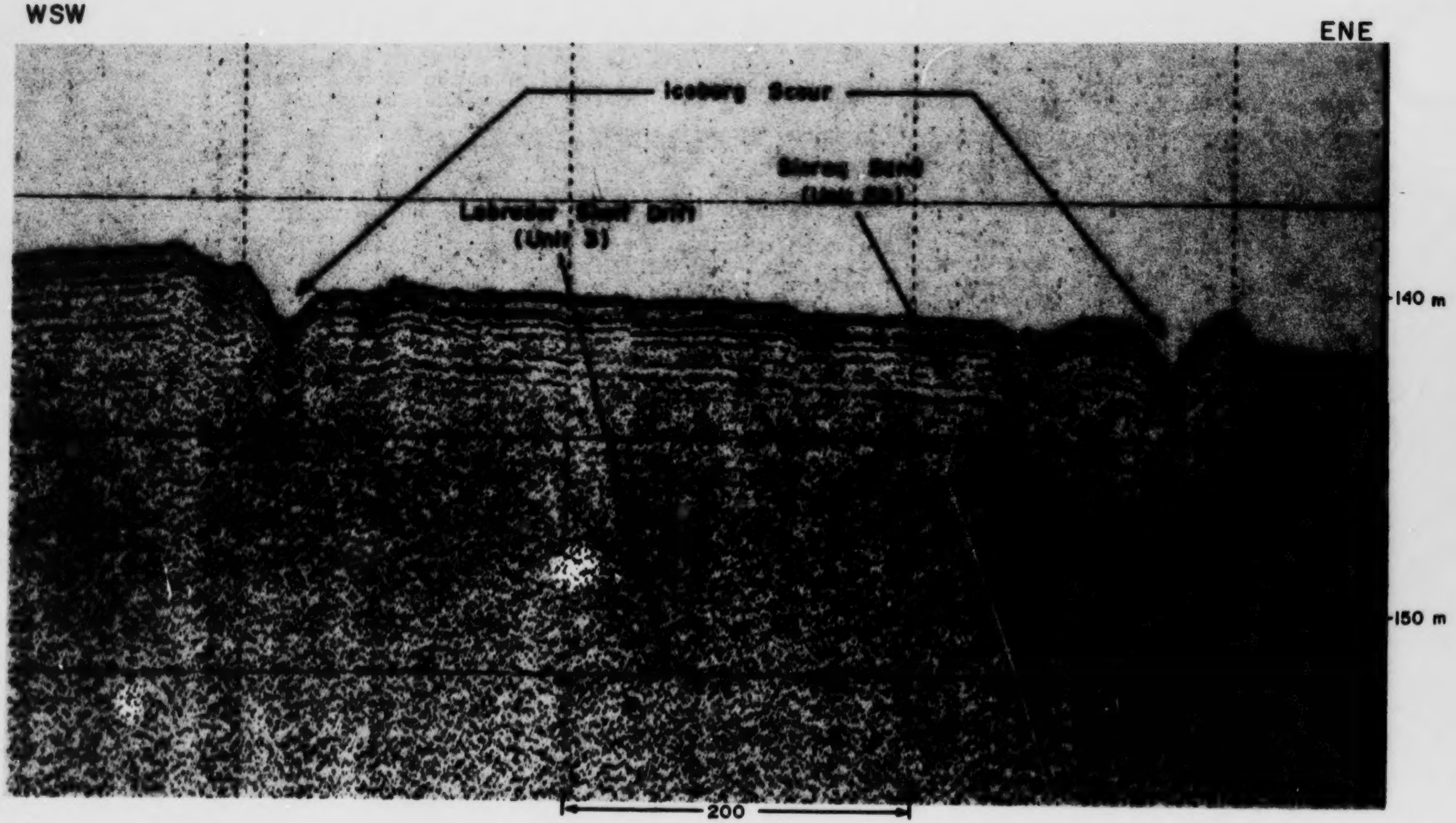

Figure 86. A DTS profile of part of Line 78 from the iceberg 'Anastasia/Deborah' site illustrating the acoustic character of the geologic units and two well-defined iceberg scours.

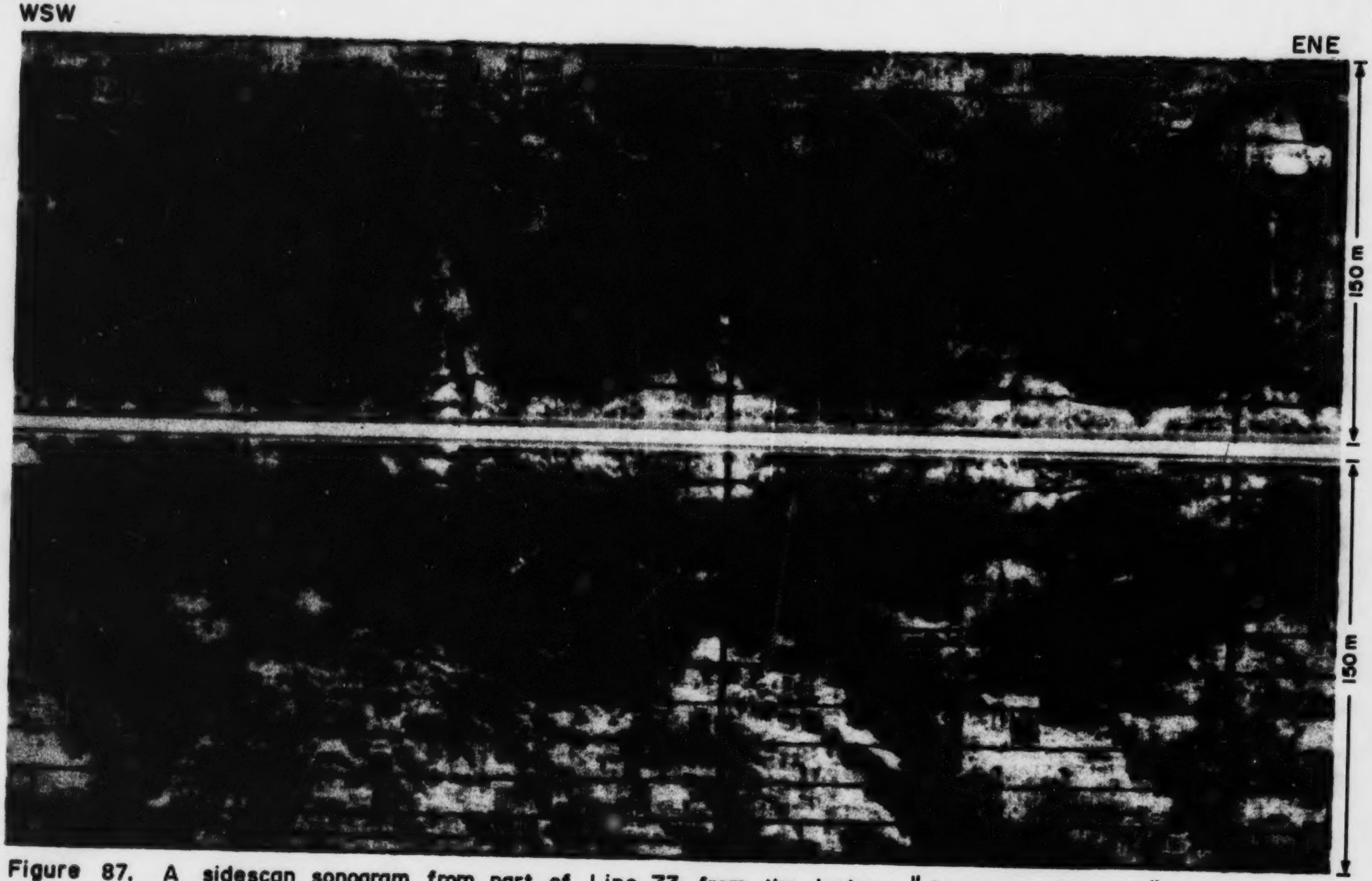

Figure 87. A sidescan sonogram from part of Line 73 from the iceberg "Anastasia/Deborah" site showing iceberg scours and pits within the Labrador Shelf Drift Formation (Unit 3).

In the southeastern half of the "Anastasia/Deborah" mosaic, Labrador Shelf Drift is draped by a southeastward-thickening cover of Sioraq Sand. This unit reaches a maximum thickness of about 6 m over the southern portion of the site. It is acoustically transparent and lacks internal stratification (see Figure 87). The seabed over this unit is flat except where buried iceberg scours come to the surface. Where it is thin, Sioraq Sand fills in hollows rather than draping the underlying material. This character is well illustrated in Figure 88 which shows an almost completely buried iceberg scour.

Bedforms. No bedforms were observed on the "Anastasia/Deborah" mosaic. BRUTIV data collected just north and west of the mosaic area show scattered ripples and large, symmetrical ripples on the seabed. In addition, a mottled texture has been noted in some of the sandier areas between survey lines 6 and 7.

Iceberg Scours and Other Ice-Related Features. A total of 214 iceberg scours and pits have been documented and measured from the "Anastasia/Deborah" sidescan sonar data (Appendix 10). Orientation, width, and length measurements were made from a preliminary 1:5000 scale mosaic. Available DTS data were used to document 38 scour depths and, where possible, these were correlated with scours identified on the mosaic.

Scours have a strongly preferred northwest-southeast trend (Figure 89). Average measured scour widths are 18.5 m for Unit 5b and 16.5 m for Unit 3. Pit widths are appreciably larger: 44.3 m for Unit 5b and 35.8 m for Unit 3. Average scour depths are 1.0 m for Unit 5b and 1.2 m for Unit 3. The maximum upslope/downslope range observed is 4 m.

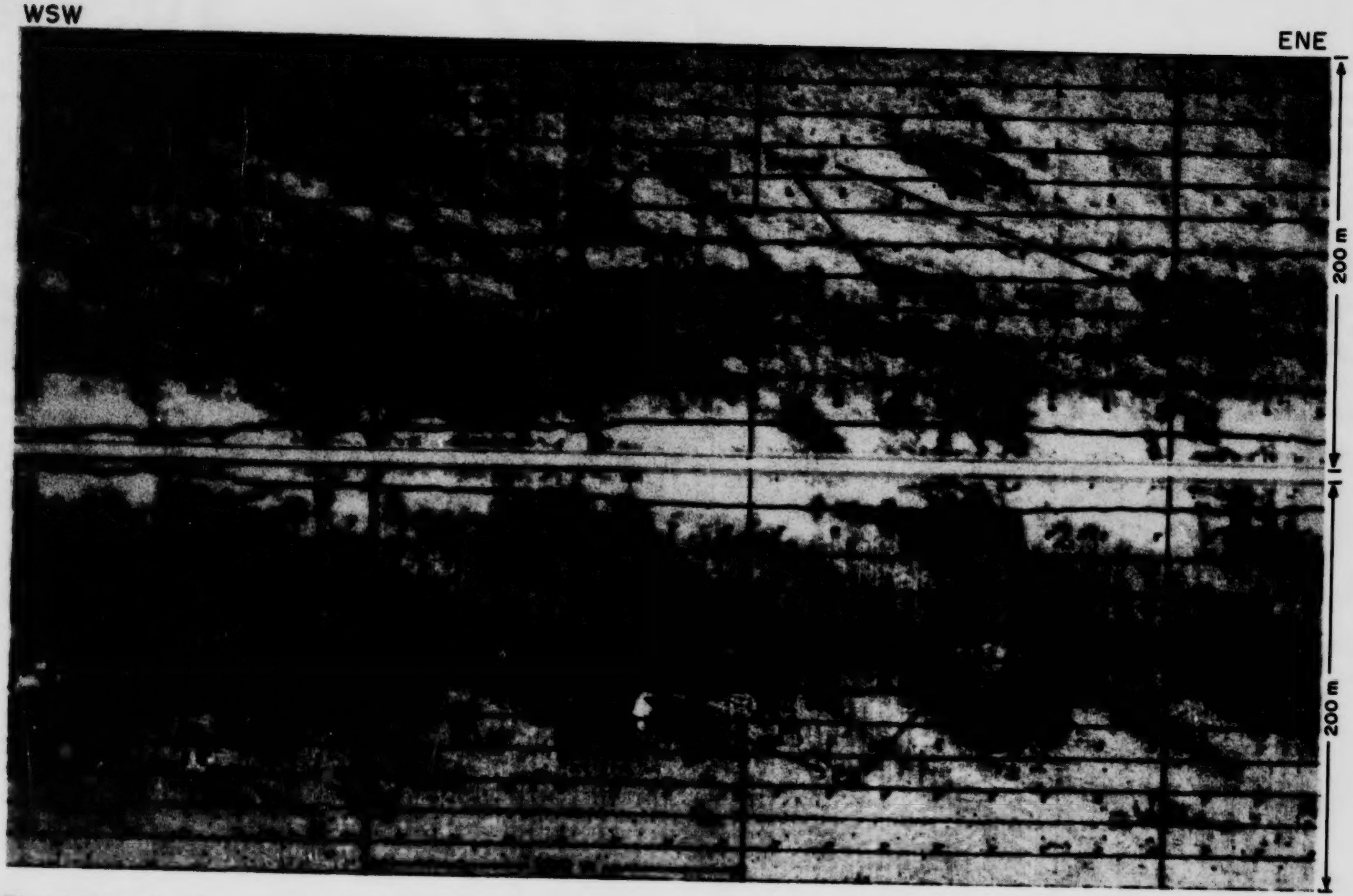

Figure 88. A sidescan sonogram of part of Line 72 from iceberg "Anastasia / Deborah" site showing a partially infilled scour as well as a number of pits within Sioraq Sand.

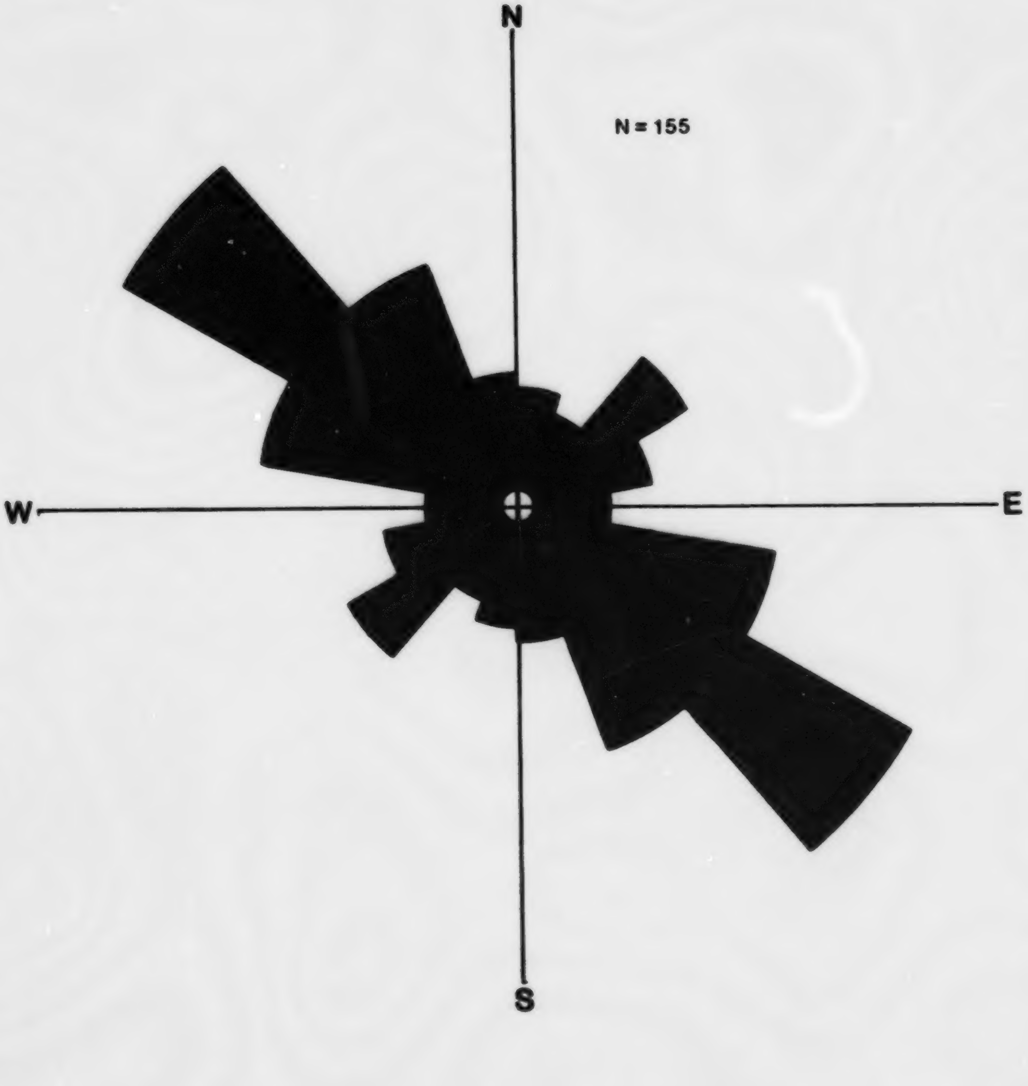

Figure 89. Iceberg scour orientations – Iceberg "Anastasia/Deborah" site.

Iceberg scours occur over the Labrador Shelf Drift Formation (Unit 3) within the mosaic area and are generally straight and consistently oriented. Those in Sioraq Sand (Unit 5b) are less well oriented but are fresher in appearance. This could be the result of the influence of different current regimes operating on the slope and top of Makkovik Bank. It is noteworthy that most pits observed on the mosaic are fresh looking and most are located in the Sioraq Sand unit.

"Gladys" Sidescan Composite

Bathymetry. The "Gladys" site is situated on the southeast corner of Makkovik Bank (Chart 3). The bathymetry for the area is presented on Chart 5.17. Water depths over the site range from a minimum of 122 m along the southern edge to 146 m at the eastern boundary. In the extreme southern part of the area water depths decrease from 128 m to 122 m over a topographic high before increasing northward toward the central part of the site for about 2 km with an average slope of about 1:133 (.75 percent). The 140 m isobath defines the relatively flat northern region. The seabed in this area gradually deepens to the north and east to depths of 144 m and 146 m respectively with slopes averaging 1:500 (0.11°).

Surficial Geology. Two surficial geologic sequences have been identified. The Labrador Shelf Drift Formation (Josenhans et al. 1986) underlies the entire site, however, insufficient data were acquired to allow accurate definition of the Upper Till and Lower Tills. Along the southern edge of the site, in water depths of less than 132 m, the formation is exposed at the seabed. Where exposed, the surface appears quite disturbed, possibly indicative of a high degree of iceberg scouring (Chart 18).

In water depths greater than 132 m, encompassing the entire central and northern part of the sidescan composite, the Labrador Shelf Drift Formation is overlain by a continuous surficial cover of post-glacial material interpreted as Sioraq Sand (Josenhans et al. 1986) (Figure 90). Although DTS records fail to define accurately the contact between the Sioraq Sand and Labrador Shelf Drift they do indicate a relatively uniform unit thickness of between 5 and 7 m. The upper surface of the unit appears quite smooth, occasionally interrupted by iceberg scours. No bedforms are evident on any of the data acquired at the site.

Iceberg Scours and Other Ice-Related Features. A total of 209 iceberg scours and pits have been measured from Huntec DTS (internal hydrophone) data from the "Gladys" site (see Appendix 10). No attempt was made to measure scour dimensions or orientations from the uncorrected sidescan sonograms.

Of 209 scours measured, 144 were located within the Sioraq Sand (Unit 5b) and the remainder in the Labrador Shelf Drift Formation (Unit 3). The average scour depth within Unit 3 is 0.98 m compared with 1.02 m in Unit 5b. The maximum depth recorded was 4.2 m, occurring within the Sioraq Sand unit.

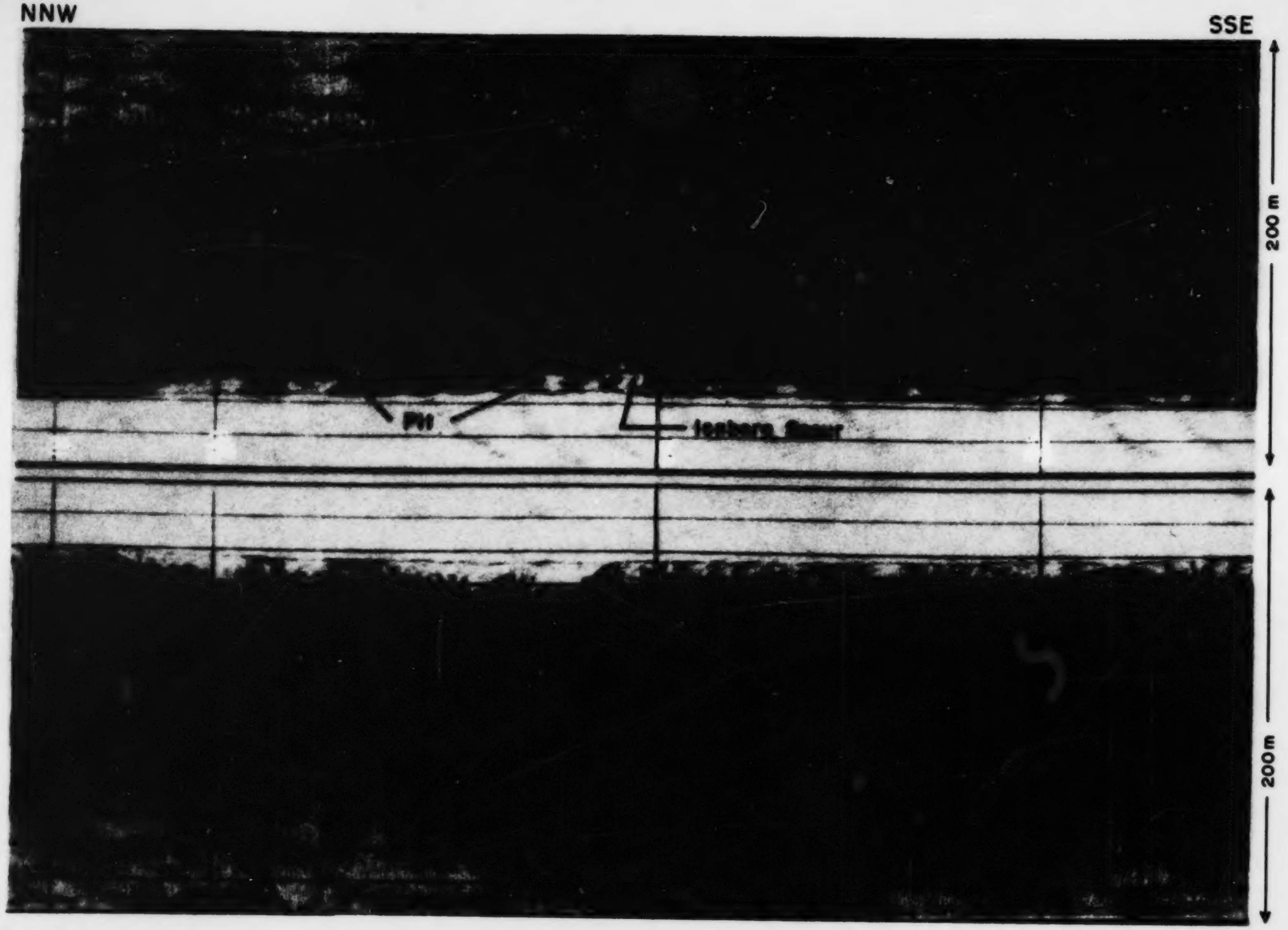

NNW
SSE
200 m
Pit
Iceberg Scour
200m

Figure 90. A sidescan sonogram of Line 37 from the iceberg "Gladys" site illustrating the scoured seabed typical of the site. The surficial material is interpreted to be Sioraq Sand (Unit 5b).

SEDIMENT TRANSPORT

Current meter results from the 18-day period were dominantly controlled by tides (Chapter 2) and only two significant events occurred that could have resulted in sediment transport.

The first event occurred on August 4 when velocities reached a maximum of 0.33 m/s one metre above the seafloor. The currents relate primarily to spring tidal currents with peak flows to the south-southwest.

The second series of events occurred on August 15, 16, and 17. These events occurred during the next spring tide and during a period when waves had a mean significant wave height of 2.3 m and a period of 10 s. The mean current speed 1 m above the seafloor during these events was approximately 0.28 m/s whereas the bottom orbital velocity was negligible. Hence, sediment transport was primarily controlled during this short observation period by semi-diurnal and diurnal spring tidal flow. The dominant current flow direction is southwest to west with a smaller component flowing southeast to east. The highest current velocities and the longest flow duration were to the southwest.

Sediment Tracer Results

During dive number 8 of the Pisces IV submersible, a 50 m grid of five sample stations (see Appendix 9) was established in the area of the shallow current meter. About 20 g of material were obtained in each sample, using the suction sampler on the Pisces IV.

The original buoy deployed with the tracer sand was not relocated; therefore, the sampling grid was set up based on the ship's position during deployment of Pisces IV. The grid is therefore offset, because of navigational errors of the submersible, from the original point of deployment.

Analysis was carried out by Atomic Energy of Canada on the five suction samples collected. The highest concentration of cesium found was in sample #5 where the cesium content was 0.6 ppm (Table 7).

Predicted Sediment Transport

Based on current meter and tracer sample results (Table 7) and the orientation of the large symmetrical ripples, a net transport direction to the southwest can be predicted. It is difficult to derive accurate direction and total sediment transport from the pollucite tracer sand results because the position of the original dump site is uncertain.

From the current data collected during the August 15, 16 and 17 events, bottom shear velocities have been calculated based on the Bijker (1967) method. This method assumes that the formulae for the prediction of sediment transport rate under unidirectional flow remain valid for transport under the combined action of waves and currents with the exception that the shear velocity (U*c) is replaced by the resultant shear velocity (U*wc) in the presence of waves and currents. The expression used is:

$$U^{*}wc = U^{*}c \left[1 + 0.5 \left(\xi \, U\underline{m} \right)^{2} \right] 0.5 \qquad (2)$$

Table 8

Cesium concentration in sediment samples collected after 19 days.

Sample number	Cesium concentration (ppm)
1	<0.1
2	<0.1
3	0.3
4	0.5
5	0.6
Background level	<0.1

where ξ is a function of the wave friction factor (Jonsson 1966) as expressed by Swart (1976) and Pattiaratchi and Collins (1984), Um is wave orbital speed and U is the current speed. As the principal tidal current is in the same general orientation as the waves, the Bijker method can be considered reasonably valid.

The results are a measure of the mean bottom shear stress and can only be used as a first-order calculation. The maximum bottom shear velocity would be 0.39 m/s in a west-southwest direction. This would result in considerable sediment transport of fine sand in the area during those short periods of enhanced current.

CHAPTER 5

ICEBERG DYNAMICS AND SEDIMENT RESPONSE

ANALYSIS OF OBSERVED ICEBERG/SEABED INTERACTIONS

In this section, analyses are presented to account for the observed behaviour of the three icebergs known to have interacted with the seabed: "Bertha", "Gladys", and "Julianna". For all three icebergs, information on above- and below-water shape has been used to examine static stability. Where appropriate, dynamic analyses of interaction events are also presented.

The two main objectives of these analyses are: (a) to produce quantitative estimates of forces interacting between iceberg and seabed; and (b) to demonstrate qualitative agreement between observed and simulated interaction behaviour as a means of gaining confidence in model performance.

The numerical model used for iceberg stability calculations and dynamic simulations was based on an extension, to three dimensions, of the work by Bass and Peters (1984) and Bass et al. (1986).

The original iceberg shape data were in terms of offsets for horizontal cross-sections. These sections were used to calculate the centres of gravity of the above- and below-water portion of the iceberg. This information, together with observations and photographic evidence were used in placing the iceberg "top" on the iceberg "bottom". In particular, as "Bertha" was free-floating at the time of data acquisition, the calculated positions of the centres of gravity were used to ensure static equilibriums of the final iceberg ensemble.

In the analysis of stability it is necessary to tilt the iceberg in various directions. To ensure accurate calculation of the geometric characteristics for different water-line positions, it is necessary to obtain a representation of the iceberg by vertical cross-sections (and thence by vertical trapezoidal prisms). The procedure of deriving vertical cross-sections of a three-dimensional shape from given horizontal cross section data is non-trivial for a complex irregular shape such as an iceberg. A certain amount of "smoothing" was applied in the derivation process which resulted in small variation (typically less than 1%) in calculated values of volume, moments of inertia, and so on, between the horizontal and vertical representations. Because the shape data themselves were subject to much larger uncertainty, the horizontal and vertical representations developed for each iceberg were felt to be equivalent.

Quasi-static stability maps were generated by rotating the icebergs about various axes. The resulting changes in potential energy were expressed in terms of the changes in the vertical separation of the centres of gravity and buoyancy for constant underwater volume. The potential energy is equal to this separation or potential height times the iceberg's weight. For the iceberg to be stable, its present orientation must be one of minimum potential energy locally.

The dynamic analysis was carried out using a time-domain simulation program built around the aforementioned static-analysis computer program. Briefly, the simulation program follows the movement of the centre of gravity of the iceberg together with the rotations of axes fixed in the body relative to some absolute system of axes at the waterline. The rotation of the body axes are described by means of modified Euler angles with rotation relative to the x, y, and z axes described as roll, pitch, and yaw (respectively), following the terminology adopted by naval architects; the convention for the rotation order follows that of Blagoveshchensky (1955).

For free-floating icebergs, the rigid body motion equations solved (numerically) at each time step are given as follows:

$$[M + \delta M]\,\ddot{\underline{r}} + [Bx]\,\ddot{\underline{r}} = \mathrm{HSFOR} \qquad (3)$$

$$[I + \delta I]\,\ddot{\underline{\omega}} + \underline{\omega} + I\,\underline{\omega} + [B\omega]\,\underline{\omega} = \mathrm{HSMOM} \qquad (4)$$

where:

$[M]$ and $[\delta M]$ are the mass and added mass matrices;
$[I]$ and $[\delta I]$ are the inertia and added inertia matrices;
$[Bx]$ is the damping matrix for translational modes;
$[B\omega]$ is the damping matrix for rotational modes;
$\underline{r}$ is the position vector of the centre of gravity of the iceberg relative to some absolute frame;
$\underline{\omega}$ is the angular velocity of the instantaneous body axes;
HSFOR is the vector of hydrostatic forces acting on the body, in absolute axes;
HSMOM is the vector of moments of hydrostatic forces acting on the body in terms of relative axes about the centre of gravity.

Crude estimates of the hydrodynamic coefficients were used in the simulations based on previous work (Bass and Sen 1985). Although some coupling between motions was modelled in the rotational modes with the non-zero products of inertia terms in the inertia matrix [I], no hydrodynamic coupling was included in $[\delta I]$ as such terms would be of second order.

For the analysis of motion during impact of the iceberg with the seabed, the same motion equations (3, 4) were used, but with the addition to the right-hand side of a scour force term SCFOR and an ocean current drag term CRFOR to the first equation, the corresponding moments to the second. With few data on currents, the main use of the current term was to investigate its effect on the "Bertha" roll and pitting behaviour.

The scour forces and moments were based on models used in previous work (Bass et al. 1986). In the three-dimensional modelling, the velocity and direction of some point on the iceberg keel were determined, together with the position of this point relative to the seabed. From that data, the direction and magnitude of the scour force was determined together with its moment relative to the centre of gravity (CG) of the iceberg. The point chosen on the iceberg keel was assumed to be the centre of pressure for the scour force. The keel had variable geometric dimensions, but only "indentor width", and horizontal (projected) cross-sectional area were used in the present simulations.

The vertical force exerted on the keel by the seabed, as a result of the downward motion, was taken to be directly proportional to the bearing capacity of the soil, the area of contact of the keel with the seabed and the depth of penetration. The horizontal seabed force was based on the model of Chari (1979).

In the situation where the keel was embedded in the seabed but was moving out, the vertical force was taken to be zero. For the situation in which the keel reentered the already formed pit (as with "Gladys") a much lower vertical force was applied, which was intended as a quasi-static reaction to the imbalance of weight over buoyancy. In such cases, in which buoyancy exceeded weight, no vertical soil reaction was applied. This procedure permitted smooth reapplication of vertical soil force upon keel reentry. Because the horizontal direction of keel motion varied significantly during seabed interaction, those forces were not modified on pit reentry. The main consequence of this may be that pit horizontal dimensions are underestimated. In fact the soil mechanics of the process are too poorly understood for any definitive conclusion.

As with any initial value problem, the time domain solution is significantly dependent on initial conditions. For example in the "Bertha" motion it is apparent that for the iceberg to move off and to impact the seabed some 35 m distant from its original grounded situation, it must have been impelled by the reaction of the seabed to its rotational motion. The initial angular orientation of the iceberg relative to its final free-floating orientation significantly affects the "propulsion" of the iceberg forward to its next impact site, which in turn affects the next impact, and so on.

Similarly, the initial position of the centre of gravity of the iceberg relative to the waterline is a major factor in determining impact behaviour. Vertical motions of the iceberg are difficult to extricate from the rotational modes in the observed motion data, so it is impossible to determine the degree of heave motion that takes place during roll over.

For "Gladys", placement of the initial CG position was governed by the need to align the grounded section with its pre-split orientation, quantitatively described by the above-water contour map.

Unfortunately, no stereophotographs were obtained for "Bertha" in its grounded state. Thus, the choice of initial CG position for "Bertha" (3 m above its final position) was dictated by the requirement of initial keel penetration of sufficient (but not too great) depth to provide the initial impetus for forward motion. Such a choice was therefore dependent on the assumption of correct keel geometry as well as soil shear strength, and therefore subject to some uncertainty.

"Bertha" Roll and Pitting Event

At about 1030 hrs GMT on August 5, calving initiated the roll of the previously grounded iceberg "Bertha". The iceberg drifted towards the northwest, and subsequent survey work revealed the creation of a set of four pits along this direction from its initial grounding site (see Figure 65). The motions recorded during this period by the C-CORE sensor package are shown in Figures 51-53. Profile data are also available for this iceberg, so it is possible to recreate the event and compare predicted versus observed behaviour.

A plot of the potential energy, or stability surface, for "Bertha" is shown in Figure 91. The iceberg was

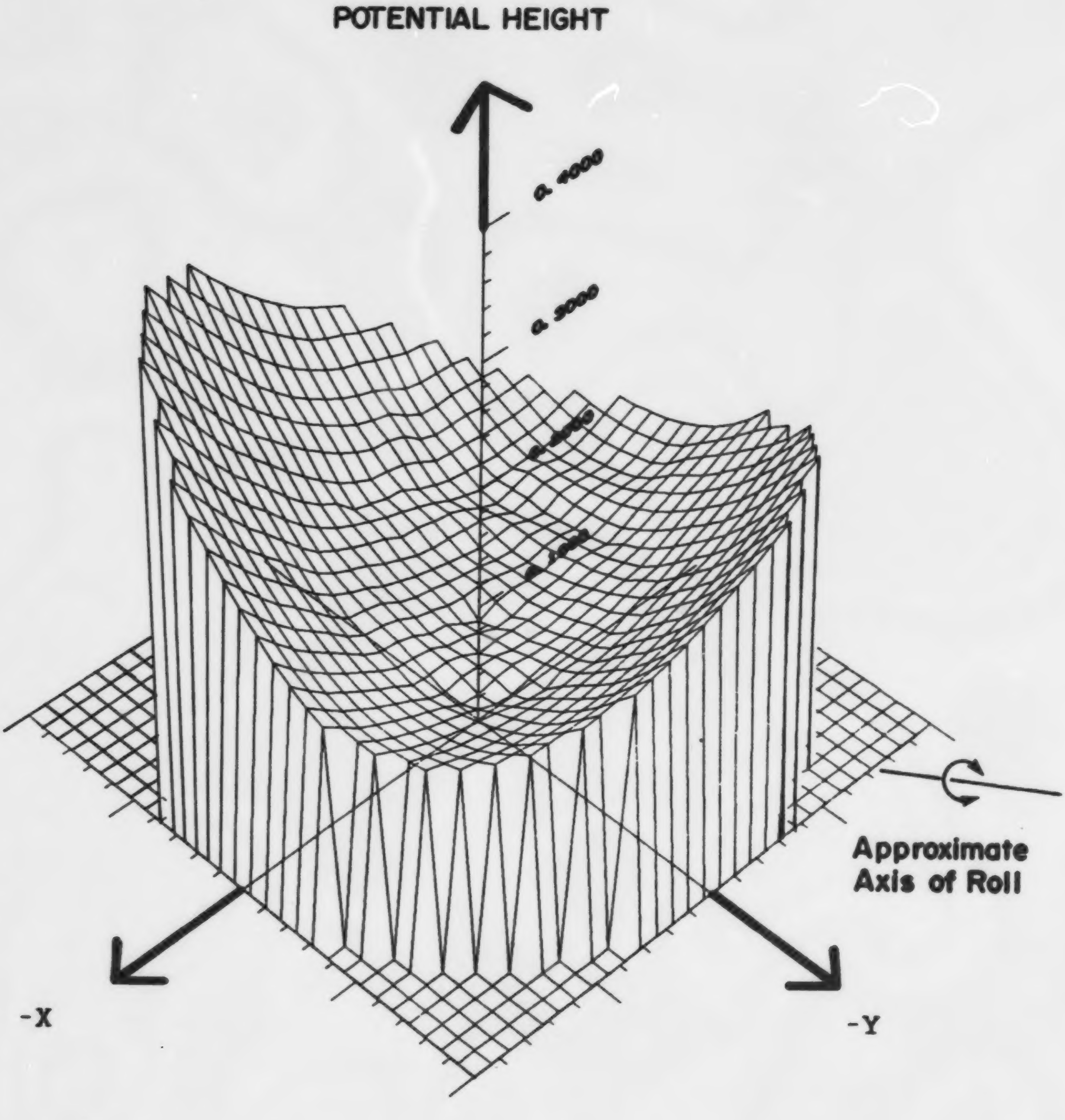

Figure 91. Potential energy plot for "Bertha".

free-floating at the time of above- and below-water dimensioning, and the stability map shows that "Bertha" was indeed stable about all axes of rotation. The stiffest axes for roll are seen to lie in the range of 40° to 50° yaw (counter clockwise angle with respect to X axis on Figure 26), with potential height changes of approximately 0.2 m over ±10° roll. The weakest roll axes are seen to lie in the range of -50° to -60° yaw, with potential height changes of only 0.03 to 0.06 m over +10° roll (see Figure 91). That is, the iceberg is predicted to rotate much more easily about axes nearly parallel with its longest waterplane dimension. In fact, the roll and pitting event on August 5 and the free-floating roll behaviour on August 6 (see Chapter 3) both occurred about axes within this range of least stability.

During the day between aerial photography and the completion of underwater profiling of "Bertha", several calving events took place (see Chapter 3). Furthermore, the exact circumstances which initiated the roll and pitting behaviour, such as where and how much ice was calved and the actual current regime, are not known. Lack of this information makes it difficult to recreate the initial stages of the event with certainty. However, it was apparent from the early simulation runs that the current alone could not have accelerated the iceberg rapidly enough to account for the large initial space between the pits. It appears that ice was calved in such a way that "Bertha" pushed off the seabed in the direction of travel, and this behaviour was in fact used in the later simulations to initiate the event.

Additional difficulty in recreating this and the other events of observed seabed interaction lies in the imperfect knowledge regarding the geometry of the keel and area of the ice contact surface and seabed contact surface. The geometry of the ice at the keel is not known accurately as profiling observations of the most deeply submerged part of the iceberg were subject to greatest measurement error with the profiling technique used. Because geotechnical measurements were not made, the seabed soil strength is unknown. Finally, it is not clear to what degree ice failure at the interface between keel and seabed interface took place, if at all.

In spite of these difficulties, dynamic simulations of the "Bertha" roll and pitting event were nevertheless conducted. Table 9 lists the conditions used in the final simulation.

The simulated motions of "Bertha" are shown in Figures 92-94. Here, the x,y,z translations are measured in a space-fixed co-ordinate system based on the starting orientation of the iceberg, (see Figure 26). The x,y,z rotations are about the respective body-fixed axes under right-hand convention.

In comparing the simulation results with observed motion data, the following differences should be noted: (a) the simulation yields linear displacements in a space-fixed co-ordinate system whereas the sensor package gave linear accelerations in the body-fixed frame; (b) the simulation X axis and Y axis rotations correspond approximately to the sensor package Y-Tilt and X-Tilt, respectively. Because of noise, and data rate problems with the data loggers, it was decided not to convert measured linear accelerations to fixed reference frame displacements. Hence, the observed accelerations include large gravitational components associated with body rotations and yield essentially the same information as the tiltmeters. Fortunately, the

Table 9

Conditions for "Bertha" Simulation

Water depth: 112 m

Current speed: 0.3 m/s

Current heading: -140°

Centre of pressure: (17,-6,-31)m

Drag coefficient: 1.5

Projected area for current: 17,000 m^2

Added mass coefficient: 0.8

Soil strength: 200 kPa

Scour breadth: 35 m

Horizontal contact area: 200 m^2

Seabed slope: 0.02

Keel slope: 0°

Keel contact point: (52,-2.3,-110)m

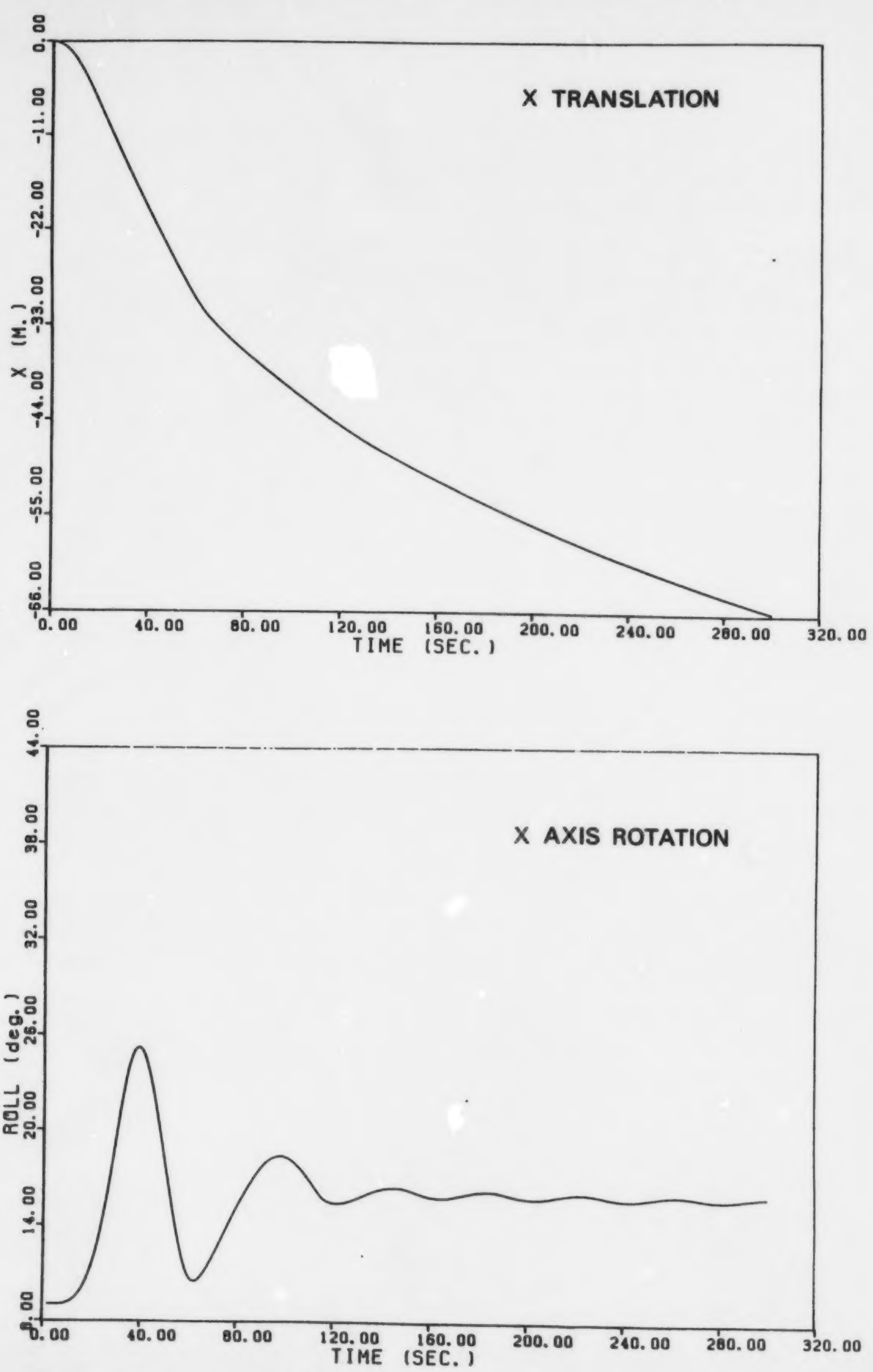

Figure 92. Simulated motions of "Bertha" during roll/pitting event, X axis translation and rotation.

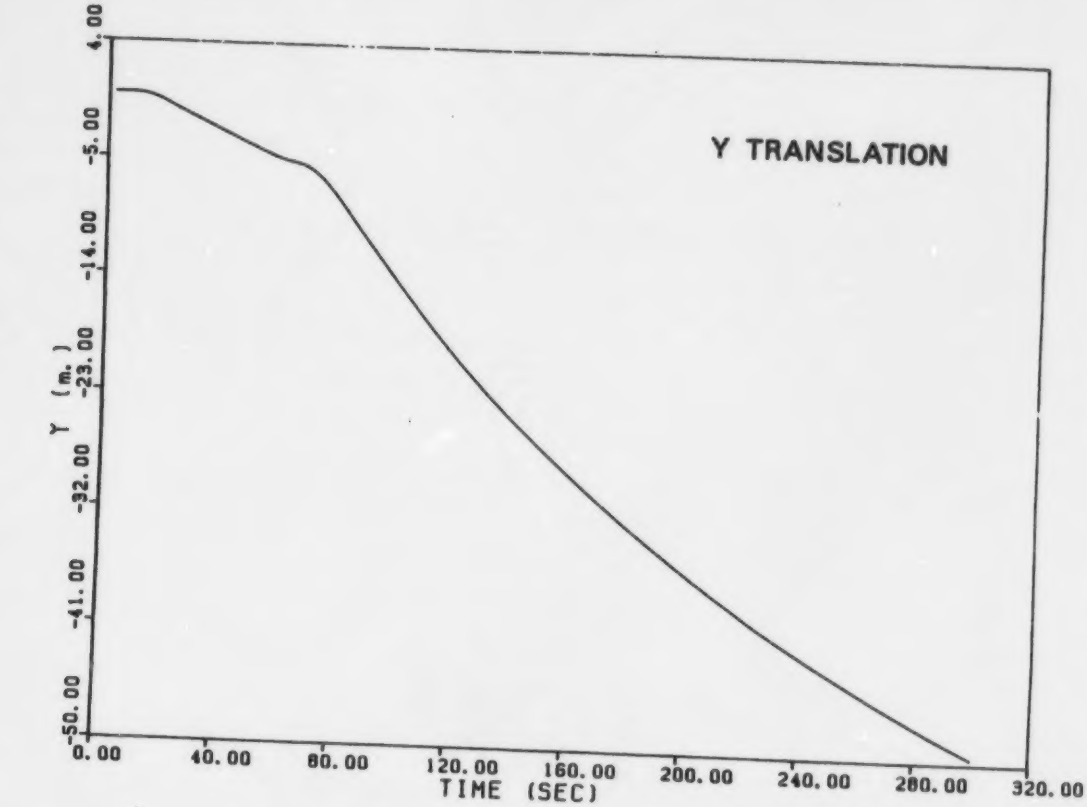

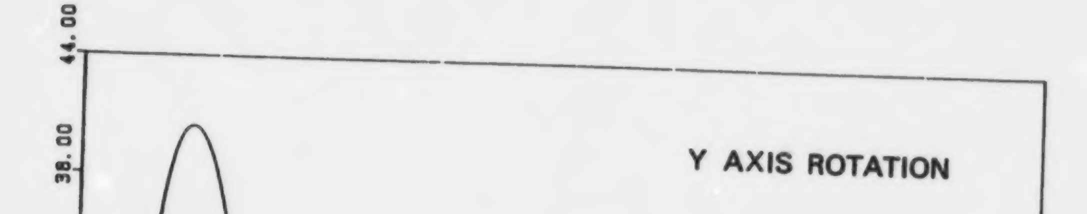

Figure 93. Simulated motions of "Bertha" during roll/pitting event, Y axis translation and rotation.

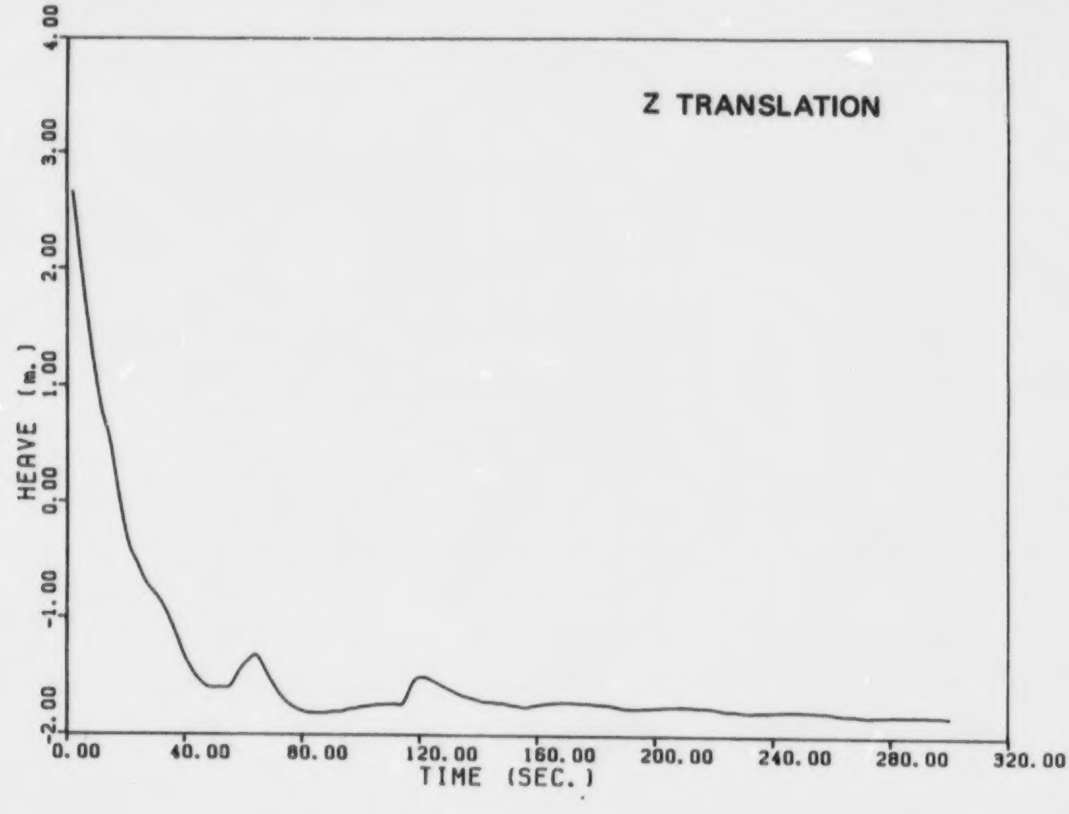

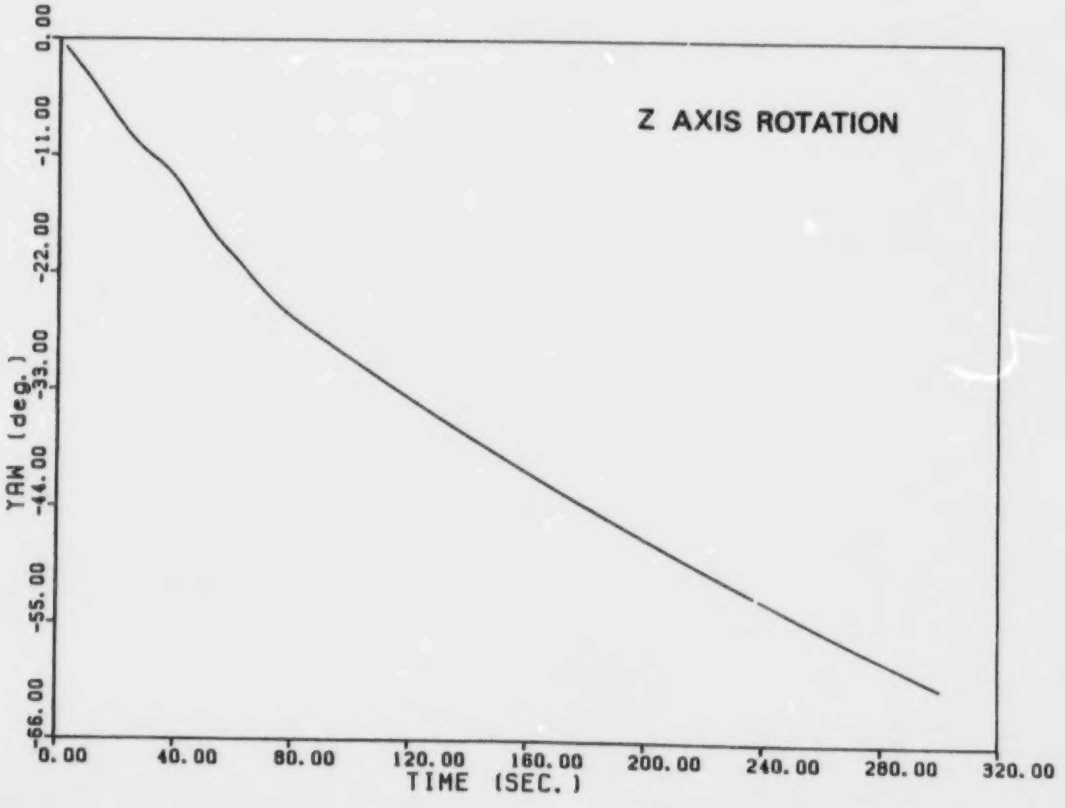

Figure 94. Simulated motions of "Bertha" during roll/pitting event, Z axis translation and rotation.

"Bertha" event is primarily a rotation-induced pitting sequence and, hence, comparison of simulated and observed rotational motion yields sufficient insight.

Comparison of Figures 92-94 with Figures 51-53 shows reasonably good agreement between the observed and predicted behaviour of iceberg "Bertha". The predicted large initial rotation of 28° about the Y axis agrees well with the observed 22° change in X-Tilt. Smaller initial rotations about the X axis (Y-Tilt) are seen in both the simulated and observed results (16° versus 7° respectively). The predicted roll periods of 60 s agree reasonably well with the observed periods of about 70 s, although the rate of decay of the oscillations appears to be higher in the simulated results.

Pitting behaviour is also predicted by the simulations. The first pit is predicted to occur on the downswing about 60 s after initiation of the event. This first pit is predicted to lie about 35 m from the initial grounding site. A maximum penetration of 3.4 m is predicted in soil of 200 kPa shear strength, and the pit would measure 35 m wide by 15 m long. Vertical soil forces of 220 MN are predicted, which translate to soil pressures of about 1,100 kPa (as expected for the static bearing capacity formula employed). Horizontal soil forces are predicted to be considerably smaller than vertical ones, because of smaller contact areas (maximum 120 m^2 versus 200 m^2) and lower soil pressures (450 kPa versus 1,100 kPa).

The remaining two pits are predicted to have reduced spacing (18 m, and 12 m separations) with substantially shallower depths of penetration and hence even lower horizontal forces. The progressive reduction in pit spacing agrees with the observed behaviour (observed spacing about

35 m, 25 m, and 20 m, see Figure 65) and suggests that the iceberg did indeed push off the bottom in the direction of travel. If initiation were solely the result of current forces, an increase in pit spacing would be expected. This pushing action also increases the size of the grounding site pit.

It is possible to compare rotational kinetic energies between the observed and simulated results. The maximum observed rotational velocities on the downswing leading to the first pit, as obtained from Figures 51 and 52, were approximately 0.20 ± 0.04°/s on both X- and Y-Tilt. The mass moments of inertia (including added mass) through the CG are (4.1 ±0.6) x 10^{12} Kg m^2 about both the X and Y axes. Thus, the observed maximum rotational kinetic energy of "Bertha" prior to creation of the first pit was approximately 50 ±30 MJ.

By comparison, the maximum rotational velocities obtained from the dynamic simulation are approximately 1.2°/s about both X and Y axes, or about 6 times higher than the observed values. Thus, the maximum rotational energy based on the simulation would be 36 times higher than that actually observed, or about 1,800 MJ. A check of the calculated stability map for "Bertha" shows that for a 20° roll about its weakest axis, a potential energy change of 1,100 MJ would be predicted. That is, the dynamic simulation results are consistent with the potential energy calculations based on the measured iceberg shape. It can be concluded that "Bertha" must have been much less stable for roll about its weakest axis than the measured shape data imply. It is likely that the non-simultaneous measurement of above- and below-water shapes, plus the inaccuracies inherent in the underwater dimensioning and positioning of the top on the bottom, have combined to yield a shape for

"Bertha" which is in fact substantially more stable than the actual iceberg.

One important implication of this result is that energy available to "Bertha" for seabed disruption was much lower than the simulation would suggest. Presumably the crater chain left by the iceberg was made in weaker soil than 200 kPa and/or the individual pits are not as deep as those predicted by the simulation.

Unfortunately, the quality of full-scale information available makes it extremely difficult to refine the simulation results. The exact number and sizes of pits are strongly dependent on the soil strength, keel geometry, initiation conditions, and overall iceberg shape. Nevertheless, present simulations show sufficiently good qualitative agreement with the observed behaviour to yield some confidence in the model and in the interpretation of the circumstances surrounding the event.

"Gladys" Split and Grounding Event

At about 1320 hrs GMT on August 10, "Gladys" split into two parts. The motion of "Gladys" as it rolled and grounded solidly with the seabed is shown in Figures 56-58. The shape of "Gladys" as measured following this event is shown in Figure 38.

The underwater profile data were of particularly poor quality for the lowest segments of the keel of the grounded portion of "Gladys", and an interpreted extension of the keel was required from 110 m depth to the seabed. This extension could not be located so as to achieve static equilibrium for both vertical and rotational motions using an average ice density of 0.90 tonnes/m^3. Rather than adjust the shape of the iceberg above the keel extension, it was decided to increase the average ice density used in the dynamic simulations to approximately 0.94 tonnes/m^3 to achieve static equilibrium. Although this value exceeds the density for pure ice of 0.917 tonnes/m^3, it was felt to be the best compromise. Static equilibrium of the final grounded state is a requirement for reliable dynamic simulation. By comparison, the approximately 3% increase in total mass resulting from the increased ice density has little effect on the computed inertial forces. Furthermore, the actual indentor shape may be independently specified in the simulation model. Thus, the extrapolated keel shape does not significantly influence the dynamic results, provided static equilibrium of the final grounded configuration is achieved.

The horizontal profiles of the keel extension on "Gladys" have been added to the digital magnetic tape of the shape data and were used in the construction of the three dimensional perspectives shown in Figure 38.

The potential energy plot for "Gladys" after it grounded (Figure 95) illustrates the steep potential gradient along the direction followed by the iceberg during the event (roll axis orientation of 10° to 20° relative to X axis on Figure 39). The calculated drop in potential energy for a 10° roll along this steep gradient is approximately 63,000 MJ. As will be shown later, this figure is in good agreement with the kinetic energy at the time of seabed impact. The map also shows that the iceberg is stable for rotations about other axes, a fact consistent with its stable grounded condition. These consistencies between the computed stability map and the observed behaviour of the iceberg lend some confidence to the overall shape determination.

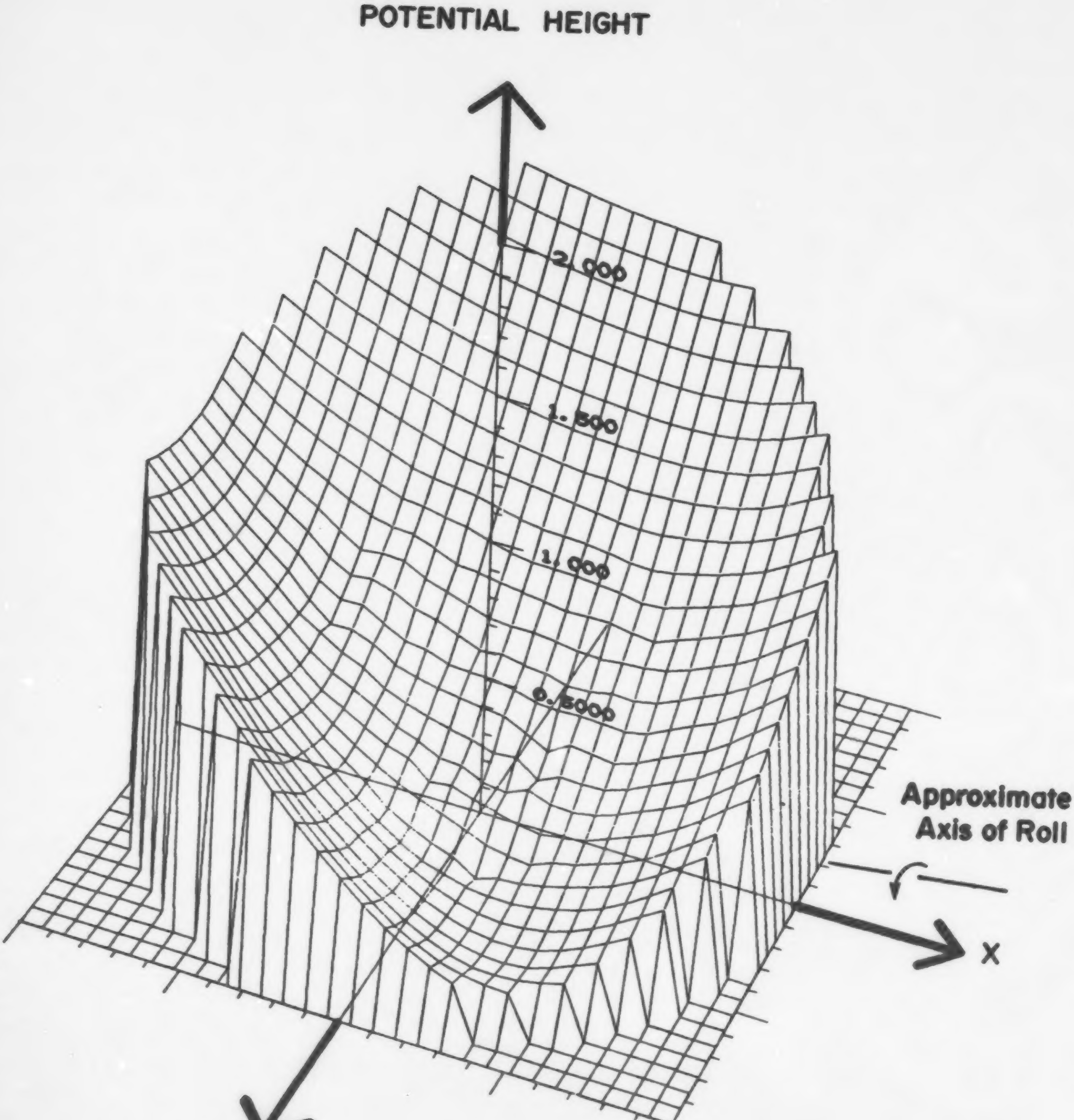

Figure 95. Potential energy plot for the grounded portion of "Gladys".

The observed motion of "Gladys" (see Figures 56-58) may be interpreted as follows. The near instantaneous splitting of the iceberg resulted in a huge unbalanced buoyancy moment acting about the centre of gravity (CG). This moment initiated a fairly rapid roll behaviour about an axis 10°-20° counter-clockwise from the X axis shown on Figure 39. The C-CORE instrument package registered this initial motion primarily as large changes in Y-Acceleration, and Y-Tilt. Some changes in X-Acceleration, X-Tilt and Z-Accleration were also seen.

Careful examination of the data in Figures 56-58 reveals that the roll velocity increases rapidly from time 68 s to time 85.25 s. However, the next data packet, at 89.5 s, reflects abrupt changes in this roll behaviour as evidenced by the jumps in X-Acceleration, X-Tilt and Z-Acceleration, and the reduced rates of increase of Y-Acceleration and Y-Tilt. The behaviour of the iceberg following this time may be interpreted as damped oscillation about its keel. It is thus felt that "Gladys" struck the seabed abruptly during the 4.25 s gap in the data record following the 85.25 s time mark. Although contact with the seabed could have begun before this time, the interaction forces were clearly insufficient to alter the iceberg's behaviour significantly.

Although this roll event was dramatic, the linear accelerations at the sensor package location were in fact quite small. The changes in the accelerometer readings (see Figures 56-58) may be accounted for by the changing components of gravity as a result of roll motion, within the accuracy of the measurement system. This result suggests that the iceberg was in near-vertical and horizontal equilibrium during its initial roll, and permits a significant simplification in the description of the event: prior to seabed contact, "Gladys" essentially rotated about its stationary CG because of a large, unbalanced buoyancy moment. Following impact with the seabed, damped oscillations about the grounded keel were observed. Both motions may be described in terms of a single rotational degree-of-freedom. Because the duration of contact was short relative to the time scales of motion before and after contact, the interaction may be analysed using the impulse theorem (see, for example, Fowles 1970). Results from this simplified analysis may then be compared quantitatively with corresponding results from the full dynamic simulation.

It should be noted that the drift velocity of "Gladys" immediately prior to splitting was quite small, probably less than 0.1 m/s. The reason for the uncertainty lies with the difficulty in determining the iceberg's range and bearing from the ship's radar when alongside the iceberg. The lateral dimensions of "Gladys" were comparable to the changes in its position over the one hour interval between sightings. Thus, the reported positions of the iceberg were significantly affected by the choice of location on the radar screen used to determine range and bearing. For example, by targeting on the nearest face, the iceberg's reported position could change by ± 300 m depending upon which side of "Gladys" the Polar Circle was located at the time of measurement.

The drift kinetic energy of "Gladys" was inconsequential compared with the large rotational energy involved in the split/grounding event. As a result, the drift motion of the iceberg is ignored in the following analyses.

Simplified Analysis. A schematic representation of the "Gladys" split and grounding event is shown in Figure 96. If it is assumed that for the portion of "Gladys" which grounded, the buoyancy force, B, just after splitting is

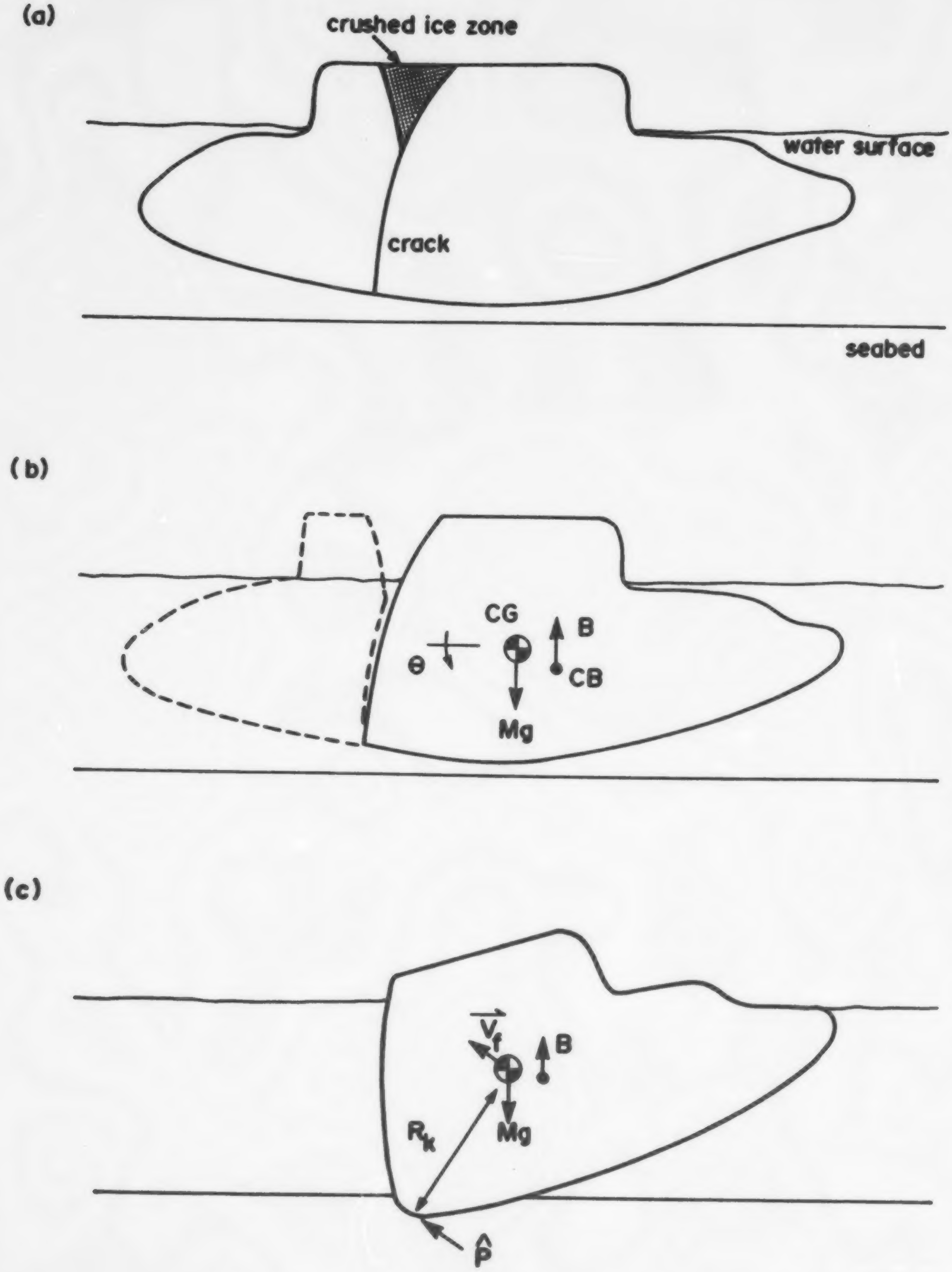
(a)
crushed ice zone
water surface
crack
seabed
(b)
CG
B
θ
CB
Mg
(c)
$\vec{V}_f$
B
R_k
Mg
$\hat{P}$

Figure 96. Schematic representation of "Gladys" split and grounding event (a) splitting in two; (b) key forces just prior to rolling; (c) key forces on contact with seabed.

about equal to the iceberg's weight, Mg, then the iceberg rolls about its CG as indicated. During seabed contact, an impulsive force, $\hat{P}$, is generated at the keel/soil interface which is just sufficient to change the motion to rotation about the keel. The iceberg then oscillates about this point with decreasing amplitude because of soil, wave, and viscous damping. The recorded rotational motions may be used to obtain the impulsive soil force $\hat{P}$ based on the change in momentum of the iceberg during the impact. An energy balance may then be formed to estimate the depth of penetration of the keel into the seabed.

Newton's second law may be written in vector form as:

$$\underline{F} = M\frac{d\underline{v}}{dt} \tag{5}$$

where $\underline{F}$ is the vector sum of the forces acting, and $\underline{V}$ is the velocity of the CG. The integral of this yields the impulse theorem:

$$\hat{P} = \int \underline{F}\, dt = M(\underline{v}_2 - \underline{v}_1) \tag{6}$$

That is, the net impulse may be computed from the change in CG velocity over the impact. Since the buoyancy force is assumed to cancel the iceberg's weight, and the damping, current and wind forces may be shown to be small, the only impulsive force of significance is the seabed force, $\hat{P}_{soil}$. Furthermore, for rotation about the CG, the initial velocity $\underline{V}_1$ is zero, hence:

$$\hat{P}_{soil} = Mv_2 \tag{7}$$

The velocity after the impact, V_2 may be obtained from the measured rotational velocity, since the iceberg was oscillating about its keel. The soil impulsive force thus acts normal to the line connecting the keel and the CG, to set up the rotation about the keel.

The rotational velocity after the impact, ω_2, may be obtained from the observed motions shown in Figures 56 and 57, so that

$$\hat{P}_{soil} = MR_k \omega_2 \tag{8}$$

where R_k is distance from the keel/soil interface to the CG. To simplify the problem further, only rotation along the Y-Tilt direction, the major roll component, will be considered. It may be shown that the kinetic energy associated with the X-Tilt rotational component is negligible by comparison with that associated with Y-Tilt.

In recognition of the high noise levels on the motion data, the value of ω_2 was obtained in two ways: (a) from the slope of the Y-Tilt curve (Figure 57) immediately following the impact; (b) from a calculation of the initial velocity associated with the damped, post-impact oscillations recorded as Y-Tilt. Method (a) yielded 0.69°/s whereas method (b) yielded 0.49°/s. A value of 0.6 ±0.1°/s will thus be used.

The distance from the zone of keel/soil contact to the CG was about 130 ±10 m, based on the measured profile data. The total mass of the grounded portion of "Gladys", assuming an average ice density of 0.90 ± 0.01 tonnes/m^3 and an added mass coefficient of 0.8 ±0.1 (Bass and Sen 1985), is estimated at $(10.5 \pm 1.5) \times 10^9$ Kg.

The impulsive soil force calculated using equation (8) is thus (1.4 ± 0.3) 10^{10} Ns. This may be related to the average soil pressure, P_{soil} by the relationship

$$\hat{P}_{soil} = P_{soil} \; A_{keel} \cdot \Delta t \qquad (9)$$

where A_{keel} is the area of the keel/soil interface and Δt is the duration of the impact. Estimates must be made of these latter parameters. Because the impact lasted no more than 4.25 s, and allowing for some rise time, $\Delta t = 3 \pm 1$ s is felt to be reasonable. The deepest measured profile, obtained at 110 m, had an area of 16,000 m^2. A quarter of this value, or 4,000 ± 2,000 m^2 would correspond to an area of contact equivalent to a 70 ± 20 m diameter circle. These dimensions and confidence limits are also felt to be reasonable.

Using these values for Δt and A_{keel}, an average soil pressure of 1.2 ± 0.8 MPa is obtained from equation (9). This pressure corresponds roughly to the bearing capacity of 210 ± 130 kPa shear strength for cohesive soil. Sub-bottom profiles at the grounding site reveal a veneer (<50 cm thick) of Sioraq Sand lying above the Lower Till. The Till is inferred to be very stiff, possibly greater than 100 kPa, having resisted all sampling attempts with conventional grab samplers, piston, and vibro-corers.

Continuing the simplified analysis of the "Gladys" impact, it is possible to determine the energy dissipated during the interaction period. Assuming that little change in orientation occurs during this brief period, potential energy changes can be ignored. Thus, the energy dissipated becomes the difference in kinetic energies before and after the impact. For initial rotation about the CG, the energy before the impact may be written as:

$$KE_1 = 1/2\ I_{CG}\,\omega_1^2 \qquad (10)$$

where I_{CG} is the mass moment of inertia about CG, and w_1 is the rotational velocity immediately prior to impact.

For final rotation about the keel, the energy after the impact may be written as:

$$KE_2 = 1/2\ I_{keel}\,\omega_2^2 \qquad (11)$$

where I_{keel} is the mass moment of inertia about the keel/soil contact point. For the simplified case of motion in the plane of the Y-Tilt sensor, $\omega_1 = 2.5 \pm 0.3$ °/s, and $\omega_2 = 0.6 \pm 0.1$°/s are obtained from the readings of this sensor before and after the impact (Figure 57), and the moment of inertia may be written as:

$$I_{keel} = I_{CG} + MR_K^2 \qquad (12)$$

Based on the measured shape data, and assuming an average ice density of 0.9 ± 0.01 tonnes/m and an added mass moment of inertia coefficient of 0.8 ±0.1 (Bass and Sen 1985), $I_{CG} = (6.6 \pm 0.9) \times 10^{13}$ Kg m^2 and $I_{keel} = (2.4 \pm 0.4) \times 10^{14}$ Kg m^2 are computed. Thus the energy dissipated during the impact is estimated as

$$\begin{aligned} \Delta KE &= KE_1 - KE_2 \qquad (13)\\ &= (6.3 \pm 1.5) \times 10^{10} - (1.3 \pm 0.5) \times 10^{10} J\\ &= (5.0 \pm 1.6) \times 10^{10} J\\ &= 50{,}000 \pm 16{,}000 \text{ MJ} \end{aligned}$$

To put this figure into perspective, consider that the 1% exceedence drift velocity for icebergs in the Labrador

Sea is about 0.7 m/s (Lever and Sen 1986). Even for this extreme speed, the drift kinetic energy of "Gladys" would be only 2,500 MJ, that is, a factor of 20 less than the energy dissipated during this rotational impact event. By comparison, the drift kinetic energy of "Gladys" prior to splitting (assuming an average drift speed of 0.1 m/s) was only 70 MJ, an inconsequential value in comparison with the rotational energies involved in the split/grounding event. It is also interesting to note that the average rate of dissipation of the 50,000 MJ over the three-second event duration was about 17,000 MW - more than three times the power output of the entire Churchill Falls hydroelectric generating station!

The depth of penetration, ΔZ, of the ice keel into the seabed can be estimated by the relationship

$$\Delta KE = P_{soil} \cdot A_{keel} \cdot \Delta Z \qquad (14)$$

The product $P_{soil} \cdot A_{keel}$ may be found directly from equation (9), yielding

$$\Delta Z = \Delta KE \ . \Delta t / \hat{P}_{soil} \qquad (15)$$

If it is assumed that no ice failure occurred, the maximum depth of penetration is predicted to be 10 ± 5 m via equation (15).

It should be noted that the above analysis ignores the possibility of energy dissipation through ice failure. The average ice/soil interaction pressure of 1.2 ± 0.8 MPa could have been generated as a result of ice or soil failure, or a combination of both. Uniaxial compressive strength tests on glacial ice samples at high strain rates have shown mean strength values of ~7 MPa at -5°C (El-Tahan et al. 1984), and the effect of confinement would be to raise ice strength. However, because ice in the outer layers of the keel is likely to be warmer than -5°C (Diemand 1984), it is possible that some ice failure might have occurred during the 3 s impact. In such a case, the energy dissipated by ice failure would have reduce the depth of penetration.

Failure of warm ice layers during the early stages of the roll of "Gladys" would not affect the foregoing analysis, because the interaction forces were clearly small in comparison with those generated during the 3 s impact. Indeed, the fact that "Gladys" was solidly grounded for several weeks following the impact suggests that significant penetration, and hence significant energy dissipation in soil failure, did take place. It is also interesting to note that the iceberg did not fracture as a consequence of the impact. Such fracture is common for sea ice interacting with a structure at large scale and its absence during the "Gladys" impact suggests this failure mechanism may not occur during an iceberg/structure interaction.

A survey of the "Gladys" grounding site would be extremely helpful in refining this simplified analysis. In particular, knowledge of the pit diameter would lead to a more reliable estimate of the average ice/soil interaction pressure. Also, the measured pit depth could be used to estimate the energy dissipated by ice failure during the impact. However, the other major characteristics involved in this analysis (overall iceberg shape, average ice density, initial and final velocities, duration of impact, added mass coefficient) have smaller ranges of variability. It is thus felt that this simplified analysis gives a reasonably reliable quantitative description of the "Gladys" split and grounding event, to within the accuracy of available data.

Dynamic Simulation. As mentioned earlier, the requirement of final static equilibrium dictated that an average ice density of 0.94 tonnes/m^3 be used in the dynamic simulation of the "Gladys" split and grounding event. Although using this ice density figure leads to a slight distortion of the dynamic behaviour, it was felt to be a better compromise than making large and somewhat arbitrary modifications to the iceberg's profile data.

The remaining conditions used in the simulation are shown in Table 10. Because the drift motion of "Gladys" was of minor importance, it was decided to set the current velocity to zero in order to concentrate on the rotational behaviour of the iceberg.

The simulated motions of "Gladys" are shown in Figures 97-99. The initial configuration of the iceberg was found by rotating the measured grounded iceberg shape until orientation and above-water dimensions corresponded approximately to the pre-split "Gladys" (as documented by surface and aerial photographs).

The iceberg was "released" at t=0, and allowed to respond to the unbalanced buoyancy forces. The model predicts keel/soil contact after about 8 s of roll. Although this is substantially less than the observed 17 s, the likely cause is the imperfect specification of the keel extension. The iceberg has only rolled through approximately 11° by this time. A different keel extension would alter this time of first contact. It is more important to note that prior to contact, the CG has not moved at all in the X or Y directions and has dropped only about 0.8 m in the Z direction. That is, the full dynamic simulation validates the assumption of essentially pure

Table 10

Simulation conditions for "Gladys"

Water depth: 140 m

Current speed: 0 m/s

Current heading: 0°

Centre of pressure: (0,-26,-36) m

Drag coefficient: 1.5

Projected area for current: 150,000 m^2

Added mass coefficient: 0.9

Soil strength: 200 kPa

Scour breadth: 65 m

Horizontal contact area: 4000 m^2

Seabed slope: 0°

Keel slope: 0°

Keel contact point: (0, -70, -149) m

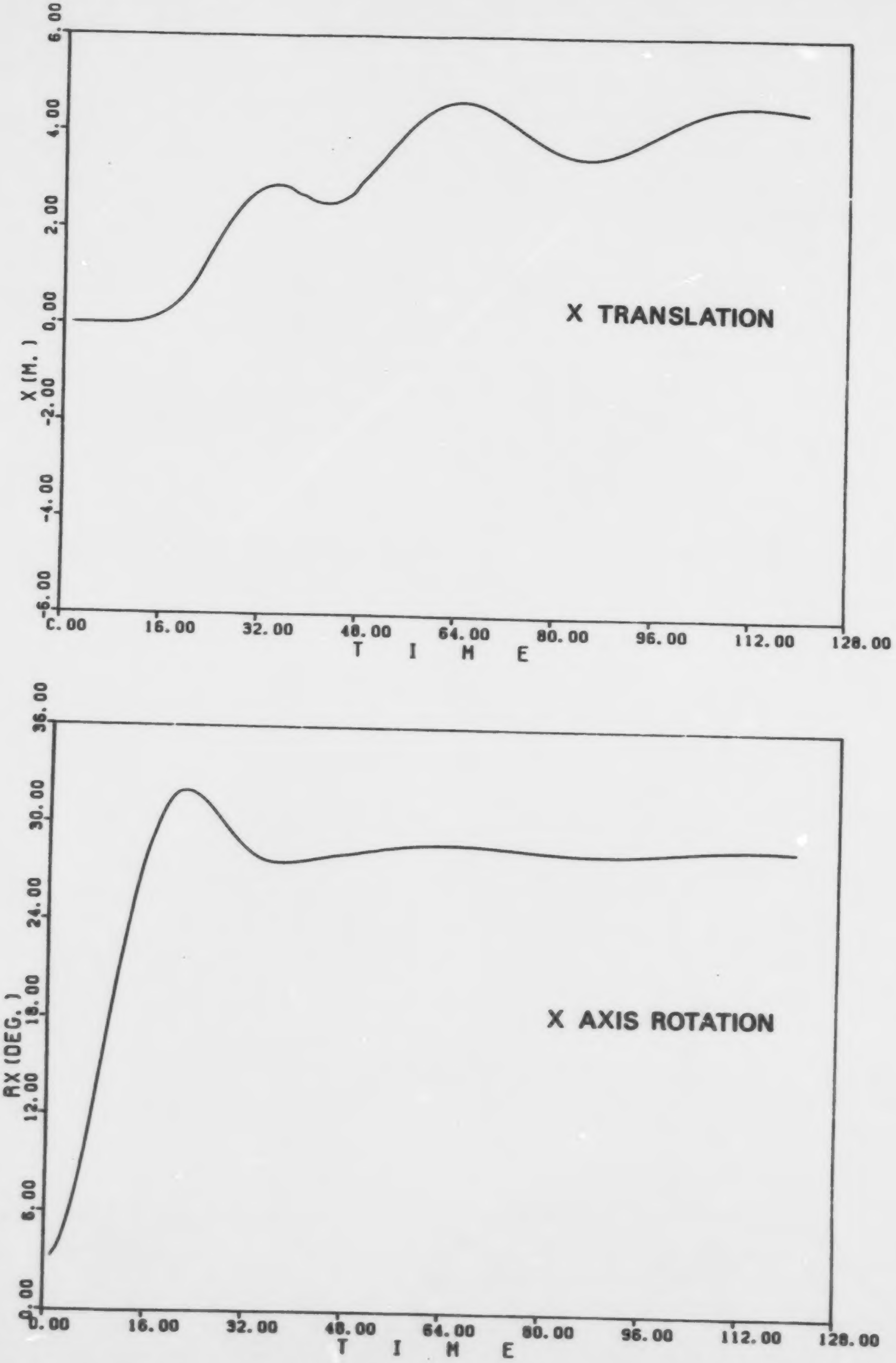

Figure 97. Simulated motions of "Gladys" grounding, X axis translation and rotation.

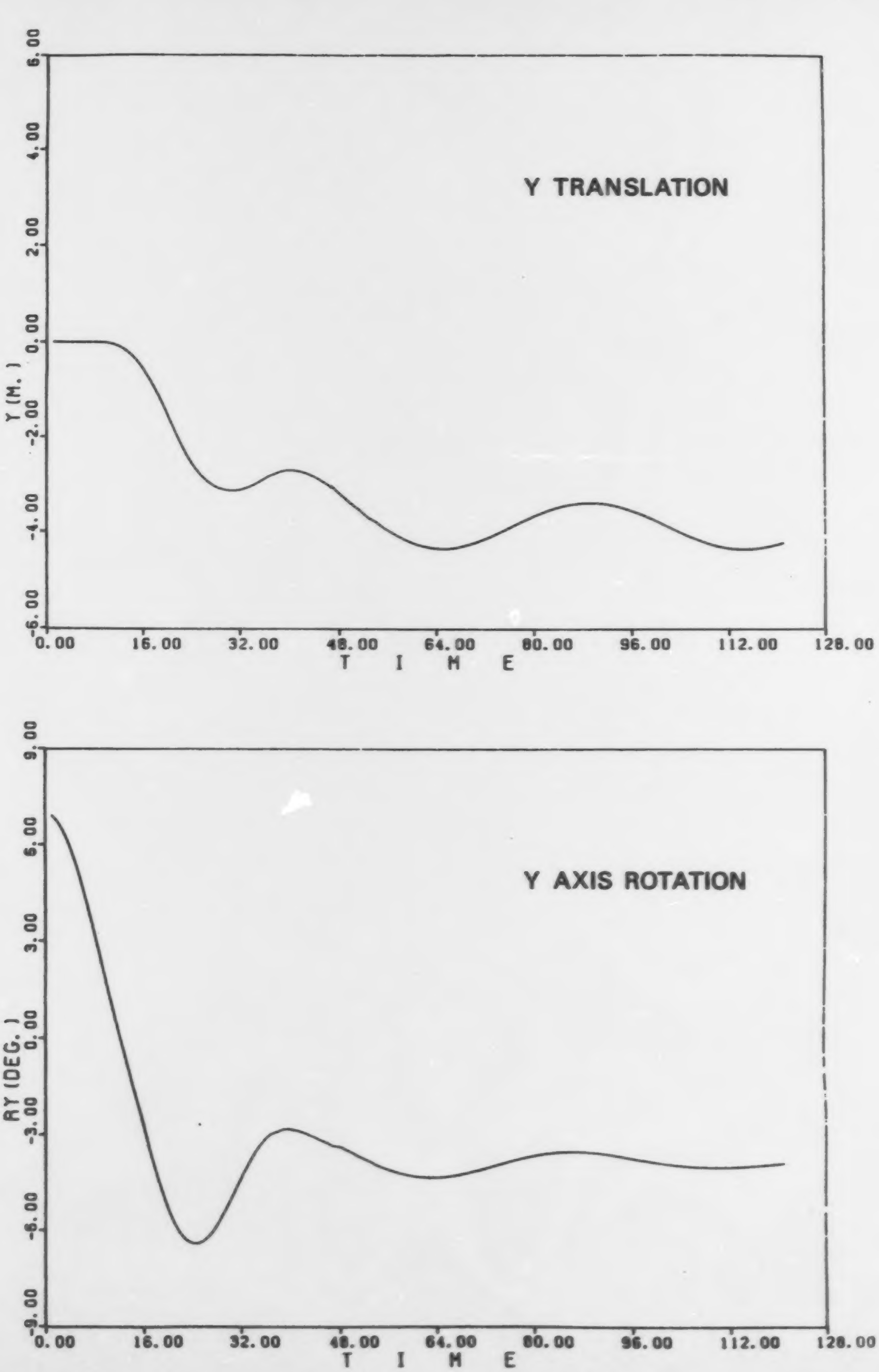

Figure 98. Simulated motions of "Gladys" grounding, Y axis translation and rotation.

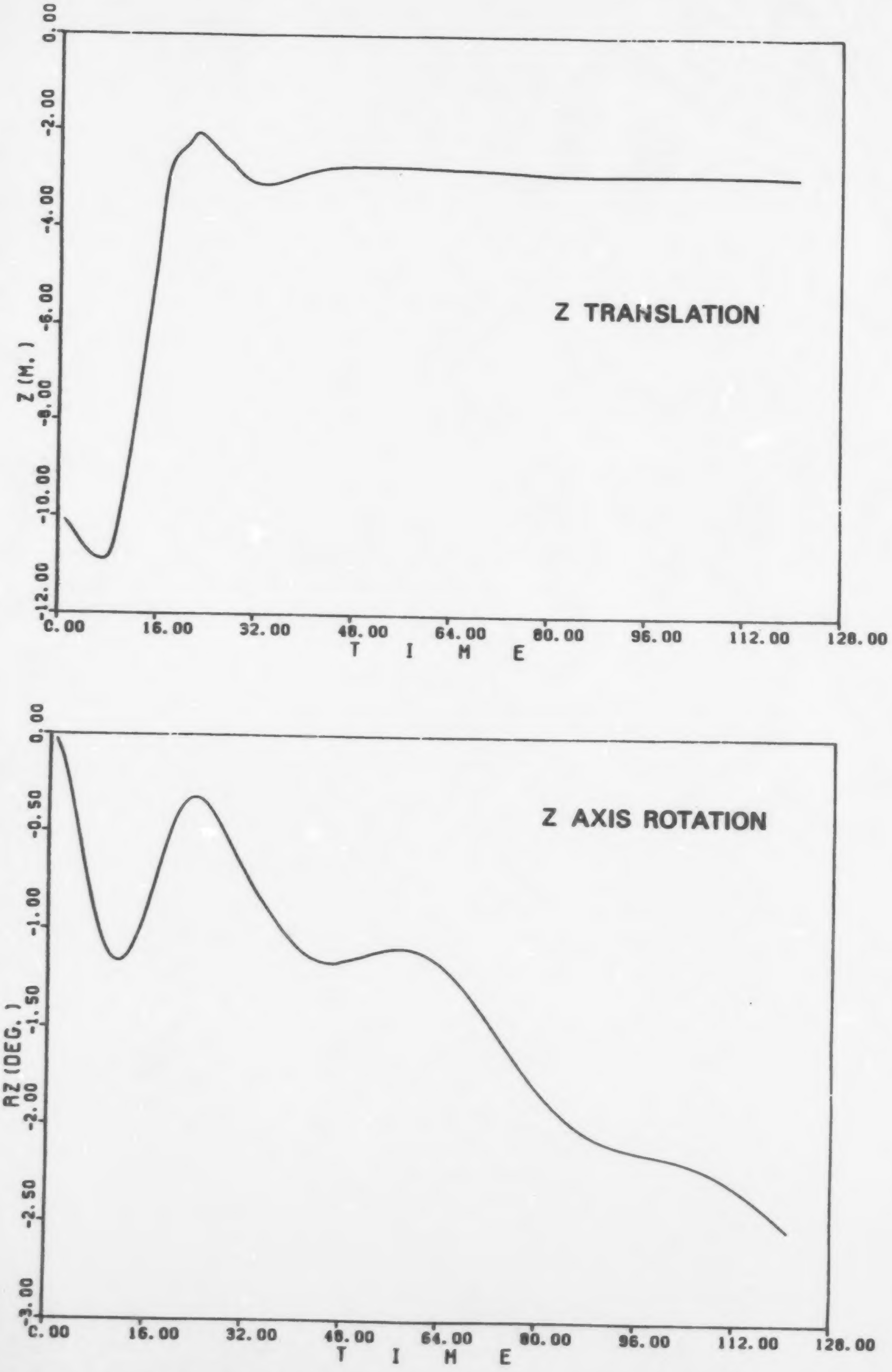

Figure 99. Simulated motions of "Gladys" grounding, Z axis translation and rotation.

rotation about the CG prior to seabed impact, as used in simplified analysis.

The maximum changes in the angles of roll (X axis rotation) and pitch (Y axis rotation) are found to be about 29° and 13° respectively, occurring 20 s to 25 s into the event. These angles and times are in quite good agreement with the observed values. Similarly, the maximum depth of penetration was found to be 12.3 m occurring at about 21 s. These values are in excellent agreement with the simplified analysis presented earlier. Because a maximum roll velocity of 2.2°/s is predicted by the simulation (versus 2.5 ± 0.3°/s observed), and because the area of contact and soil strength were chosen to be in keeping with the simplified analysis, one would expect reasonably good agreement between these analyses based on energy considerations. Note also that the keel ice has been taken to be infinitely stiff for this simulation. The peak vertical pressures of about 1.2 MPa are predicted by the simulation, which are as expected based on bearing capacity failure of 200 kPa for soil. The horizontal forces acting on the keel are an order of magnitude smaller than the vertical forces, because of the combination of lower soil pressures and contact areas.

Following pit creation, the simulated pitch and roll oscillations display similar decaying behaviour to those observed. The periods of the predicted damped oscillations are 41 s for roll and 47 s for pitch. The corresponding observed values are 37 s and 50 s, respectively. However, the assumed rates of decay of these oscillations are somewhat arbitrary, because of incomplete knowledge of soil and fluid damping phenomena.

Overall, it is felt that the dynamic simulation of the "Gladys" split and grounding event yielded quite good results, both quantitatively and qualitatively. Because the event was driven by a large unbalanced buoyancy moment, the simulation results are not sensitive to small changes in most conditions. As with the simplified analysis, refinement of the simulation would be possible with the addition of information on pit diameter and soil strength, the two most important parameters.

"Gladys" Post-Grounding Behaviour

Following the split and grounding event on August 10, "Gladys" remained in contact with the seabed for the duration of the field program. Motion data were collected until 0910 hrs GMT on August 12. "Gladys" modified its orientation continuously during this period (see Figure 55), with sediment laden growlers calved from the keel at 2100 hrs on August 10, and a major adjustment in X-tilt at 0118 hrs on August 11. This latter event (event #2) was felt to be a result of additional soil failure.

It would be desirable, in principle, to analyse event #2 to determine ice/soil interaction forces. However, it has already been noted that the underwater profile data for "Gladys" is statically inconsistent. Because analysis of event #2 would involve the change in static buoyancy forces resulting from the observed orientation change, such an analysis would be quite unreliable for an iceberg that is statically inconsistent. Adjustment of the average ice density was justifiable for the split and grounding event because of the predominance of dynamic forces. That approach is felt to be inappropriate here, where the static load alone is believed to have caused soil failure. Instead, a qualitative discussion of the observed post-grounding behaviour of "Gladys" is presented.

The "Gladys" split and grounding event represented a large roll in the direction of Y-Tilt. In the resulting grounded position, further rotation in the same direction was resisted by a large seabed force. It is not surprising that the remaining observed grounded behaviour of "Gladys" shows a fairly continuous increase in Y-Tilt as the soil and iceberg slowly accommodate to this large static ice/keel interaction force (see Figure 55).

The situation is not as simple for rotation in the direction of X-Tilt. The split and grounding event resulted in a sharp decrease in X-Tilt. Additional roll in this same direction was apparently resisted by the soil, because a slow additional decrease in X-Tilt is seen on Figure 55 prior to the calving of the dirty growlers. The slow rate of change and the subsequent calving of keel ice suggests that accommodation of this force was primarily by the iceberg.

Event #2 at 0118 hrs on August 11, shows an abrupt increase in X-Tilt; that is, a rotation in the opposite direction to previous behaviour. No growlers were reported at this time, so that soil failure was likely responsible for the change. It seems probable that the previous ice accommodation overcompensated, and resulted in a stress build up on the opposite side of the keel. This stress build up was then relieved by the soil failure of event #2.

From this point on, orientation changes in the grounded "Gladys" occurred more slowly. Nevertheless, accommodation to the ice/soil interaction stresses continued to alternate directions on X-Tilt. As mentioned, Y-Tilt showed essentially steady increase throughout this same period. The potential energy map (see Figure 95) confirms that the iceberg was strongly unstable along the direction of Y-Tilt, yet stable along X-Tilt. This condition is in agreement with the observed post-grounding behaviour of continuous increase in Y-Tilt, yet alternating changes in X-Tilt.

Finally, it should be noted that the tidal changes were relatively small (0.5-0.6m) during this period, and show no correlation with the observed orientation changes. The numerous above-water calvings also do not appear to have triggered these changes. It is thus felt that adjustments in the orientation of the grounded "Gladys" resulted from accommodation of soil and ice to the high interaction stresses generated as a consequence of the initial split and grounding event.

"Julianna" Post-Grounding Behaviour

"Julianna" was aground in just over 170 m of water throughout the observation period of August 16-21. Because no dynamic seabed interaction events were observed during this period, a static calculation is presented to determine the average vertical load on the seabed.

The measured shape data give above-water and below-water volume estimates as 1,403,000 ± 28,000 m^3 and 7,300,000 ± 1,100,000 m^3, respectively. A balance of forces in the vertical direction yields the expression for the upward seabed force, F_s, as:

$$F_s = g\left[V_a \cdot \rho_i - V_b - (\rho_w - \rho_i)\right] \qquad (16)$$

where g is the gravitational acceleration, 9.81 m/s^2.

Assuming an average ice density of 0.90 ± 0.01 $tonnes/m^3$, the upward seabed force is found to be (3.4 ±

1.6) x 10^9 N. Using an area of contact of 20,000 ± 3,000 m^2 based on the 170 m depth profile, the average ice/soil contact pressure is found to be 170 ± 80 kPa. Such a pressure suggests that the shear strength of the soil supporting "Julianna" was at least 32 ± 15 kPa.

The calculated potential energy plot for "Julianna" is shown in Figure 100. It can be seen that the buoyancy forces exert a considerable moment which must be resisted by the upward soil force. The magnitude of this moment requires that the soil force act through a centre of pressure which is approximately 100 ± 80 m from the CG. This estimated range for the centre of pressure overlaps with the contact area obtained from the underwater profile data. Overall, the shape data for "Julianna" are consistent with the fact that the iceberg was grounded when these data were acquired.

ICEBERG DETERIORATION AND ITS INFLUENCE ON SEABED INTERACTION

It has long been appreciated that calving and/or continuous ablation of ice can lead to the unstable roll of icebergs. Bass and Peters (1984) showed that icebergs can increase their draft during a rolling event. Hence, continuous ablation and/or calving can lead to seabed pitting via unstable roll. This seabed interaction mode has been the subject of recent investigations (Bass et al. 1986; Bass and Woodworth-Lynas 1988). The movement of "Bertha" away from its grounded position was initiated by a minor calving event and the resulting crater chain was developed by the mechanism of weakly unstable roll.

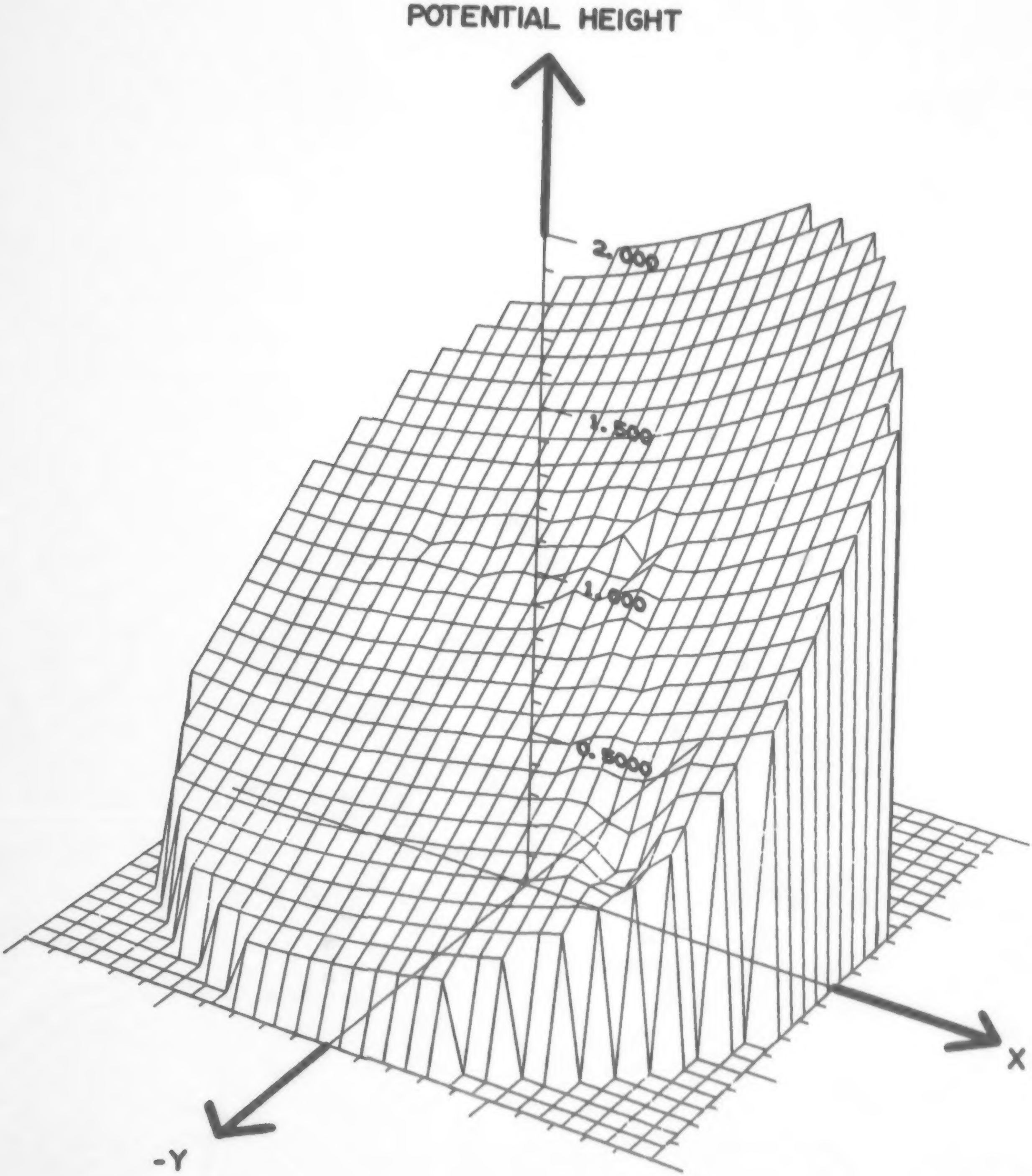

Figure 100. Potential energy plot for "Julianna".

The loss of maior portions of a parent tabular iceberg, such as the ram loss and later splitting observed for "Frieda" and the splitting of "Gladys", represent another deterioration mechanism that may result in iceberg/seabed interaction. the splitting mechanism is believed to be an important component in the transition of large tabular icebergs to tilted tabular and other more deteriorated shapes (Diemand and Lever 1986b). Iceberg deterioration proceSses and their possible consequences, as inferred from the DIGS experiment observations are summarized schematically in Figure 101.

Wave-driven erosion at the water-line is the predominant deterioration mechanism for icebergs in open water (White et al. 1980). From late summer through early fall along the Labrador Shelf, the combination of relatively high water-particle velocities (1-3 m/s) and high surface-water temperatures (5-9°C) results in rapid waterline ablation. When ablation has developed a sufficient incision, the overhanging cliffs of ice calve, leaving near vertical faces which are subject to further wave-driven erosion. The ablation of ice below-water, however, proceeds at a much slower pace, because of the lower water velocities and considerably colder subsurface water (-1.5°C). Through this preferential surface erosion and calving process in comparison with underwater ablation, large tabular icebergs retain nearly vertical faces, yet develop underwater rams which often extend outward to some appreciable fraction of the above-water dimensions of the iceberg.

The slow pace of underwater ice ablation also allows the outer shell of the iceberg keel to warm, leading to a significant reduction in strength (Diemand 1984). This effect likely contributes to failure of the keel ice and

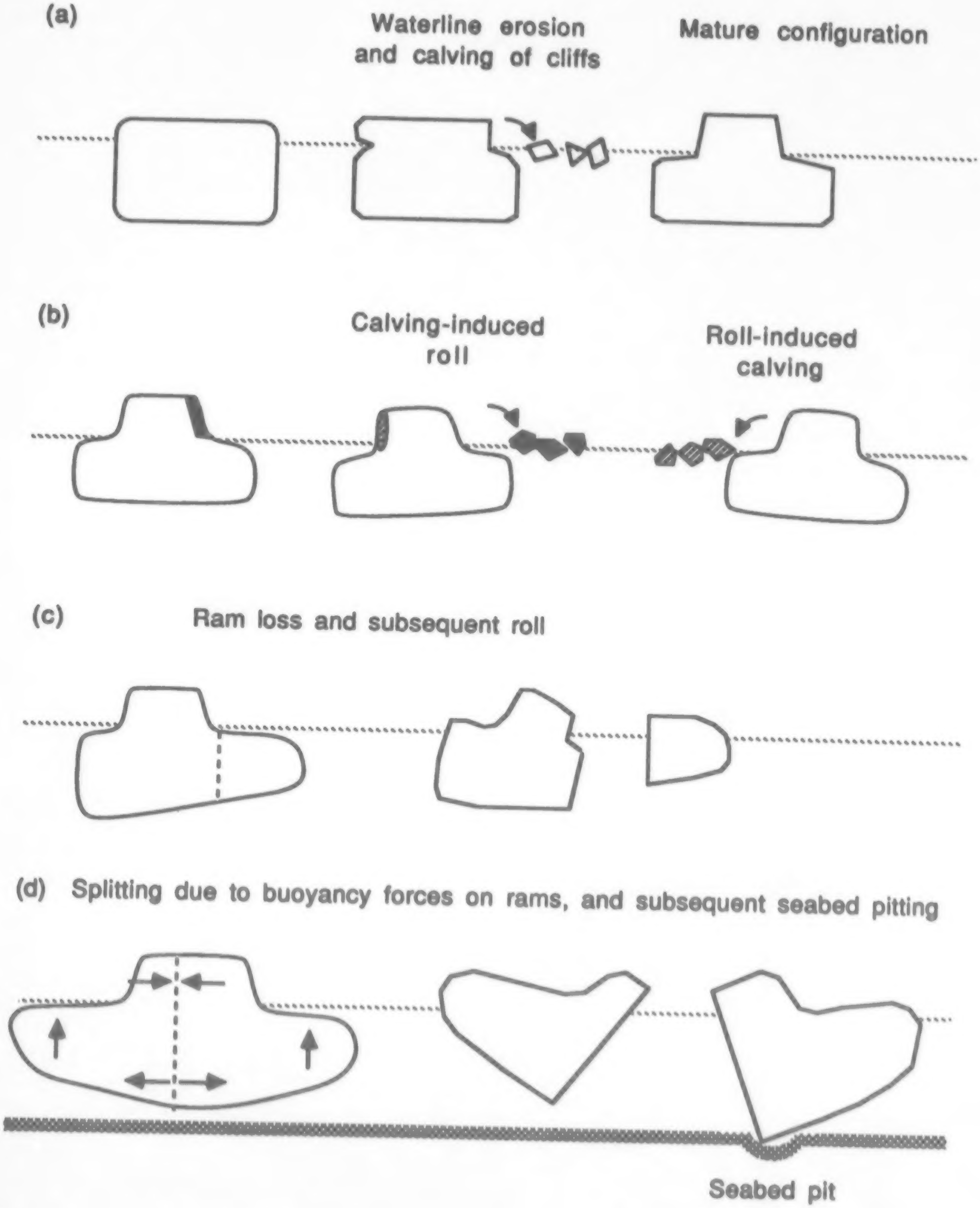
(a)
Waterline erosion and calving of cliffs
Mature configuration
(b)
Calving-induced roll
Roll-induced calving
(c)
Ram loss and subsequent roll
(d) Splitting due to buoyancy forces on rams, and subsequent seabed pitting
Seabed pit

Figure 101. Iceberg deterioration processes and their possible consequences.

exposure of cold hard ice during periods of iceberg/seabed interaction, as discussed later.

The upward buoyancy forces exerted by the submerged rams are displaced laterally from the downward gravitational force on the above-water mass. This results in significant bending and shear stresses on such icebergs. Diemand et al. (1987) have shown that the tensile stresses generated in an idealized tabular iceberg resulting from the existence of large rams can exceed the stress needed to initiate tertiary creep or failure of the ice. It is thus probable that the development of large underwater rams eventually leads to large-scale splitting for the majority of tabular icebergs.

Such splitting immediately produces a large imbalance in buoyancy forces and thus results in the kind of rapid rolling behaviour exhibited by "Gladys". If the iceberg keel contacts the seabed during such a split and roll, the forces generated are likely to be enormous because of the large masses and high rates of rotation involved. By comparison, continuous deterioration leads to smaller imbalances in buoyancy forces, and hence to less energetic behaviour.

The calve and roll, and split and roll phenomena are likely to be common occurrences rather than rare events, because they arise as a result of normal iceberg deterioration processes. These roll phenomena are likely to lead to seabed disruption in areas of suitable water depth on the Labrador Shelf and Grand Banks of Newfoundland, where iceberg deterioration processes are seasonally rapid. Because large tabular icebergs are more prevalent along the Labrador coast than on the Grand Banks, the highly energetic split and roll mechanism probably disrupts the seabed more frequently in the former region.

ICEBERG SCOUR PROCESSES

Iceberg Dynamics

In this qualitative discussion of the dynamic behaviour of icebergs during seabed interaction, distinction is made between linear and point seabed disturbances. Each is further subdivided according to the dynamic characteristics of the icebergs involved.

Linear Features. Horizontal translation of an iceberg can lead to a linear scour if the iceberg's static draft exceeds the local bathymetry and the driving forces or initial momentum are sufficiently high to keep the iceberg moving. As the iceberg scours into shallower water, stability considerations dictate that the soil force acting on the keel will cause the iceberg to roll to some new equilibrium orientation. Some overall uplift of the iceberg will also occur. The final configuration of the iceberg will be one that minimizes the potential energy increase because of these changes. Because rotation of the keel can accommodate the necessary change in bathymetry, the iceberg seeks out its weakest axis of roll. That is, the iceberg yaws about its vertical axis until the scour force acts normal to the axis of minimum potential energy change because of roll. These rotations also have the effect of minimizing the ice/soil interaction force. The magnitude of this force and the resulting scour morphology thus depend, in part, on the strength of the iceberg's weakest roll axis.

If this axis is very weak (i.e., small potential energy change for large roll angles), the keel can easily rotate with little increase in soil force. The iceberg can scour up and down slope with essentially no change in keel force and hence little change in scour morphology. Scour length is a maximum for such a case. Iceberg yaw and pitch adjustment resulting from seabed contact forces has been suggested by Woodworth-Lynas et al. (1985) to explain up- and down-slope scour behaviour.

"Bertha" was an example of an iceberg possessing a low, flat potential energy plateau for roll about a range of axes. In fact, "Bertha" was seen to roll about an axis in this range, during and after its seabed interaction event. This weak axis roll behaviour is in agreement with the observation that scours do not preferentially increase in incision depth and width as they proceed upslope (Woodworth-Lynas et al. 1986). Such would not be the case if uplift of the entire iceberg occurred, because the soil force would necessarily increase, and hence the scour would tend to deepen and widen as the iceberg moved upslope. It should also be noted that pack ice forces acting in the direction of scour both assist in the roll of the iceberg and help overcome soil resistance, leading to longer scours and easier up-slope compliance.

If the iceberg's weakest axis is stiff (large potential energy change for small roll angles), the keel does not easily rotate in response to scour forces. In weak soils, the iceberg ploughs horizontally, leading to a progressive deepening and broadening of the scour and a corresponding build-up in forces (e.g., Chari 1979). In very stiff soils, the iceberg increases its potential energy by riding up the seabed slope, rather than by rotation. In either case, the ice/soil interaction forces increase more rapidly with scour length, leading to generally shorter scours, than if the iceberg possessed a very weak axis for roll. "Julianna" was an example of an iceberg displaying a large increase of potential energy with roll. Sidescan records of the seabed in the vicinity of the grounding site showed no evidence of a lead-in scour, suggesting that "Julianna" did indeed stop abruptly on contact with the seabed.

Point Features. Discrete point features, or pits, may result from rotational or vertical translational contact of an iceberg with the seabed. An increase in the instantaneous draft of an iceberg during roll behaviour may result in the creation of a pit by rotational motion. Similarly, tide changes or heave resonance may lead to point seabed contact by vertical translational motion. These mechanisms are discussed below.

As mentioned earlier, continuous iceberg ablation leads to the development of weak rotational instability. The low rotation energies associated with the roll of such icebergs may lead to the formation of small, shallow pits on contact with the seabed. Because these icebergs are only weakly unstable, large rebound of the keel is possible, potentially leading to the development of a crater chain (e.g., Bass and Woodworth-Lynas 1986). The long roll periods involved suggest that pits in the chain will be well spaced out. "Bertha" was an example of an iceberg which produced a crater chain as a result of just this type of weak roll instability.

On the other hand, when a large tabular iceberg splits, a strong rotational instability develops immediately. The resulting roll motion is highly energetic, and large ice/soil interaction forces are generated on seabed contact. Pits created through such a mechanism are probably quite deep, and some degree of ice failure at the keel is likely. "Gladys" clearly demonstrated the highly energetic nature of this split and grounding mechanism.

Vertical translational contact resulting from tide changes may lead to pit creation by static forces. As in the case of upslope scouring, the keel/soil interaction forces during such a contact are substantially reduced if the iceberg is free to roll about some axis, reducing its potential energy. If no roll is possible, then the downward load on the seabed slightly exceeds the weight of ice exposed during the tide change. However, the penetration depth would not exceed the magnitude of the tide change.

Heave resonance [illegible] ocean swell may also lead to seabed pitting. Although resonance periods and amplitudes depend on iceberg underwater shape, translational kinetic energies comparable with those resulting from weakly unstable roll are quite possible. Thus, shallow pits or crater chains might also result from heave resonance.

Ice Keel Adjustments

Results of the DIGS experiment show clearly that during the scouring process, the keel ice both modifies the seabed sediment and is in turn modified, deforming in both brittle and ductile modes. Specific processes of keel ice deformation described here have either been observed from thin-section analysis or are inferred from visual observations of the scoured seabed.

Pressure Effects - Crystallographic Changes. About 7.25 hours after "Gladys" grounded on August 10, an underwater calving event released several sediment-laden growlers that apparently originated from the iceberg's keel. Samples of ice were collected and kept frozen for subsequent analysis. In St. John's the ice was thin-sectioned and analysed. Results show that zones of fine-grained euhedral polygonal crystals are in sharp contact with zones of large-grained crystals which contain pervasive linear trains of elliptical air bubbles, characteristic of glacial ice. Porphyroclasts of glacial ice, containing air bubbles, may be seen in the groundmass of the fine-grained zones (Figure 102).

It is probable that the fine-grained euhedral crystals were generated by dynamic recrystallization of the larger-grained glacial ice crystals as a result of stress during the 7.25 hours after the grounding event. The porphyroclasts represent non-recrystallized relict glacial ice crystals.

Ice Failure and Sediment Injection. During the grounding and scouring process brittle fracturing of the keel occurs as seen from thin section analysis. Fracturing and removal of ice from the keel is also evident from the discovery of ice embedded in one of the pits at the "Bertha" grounding site, and also from the presence of ice meltout pits within the striated troughs of fresh scours (see Chapter 4). An overturned iceberg, photographed closer to shore during the WIIM study, exposed its former keel which had evidently interacted with the seabed (Figure 103). Fracturing of the ice is clearly evident in this view as is the presence of large amounts of fine sediment within the fracture planes. Coarse material (including boulders) is incorporated in the keel surface having been picked up from the seafloor during ice/seabed interaction.

The extent and geometry of keel fracturing is at present still unknown. However, where these fractures develop in ice which is in physical contact with the seabed, sediment is emplaced along the fracture planes. Fractures seen in thin section are zones of little or no displacement and are less than 0.5 mm wide. They are developed only in

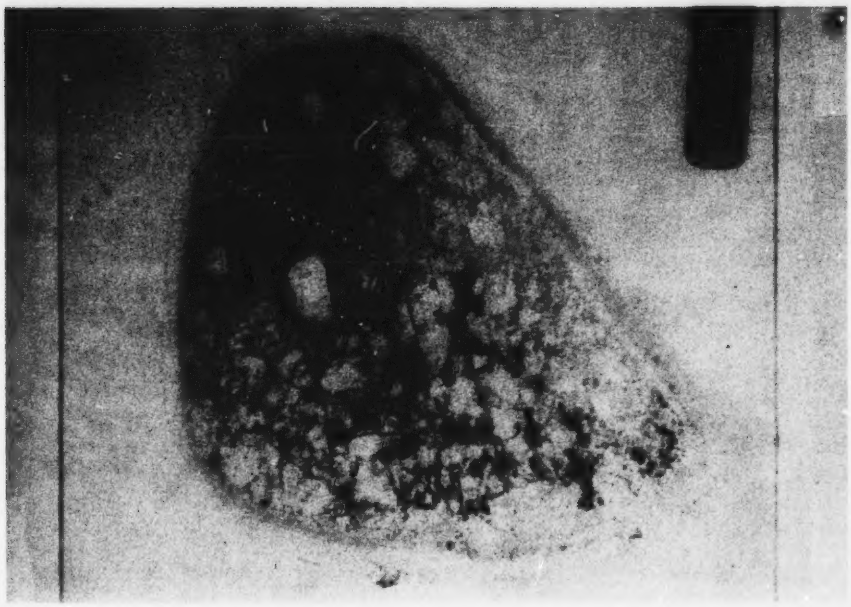

Figure 102. Thin section of ice from sediment-laden growler which calved from the grounded keel of iceberg "Gladys". Note pervasive fracture planes running across the section. Fine-grained sediment is confined to fracture planes and the recrystallized, fine-grained ice groundmass. Large porphyroclasts of relatively undeformed glacial ice are clearly evident and contain no sediment. (Photo approximately at scale).

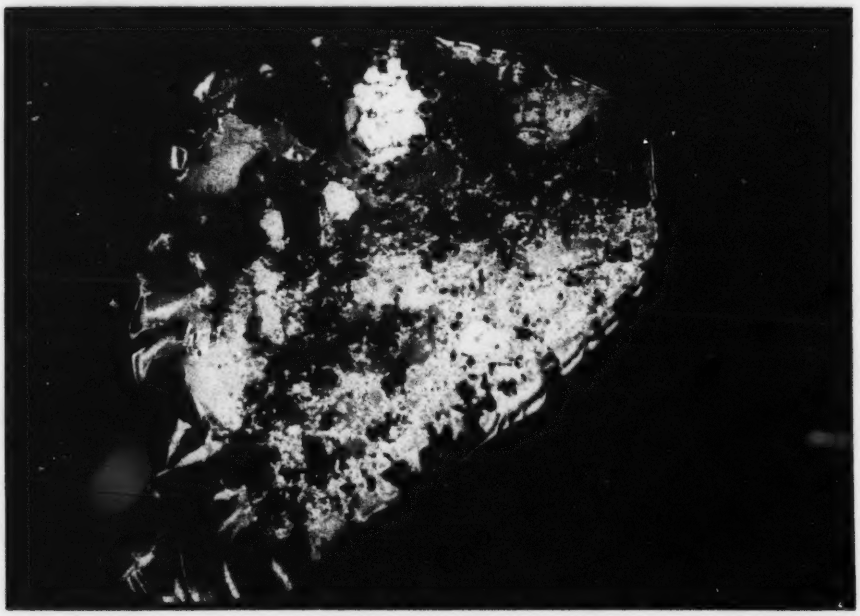

Figure 102. The same view as in (a) but with polarized light clearly show development of the recrystallized groundmass of fine-grained euhedral, polygonal grains. (Photo approx. at scale).

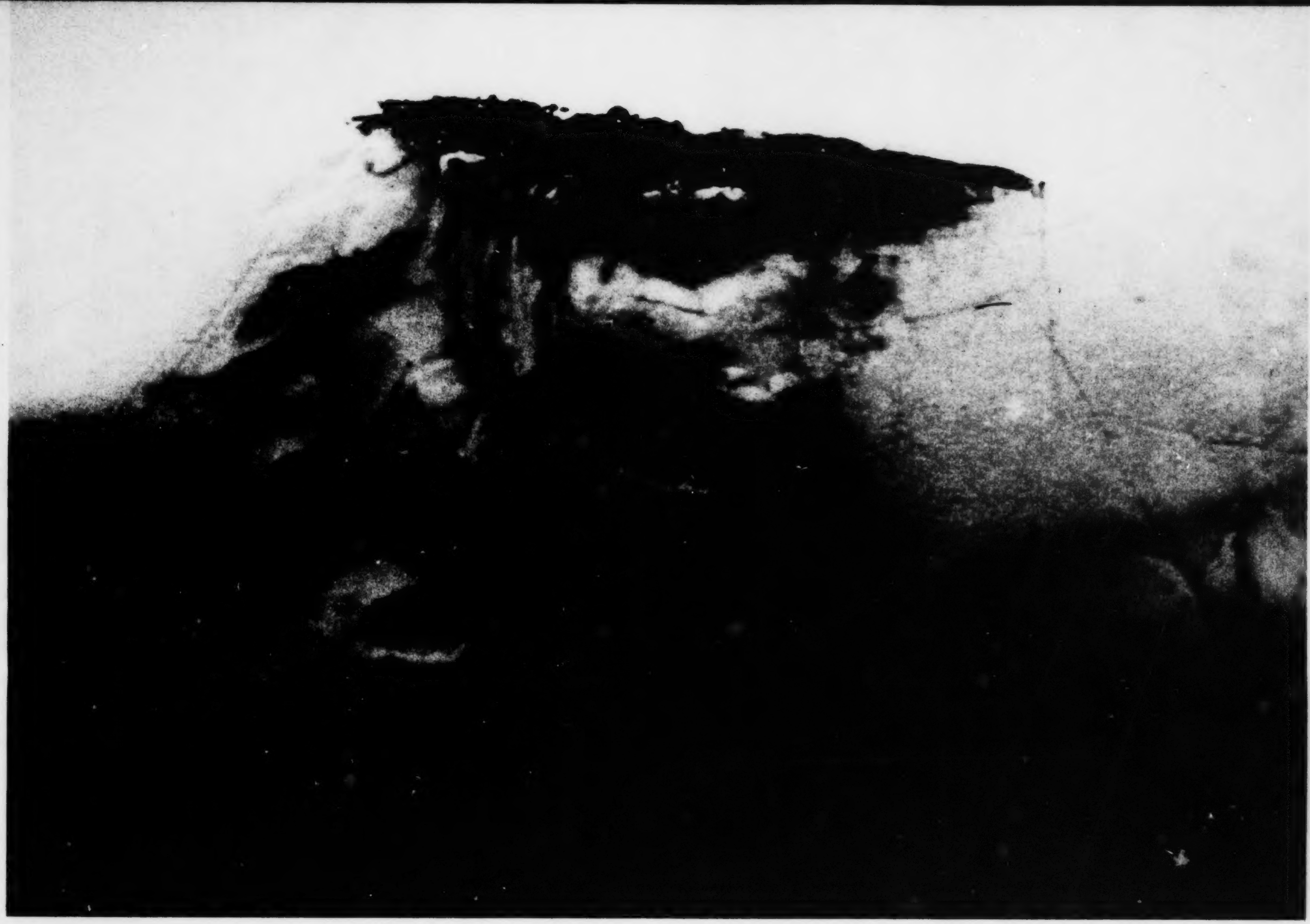

Figure 103. The former keel of a grounded iceberg is seen in this photograph. The ice has been fractured during the grounding event and vertical sediment-filled fracture planes are clearly evident beneath the flat surface. Coarse debris embedded and frozen into the keel was probably picked up from the seabed.

the original, unrecrystallized glacier ice and not in the recrystallized ground mass. It is not known whether sediment was intruded into the crack system because of the vertical pressure of the iceberg on the seabed or as a result of the generation of negative pressures in the cracks during their formation.

Keel Flattening. Keel flattening is implied based on observations of an overturned iceberg (Figure 103) and of three new linear scours during the field program. The linear scours, although characterized by small-scale ridge-and-groove topography, are essentially flat-bottomed. These scours include the asymmetric scour on the western edge of Makkovik Bank, the new scour at the "Caroline" site on Saglek Bank, and "Big Makk" (see Chapter 4). Two possible explanations for the existence of such flat-bottomed scours are either that the keel, which was originally an irregular shape, was planed flat as a consequence of contact with the seabed, or that the contact area of the keel was coincidentally flat before touchdown. The asymmetric scour observed on western Makkovik Bank was not only flat-bottomed, but also conformed to the regional seabed slope, which strongly suggests that keel flattening results from seabed interaction. Furthermore, given the wide variation in iceberg morphology, the fact that all three new scours were flat-bottomed is more easily explained by keel planation than by the coincidence of three flat keels. However, the mechanism of keel flattening is not understood, and characteristics of the process, such as its rapidity and the amount of ice removed, cannot be ascertained from the present observations.

Keel Armouring. Observations of a flat keel on an overturned iceberg (see Figure 103) showed quantities of boulders, cobbles, and finer-grained material embedded in the ice. Further evidence of scouring by "armoured" keels is the frequent association of boulders within ice melt-out pits as described in the next section.

The most likely processes of armouring during iceberg scour are mechanical embedding, and subsequent freezing into the ice, of overridden seabed material, and exposure of englacial material from within the iceberg. Mechanical embedding would involve incorporation into the ice of seabed material, such as cobbles and boulders, via the generation of high local pressures caused by passage of the keel. Based on measured temperature profiles of icebergs (Diemand 1984), planation of as little as 2 m of the keel may expose ice as cold as -13°C; such depressed temperatures would probably be capable of freezing saline seabed sediment onto the keel surface. Englacial material from within the iceberg could be exposed at the keel surface because of planation or other ice failure mechanisms. Keel armouring by any of the above processes would help protect the keel ice from further failure.

Seabed Modifications

Visual observations of "fresh" iceberg scours, made possible through use of the submersible Pisces IV, confirmed the presence of most features previously known to occur in scours based on analysis of sidescan sonograms, such as incised troughs and elevated berms. Transverse ridges between scour berms as reported by Lien (1981) were not observed. Visual observations also provided information on hitherto unknown features such as fractured, blocky berm material, trough-parallel striations; ice meltout pits commonly associated with boulders; possible sand volcanoes; and small-scale, flat-topped mounds. Perhaps the most striking observation was that all of the fresh scours observed from Pisces have flat-bottomed scour troughs which, over a few metres laterally, pass into often spectacular blocky berms which may rise up to 6 m above the seabed (see Chapter 4). Observations of these features leads directly to the inference of processes that occur during scouring that were previously unknown. The most important processes are failure of the iceberg keel, sub-scour liquefaction, and combined bulldozing and extrusion of sediment in front of, and from beneath the keel.

Displacement, Compaction, Liquefaction, and Extrusion.

Consolidated silts and clays characterize the scour berms observed from Pisces. Their existence is clear evidence that sediment has been displaced by extrusion and bulldozing by the scouring keel. Gravity forces of the iceberg on the seabed probably result in bearing capacity failures and the lateral displacement of soil away from the keel. The bulldozing effect by forward movement of the iceberg generates a surcharge of sediment in front of the keel which is displaced to either side as the keel moves forward.

Compaction and remoulding of sediment occurs in a zone adjacent to the keel. Sediments in the scour trough and in the berm are interpreted to be overconsolidated whereas the surrounding seabed appears to be normally consolidated. Spalled blocks of disrupted berm material are ramified by a network of fine cracks which do not appear to be dislocation planes. Exposed crack surfaces display vertical columnar or radial fracture patterns, features characteristic of brittle fracture (Figure 104a and 104b).

Occasional conical mounds of loose, fine-grained sediment are developed above the compacted sediment surface within the trough of "Big Makk" (see Chapter 4). These

Figure 104a. Massive blocks (1-2 m high) from the berm of the new scour at the "Caroline" site display crude vertical fracture patterns.

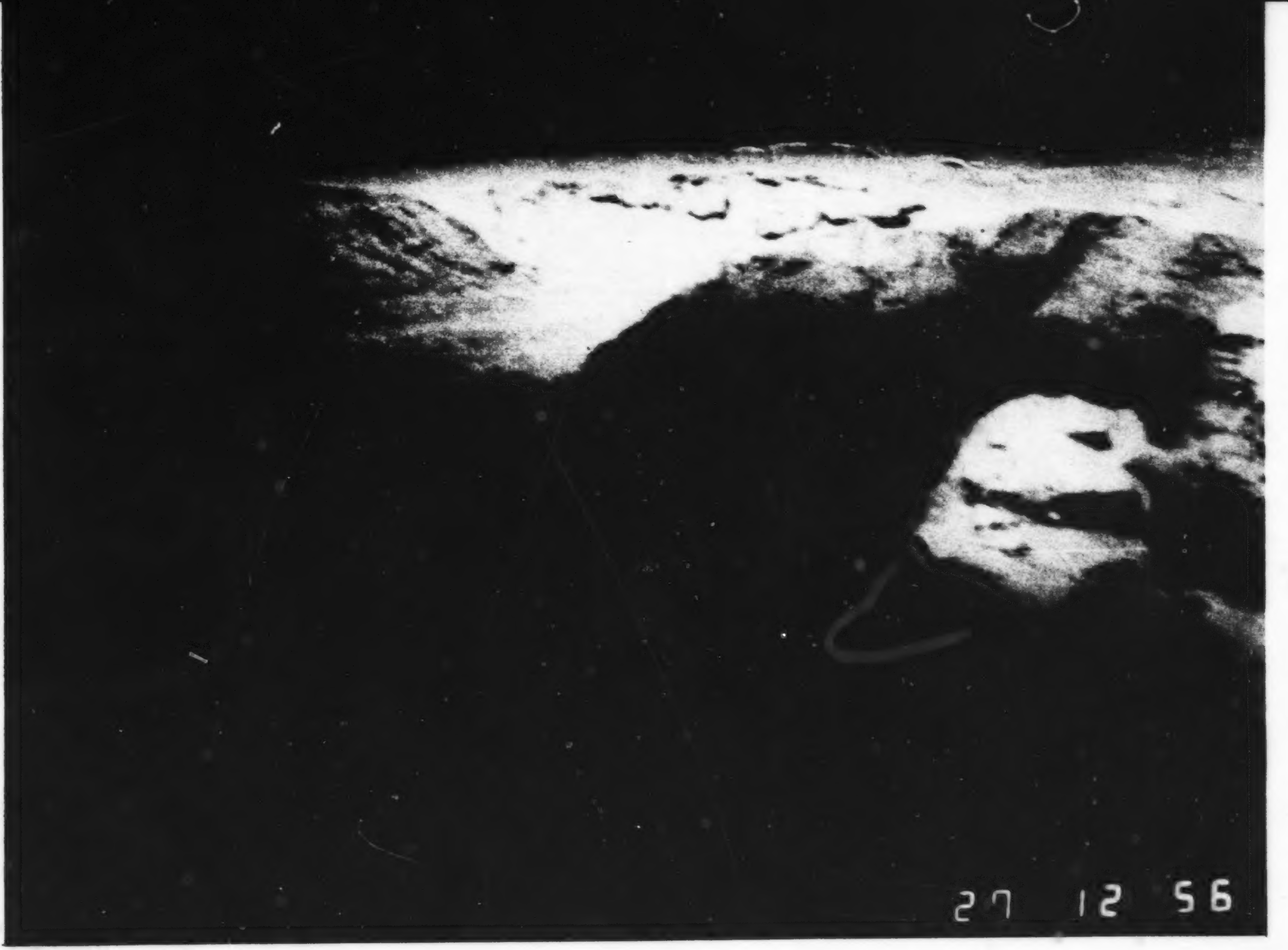

Figure 104b. Vertical face of a block (1 m across) showing a radial fracture pattern, also from the new scour at the "Caroline" site.

mounds may be sand volcanoes generated by the extrusion of sediment liquefied at depth. If they are the result of sediment extrusion then clearly they must have developed following passage of the scouring keel but during the time when the effect of keel pressure on the seabed was causing liquefaction at some depth below the surface.

Meltout Pits. Ice meltout pits, up to 1 m deep, were observed within "Big Makk", and the new scour at the "Caroline" site (see Chapter 4). Also, a boulder rimmed by ice was found in one of the pits created by "Bertha". Such pits arise by the failure of a segment of a scouring keel and its subsequent overriding by the remainder of the keel. The embedded ice later melts leaving a void in the scour trough interrupting the ridge-and-groove microtopography. Boulders, commonly found in meltout pits, are further evidence for the existence of keel armouring. The occurrence of ridge and groove microtopography in all the new scour features can be most easily explained by the existence of such "armoured" keels as explained later.

Formation of Ridge-and-Groove Microtopography. Ridge-and-groove microtopography was observed from the submersible in all three fresh linear scours and in the "Bertha" pits (see Chapter 4) (Fig. 105 (a-b)). It was also recorded on sidescan sonograms of "Big Makk" (see Fig. 68), the "Bertha" pits (see Fig. 65) and the new scour at the "Caroline" site (see Fig. 74).

Ridges and grooves may have amplitudes of only a few millimetres or as great as 20 to 30 cm. Generally speaking the millimetre-scale features are not as continuous as the larger, centimetre scale features, commonly dying out over a distance of a few metres. Larger ridges and grooves may be traced over distances of at least 500 m as seen from

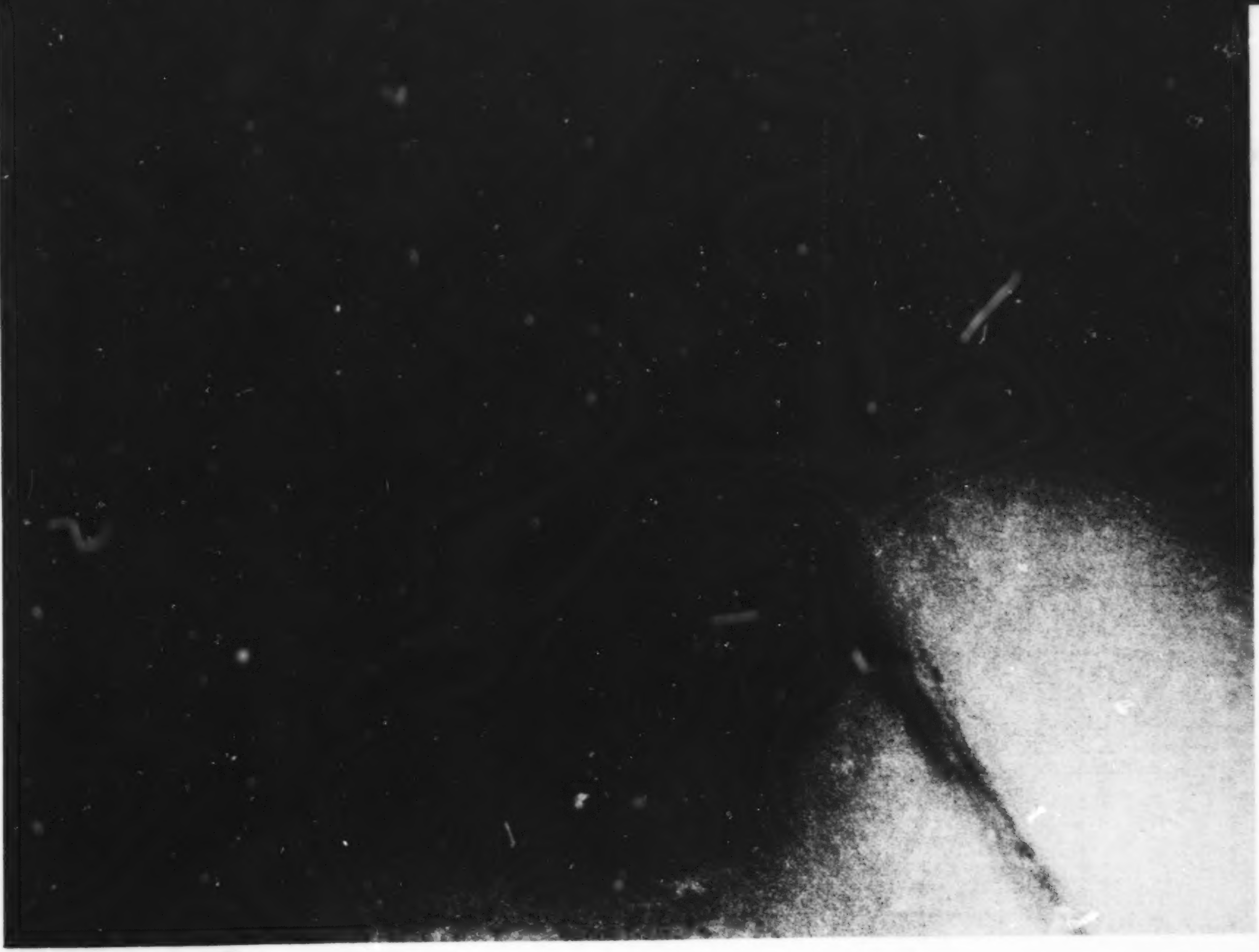

Figure 105a. An example of ridge-and-groove microtopography from the new scour at the "Caroline" site. The ridge on the right is about 20 cm high and 30 cm wide. Field of view is approximately 2 m across.

Figure 105b. Similar ridge-and-groove microtopography, with less than 5 cm relief, in the trough of "Big Makk".

sonogram records of the new scour at the "Caroline" site, and were traced by submersible for at least 90 m at this site. However, it is clear from dive observations that although large features may persist, their morphology may change considerably. Characteristic changes involve gradual reduction or increase in amplitude between a ridge and corresponding groove, or changes in width of several centimetres, and changes in the cross-sectional shape. Smooth-faced ridges may deteriorate over several metres, the ridge walls becoming "ragged" looking, before either dying out or regaining, over similar distances, their original morphologies.

Although the entire roughened surface of a scouring keel may be in direct seabed contact, the morphology of the trailing edge is responsible for generating microtopography. Evidence comes from two observational sources. Firstly, individual ridges and grooves are commonly traced out over meltout pits. This continuity can be explained by the breaking out of ice, in advance of the trailing edge, which is subsequently overridden and embedded in the scour trough. Continuous tool marks are made as the trailing edge passes over the embedded ice. Secondly, individual boulders and cobbles were found at the start of many ridges. These crag-and-tail features are probably generated when boulders and cobbles break out of the keel's trailing edge. Sediment may then be continuously forced into the void left by the clast because of vertical iceberg pressure. Such features may be used as indicators of iceberg movement direction, the ridge behind the boulder or cobble pointing "down-scour".

Alterations in microtopography reflect dynamic change occurring at the keel's trailing edge, but are not indicative of large-scale modifications in overall keel geometry. The gradual longitudinal changes in ridge-and-groove morphology probably reflect small-scale continuous adjustment of the tools that generate them.

Ridges and grooves are nearly always parallel to the scour axis clearly reflecting the rotational stability of the scouring iceberg about a vertical axis. This observation is consistent with the inferred dynamic behaviour of a scouring iceberg which is that the iceberg yaws so that roll occurs about its weakest axis of rotation. Once this condition is achieved, vertical rotations cease (eg. Woodworth-Lynas et al. 1985). Along the inside berm flanks of the new scour at the "Caroline" site ridge-and-groove microtopography developed at nearly 45° to the scour axis probably reflects plastic flow of sediment away from the flanks of the scouring keel.

Sediment Reworking and Redeposition. Although not observed in the other scours investigated by *Pisces*, "Big Makk" displayed possible evidence of deposition within the scour trough in areas of flat-floored, negative seabed relief below the scouring keel. Small-scale flat-topped mounds developed in depressed areas within the scour trough (Figure 106) may represent places where the keel was not in contact with seabed (see Chapter 4). In this situation a layer of continuously reworked sediment between the flattened keel and seabed is envisaged to fill in the depressions by a "plastering" mechanism. Where there is insufficient material beneath the keel to completely obliterate it, the unscoured seabed may be exposed.

Alternatively, overriding of continuously failing ice by the keel may have generated the depressed region, the flat-topped mounds indicating places where there were voids in the ice that was embedded in the seafloor. This explanation is considered less likely because it does not

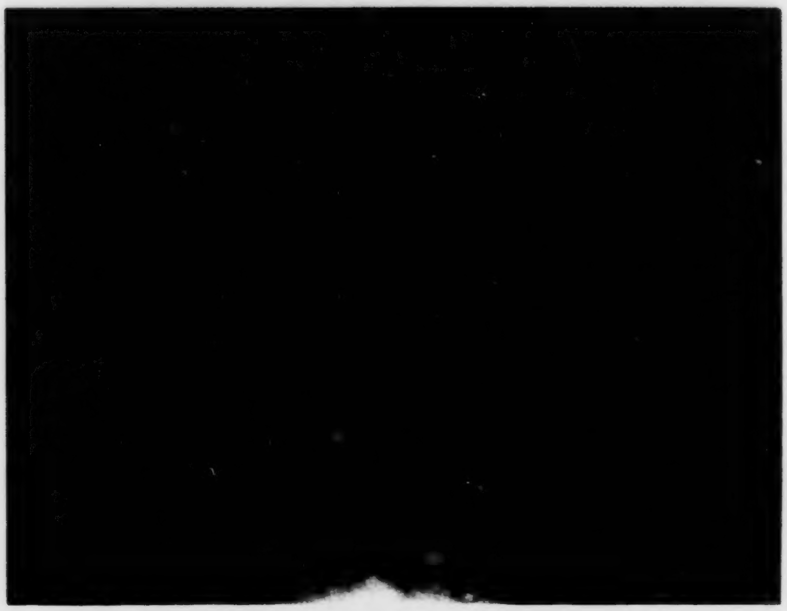

Figure 106, Sample of a flat-topped mound, about 0.5 m high, resting above apparently undisturbed seabed in a linear depressed area within the scour of "Big Makk".

account for the flat floor of the depressed area. Meltout features observed in other scours are characterized by uneven surfaces reflecting irregularities in the morphology of broken off ice blocks. Further, the flat floor appeared to be a region of old, undisturbed seabed. If ice were embedded, it is likely that the seabed would appear disturbed.

Summary of Iceberg Scour Processes and Sediment Failure Mechanisms in Cohesive Sediments. Seabed failure mechanisms thought to occur during scouring have never been observed. However, the morphology of structures seen in new scours yields information on the probable nature of soil failure.

Between the scour trough and berm crest the berm flanks characteristically consist of fractured blocks of apparently compressed clay and silt in situ. Although sometimes chaotically arranged and despite the fact that lateral displacement normal to fracture planes has occurred, it is often possible to match fracture planes on adjacent blocks as seen in the new scour at the "Caroline" site (Figure 107) (see Chapter 4). Displacement may be tensional, the blocks being separated by gaps a few centimetres across. Vertical displacement may be only a few centimetres so that, although pulled apart, the upper surface of the blocks is relatively even. The depth to which fractures occur below the surface is unknown but, based on the height of free-standing single blocks on the berm crest at the "Caroline" site, may be at least 1 m.

Although massive, the blocks are ramified by a network of hairline fractures along which no displacement has occurred. Demonstrable evidence for the existence of such networks was found in the new scour at the "Caroline" site (see Chapter 4). During sampling of a fractured berm block,

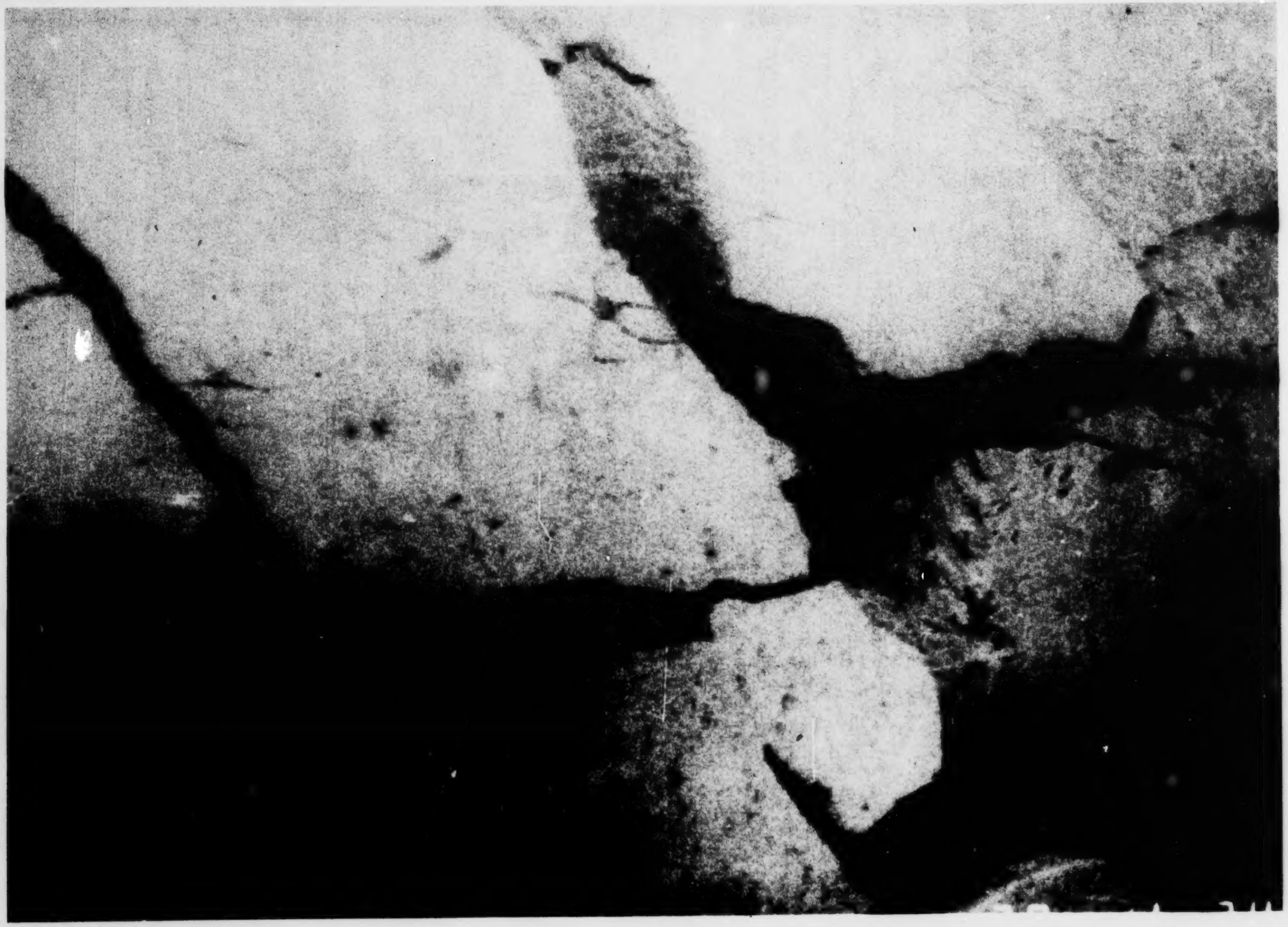

Figure 107. View of blocks fractured in situ on the inside berm flank of the new scour at the "Caroline" site. Field of view is approximately 3 m across.

the pressure of the core sampler caused expulsion of fine clouds of sediment from the upper block surface evidently from minute fractures that were otherwise not seen.

The berm crest marks a transition from relatively intact, in-situ blocky sediment, to smaller, disaggregated and chaotically arranged blocks which characterize the outer berm flanks (Figure 108). Some of the material constituting the outer berm flanks is derived from fractured sediment blocks which have spalled from the berm crest probably both during and after the scouring event. This process generates a characteristically disaggregated, rubbly outer berm slope. The smaller blocks and pieces commonly rest in a fine-grained matrix which is probably in part derived from disaggregation of originally larger blocks at the berm crest during mass wasting and by later bioturbation and current winnowing.

As an iceberg keel moves horizontally through the seabed creating a scour trough, material is displaced to both sides. Displacement occurs through passive failure mechanisms, that is the soil fails and is subsequently displaced by a structure (the iceberg keel) exerting a pressure on the soil. Vertical pressure of the keel on the seabed may cause excess porewater pressure to develop in the soil beneath the keel. The resulting loss of strength causes some of this soil to flow plastically out from under the keel. The soil may then fracture, possibly as a result of stress release, following passage of the scouring keel. Further mechanical action by the scouring keel causes break-up of the fractured sediment on the inner berm flank. At the same time lateral displacement causes blocky material along the berm crest to spall outwards forming a blocky slope on the outer berm. Observations also suggest that berm material may actually be extruded laterally by the keel

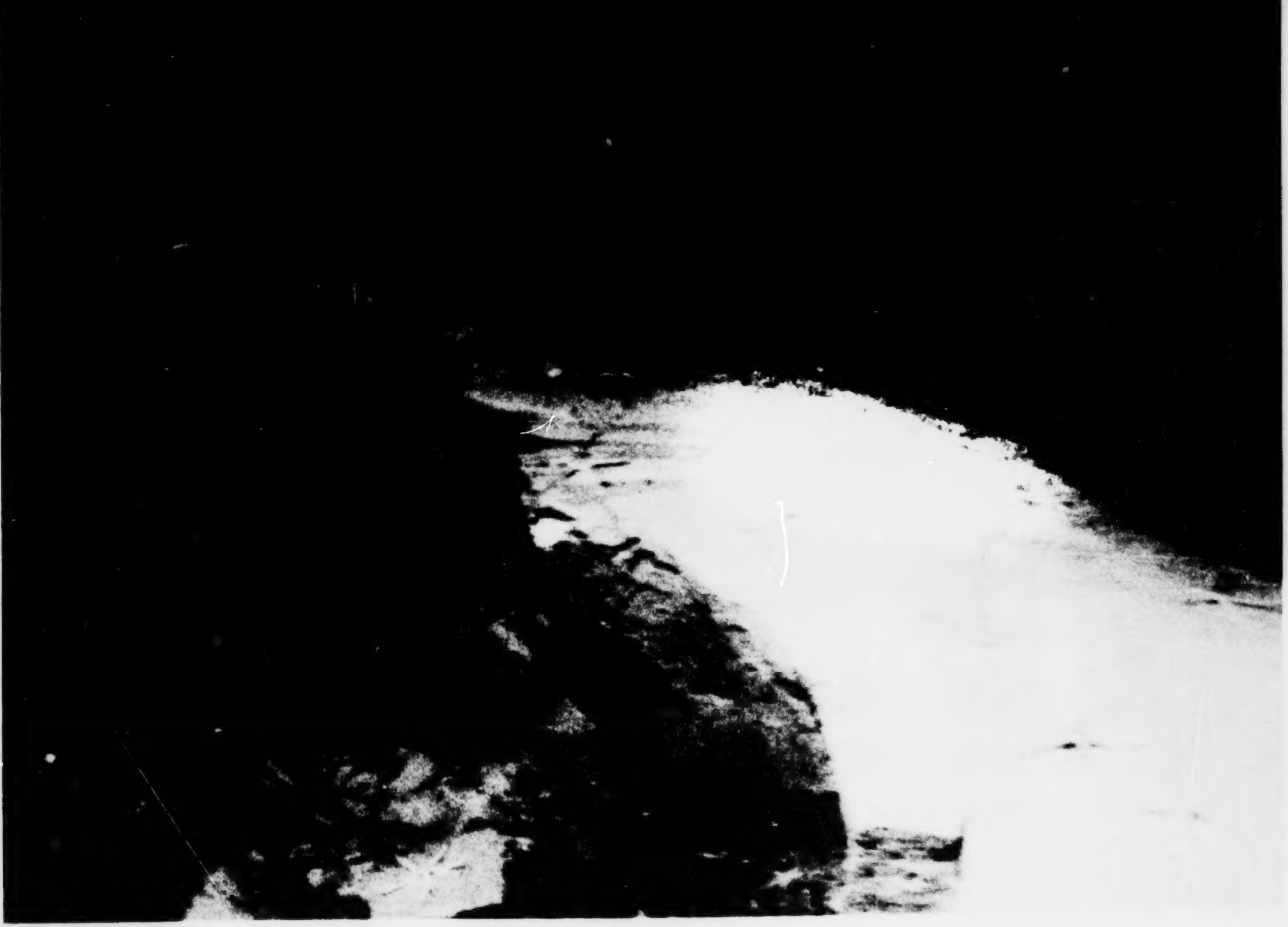

Figure 108. View of the abrupt transition from consolidated material of the inside berm flanks on the right (note the small-scale ridged and grooved surface), to disaggregrated, largely unconsolidated sediments of the outside berm flanks on the left from the "Caroline" site. Field of view is approximately 3 m across.

to form unsupported overhangs at the berm crest. These unsupported masses subsequently fail, falling beyond the berm margins to form discontinuous mounds on the seafloor.

A surcharge of bulldozed material is probably continually being formed at the leading edge and displaced by the iceberg keel. A leading edge surcharge of this type was observed at "Big Makk" (see Chapter 4) and consisted of unconsolidated material and a sandy surface lag. The surcharge material is probably generated by initial plastic and/or brittle deformation of sediment in front of the scouring keel. As the keel advances, the sediment will be continually reworked and comminuted by the mechanical bulldozing action of the keel's leading edge and by mass wasting down the outer slope of the surcharge. Lateral displacement of this material by the advancing keel probably accounts for a major portion of the loose sediment observed on the outer berm flanks of fresh scours.

Regional Aspects of Iceberg Scouring

The four sidescan mosaics from Makkovik Bank (Figure 109) offer an opportunity to study the influence of sediment type on scour morphology. The iceberg scour parameter information obtained at each of the mosaic locations is presented in Chapter 4 and Appendix 10. The scour parameters discussed in this section are illustrated in Figure 110.

This subsection describes scour dimensions measured from the sidescan mosaics. The measurements document scours of unknown age and in many cases are representative of substantially eroded scours. The occurrence of fresh scours, such as at the "Bertha" or "Caroline" sites,

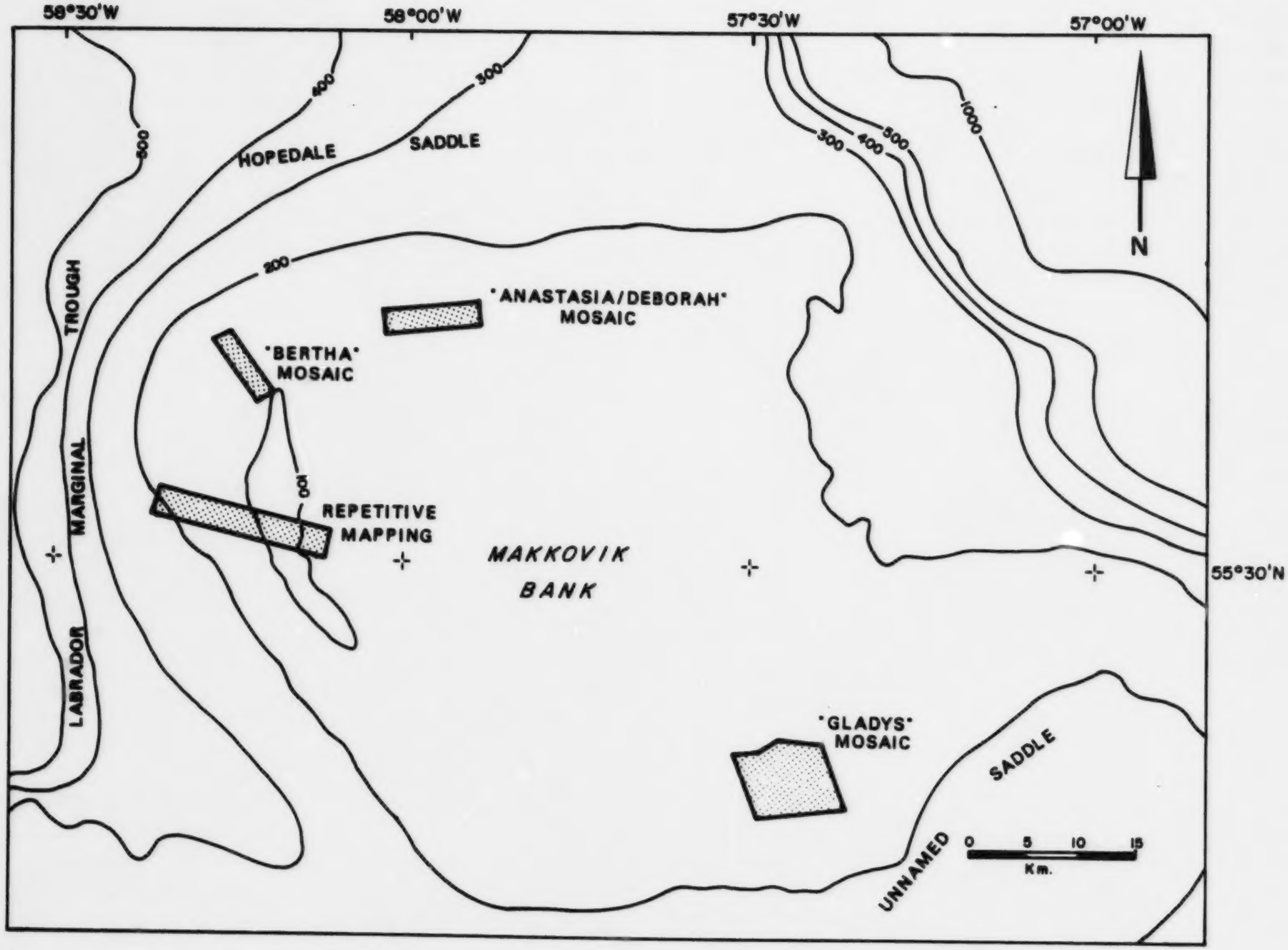
58°30'W
58°00'W
57°30'W
57°00'W
55°30'N
N
HOPEDALE
SADDLE
500
400
300
1000
500
400
300
200
100
TROUGH
MARGINAL
LABRADOR
'ANASTASIA/DEBORAH'
MOSAIC
'BERTHA'
MOSAIC
REPETITIVE
MAPPING
MAKKOVIK
BANK
'GLADYS'
MOSAIC
SADDLE
UNNAMED
0
5
10
15
Km.

Figure 109. Makkovik Bank bathymetry and location of mosaics.

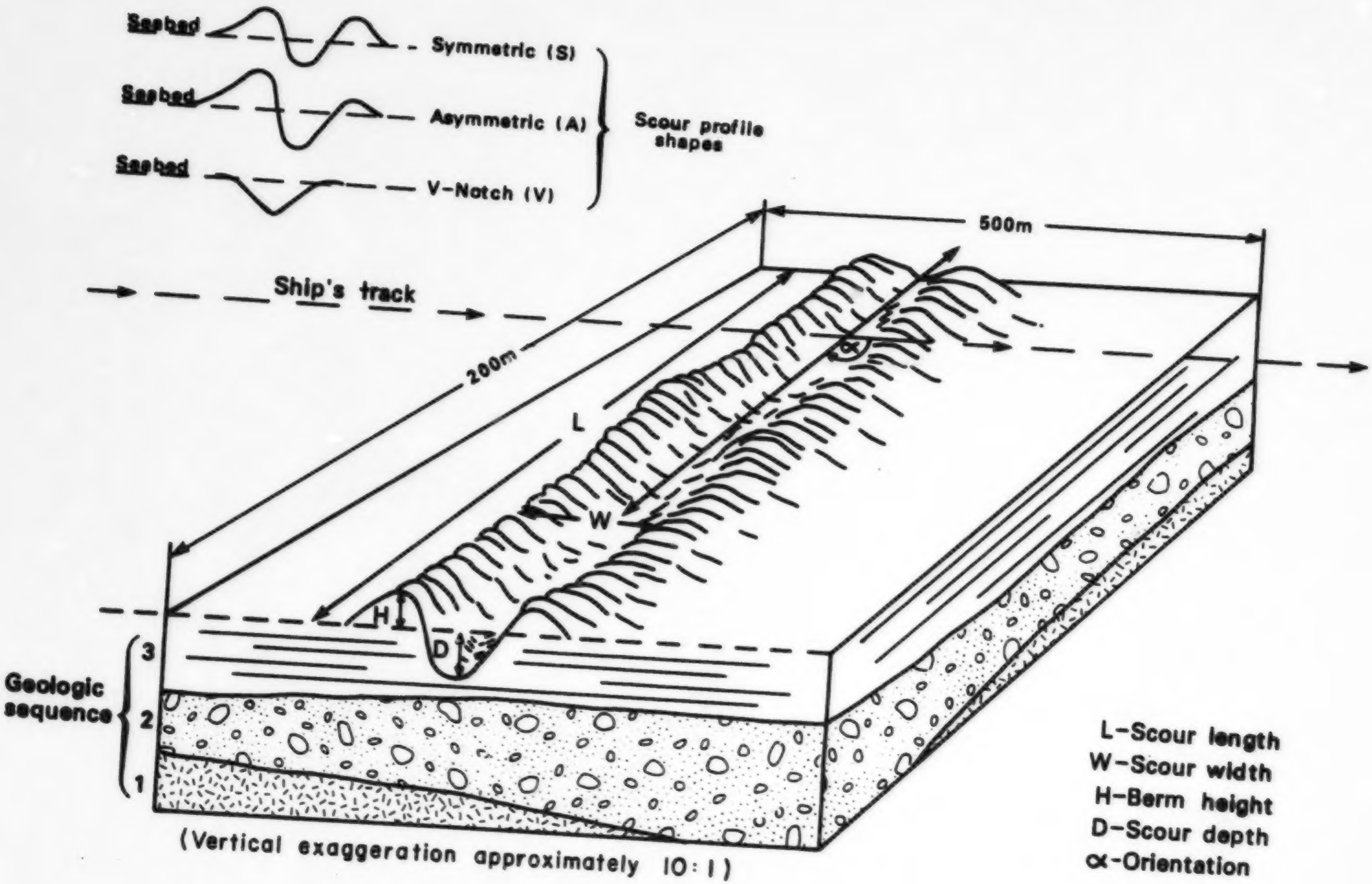
Seabed
Symmetric (S)
Seabed
Asymmetric (A)
Seabed
V-Notch (V)
Scour profile shapes
Ship's track
200m
500m
L
W
H
D
α
3
2
1
Geologic sequence
(Vertical exaggeration approximately 10:1)
L-Scour length
W-Scour width
H-Berm height
D-Scour depth
α-Orientation

Figure 110. Schematic diagram of a sample area showing (1) horizontal dimensions; (2) ship's track; (3) angle of scour orientation (relative to ship's tracks); (4) scour length, width, depth and berm height; (5) classification of scour shapes in profile view, and (6) differentiation of geologic units.

suggests that only a few of those measured represent unmodified scours. The scour depth data must therefore be treated with caution and probably do not represent original incision depths; the width data will not have been altered significantly.

Influence of Sediment Type and Thickness on Scour Depth. The depths of iceberg scours along the western edge of the Bank at the Repetitive Mapping and "Bertha" sites suggest a negative relationship between scour depth and seabed competence. Scour depths within the Labrador Shelf Drift average 0.66 m compared to an average of 0.71 m within the Sioraq Sand and 1.01 m within the Qeovik Silt. Iceberg scour widths for the same area indicate the same, although less pronounced, general trend with widths ranging from an average of 18.1 m within the Labrador Shelf Drift to 20.8 m within the Qeovik Silt.

A comparison of available geotechnical information for these units shows the Upper Till of the Labrador Shelf Drift to be slightly overconsolidated with an average shear strength of ±20 kPa, water content of 25% to 30% dry weight and bulk density of 1.8 to 1.9 g/cc. Unfortunately, no information is available for the Lower Tills. Sioraq Sand is geotechnically highly variable. Qeovik Silt is less competent than the till, characterized by shear strengths of 4 to 18 kPa, water contents of 20% to 60% and bulk densities of between 1.3 to 1.9 g/cc (Josenhans et al. 1986). Labrador Shelf Drift and Sioraq Sand are evident mainly along the Bank edge and top in water depths generally less than 120 m. Qeovik Silt occurs in the deeper waters along the side of the Bank and is therefore intuitively exposed to scouring by larger icebergs.

The "Gladys" seabed composite was surveyed on the southeastern corner of the Bank in an average water depth of about 130 m. Average scour depths for the Sioraq Sand and Labrador Shelf Drift units are 1.02 m and 0.98 m respectively. Scour widths were not measured because the sidescan data were not corrected for distortion. A comparison of scour depths from the "Gladys" composite with scours from the western side of Makkovik Bank shows a 43% increase in average scour depth for the Sioraq Sand unit and a 48% increase for the Labrador Shelf Drift within the "Gladys" composite.

This substantial increase in average scour depth is pronounced on the northeastern corner of the Bank as shown by scour measurements from the "Anastasia/Deborah" mosaic location. The average depth at this site is about 1.0 m within the Sioraq Sand and about 1.2 m within the Labrador Shelf Drift for an average depth increase of 41% and 82% respectively over scours on the western side of the Bank. Scour widths within the till are similar for the two regions.

The differences in scour depth within the Labrador Shelf Drift suggests that different till units may be exposed in the different areas. Unfortunately, the only area where the Upper and Lower Tills can be identified is at the Repetitive Mapping site where Upper Till is primarily overlain by Qeovik Silt.

Scour depths within Upper Till and Lower Tills vary considerably because of differences in geotechnical properties. The Upper Till is normally consolidated whereas the Lower Tills are interpreted to be overconsolidated (Josenhans et al, 1986). Piston cores and vibracores penetrate Upper Till but are unable to penetrate the Lower

Tills supporting the interpretation of overconsolidation. Scours developed in the Lower Tills were observed during manned submersible dives within the Repetitive Mapping site and appear as features with little or no relief.

A graph of scour depth versus water depth including geological data from each of the four mosaic locations is presented in Figure 111. Though variation is considerable the trend of scours suggests that for each geologic unit, scour depth increases with water depth, and that, for any given water depth interval, no individual unit necessarily has the deepest scours. Water depth is a significant control on scour depth possibly because of a combination of more frequent sediment reworking in shallower water on the Bank top and to the effects of increased ice mass and momentum at greater depths, particularly in the marginal trough where currents are typically stronger than the Bank top.

Scours in Labrador Shelf Drift are deeper at the "Anastasia/Deborah" and "Gladys" sites than at the Repetitive Mapping and "Bertha" sites. This difference can at least partially be attributed to the fact that the former are situated in deeper water.

Scour Orientation in Relation to Regional Seabed Morphology.

The locations of the four mosaic sites offer good geographic coverage of Makkovik Bank. The iceberg scour orientation data available from these mosaics can be used to provide additional information about the relationships between scour orientation and local Bank morphology.

The scour orientation information for each mosaic site is given in Chapter 4, with the exception of the "Gladys" site for which no attempt was made to document scour

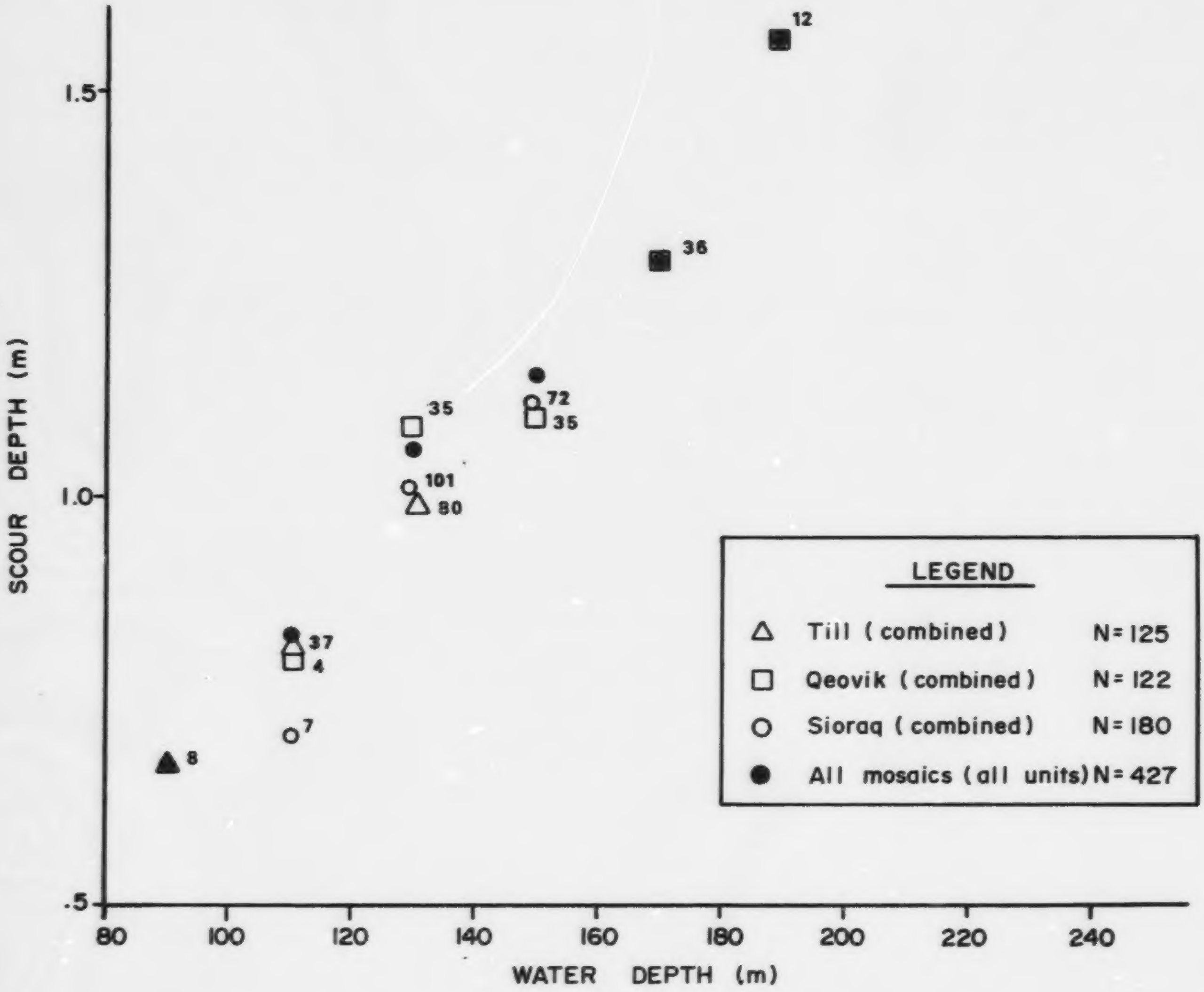

Figure 111. Scour depth vs. water depth for all mosaics, combined in 20m intervals of water depth. The number of scour depths averaged are indicated beside each mean.

orientations because of the uncorrected nature of the sidescan sonar data.

Analysis of scour orientation data from the Repetitive Mapping site, located along the western edge of the Bank, indicates three dominant trends. In water depths of greater than 120 m, the primary mode is N124°E or roughly 40° to the regional isobaths. In depths of less than 120 m, there appears to be a primary mode of approximately N130°E and a secondary mode oriented N70°E.

One well-developed scour from the Repetitive Mapping site is 3.5 km long and traverses diagonally across the isobaths at an angle of about 40 degrees along a bearing of 120°. The scour traverses a 25 m depth range (150 to 125 m) and doubles in width toward the upslope end. Other scours with similar orientations increase in width and end in a pit at the upslope termination suggesting that the dominant movement of scouring icebergs may be toward the southeast.

Of the 296 iceberg scours measured from the Repetitive Mapping mosaic, 65% traverse an upslope/downslope vertical distance of 0 to 2 m, 20% traverse 2 to 4 m, 10% traverse 4 to 6 m, and the remaining 5% of scours indicate an upslope/downslope range of 6 to 14 m. The average vertical range for scours in the mosaic area is 1.8 m. Depth measurements made at three points along a 3.5 km long scour which cuts into the Qeovik Silt unit range from 1.2 m at a water depth of 150 m; to 0.7 m at a water depth of about 140 m and 1.0 m at a water depth of about 130 m.

The "Bertha" site is situated on the northwestern edge of Makkovik Bank. Iceberg scour orientations measured from the mosaic indicate a dominant trend of N103°E which is roughly 60° to the trend of the isobaths. The maximum upslope/downslope vertical range documented is 3.0 m with an average vertical range of 0.7 m.

The "Anastasia/Deborah" mosaic is situated on the northeastern corner of Makkovik Bank. Scour orientations in the area show a strong northwest to southeast trend, normal to the regional isobaths. This orientation may reflect the southeasterly current flow along the northeastern edge of the bank. Chart 4 showing iceberg drift tracks for August of 1985 strongly supports this interpretation.

In the central portion of the "Anastasia/Deborah" mosaic, the northwest to southeast trending scours, which represent about 80% of the scour population, are buried beneath Sioraq Sand. The remaining 20% are randomly oriented short scours and pits which disturb the surficial sand. This mosaic site is one of the few areas where thick (approximately 5 to 7 m) deposits of the sand unit are found. The majority of scours are buried by Sioraq Sand, which may be as old as 8,000 years (Josenhans et al. 1986). Thus scours in this unit may range in age from 8000 years old to modern. The subdued relief of exposed scours indicates considerable erosion of these features. The maximum vertical range traversed by a scour is 4.0 m whereas the average range is approximately 0.5 m.

The northern part of the "Anastasia/Deborah" site, which consists primarily of Labrador Shelf Drift, is so heavily scoured that it is difficult to identify individual features. On the other hand, in the southern part of the site, the Sioraq Sand has comparatively few scours. Scours which traverse both units appear well defined within the till but are either not evident or are partially infilled in the sand unit.

Iceberg Scour Degradation

Degradation During the Scouring Process. Scour degradation may occur during and immediately after the scouring event as a result of several processes. Although not observed, these may include backfilling of the scour trough with suspended sediment behind the advancing iceberg, slope failure of the berms and short term erosion by enhanced currents around the keel. To separate these degradation processes from longer-term effects, the time-scale can be considered limited to the period during which the presence of the iceberg itself is significant. In particular, erosion or infilling during the scouring event should be considered as limited to the period where local hydrodynamic forces are modified by the presence of the iceberg. Within cohesive sediments, backfilling, slumping or immediate redeposition from suspension into a new scour trough has not been observed. Localized redistribution of unconsolidated surficial sand to the outer berm crest was inferred, as was slumping and fracturing of material from the steeper parts of the outer berm to the undisturbed seabed. There was no evidence of current erosion or sediment transport during the scouring event as a result of currents around the iceberg. However a significant current flow of about 0.5 m/s around the keel of iceberg "Gladys" was observed during operation of the ROV. The absence of sediment within newly formed scours suggests that increased currents inhibit sedimentation in the scour trough. Two types of infilling of new scour troughs were observed but are probably only of minor importance. These are broken rock fragments deposited from the iceberg which formed the scour and redeposition of sediment in areas of negative seabed relief below the scouring keel, interpreted from the presence of flat-topped mounds observed in the trough of "Big Makk" (see Chapter 4).

Bioturbation Effects. On Saglek Bank an iceberg scour, interpreted to be six years old and since cut by a more recent scour, was colonized by a dense and diverse community of benthic organisms. Mobile epifauna include two species of brittle star, one species of sea urchin, and one species of gastropod (Pocklington 1987). Attached epifauna include one species of crinoid, three genera of sea anemones, two genera of bryozoa, and a variety of sponges. Brittle stars, sea urchins, crabs, and gastropods are very mobile and may be able to invade a new scour within hours. Crinoids and sea anomones, although attached to the substrate, may release and swim away from physical disturbance and resettle after the disturbance has passed (Pocklington 1987). Sponges, on the other hand, are slower colonizers, perhaps taking as long as six years to become re-established (Pocklington 1987). Recolonization generates a surface veneer of reworked silty sand. The fines appear to be frequently suspended by bottom currents and transported away from the scour. This continuous process of disaggregation, suspension and winnowing of fines by the combined actions of bioturbation and bottom currents is a fundamental process in eroding the cohesive silts and clays of the scour berms in particular. To erode these cohesive silts and clays by hydrodynamic processes alone would require currents greater than those observed or recorded for this area of the Labrador Shelf.

Scour Erosion. Erosion of scour berms depends on whether seabed sediments are cohesive or non-cohesive. Also, the quantity of large clasts, particularly in non-cohesive sediments, is important in understanding the erosion of these features.

Iceberg scours formed in areas of sand or sand and gravel are subject to significant erosion particularly during storm events unless a lag or armour of coarse material is formed. Scour berms increase seabed roughness which in turn leads to increased bottom current shear stresses. Berms should thus be preferentially eroded depending on the direction of the net flow at the seabed. Erosion and reworking of berm material was noted at 230 m depth on the southern Baffin Island Shelf (see Chapter 4). However, scour troughs may channel bottom currents, and, if the flow is sufficient to prevent sedimentation, the scour trough will not infill even if the berms are eroded.

On the Grand Banks of Newfoundland, sidescan sonar surveys indicate that scours are preferentially preserved in areas of lag gravel and are noticeably less common in areas of sand, especially in thick sand ridges (Lewis and Barrie 1981). There is also a significant drop in scours per unit area in water depths shallower than 100 to 120 m on the northeastern portion of Grand Bank. This reduction is opposite to the usual situation in which iceberg scour density increases upslope (Lewis 1979; Barrie 1980; Todd 1984). Lewis and Barrie (1981) interpret the change in scour density to be partly the result of wave-induced sediment transport in water depths shallower than 110 m which is considered to be the primary mechanism of scour degradation in this area (Barrie 1983).

Observations of the processes of erosion of iceberg scours formed in cohesive sediments were made during the DIGS experiment. The sediment types encountered in this investigation are sufficiently compacted to require strong bottom flow acting over long periods to cause erosion. Maximum current velocities measured at the seabed during this field program exceeded 30 cm/s during a storm event. During submersible operations currents were observed to be stronger on the scour berms than in the troughs in most cases. In the fresh scour at the "Caroline" site on Saglek Bank (see Chapter 4) current direction was weak but parallel to the scour axis within the scour trough but normal to the scour on the berm crest. All these observations were made during calm sea conditions.

Cohesive sediments disaggregated by bioturbation are made more susceptible to erosion and transport. These effects were apparent at the "Caroline" site where the six-year-old scour and a fresh scour have a difference of 1 m in berm height at the crossover point. Because they are similar in width and are cut into the same sediment, it is assumed that they would have had similar berm heights when newly formed. This inference is reasonable as there was little variation in berm height in both scours. The berms of the old scour have been substantially rounded and reduced in height in six years and are blanketed by a coarse lag deposit that has been exposed by the armouring of fines largely disaggregated by bioturbation. Striations in the scour trough have also apparently been eroded and there was little sediment infill of the trough.

Bedform Migration. Sedimentary bedform migration can act as an agent of either scour infilling or erosion. Based on the known physics of sedimentary bedform generation and movement, degradation rates and even scour age may be determined. The distribution of bedforms (see Chapter 4) is based on the analysis of sidescan mosaic coverage and submersible observations. The principal bedforms identified are straight-crested, flat-sloped, large, symmetrical ripples found primarily in water depths of less than 120 m. They have crest orientations of generally N140°E, amplitudes of 0.3 to 0.5 m, wavelengths of 1.0 to 3.0 m and are developed in local depressions such that the ripple crests are level with the surrounding seafloor. Smaller, wave-induced ripples are also found above 120 m and are ubiquitous at the shallowest depths except in areas of lag gravel. Moribund sand waves occur on the western flank of Makkovik Bank. The large symmetrical ripples have a morphology attributed to wave-induced formation and thus may reflect the most significant sediment transport mechanism in this area. However, at present it is unclear whether they are formed primarily by unidirectional or wave-induced oscillatory currents or whether both mechanisms are involved.

As discussed in Chapter 3, mean rectilinear sediment transport is directed largely to the west-southwest with lesser east-southeastward transport. Large, symmetrical ripple migration may also be along the west-southwest axis but the actual net transport direction is undetermined.

No observations were made where large, symmetrical ripples interacted with iceberg scours. However, evidence from sidescan sonar surveys from other areas of the eastern Canadian shelf indicates the presence of bedform migration across scours (Barrie 1983; Amos and Barrie 1985). It is unclear whether bedforms become trapped after migrating into scour troughs or whether they may migrate out again with little modification of the scour morphology. In the case of many larger scours found during the DIGS experiment, the steep, high berms may act as a barrier to bedform migration until they are reduced in height through the degradation processes of bioturbation and winnowing. Small-scale current ripples observed in the troughs of two scour pits at the "Anastasia" site (see Chapter 4) indicate that some infilling had occurred.

Sedimentation. Sedimentation rates over the eastern Canadian continental shelf are low and result primarily from the reworking of surficial sediments by bioturbation, sediment transport, and iceberg scouring. Small amounts of new sediment are input by ice and iceberg rafting. Although these processes are geologically significant, the rate of sedimentation is too low within the recent scour population for detection by the sub-bottom profiler used during this study. McMillan (1973) gave rates of sedimentation by iceberg rafting of 4 cm/100 years which is considered by Gilbert and Barrie (1985) to be low. Sediment suspended and reworked by iceberg scouring may generate as much or more material for scour infill as by iceberg rafting. Using rough calculations based on present scouring frequencies on Saglek Bank on the northern Labrador Shelf, Woodworth-Lynas et al. (1984) estimate that 112 million m^3 of seabed material is reworked by the scouring process each year. This estimate was based on an erroneous scour depth estimate of 5 m. It is now known through the holdings of the ESRF Ice Scour Data Base (Geonautics, in prep.) that the average scour depth on Saglek Bank is 1.4 m. This reduces the estimate of reworked material to 31,360,000 m^3 each year.

Taking the predicted results of sediment transport (see Chapter 4) into consideration for the western portion of the Bank at 100 m, complete infill of a scour could occur in a few hundred years probably during storms such as occurred from August 15 to 17. However, the calculation of infill rates for use in defining scour equilibrium (that is where the number of new scours added to a population is equal to the number of scours removed by sedimentary processes) as defined by Lewis (1978) and developed by Gaskill et al. (1985), requires knowledge of the interaction processes between bedload and suspended load transport and iceberg scours (Lanan et al. 1986; Weeks et al. 1985).

Data acquired during the DIGS experiment together with earlier submersible observations (Josenhans and Barrie 1982), demonstrate that little sediment is available for transport despite the large potential volume of ice reworked sediment, and that erosion is the significant mechanism affecting the seabed. Scour infill, as shown by Gilbert and Barrie (1985), can be explained in terms of the availability of sediment for transport. Within sand patches enough material can be moved to infill a scour, completely or partially, whereas portions of the same scour, developed in a coarse lag deposit, may remain relatively unchanged.

Summary. Degradation of iceberg scours is initially quick. Microfeatures are eroded in just a few years whereas some large-scale features such as berms can endure for several hundred years or longer because of the process of armouring. Disaggregation and suspension of cohesive sediments by burrowing organisms coupled with removal of the disaggregated material by both oscillatory and unidirectional bottom currents are the dominant processes of iceberg scour degradation on Makkovik Bank. The effects of biogenic reworking results in smoothing of initially blocky berms and development of a localized sandy lag surface. Also, some scour trough infilling from the same disaggregated cohesive sediment occurs, as well as bedload transport of non-cohesive sediment, where available.

Scour obliteration, resulting from degradation processes, can be monitored over time by means of repetitive sidescan surveys. From these repetitive observations it should be possible to determine the rate of scour obliteration in various hydrodynamic and geologic settings.

CHAPTER 6

CONCLUSIONS AND RECOMMENDATIONS

Included in this chapter is an assessment of the strategy and methodology of the combined DIGS experiment and Repetitive Mapping study, and a summary of what are felt to be the most significant findings.

STRATEGY AND METHODOLOGY

A primary objective of the DIGS experiment was to obtain full-scale data sets of iceberg/seabed interactions for use in the verification of seabed scour models. As discussed in Chapter 1, icebergs identified as possible grounding candidates were to be profiled, driving forces measured, instruments deployed to document their motion, and ROV operations conducted to provide observations of actual scour processes. These activities were to be complemented by thorough seabed surveys along the trajectory of the iceberg, in order to document any seabed disruption. Because all iceberg monitoring operations were to be daylight activities, the Repetitive Mapping program was conducted at night, thus yielding maximum use of logistic resources. The concurrent WIIM study would also complement these efforts.

It was recognized at the onset that this first attempt to observe iceberg/seabed interaction contained an element of chance, and a consequent risk of failure. However, the extensive seabed mapping activities, consisting of well established techniques, represented a more certain means of acquiring a wealth of information on iceberg scour on Makkovik Bank. These activities, together with the availability of the submersible, Pisces IV, and the implementation of a sediment transport study, virtually assured the acquisition of a substantial set of detailed observations of scour formation and degradation processes.

Overall, it is felt that the DIGS experiment was extremely successful. Full-scale data sets of iceberg/seabed interaction were obtained, and the seabed survey and submersible activities yielded an enormous amount of new information on scour processes. The planned operational strategy worked reasonably well, requiring little modification. As with any ambitious undertaking, however, a number of difficulties in executing the strategy in detail led to a reduced operational efficiency and some data loss. Suggested solutions to these difficulties are summarized in point form below, in the hope that future experiments of this sort might yield an even greater degree of success.

(a) More lead time between the commitment of funds and the mobilization of equipment should be provided than existed for the DIGS experiment. Funding was approved in June 1985 with mobilization required by July 1985. Fortunately, motion package instrumentation development had been initiated in March 1985. However, many systems used, including the C-CORE motion sensor packages, experienced difficulties which could have been avoided with longer development time. Some equipment, (such as a large plotter) could not be acquired in time for the experiment. A 6- to 12- month lead time for mobilization would be more appropriate for a large program of this sort.

(b) All major subsystems used in the experiment should be tested and calibrated, as appropriate, prior to mobilization. Calibration checks, as far as possible, should also be conducted once equipment is installed on the vessel. The Ametek Straza Doppler Current Profiler was a notable example of an essential piece of hardware which could have been diagnosed as working improperly if on-board calibration had been conducted. Similarly, breakdowns in the ROV could have been more easily overcome with early deployment and testing. Clearly, adequate lead time and provision of additional experimental time is necessary for all major equipment to be checked thoroughly.

(c) Spare parts should be provided for instrumentation essential to the success of the program. Also, spare equipment enables cross-checks on data to be undertaken. Furthermore, on-site data verification should be possible for all essential systems. Operators should be sufficiently well trained to recognize bad data and should be able to take corrective action.

(d) Although the underwater iceberg profiling technique was the most advanced one available, several modifications are recommended. The vessel used as a platform should possess bow and stern thrusters for greater maneuverability, as profiling time must be kept to a minimum for large icebergs that are deteriorating rapidly. Additional transponders should be deployed to maintain an adequate acoustic positioning network around very large icebergs. Improved profiling accuracy in the vicinity of the keel/soil interface would also be extremely desirable, gained perhaps with the use of a vertically scanning transducer head. As with other instrumentation, calibration of the profiling system is recommended. Finally, much larger transponder floats should be used to assist in the determination of water-line location from aerial photographs, and to help position the underwater shape information relative to the above-water orientation.

(e) An ROV represents perhaps the only means of safely observing the keel/soil interface during a grounding event. It also can operate in more extreme weather than a manned submersible, with no problems associated with power supply exhaustion. However, the UFO 300 used during the DIGS experiment was clearly under-powered for the conditions encountered. The loss of its acoustic positioning system only aggravated control problems. A more powerful ROV with its own navigation sonar, such as the Hydra 5000, is recommended. Otherwise, costs associated with the ROV would be better dedicated to more productive experimental tools.

(f) The Huntec DTS sub-bottom profiler system worked well, yet the problem of interpreting the real depths of scours from the acoustic records still remains. Even on a slow pass over the "Big Makk" scour, parabolic reflectors resulting from the wide acoustic footprint of the beam masked much of the scour morphology. For example, either a sub-bottom profiling system mounted on an ROV or an echo sounder mounted on BRUTIV would enable the sound source to be located very close to the seabed and would likely solve the problem of acoustic footprint.

(g) Although iceberg targets were successfully tracked using the ship's radar and Syledis position fixes, the method of target coding could be modified. Assigning sequential codes for all sightings made it difficult in many cases to determine trajectories of individual icebergs. It would be better to reidentify targets when logged to improve operational decision making and post-cruise iceberg drift analysis. Target reidentification could be done either by the ice observer or by using suitable software based on previous trajectory information. Also, the lack of full radar coverage of the entire Bank made selection of grounding candidates difficult at best, and some grounding events may have been missed. Whenever the vessel changed location on the Bank, valuable time was used in acquiring drift trajectories for the icebergs near the new location. Unfortunately, full radar coverage of a region as large as Makkovik Bank must await the development of shore-based over-the-horizon radar. The availability of such a system, even in prototype stage, would substantially increase the likelihood of successful iceberg selection. Alternatively, for improved iceberg tracking, the experiment could be conducted in the vicinity of a fixed platform, such as an oil exploration or production drilling rig, or a vessel conducting geotechnical investigations.

(h) The compilation of sidescan mosaics at sea would have been of great benefit in interpretation of scour morphology and surficial geology, and would have assisted in decision-making for follow-up submersible dives. Mosaic construction would require a plotter, dedicated space, and at least one person.

(i) The method of quantifying sediment transport using pollucite tracer sand has one major shortcoming: the deployment area must be resampled within about 18 months, as pollucite is estimated to lose most of its naturally-occurring cesium into solution by this time. Except for one sampling during the DIGS experiment, follow-up sampling was not conducted during the required period.

Depth-of-disturbance rods have a far longer survival time than pollucite. However, if not revisited regularly, their value for quantifying net erosion/sedimentation rates is reduced. Revisitation does not necessarily require the use of a submersible; a video-equipped ROV could make the required observations at far less expense. If equipped with sufficiently powerful thrusters and manipulator arms, an ROV could also reset the rods for future visits.

Both of the above methods require firm commitments to return to the deployment sites. Naturally, it is difficult to allocate long range funds for this purpose, yet this requirement should be considered when the decision is made to incorporate sediment transport studies within larger programs.

Although difficulties were encountered with many aspects of the DIGS experiment, some systems yielded such satisfying results that these are recommended for any future large scale iceberg/seabed interaction experiments.

(a) The twin-engine Twin Star helicopter was an invaluable, multipurpose tool. It was used for iceberg reconnaissance, equipment and personnel transfer, instrument package deployment, aerial photography, and so on. Equipped with good navigation and communications equipment, and able to use the Polar Circle as an offshore base, this aircraft extended the field operations zone to virtually all of Makkovik Bank.

(b) A manned submersible is probably the best way to get a "feel" for the seabed, and perhaps cannot be bettered even by a good ROV equipped with video and still cameras. The advantage of direct observation more than compensates for the limited weather window and bottom time in comparison with an ROV, certainly if cost is not considered. The combined Hydrostar and Syledis navigation systems used on the Makkovik Bank dives illustrated the value of good on-board navigation capability. Nevertheless, improvement in the usefulness of a submersible could be made with the inclusion of a better means of taking core samples.

(c) The Syledis navigation hardware provided an outstanding reference system for iceberg tracking, seabed mapping, and so on. Although all-weather back-up capability would be desirable, the high resolution and accuracy of Syledis makes it the preferred single-system choice for nearshore experiments.

(d) The provision of telemetry and on-board data logging was found to be essential to the acquisition of iceberg motion data. This back-up capability to internal package logging helps to ensure data acquisition in the event of failure or loss of the package after an event. It also provides useful information on the status of an iceberg, to assist in the scheduling of other experiment resources. The availability of multiple, self-contained, long-duration motion sensor packages is also recommended for future experiments, although longer lead time is clearly desirable to ensure better performance than was experienced.

Finally, although it is felt that the overall strategy for the DIGS experiment was sound, attempts to gather further full-scale iceberg grounding and scouring data sets should be made with the following comments in mind.

(a) Analysis of the seabed interaction events documented in this report is hampered by the lack of geotechnical and post-experiment survey work. Although expensive, such additional investigation of any observed seabed disruption would significantly improve quantitative analysis of the corresponding events. In particular, it is recommended that the "Gladys" grounding site receive specific attention in any further study of scours on Makkovik Bank.

(b) The importance of pack ice driving loads in the generation of long scours has yet to be quantified. The nature of pack ice/iceberg interaction should receive systematic theoretical and experimental attention. It may well be that long scours are primarily generated by icebergs embedded in the Labrador ice pack. If true, consideration should be given to possible winter iceberg monitoring, with follow-up summer seabed mapping, as an overall strategy to investigate this phenomenon.

ACCOMPLISHMENTS AND RECOMMENDATIONS OF THE REPETITIVE MAPPING PROGRAM

The primary objective of Repetitive Mapping was to mosaic a series of sites on Makkovik Bank and document iceberg scour dimensions and their relationship to bathymetry and surficial geology as a basis for future resurveying programs.

Four mosaics were prepared providing good geographic coverage of the Bank. Data quality is excellent and allows for accurate documentation of iceberg scours. Measurements from sidescan mosaics and sub-bottom profiles of Makkovik Bank reveal the variability in the dimensions and orientations of the observable scours in relation to water depth, sediment type and bank morphology. Iceberg scours and pits dominate the seafloor from bank-top to the deepest surveyed areas (200 m) in the Labrador marginal trough. No data were obtained from the outer shelf edge. Iceberg scour orientation distributions on the flanks of the marginal trough are typically unimodal with a southeast trend. This trend may lie up to 40° to the regional isobaths. Individual scour features in deeper water were traced upslope over ranges as great as 25 m. On the bank-top, scour orientation distributions are more diverse and are typically bimodal with southeast and southwest trends. These observations are consistent with the general circulation pattern on Makkovik Bank, in which ocean currents that drive scouring icebergs are more variable and sluggish on the bank-top compared with those in the marginal trough.

Scour depths vary between geological units with deeper average scour depths occurring in the weaker units, as expected. However, this variation is quite small, and is dominated by a stronger correlation with water depth in which the deepest mean scour depths occur in the deeper water. Though a thorough statistical analysis has not been done, the correlation between scour depth and water depth is clear suggesting that the following factors may be important: (1) deeper draft icebergs in the Labrador marginal trough are less compliant than scouring icebergs on the bank-top; and (2) bank-top scours in the shallower water where sandy sediments are present are more susceptible to degradation processes such as sediment transport, and infill.

Future repetitive mapping programs should use a towfish positioning system to ensure accurate mosaicing and to simplify the correlation between sidescan and sub-bottom profiler data. The 50- and 100-kHz Klein sidescan systems used for Repetitive Mapping are highly recommended for future programs of this sort. Towed at the same time, the two systems provide complementary information. The 50-kHz sidescan, which was an integral part of the Huntec DTS system, provided a wide (375 m) scanning range capable of resolving gross seabed features such as general scour morphology and surficial geology distribution patterns. The 100-kHz system operated at closer range (200 m) and provided details not seen on the 50-kHz records, such as striations and meltout pits in scours and small sand ripples. The 100 kHz records were sufficiently detailed that they could be used in the submersible for highly accurate navigation, such as along the "Big Makk" scour. Track plots of the two submersible dives on this scour were in fact compiled based on features matched between the visual observations and the 100-kHz sidescan record.

Resurveying of the sites investigated during the 1985 field program should be undertaken using the same sidescan sonar systems and following the same line orientations as the initial surveys to ensure compatibility between corresponding data sets.

ADVANCES IN UNDERSTANDING OF SCOUR PROCESSES

As a result of the intensive study of iceberg scour activity on Makkovik Bank and the multi-disciplinary nature of the data analysis team, the DIGS experiment has led to several advances in the understanding of iceberg scour processes. In some cases, full-scale confirmation was obtained for previous theoretical hypotheses; in other cases, entirely new phenomena were discovered. Summarized here are what are felt to be advances in understanding of scour processes directly attributable to the DIGS experiment and repetitive mapping program. New contributions to the study of iceberg deterioration and iceberg/structure interaction are also noted, where appropriate.

(a) Verification of Seabed Pitting Mechanism

The "Bertha" roll and pitting event provides documented evidence of point seabed disruption by weak iceberg rotational instability as a result of continuous ablation or minor calving. This seabed disruption mechanism has been postulated as the cause of observed pits on the Grand Banks and has received considerable theoretical attention (see, for example: Bass and Peters 1984; Woodworth-Lynas et al. 1986; Bass et al. 1986; Bass and Woodworth-Lynas 1986). The "Bertha" data set, which includes measured motions, above- and below-water shape, sidescan records, and submersible observations, represents the only full-scale documentation of this phenomenon to date.

(b) Observation of Iceberg Split and Grounding Mechanism

The "Gladys" split and grounding event represents the first recorded description of high-energy rotational iceberg/seabed interaction resulting from the splitting of an iceberg into two large fragments. Previous to the DIGS experiment, no mention of this mechanism existed in the literature. One consequence of the high rotational energies involved is that much deeper pits are likely to result from this mechanism, in comparison with pitting resulting from weak iceberg rotational instability arising from continuous ablation and/or minor calving.

It should also be noted that the documented split and grounding behaviour of "Gladys" provides a means of estimating average iceberg/structure interaction pressure over an area of contact three orders of magnitude larger than any previous experimental measurement. In fact, this event represents the only documented full-scale iceberg impact of any sort. The estimated 1.2 ± 0.8 MPa average pressure obtained over a 4,000 ± 2,000 m^2 contact area provides a valuable data point for determining interaction pressures appropriate in the design of oil production platforms and associated seabed installations designed to resist iceberg impact. The fact that "Gladys" did not fracture as a consequence of the impact suggests that this failure mechanism may not occur during an iceberg/structure interaction.

(c) Identification of Splitting as a Significant Iceberg Deterioration Process

The ram loss and later split of "Frieda" and the split of "Gladys" represent the first thoroughly documented accounts of this significant iceberg deterioration mechanism. The predominance, over underwater ablation, of wave-driven waterline erosion and the subsequent calving of overhanging ice leads to the production of icebergs with large underwater rams. It is now believed that tabular icebergs split as a result of the buoyancy stresses generated by these extensive underwater rams (Diemand and Lever 1986a; Diemand et al. 1987). This mechanism is probably common and represents the first major transition of icebergs from tabular to tilted tabular and other shapes.

The iceberg splitting process has important implications for iceberg deterioration, population, and flux modelling, as well as being the source of energetic seabed pitting events. Splitting locally increases the number of icebergs while repopulating the lower mass categories which have become depleted through normal ablation. Thus iceberg population models that ignore splitting would underestimate total population and overestimate median iceberg size (Diemand and Lever 1986b). Furthermore, the calculation of iceberg flux (in the absence of direct iceberg tracking) is based on changes in local iceberg density (Anderson 1971; Ebbesmeyer et al. 1980). Hence, models which infer iceberg flux and the derived risk of collision based on measured population densities (see, for example, Gustajtis 1979) will need to be updated to account for the effect of population increase resulting from splitting.

The incidence of iceberg splitting is probably highly seasonal, being enhanced by wave action and warm surface-water conditions of summer and constrained by the low sea state, cold surface water, and sea ice conditions of winter. Thus, seabed pitting arising from the iceberg splitting processes will be more common in summer than in winter. In winter, with seabed pitting suppressed, iceberg furrowing is likely to be relatively more common, particularly with the presence of pack-ice driving forces.

(d) Categorization of Iceberg Scour Effects based on Iceberg Stability

The number of documented groundings was limited during the DIGS experiment. Nevertheless, a progression of iceberg behaviour and iceberg scour effects, which may be related to iceberg stability (resistance to roll), is suggested by the data. For example, "Anastasia", a weakly unstable iceberg, executed a low-energy roll and drifted free from a barely perceptible scour mark. "Bertha", only moderately more stable and energetic, oscillated as it rolled free of its grounding site and created a distinct but minor series of pits on the seafloor. At the other extreme, after splitting, the highly unstable "Gladys" executed an astonishingly energetic roll that probably produced a deep seabed pit.

These same stability considerations may be applied to the interpretation of linear scour features. In general, icebergs usually rotate when encountering grounding resistance, then tilt about their weakest axes of roll; the degree of tilt is inversely related to their stability. The tilting of a scouring iceberg tends to minimize the depth of keel penetration and hence minimize the seabed resistance. Although furrowing events were not observed during the DIGS experiment, in general these would arise from the tilting behaviour of moderately stable icebergs under the influence of horizontal driving forces such as current and wind drag and stress from pack ice. The rotational stability of icebergs must play a particularly important role in the accommodation of a scouring keel to bathymetry changes. That is, long scours which traverse many metres of relief with little change in scour profile are likely to be generated by icebergs with at least one weakly stable roll axis.

The Chari (1979) model of a non-tilting iceberg, which furrows into a seabed slope, does appear to have been observed in the case of iceberg "Julianna". This strongly stable iceberg (as confirmed by the shape data) showed little or no tilt while furrowing at most a very short distance to its grounding site. Therefore, this model is valid for icebergs of highly stable shape. However, it may not be the most conservative model in terms of potential scour depth. It appears that the rotational kinetic energies available during a split and grounding event, such as by "Gladys", are an order of magnitude greater than drift kinetic energies available for translational seabed contact. However, the risk posed by these energetic rotational impacts depends on their frequency, depth, and amount of seabed disrupted; parameters as yet unknown.

(e) Identification of Discontinuous Keel-Ice Failure

Evidence provided by observations of melt-out pits, the underwater calving of sediment-laden growlers from iceberg "Gladys", the ubiquity of flat-bottomed scour troughs and the observation of a flat keel on an overturned iceberg, demonstrate clearly that ice failure does take place at the keel/seabed interface. However, adjustment of the keel by ice failure probably occurs quickly, near the beginning of a scour, because linear scours traced over large distances show no evidence of continuous ice failure through a similarly continuous change in morphology. The latter observation has important engineering implications; the largest part of any single linear scour feature can be treated as having been formed by a rigid indentor.

The situation is not as clear for high-energy rotational impacts, and the possibility of pit depths being limited by keel-ice failure requires further attention. Determination of the depth of the "Gladys" grounding pit would significantly aid in the assessment of the importance of ice failure during seabed pitting events.

(f) Deposition Beneath the Keel

It is possible that a flat keel which is scouring through an undulating seabed (e.g., a previously scoured surface) will encounter topographic lows that are deeper than the incision depth of the keel. If the depression is narrower than the keel width and the iceberg is thus prevented from making vertical adjustments, a physical space between the keel and seabed is produced. Sediment bulldozed by the leading edge of the keel may fill the space as the keel advances. If insufficient material is present the space may be only partially filled. This depositional mechanism has been used to explain the existence of the small-scale flat-topped mounds in the trough of "Big Makk" and is believed to be the first observation of deposition of reworked sediment beneath a scouring keel.

(g) Recognition of Keel Armouring

Boulders and cobbles embedded in an overturned iceberg keel, boulders associated with ice melt-out pits, and the existence of ridge-and-groove microtopography offer direct and indirect evidence of shielding of the keel ice from direct seabed contact. Three possible armouring processes are (1) mechanical incorporation of seabed material; (2) adfreezing of seabed material; and (3) exposure of englacial sediment through failure of outer ice layers. By so protecting the keel, these armouring processes inhibit continuous ice failure, thereby accounting in part for the observed consistencies in linear scour morphologies.

(h) Observation of Ridge-and-Groove Microtopography

Although commonly associated with Beaufort Sea pressure-ridge keel gouges, small-scale ridge-and-groove microtopography had only rarely been identified as a feature common to iceberg scours on the eastern Canadian continental shelf. During the DIGS experiment, these features were studied in detail in all three fresh linear scours and in the "Bertha" pits.

Although the entire roughened surface of a scouring keel in direct seabed contact causes continuous reworking of near-surface sediments as the keel moves forward, the morphology of the keel's trailing edge is responsible for generating the microtopography. Either the armouring material and/or the ice itself are the tools that shape the ridges and grooves.

Ridges and grooves parallel to the scour axis are clear indicators of the rotational stability of a scouring iceberg about its vertical axis. This observation is entirely consistent with the inferred dynamic behaviour of a scouring iceberg, namely that it yaws such that tilt occurs about the iceberg's weakest axis of roll. Once this state is achieved, vertical rotations cease.

(i) Degradation of Iceberg Scours

Scour degradation is largely controlled by the cohesive or non-cohesive nature of the seabed substrate. In cohesive sediments, disaggregation of fine-grained sediment by the benthic communities and suspension of the fine fraction by filter feeders, coupled with removal of the disaggregated material by the bottom currents, whether oscillatory or unidirectional, are the dominant processes of degradation. The effects of biogenic reworking results in smoothing of the blocky berms and the exposure of large clasts which eventually form a protective armour. Microfeatures, such as ridges and grooves in the scour trough, are eroded quickly. In non-cohesive sediments current erosion of berms and sediment infilling of troughs, depending on the sediment supply, is of greater importance.

Sediment transport occurs on Makkovik Bank during periods of peak tidal flow and significant storm events. During the DIGS experiment, two periods (4 days total) of strong current flow (>2 m/s) resulted in the entrainment and movement of sand. The occurrence of large oscillation ripples (<3.0 m wavelength), developed in erosional troughs on the seabed, further suggests that periodic erosion and sediment transport takes place above about 120 m water depth.

REFERENCES

Amos, C.L. and J.V. Barrie. 1985. The frequency of ice scouring on the northeastern Grand Banks of Newfoundland using the interrelationship of scours and bedforms. Workshop on Ice Scouring, 15-19 February 1982. National Research Council of Canada Technical Memorandum No.133: 220-221.

Amos, C.L. and E.L. King. 1984. Bedforms of the Canadian eastern seaboard: a comparison with global occurrences. Marine Geology, 57:167-208.

Anderson, C. 1971. The flow of icebergs along the Canadian east coast. Proceedings of the Canadian Seminar on Icebergs, Maritime Command Headquarters, Halifax, Nova Scotia, 6-7 December 1970: 52-61.

Andrews, J.T. 1963. End moraines and late-glacial chronology of the northern Nain-Okak section of the Labrador Coast. Geogr. Annal. No. 45: 158-171.

Atmospheric Environment Service. 1984. Climatology of the east coast marine areas. Contract report prepared by Meteorological and Environmental Planning Limited for the Atmospheric Environment Service, Downsview, Ontario. 142 p.

d'Apollonia, S.J. and C.F.M. Lewis. 1981. Iceberg scour data maps for the Grand Banks of Newfoundland between 46 N and 48 N. Geological Survey of Canada Open File Report 819. 13 p.

Banke, E.G. and S.D. Smith. 1984. A hindcast study of iceberg drift on the Labrador coast. Canadian Technical Report of Hydrography and Ocean Sciences, Canada Department of Fisheries and Oceans. No. 49, 161 p.

Barrie, C.O. and D.J.W. Piper. 1982. Late Quaternary marine geology of Makkovik Bay, Labrador. Geological Survey of Canada, Paper 81-17: 37 p.

Barrie, J.V. 1980. Iceberg/seabed interaction (Northern Labrador Sea). Proceedings of the Conference on Use of Icebergs: Scientific and Practical Feasibility, Cambridge, 1-3 April 1980, Annals of Glaciology, 1:71-76.

Barrie J.V. 1983. Sedimentary processes and the preservation of iceberg scours on the eastern Canadian continental shelf. Proceedings of the 7th International Conference on Port and Ocean Engineering Under Arctic Conditions, Helsinki, Finland, 4:635-653.

Barrie, J.V., W.T. Collins, J.I. Clark, C.F.M. Lewis, and D.R. Parrott. 1986. Submersible observations and origin of an iceberg pit on the Grand Banks of Newfoundland: Current Research, Part A, Geological Survey of Canada, Paper 86-1A: 251-258.

Barrie, J.V. and W.T. Collins. 1985. Preliminary results of investigations into seabed stability in the Hibernia region of Grand Banks during operations of the HMCS Cormorant and SDL-1 Submersible. Contract Report to Geological Survey of Canada, 39 p.

Bass, D., H.S. Gaskill, and W. Carter. 1986. Iceberg generated pits: a theoretical study. Proceedings of the 5th International Offshore Mechanics and Arctic Engineering Symposium, 81-88.

Bass, D. and G.R. Peters. 1984. Computer simulation of iceberg instability. Cold Regions Science and Technology, 9(2):163-169.

Bass, D.W., and S. Sen. 1985. Added mass and damping coefficients for some realistic iceberg models. Cold Regions Science and Technology. 12:163-174.

Bass, D.W. and C. Woodworth-Lynas. 1986. Iceberg crater chains and scour up-down slope. Ice Scour and Seabed Engineering, Environmental Studies Revolving Funds Report, No. 49: 122-126, Ottawa.

Bass, D.W. and C. Woodworth-Lynas. 1988. Iceberg crater marks on the seafloor, Labrador Shelf. Marine Geology, 79:243-260.

Bijker, E.W. 1967. Some considerations about scales for coastal models with moveable beds. Delft Hydraulics Laboratory. Report No. 50, 142 pp.

Blagoveshchensky, V. 1955. Theory of Ship Motions, Dover.

Bursey, J.O., W.J. Sowden, A.D. Gates, and C.L. Blackwood. 1977. Proceedings of the 4th International Conference on Port and Ocean Engineering under Arctic Conditions. Memorial University of Newfoundland, 26-30 September, 1977.

Chari, T.R. 1979. Geotechnical aspects of iceberg scours on ocean floors. Canadian Geotechnical Journal, 16: 379-390.

Chari, T.R. and J.H. Allen. 1972. Iceberg Grounding - a preliminary theory. Applications of Solid Mechanics, Proceedings of the Symposium, 26-27 June, University of Waterloo, Waterloo, Ontario: 81-95.

Chari, T.R. and H.P. Green. 1981. Iceberg scour studies in medium dense sands. Proceedings of the 6th International Conference on Port and Ocean Engineering Under Arctic Conditions, Quebec, Canada, 1: 1012-1018.

Chari, T.R. and G.R. Peters. 1981. Estimates of iceberg scour depths. Production and Transportation Systems for the Hibernia Discovery, (W.E. Russell and D.B. Muggeridge eds.) Newfoundland Petroleum Directorate, St. John's, 178-188.

Chari, T.R., G.R. Peters and K. Muthukrishnaiah. 1980. Environmental factors affecting iceberg scour estimates. Cold Regions Sciences and Technology, 1: 223-230.

Collins W.T. and D. Diemand. 1983. Norploy '82 cruise report August 1982; Centre for Cold Oceans Resources Engineering, Memorial University of Newfoundland St. John's, Newfoundland, C-CORE Publication 83-4, 31p.

Danish Hydraulic Institute. 1979. Environmental conditions offshore west Greenland. Vol. IV Icebergs, Greenland Technical Organization, November 1979.

Denton, G.H., and T. Hughes. 1981. The last great ice sheets. John Wiley and Sons, New York, 484 p.

Diemand, D. 1984. Iceberg temperatures in the north Atlantic, theoretical and measured. Cold Regions Science and Technology, 9: 171-178.

Diemand, D. and J.H. Lever. 1986a. Iceberg stress state. Iceberg Research. No.12: 20-26.

Diemand, D. and J.H. Lever. 1986b. Iceberg splitting and its implications for deterioration modelling. Proceedings of Canadian East Coast Workshop on Sea Ice, Dartmouth, N.S. Canadian Technical Report on Hydrography and Ocean Sciences, No. 73: 427-440.

Diemand, D., W.A. Nixon, and J.H. Lever. 1987. On the splitting of icebergs - natural and induced. Proceedings of the 6th International Symposium on Offshore Mechanisms and Arctic Engineering, Houston, Texas: 379-385.

Ebbesmeyer, C.C., A. Okuba, and J.M. Helseth. 1980. Description of iceberg probability between Baffin Bay and the Grand Banks using a stochastic model. Deep Sea Research 27a: 975-986.

El-Tahan, M., H. El-Tahan, D. Courage, and P. Mitten. 1985. Documentation of iceberg groundings, Environmental Studies Revolving Funds Report No. 007: 162 p. Ottawa.

El-Tahan, H., A.S.J. Swamidas, M. Arockiasamy, and D.V. Reddy. 1984. Strength of iceberg and artificial snow ice under high strain rates and impact loads. Proceedings of 3rd International Symposium on Offshore Mechanics and Arctic Engineering, New Orleans, 3: 157-165.

Engelund, F. and E. Hansen. 1967. A monograph on sediment transport in alluvial streams. Tekrisk Vorlag. Copenhagen, Denmark.

Fader, G.B., and L.H. King. 1981. A reconnaissance of the surficial geology of Grand Banks of Newfoundland; Current Research, Part A. Geological Survey of Canada Paper 81A-1A: 45-56.

Fenco Consultants Ltd. 1975. An analytical study of ice scour on the sea bottom: Arctic Petroleum Operators Association (APOA) Project 69-1 (eds. G.R. Pilkington and H. Iver), Calgary: 185 p.

Fillon, R.H. 1975. Deglaciation of the Labrador continental shelf. Nature, 253: 429-431.

Fillon, R.H. 1980. High-resolution sub-bottom profiles across the northern Labrador shelf: do they provide evidence of glaciation? Program with Abstracts, Geological Association of Canada, 5: p A53.

Fillon, R.H., and R.A. Harmes. 1982. Northern Labrador shelf glacial chronology and depositional environments. Canadian Journal of Earth Sciences, 19: 162-192.

Fissel, D.B. and D.D. Lemon. 1982. Analysis of physical oceanographic data from the Labrador shelf, summer 1980. Offshore Labrador biological studies program. Report to Petro-Canada Exploration Inc. Calgary, Alberta.

Folk, R.L. 1980. Petrology of sedimentary rocks; Hemphill Publishing Company, Austin, Texas, 182 p.

Fowles, G.R. 1970. Analytical mechanics. 2nd Ed. Holt, Rinehart and Winston, New York, pp. 211-215.

Gaskill, H.S., L. Nicks and D.I. Ross. 1985. A non-deterministic model of populations of iceberg scour depths. Cold Regions Science and Technology, 11:107-122.

Geonautics Limited. 1987. Design of an iceberg scour repetitive mapping network for the Canadian east coast. Environmental Studies Revolving Funds Report No. 043: Ottawa.

Geonautics Limited. In Pres. Regional ice scour data base update studies. Environmental Studies Revolving Funds Report Series.

Gilbert, G., and J.V. Barrie 1985. Provenance and sedimentary processes of ice scoured surficial sediments, Labrador shelf. Canadian Journal of Earth Sciences, 22: 1066-1079.

Grant, A.C. 1972. The continental margin off Labrador and eastern Newfoundland: morphology and geology. Canadian Journal of Earth Sciences, 9: 1394-1430.

Green, H.P. and T.R. Chari. 1981. Sediment compaction below iceberg furrows. Oceans '81 Conference Record, September 16-18, 1981, Boston, Mass. Institute of Electrical and Electronic Engineers, New York, 1: 223-227.

Green, H.P., A.S. Reddy, and T.R. Chari, 1983. Iceberg scouring and pipeline burial depth. Proceedings of the 7th International Conference on Port and Ocean Engineering Under Arctic Conditions, Helsinki, Finland, 1: 280-288.

Gustajtis, K.A. 1979. Iceberg population distribution study in the Labrador Sea. C-CORE Report No. 79-8, 41 p.

Gustajtis, K.A. and T.J. Buckley. 1977. A seasonal iceberg density along the Labrador coast. Proceedings of the 4th International Conference on Port and Ocean Engineering Under Arctic Condition, St. John's, Newfoundland, 2:972-983.

Harris, I.McK. 1974. Iceberg marks on the Labrador shelf. Offshore geology of eastern Canada (ed. B.R. Pelletier). Geological Survey of Canada, Paper 74-30, p. 97-101.

Harris, I.McK. and P.G. Jollymore. 1974. Iceberg furrow marks on the continental shelf northeast of Belle Isle, Newfoundland: Canadian Journal of Earth Sciences, 11: 43-52.

Ives, J.D. 1978. The maximum extent of the Laurentide ice sheet along the east coast of North America during the last glaciation. Arctic, 31: 24-53.

Jonsson, T.G. 1966. Wave boundary layers and friction factors. Proceedings of the 10th Conference of Coastal Engineering (ASCE), Tokyo, 1: 127-148.

Josenhans, H.W. 1983. Evidence of pre-late Wisconsin glaciations on Labrador shelf, Cartwright Saddle region. Canadian Journal of Earth Sciences, 20: 225-235.

Josenhans H.W. 1986. Regional geology and seabed dynamics at the proposed iceberg scour (DIGS) experiment site. (C.F.M. Lewis et al. eds.) Ice Scour and Seabed Engineering, Environmental Studies Revolving Funds Report No. 049: 132-137, Ottawa.

Josenhans, H.W., and J.V. Barrie, 1982. Preliminary results of submersible observations on the Labrador shelf. Current Research, Part B. Geological Survey of Canada Paper 82-1B: 269-276.

Josenhans, H.W., and J. Zevenhuizen. 1984. Seafloor dynamics on the Labrador shelf. (Abstract). Proceedings of Sedimentology of Shelf Sands and Sandstones, Calgary, 1984.

Josenhans, H.W., J. Zevenhuizen and R.A. Klassen. 1986. The Quaternary geology of the Labrador shelf. Canadian Journal of Earth Sciences, 23, (8): 1190-1213.

King, L.H. 1970. Surficial geology of the Halifax-Sable Island map area. Marine Sciences Paper 7; Geological Survey of Canada Paper 74-31, 31 p.

King, L.H., and B. MacLean. 1976. Geology of Scotian shelf and adjacent areas. Geological Survey of Canada Paper 74-31: 31 p.

Kivisild H.R. 1981. Use of mathematical models to estimate ice scour. Conference on Canadian Offshore Drilling and Downhole Technology, 14-16 September, 1981, Edmonton Alberta; 68-75.

Kovacs A. and M. Mellor. 1974. Sea ice morphology and ice as a geologic agent in the southern Beaufort Sea. (J.C. Reed and J.E. Sater eds.) The coast and shelf of the Beaufort Sea; Arctic Institute of North America, Arlington Va. pp. 113-181.

Lanan G.A., A.W. Niedoroda and W.F. Weeks. 1986. Ice gouge hazard analysis. Proceedings 18th Offshore Technical Conference, Houston Texas, 5-8 May, No OTC 5298.

Lever J. 1986. Iceberg dynamics of the DIGS experiment; (C.F.M. Lewis et al. eds.) Ice Scour and Seabed Engineering, Environmental Studies Revolving Funds Report No. 049: 138-142, Ottawa.

Lever, J.H. and D. Diemand. 1988. Te hazard potential of glacial ice masses offshore Newfoundland and Labrador. Natural Sciences and Engineering Research Council of Canada, 15 p.

Lever, J.H. and D. Sen. 1986. A method to upgrade iceberg velocity statistics to include wave-induced motion. Proceedings 5th offshore Mechanics and Arctic Engineering Symposium, Tokyo, 1986, Vol. IV: 320-327.

Lever, J.H., K. Klein, and D. Diemand. 1986. Design, development and deployment of instrument packages to monitor the motion of glacial ice masses at sea. Ice Technology, Proceedings of the 1st International Conference, Cambridge, Mass. June 1986. Springer-Verlag, New York: 255-236.

Lewis, C.F.M. 1978. The frequency and magnitude of drift ice groundings from ice-scour tracks in the Canadian Beaufort Sea. Proceedings of the 4th International Conference on Port and Ocean Engineering under Arctic Conditions, Memorial University of Newfoundland, St. John's, Newfoundland: 568-579.

Lewis, C.F.M. 1986. Dynamics of iceberg grounding and scouring (DIGS) experiment. (C.F.M. Lewis et al., eds.), Ice Scour and Seabed Engineering, Environmental Studies Revolving Funds Report No. 049: 129-131 Ottawa.

Lewis, C.F.M. and J.V. Barrie. 1981. Geological evidence of iceberg groundings and related seafloor processes in the Hibernia discovery area of Grand Bank, Newfoundland. (W.E. Russell and D.B. Muggeridge, eds.) Proceedings of the Symposium on Production and Transportation Systems for the Hibernia Discovery, Newfoundland and Labrador Petroleum Directorate, St. John's, Newfoundland: 146-147.

Lewis, C.F.M., B. MacLean, and R.K.H. Falconer. 1980. Ice scour abundance in Labrador Sea and Baffin Bay; a reconnaissance of regional variability: First Canadian Conference on Marine Geotechnical Engineering, April 25-27, 1979, Calgary, Alberta. The Canadian Geotechnical Society, Montreal: 79-94.

Lewis, C.F.M., H.W. Josenhans, G.B. Fader, B. MacLean, S.J. d'Apollonia, and J.V. Barrie. 1982. The distribution and shape variability of iceberg scour marks on Canadian continental shelves (Abstract): Joint Oceanographic Assembly, Halifax, Nova Scotia, 2, p. 40.

Lewis, C.F.M., D.R. Parrott, S.J. D'Apollonia, H.S. Gaskill, and J.V. Barrie. 1987. Methods for estimating rates of iceberg scouring on the Grand Banks of Newfoundland; Proceedings of the 9th International Conference on Port and Ocean Engineering Under Arctic Conditions, Geophysical Institute, University of Alaska, Fairbanks, Alaska. In press.

Lewis, C.F.M. and G.B. Fader. 1985. Submersible observations of iceberg furrows in glacial till, northeast Newfoundland shelf: and in sand and gravel, Grand Banks of Newfoundland (Abstract). (G.R. Pilkington ed.) Workshop on Ice Scouring, National Research Council of Canada Technical Memorandum No. 136. p. 101.

Lewis, C.F.M., D.R. Parrott, P.G. Simpkin and J.T. Buckley (eds). 1986. Ice scour and seabed engineering. Environmental Studies Revolving Funds Report No. 049, Ottawa, 322 p.

Lewis, J.C. and G. Bennett. 1984. Mounte Carlo calculations of iceberg draft changes caused by roll. Cold Regions Science and Technology, 10(1):1-10.

Lien, R. 1981. Seabed features in the Blaaenga area, Weddell Sea, Antarctica. Proceedings of the 6th International Conference on Port and Ocean Engineering under Arctic Conditions, Quebec, 2: 706-716.

Lopez R.J. 1981. Hydrodynamic effects on iceberg gouging. Cold Regions Science and Technology 4: 55-61.

Maclean B. 1982. Investigations of Baffin Island shelf from surface ship and research submersible in 1981. Geological Survey of Canada Paper 82-1A: 445-447.

McMillan, N.J. 1973. Shelves of Labrador Sea and Baffin Bay, Canada. (R.G. McCrossan ed.) The future petroleum provinces of Canada - their geology and potential. Memoir of the Canadian Society of Petroleum Geologists, No. 1: 473-577.

Moran K. 1986. Geotechnical aspects of the DIGS experiment: (C.F.M. Lewis et al. eds.) Ice Scour and Seabed Engineering, Environmental Studies Revolving Funds Report No. 049:143-144, Ottawa.

NORDCO Limited. 1979. Current meter analysis, drillsite Bjarni O-82. Report to Total Eastcan Exploration Ltd. St. John's, Newfoundland.

NORDCO Limited. 1980. Offshore Labrador initial environmental assessment-physical environment component. Petro-Canada Report No. 68-80, St. John's, Newfoundland, 83 p.

NORDCO Limited. 1984. Surficial geology of the Labrador shelf. Geological Survey of Canada open file report 1081.

Pattiaratchi, C.B. and M.B. Collins. 1984. Sediment transport under wave and tidal currents: a case study from the northern Bristol Channel, UK. Marine Geology, 56: 27-40.

Pocklington, P. 1987. Ageing iceberg scours by studying dominant recolonizing biogenic element. Report for Atlantic Geoscience Centre, Bedford Institute of Oceanography. 43 p.

Prasad K.S.R. and T.R. Chari. 1985. Some factors influencing iceberg scour estimates. Proceedings of Fourth International Symposium on Offshore Mechanics and Arctic Engineering, 17-22 February, 1985, Dallas, USA, pp. 302-309.

Prest, V.K. 1970. Quaternary geology. In Geology and Economic Minerals of Canada. Geological Survey of Canada, Economic Geology Report 1:675-764.

Robe, R.Q. and Farmer, L.D. 1975. Physical properties of icebergs - total mass determination, Report of the International Ice Patrol Service in the North Atlantic Ocean, Season of 1975 U.S. Coast Guard Bulletin No. 61, CG-188-30: 61-66.

Rogerson, R.J. 1977. Glacial geomorphology and sediments of the Porcupine Strand area, Labrador, Canada. Unpublished Ph.D. Thesis, Macquarie University, North Ryde, Australia, 275 p.

Schafer, C.T., H. Josenhans, and D. Frobel. 1986. Submersible investigations: videotape of east coast Baffin Island fiords and along the edge of the Labrador continental shelf. Geological survey of Canada Open File 1297, 13.5 minutes.

Shearer J., B. Laroche, and G. Fortin. 1986. Canadian Beaufort Sea 1984 repetitive mapping of ice scour. Canada Environmental Studies Revolving Funds Report 032: 43 p, Ottawa, Canada.

Smith, E.H. 1931. The Marion expedition to Davis Strait and Baffin Bay - 1928. Scientific results, part 3. U.S. Treasury Dept. Bulletin 19: 221 p.

Smith, E.H., F.M. Soule, and O. Mosley. 1937. The Marion and General Greene expeditions to Davis Strait and Labrador Sea. U.S. Coast Guard Bulletin 19: 259 p.

Sowden, W.J., and F.E. Geddes. 1980. Weekly median and extreme ice edges for eastern Canadian seaboard and Hudson Bay. Environment Canada, Atmospheric Environment Service, Ice Climatology and Applications Division. 56 p.

Swart, D.H., 1976. Coastal sediment transport: computation of longshore transport. Waterloopkundig Laboratorium (Delft Hydralics Laboratory). Report R968.

Syvitski, J.P.M., G.B. Fader, H.W. Josenhans, B. MacLean, and D.J.W. Piper. 1983. Seabed investigations of the Canadian east coast and Arctic using PISCES IV. Geoscience Canada, 10, No. 2: 59-68.

Todd, B.J. 1984. Iceberg scouring on Saglek Bank, northern Labrador shelf. Unpublished MSc thesis, Department of Geology, Dalhousie University, Halifax, Nova Scotia.

Todd, B.J. 1986. Iceberg scouring on Saglek Bank northern Labrador shelf. In (C.F.M. Lewis et al. eds.) Ice Scour and Seabed Engineering. Environmental Studies Revolving Funds Report No. 049: 182-193, Ottawa.

Todd, B.J., C.F.M. Lewis, and P.J.C. Ryall. In press. Comparison of trends of iceberg scour marks to iceberg trajectories and evidence of paleocurrent trends on Saglek Bank, northern Labrador shelf. Canadian Journal of Earth Sciences.

van der Linden, W.J.M., R.H. Fillon, and D. Monahan. 1976. Hamilton Bank, Labrador margin: origin and evolution of a glaciated shelf. Geological Survey of Canada Paper 75-40 and Marine Sciences Paper 14, Ottawa, 31 p.

Weeks, W.F, W.B. Tucker, and A.W. Niedoroda. 1985. A numerical simulation of ice gouge formation and infilling on the shelf of the Beaufort Sea. Proceedings of the 8th International Conference on Port and Ocean Engineering Under Arctic Conditions, Narssarssuaq, Greenland, 1:393-407.

White, F.M., M.L. Spaulding, and L. Gominho. 1980. Various mechanisms involved in iceberg deterioration in the open ocean environment. U.S. Coast Guard Report No. CG-D-62-80, 126 p.

Woodworth-Lynas, C.M.T. A possible submarine mud volcano from the southeast Baffin Island shelf. C-CORE Technical Report 83-2. 35 p.

Woodworth-Lynas, C.M.T., D.W. Bass, and J. Bobbitt. 1986. Inventory of upslope and downslope iceberg scouring. Environmental Studies Revolving Funds Report No. 039: 103 p., Ottawa.

Woodworth-Lynas, C.M.T., A. Simms and C.M. Rendell. 1984. Iceberg grounding and scouring frequency, Labrador Sea. OCEANS '84, Conference Record, Washington D.C. 10-14 Sept: 259-262.

Woodworth-Lynas, C.M.T., A. Simms and C.M. Rendell. 1985. Iceberg grounding and scouring on the Labrador continental shelf. Cold Regions Science and Technology, 10: 163-186.